DISSERTATIONS IN
FORESTRY AND
NATURAL SCIENCES

Anna Kaasinen

Optimal Control in Process Tomography

Publications of the University of Eastern Finland
Dissertations in Forestry and Natural Sciences

UNIVERSITY OF
EASTERN FINLAND

ANNA KAASINEN

Optimal Control in Process Tomography

Publications of the University of Eastern Finland
Dissertations in Forestry and Natural Sciences
No 128

Academic Dissertation
To be presented by permission of the Faculty of Science and Forestry for public examination in the Auditorium L21 in Snellmania Building at the University of Eastern Finland, Kuopio, on October, 29, 2013,
at 12 o'clock noon.

Department of Applied Physics

Kopijyvä Oy
Kuopio, 2013
Editors: Prof. Pertti Pasanen, Prof. Kai Peiponen,
Prof. Matti Vornanen, Prof. Pekka Kilpeläinen

Distribution:
University of Eastern Finland Library / Sales of publications
P.O. Box 107, FI-80101 Joensuu, Finland
tel. +358-50-3058396
http://www.uef.fi/kirjasto

ISBN: 978-952-61-1278-7 (printed)
ISSNL: 1798-5668
ISSN: 1798-5668
ISBN: 978-952-61-1279-4 (pdf)
ISSNL: 1798-5668
ISSN: 1798-5676

Author's address:
University of Eastern Finland
Department of Applied Physics
P.O. Box 1627
70211 KUOPIO
FINLAND
email: Anna.Kaasinen@uef.fi

Supervisors:
Professor Jari Kaipio, Ph.D.
University of Eastern Finland
Department of Applied Physics
P.O. Box 1627
70211 KUOPIO
FINLAND
email: jari@math.auckland.ac.nz

Docent Aku Seppänen, Ph.D.
University of Eastern Finland
Department of Applied Physics
P.O. Box 1627
70211 KUOPIO
FINLAND
email: Aku.Seppanen@uef.fi

Reviewers:
Professor Hugh McCann, Ph.D.
University of Edinburgh
School of Engineering
Faraday Building
The King's Building
Mayfield Road
EDINBURGH, EH9 3JL
UNITED KINGDOM
email: H.McCann@ed.ac.uk

Professor Brent R. Young, Ph.D.
University of Auckland
Department of Chemical & Materials Engineering
Private Bag 92019
Auckland Mail Centre
AUCKLAND 1142
NEW ZEALAND
email: b.young@auckland.ac.nz

Opponent:
Professor Brian Hoyle, Ph.D.
University of Leeds
School of Process, Environmental and Materials Engineering
LEEDS, LS2 9JT
UNITED KINGDOM
email: b.s.hoyle@leeds.ac.uk

ABSTRACT

One of the key issues in process control is that the controller obtains quantitative and reliable information about the process in real time. As the quantities of interest in industrial processes have typically both spatial and temporal variations, a nonstationary estimate of the three-dimensional distribution of the unknown quantity is often preferred to a stationary single-point estimate of the unknown quantity. Process tomography is a monitoring technique that provides the controller with three-dimensional and real time information about the process. Furthermore in process tomography, non-intrusive measurements are used and, thus, the measurements do not disturb the process. Consequently, process tomography has been acknowledged as a potential sensor for various process control systems.

When using diffusive tomography, such as electrical impedance tomography, for process monitoring, the challenge is that the reconstruction problem is an ill-posed inverse problem and the results are known to be sensitive to measurement and modelling errors. The models for industrial processes are typically based on partial differential equations and when using the PDE-based models, there are often unavoidable modelling errors. Such modelling errors result, for example, from unknown boundary data or from numerical approximation of the models. Furthermore, as the unknown quantities in industrial processes are often rapidly varying, traditional stationary reconstruction methods are inapplicable. Formulating the reconstruction problem as a state estimation problem and constructing models for the errors has been shown to produce feasible reconstructions in the case of nonstationary quantities.

In this thesis, designing a model-based control system for a convection-diffusion process is considered when the process is monitored with electrical impedance tomography. Two controllers, the approximate linear quadratic Gaussian controller and the approximate $\mathcal{H}_\infty$ controller, are considered. The performance of the control system is evaluated with numerical simulations. The numerical

simulations indicate that it is possible to base a control system on electrical impedance tomography measurements. Furthermore, the results show that the control system is quite robust to certain kinds of modelling errors provided that the overall structure of the process is adequately accurately modelled.

Universal Decimal Classification: 517.977.5, 621.317.33, 658.562.44, 681.513.5
INSPEC Thesaurus: process control; process monitoring; optimal control; linear quadratic Gaussian control; $\mathcal{H}_\infty$ control; state estimation; tomography; electric impedance imaging; inverse problems; numerical analysis; simulation
Yleinen suomalainen asiasanasto: säätö; prosessinohjaus; optimointi; estimointi; tomografia; impedanssitomografia; numeerinen analyysi; simulointi

Acknowledgements

This work was mainly carried out at the Department of Applied Physics at the University of Eastern Finland.

I am very grateful to my supervisors Professor Jari Kaipio and Docent Aku Seppänen for their guidance and encouragement during these years. I also want to thank Professor Stephen Duncan for his guidance and for the fruitful discussions. Furthermore, I want to thank my co-author Professor Erkki Somersalo. I am also grateful to Professor Marko Vauhkonen for his help during the final steps of this work.

I thank the official reviewers Professor Hugh McCann and Professor Brent Young for the assessment of this thesis and for their comments.

I want to thank the staff of the Department of Applied Physics. It is a pleasure to work with you all. I thank the members of the Inverse Problems group. Especially, I am grateful to Docent Tanja Tarvainen for her friendship and support during these years. Furthermore, I thank the teaching staff of the department for creating a friendly working atmosphere. Especially, I want to thank Ville Ramula, PhD, for all the scientific and non-scientific discussions. I also thank the administrative and technical staff of the department for their valuable help. Especially, I want to thank Mauri Puoskari, PhD, for the computer related assistance during these years.

I want to thank my parents Riitta and Juhani Ruuskanen for their support and encouragement during the years. I am also grateful to my friends and to my numerous team-mates in Vipinä, Puijo Wolley, and HuPi. Finally, I would like to express my deepest gratitude and love to my husband Juha and to our daughters Senja and Alisa.

This study was supported by the Finnish Foundation for Technology Promotion, the Finnish Concordia Fund, the Jenny & Antti Wihuri Foundation, and The Graduate School of Inverse Problems.

Kuopio October 2, 2013 *Anna Kaasinen*

ABBREVIATIONS

BEM	Boundary element method
CD	Convection-diffusion
CDR	Convection-diffusion-reaction
CEM	Complete electrode model
CFD	Computational fluid dynamic
CM	Conditional mean
DPS	Distributed parameter system
ECT	Electrical capacitance tomography
EIT	Electrical impedance tomography
EMT	Electromagnetic tomography
ERT	Electrical resistance tomography
FDM	Finite difference method
FE	Finite element
FEM	Finite element method
FVM	Finite volume method
GLS	Galerkin least squares
LDG	Local discontinuous Galerkin
LQ	Linear quadratic
LQG	Linear quadratic Gaussian
LQR	Linear quadratic regulator
LP	Linear programming
MAP	Maximum a posteriori
MCMC	Markov Chain Monte Carlo
MIMO	Multiple-input and multiple-output
MLP	Multilayer perceptron
MPC	Model predictive control
NN	Neural network
ODE	Ordinary differential equation
P	Proportional
PD	Proportional-derivative
PDE	Partial differential equation
PI	Proportional-integral
PID	Proportional-integral-derivative
PT	Process tomography
QP	Quadratic programming
SMC	Sequential Monte Carlo
SUPG	Streamline upwind Petrov-Galerkin

NOMENCLATURE

A_t	State transition matrix
$B_{1,t}$	State noise input matrix
$B_{11,t}$	State noise input matrix in $\mathcal{H}_\infty$ control
$B_{22,t}$	Control input matrix in $\mathcal{H}_\infty$ control
C_t	Control output matrix
$C_{1,t}$	State weighting matrix in the objective equation
$C_{2,t}$	Observation matrix in $\mathcal{H}_\infty$ control
c	Concentration
$D_{11,t}$	Disturbance input weighting matrix
$D_{12,t}$	Control input weighting matrix in the objective equation
$D_{21,t}$	Observation noise input matrix
$D_{22,t}$	Control input matrix in the observation equation
e_ℓ	Electrode
F_t	Kalman gain
$\vec{f}$	External forces acting on a system in Navier-Stokes equations
$G_{1,t}$	Observation matrix
g_t	Observation vector
H	Final state weighting matrix
H_y	Final output weighting matrix
I	Identity matrix
I_ℓ	Electric current
J	Cost function in LQG control
J_γ	Cost function in $\mathcal{H}_\infty$ control
$\mathcal{J}$	Jacobian matrix
$\bar{J}$	Interpolation matrix
K_t	Optimal feedback gain matrix
$\mathcal{L}$	Characteristic length of the flow region
M_f	Molar mass of the fluid
$M_{(\cdot)}$	Controllability matrix
n_V	Number of measurements
n_e	Number of electrodes
n_g	Number of observations
n_u	Number of control inputs
n_x	Number of states
n_y	Number of control outputs
$\vec{n}$	Outward unit normal
O	Zero matrix
$O_{(\cdot)}$	Observability matrix
p	Pressure
Q_t	State weighting matrix
$Q_{y,t}$	Output weighting matrix
q	Control source term

R_t	Control input weighting matrix
$\mathcal{R}$	Resistance matrix
r_t	Reference input
$\tilde{r}$	Pipe width
$\vec{r}$	Spatial coordinate vector
s_t	Process input
t	Time
U_ℓ	Potential on electrode
u_t	Control input
$u^{(j)}$	Flow rate of j^{th} injector
V_i	Voltage
v_t	Observation noise
v_{mean}	Mean velocity
$\vec{v}$	Velocity field
w_t	Disturbance input
$w_{1,t}$	State noise
x_t	State vector
$x_{t\|t}$	Optimal state estimate in LQG control
$x_{t\|t-1}$	Predicted state estimate in LQG control
$x_{t\|t}^{\text{CM}}$	Conditional mean
$x_{t\|t}^{\text{MAP}}$	Maximum a posteriori estimate
$\hat{x}_t$	State estimate in $\mathcal{H}_\infty$ control
y_t	Control output
z_t	Control objective
$\bar{z}_\ell$	Contact impedance
$\Gamma_{(\cdot)}$	Covariance matrix
ϵ_t	Tracking error
κ	Diffusion coefficient
Λ	Boundary of the computational domain
μ	Viscosity
ν	Kinematic viscosity
$\pi(\cdot)$	Probability density
$\pi(\cdot,\cdot)$	Joint probability density
$\pi(\cdot\|\cdot)$	Conditional probability density
$\pi_G(\cdot)$	Gaussian approximation of the probability density
ρ	Density
σ	Conductivity
ϕ	Electric potential
Ω	Computational domain
$\bar{0}$	Zero vector

Contents

1 INTRODUCTION **1**

2 ON CONTROL PROBLEMS **9**
2.1 State-space model 11
2.2 Linear quadratic Gaussian control problem 12
2.3 $\mathcal{H}_\infty$ control problem 25
2.4 Model predictive controller 30
2.5 Proportional-integral-derivative controller 31
2.6 Controllability and observability 33
2.7 Discussion 35

3 STATE-SPACE MODELLING IN ELECTRICAL PROCESS TOMOGRAPHY **39**
3.1 Stochastic convection-diffusion model 39
3.2 EIT observation model 48
3.3 Discussion 65

4 PROCESS CONTROL USING ELECTRICAL PROCESS TOMOGRAPHY **71**
4.1 Electrical process tomography in process control 71
4.2 Controller for the CD process monitored with EIT 75
4.3 Potential industrial applications 84
4.4 Discussion 88

5 SIMULATIONS USING APPROXIMATE LINEAR QUADRATIC GAUSSIAN CONTROLLER **91**
5.1 Two-dimensional approximate LQG controller simulations . 91
5.2 Three-dimensional approximate LQG controller simulations 108
5.3 Approximate LQG controller simulations with nonstationary velocity fields 118
5.4 Comparison of effects of two state estimators on control performance 126

6 SIMULATIONS USING APPROXIMATE $\mathcal{H}_\infty$ CONTROLLER **137**
6.1 Construction of the approximate $\mathcal{H}_\infty$ controller 137
6.2 Approximate $\mathcal{H}_\infty$ controller simulation results 138

6.3 Comparison of the optimal LQ tracker and the approximate $\mathcal{H}_\infty$ controller 141
6.4 Discussion of approximate $\mathcal{H}_\infty$ controller simulations 143

7 OPTIMAL INJECTOR SETTING **145**
7.1 Simulation of the concentration evolution and the EIT observations 146
7.2 Simulation results using different injector settings 147
7.3 Discussion of optimal injector setting 150

8 CONCLUSIONS **153**

REFERENCES **157**

A FE APPROXIMATION OF STOCHASTIC CD MODEL AND CONSTRUCTION OF STATE NOISE COVARIANCE MATRIX **181**

1 Introduction

Process tomography (PT) is a technique for monitoring the progress of an industrial process using tomographic imaging methods. The basic idea of PT is to distribute measurement sensors around the boundary of the object of interest, and on the basis of the measurements to determine the three-dimensional distribution of some physical quantity in that object. Process tomography is suitable for monitoring both spatial and temporal variations of the unknown quantity. It can be used, for example, to gather information on efficiency of mixing or separation of components in a multicomponent flow, or on completion of a chemical reaction. This information can subsequently be utilized in optimizing the operation of a process or in process control. Furthermore, experimental tomographic data can benefit the model validation task during model development for industrial processes.

There are two essential benefits of PT in comparison to many other conventional single-point sensors that are widely used in the process industry such as bypass flow meters for measuring fluid flow rates or conductivity probes for conductivity (and concentration) measurements. Firstly, as only indirect boundary measurements are used, PT is a non-intrusive technique. In other words, the measurement sensors do not enter into the medium of the object, but they may, however, be invasive penetrating, for example, the wall of a vessel or a pipe. Consequently, the sensors do not usually disturb the process and they can provide essential quantitative information about the physical properties of the process from locations that may be inaccessible with conventional monitoring instruments. Secondly, PT yields directly a three-dimensional distribution of the physical quantity instead of a single-point estimate provided by a single-point sensor.

The idea of tomographic imaging in general originates from the need for a method to represent an image of a slice of a human body. The discovery of X-rays and taking the first X-ray images during the last decades of the 19th century initiated the study of tomography, the attempts to built equipment for tomographic imaging, and the development of the mathematical theory behind the tomographic reconstruction. However, it was not until the 1970s when the first commercial computed tomography scanner was introduced. From then on, the medical imaging methods have been developed and instruments for medical applications have been

manufactured.

In addition to medical applications, tomographic imaging has also been applied to imaging of industrial processes. In the 1970s, the first PT applications were invented. In the applications, radiation-based tomographic techniques were used. In the 1980s, research on electrical PT techniques began [1], [2]. By the early 1990s, the work on applying also other imaging modalities, such as ultrasound-based tomography, microwave tomography, and positron-emission tomography, to process imaging had began. See [3], [2] for a review of the modalities. Due to the promising results achieved in the field using a variety of imaging modalities, by the 1990s it was established that tomographic imaging is a potential technique for monitoring industrial processes. From then on, research in the field has focused on improving the hardware, developing the reconstruction techniques, and introducing new modalities. The first book covering the development of PT was published in 1995 [3]. In [2], achievements in the field up to the year 2005 were summarized.

In this thesis, the focus is on electrical PT techniques. The electrical PT techniques include electrical impedance tomography (EIT), electrical capacitance tomography (ECT), and electromagnetic tomography (EMT). The first industrial applications using electrical PT were aimed for imaging multicomponent flows in oil wells and pneumatic conveyors. In the first applications, the imaging modality was ECT. Also EIT that had been investigated as a method for medical imaging was adapted to industrial processes and utilized for monitoring process vessels containing electrically conductive fluids. One of the main reasons that these electrical techniques were and still are preferred for industrial applications is the fast dynamic response of the sensors. Due to fast data collection, electrical tomography techniques are suitable, for example, for monitoring of fast moving targets such as fluids flowing in pipelines. Furthermore, the electrical tomography equipment is typically inexpensive and movable, and the measurement modalities are safe. The limiting issue related to electrical tomography techniques is their relatively poor spatial resolution in comparison to other imaging techniques such as magnetic resonance imaging, for example.

The reconstruction problem in electrical PT is an *inverse problem* [4], [5]. An inverse problem is an inverse of a forward problem. When solving the forward problem in electrical PT, one defines the mapping, that is, the forward model, from the unknown quantity to be reconstructed to the error-free quantity that is measured. Often, the forward model is derived on the basis of physical theory. When solving the inverse problem in elec-

trical PT, one determines the distribution of the unknown quantity on the basis of indirect noisy measurements and the knowledge of the forward model. In general, solutions of inverse problems are sensitive to modelling and measurement errors. For example, even small errors in the observations can cause large errors in the determined distribution of the unknown quantity. Consequently, it is often stated that accurate measurements, an accurate forward model, and in nonstationary case, an adequately accurate evolution model for the industrial process are needed when solving inverse problems. In practice, however, the measurement noise may not be small and the models cannot fully approximate the reality. In such cases, the key issue is to model also the measurement errors and the discrepancies between the models and the reality and take those models into account when solving the reconstruction problem [5].

In numerous publications, one of the main potential application areas for electrical PT is stated to be *process control* [6], [7], [8], [9], [10], [11], [12], [13], [14], [2]. Process control is a field of engineering referring to the methods for changing the conditions of industrial processes so that the performance of the process fulfils some specific requirements regardless of external inputs. Efficient process control can lead to increase in productivity, improvement in product quality, economical improvements, and ability to meet environmental requirements. The quantitative information provided by electrical PT can be utilised in process control to determine the changes required in order to achieve a desired process performance.

Figure 1.1 illustrates the general idea of using (electrical) PT for process monitoring in process control systems. One could consider, for example, fluid flowing in a pipeline. The aim could be to control the concentration of a chemical substance in the fluid by adding strong concentrate into the fluid flow if needed. The sensors would be attached to the boundary of the pipeline and the measured data would be passed on to the state estimator. The state estimator would yield the estimated concentration distribution and this information would be, in turn, passed on to the controller. On the basis of that information the control variable would be computed with respect to the control objective and information about the control variable would be passed on to the actuation mechanism. For example in this case, the actuation mechanism could consist of injectors the flow rates of which are controlled using flow valves. To be more specific, the control variable would be the flow rates of the injectors.

In the early 1900s, process control was exercised by making manual adjustments. From then on, the technological development in the field of process control has been extensive following the new achievements in con-

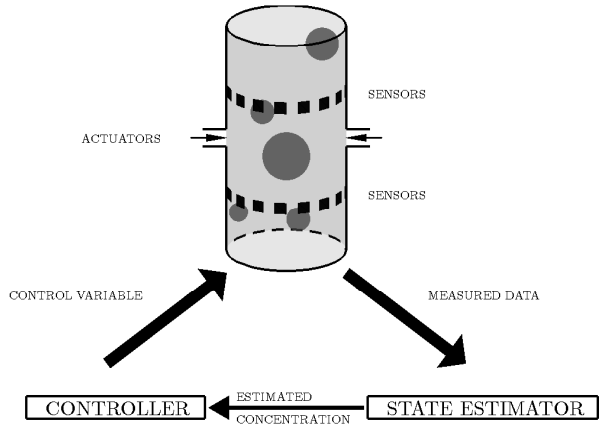

Figure 1.1: Illustration of the general idea of using PT for process monitoring in a process control system.

trol theory and the improvement in the availability of high capacity digital computers. However, the practical applications lag behind the achievements in control theory by even a decade or more. This is especially true in the field of process control since in many countries the focus of research has been on military and aerospace industries. On the other hand, many achievements in those industries have later been applicable in the field of process control.

The controllers that have been applied to industrial processes range from simple proportional-integral-derivative (PID) controllers to more complicated model predictive controllers. The PID controllers [15] have been very popular, also in the process control industry, from the early decades of the 20th century. In the late 1970s, research in the field of process control focused also on controllers based on *optimal control* methods that had already been applied successfully, for example, in military and space industries. An optimal controller aims to direct or regulate the performance of a process in the best way possible. To be more specific, the aim is to stabilize a process, to minimize the influence of disturbances, and to optimize the overall performance. The directing or regulating, that is the controlling, of the process is done by applying control inputs, that are optimal in some sense, to a process.

The obstacles in implementing optimal controllers include the lack of accurate process models, the complexity of the controllers, and, conse-

quently, the computational requirements. Despite the obstacles, model predictive control (MPC) [16], [17], [18] has gained acceptance in the process industry and it has been applied to a variety of processes by the beginning of the 21st century. However, MPC may be unsuitable for real time control of rapidly changing processes, since it is based on the repeated solution of an optimal control problem subject to a performance specification, constraints on process states and control inputs, and a process model. In addition to MPC, also other optimal controllers, such as the linear quadratic Gaussian (LQG) controller and the $\mathcal{H}_\infty$ controller, have been applied in process industry but not to the same extent as model predictive controllers. With the development of accurate process models and real time monitoring systems, such as PT, and with the growth in computer capacity, all of the optimal control methods will likely gain more popularity in the field of process control.

A special class of industrial processes consists of processes that are distributed in nature and can be considered as *distributed parameter systems* (DPSs). The DPSs are characterized by the feature that the state variables, the control variables, the observations, and/or the system parameters exhibit both spatial and temporal variations. Examples of DPSs are encountered in many process industries involving mass and/or heat transfer or chemical reaction. In many *chemical processes*, the aim is to control the flows of both heat and mass in the presence of possible simultaneous chemical reactions. The control problem is often highly complex and requires sophisticated control methods. Consequently, although laboratory or pilot case studies have been published since the early 1970s [19], [20], [21], [22] and the references therein, full-size real time distributed parameter control systems have not been widely implemented. By contrast, many simulation studies have been published applying distributed parameter control methods to chemical processes. For example, the control of a fixed-bed bioreactor [23], [24], [25], of a nonisothermal packed-bed reactor [26], [27], of a batch fluidised-bed reactor [28], and of a plug-flow reactor [29], [30] has been investigated with numerical simulations. Furthermore, the control of flow of mass is encountered, for example, in papermaking [31], [32], in polymer film extrusion [33], and in a wide range of coating processes. Control systems for the control of heat transfer have been implemented in processes such as thawing of foodstuff [34], [35], welding [36], [37], and metal spraying [38], [39], and in many processes in semiconductor manufacturing [40]. However, PT has not been used as a sensor in any of the published distributed parameter control systems although the spatial and temporal changes of the process quantities en-

countered in DPSs could be monitored with PT.

When designing *model-based control systems* for DPSs, mathematical models of DPSs are required. The DPSs are modelled, for example, with partial differential equations (PDEs) or integral equations. The PDE models are infinite-dimensional, and the controllers designed on the basis of these models are also infinite-dimensional. The infinite-dimensional controllers, however, are not typically implementable in practice for example due to the discrete nature of actuators and measurement sensors. There are two approaches to overcome the problem of infinite-dimensionality. Firstly, an infinite-dimensional controller is designed using an infinite-dimensional PDE model and then reduced to a finite-dimensional controller. This approach has been proven to be applicable for DPSs described by hyperbolic PDEs [29], [41], [30]. Secondly, the infinite-dimensional PDE system is approximated with a set of finite-dimensional ordinary differential equations (ODEs), and a finite-dimensional controller is then derived for that ODE system. Several methods have been proposed for the spatial discretisation of the PDE system. These methods include the orthogonal collocation method [23], [24], the finite element method (FEM) [42], [25], the finite volume method [40], and the finite Fourier transform technique [43]. Although these two approaches are widely-used, there are no guarantees that a finite-dimensional controller is actually able to control the process modelled with an infinite-dimensional PDE system. Theoretical results on the matter have begun to appear involving especially the linear PDE systems.

Although electrical PT has been applied to the monitoring of industrial processes, research efforts have only recently been directed to combining electrical PT and (optimal) control of PDE-based DPSs. Designing a distributed parameter control system using electrical PT as a sensor is not a trivial task and only a few industrial automatic *physical model-based control systems* employing electrical PT for process monitoring have been considered [44], [28]. There are several important reasons for the lack of applications. The information provided by the methods for solving the reconstruction problem associated with electrical PT has traditionally been more qualitative than quantitative in nature. For some specific fault detection processes, the qualitative information may be adequate, but automatic controllers require quantitative and real time information about the process. Furthermore, a model-based control system requires a model describing the evolution of the process. However in many occasions, the appropriate models are PDE-based and the spatial discretisation leads to a finite-dimensional control system of high dimension increasing

the computational load and at worst even hindering real time computations. Also the observation model, for example in EIT, is PDE-based and the spatial discretisation yields a finite-dimensional system of high dimension. A common way to reduce the dimensionality of the models is to use model reduction techniques, see [45], [46], [47], [48] for parabolic PDE systems and [41], [30] for hyperbolic PDE systems. However, the reconstruction problem in EIT is an ill-posed inverse problem and, thus, sensitive to modelling errors such as the errors due to numerical approximation of the PDE models. Therefore, model reduction often leads to infeasible reconstructions if not handled appropriately and, especially, if not taking into account the characteristic nature of ill-posed inverse problems [49], [50], [51].

THE AIMS AND CONTENTS OF THE THESIS

The overall aim of this thesis is to determine with numerical simulations whether it is possible to design an optimal distributed parameter control system for a convection-diffusion (CD) process when EIT is used for process monitoring. The control system is required to be closed-loop, automatic, model-based, and to operate in real time. The key issue is whether the quality of the data provided by EIT is adequate for the optimal controller when there are inevitable modelling and measurement errors involved. Furthermore, the idea is to consider errors that will render the quality of the state estimates inadequate for efficient process control. This study is intended as an initial feasibility study on the subject of combining optimal control of a specific industrial process described by a PDE-based DPS and EIT measurements.

In this thesis, the difference between the performance of the approximate LQG controller and the performance of the approximate $\mathcal{H}_\infty$ controller is studied in the case of EIT measurements. Also the robustness of the proposed control systems is tested. It is investigated which of the controllers is more suitable for controlling the CD process when indirect EIT measurements provide the controller with the information on the controlled quantity and when there are inaccuracies in the modelling of the CD process. Furthermore, it is studied whether the selection of a state estimator and the locations of actuators have an effect on the performance of the control system in the case of the approximate LQG controller.

Some of the results presented in this thesis have already been published [44], [52], [53], [54], [55], [56], [57]. In this thesis, the intention is to give a theoretical background for the applied methods, to provide a de-

tailed discussion of the research topics, and to present additional results.

This thesis is divided into six chapters. In Chapter 2, a short introduction to two optimal controllers, the LQG controller and the $\mathcal{H}_\infty$ controller, is given. In Chapter 3, the stochastic CD model, which is used as a process model, is considered. Furthermore, EIT that is used as a sensor in the control system is discussed. In Chapter 4, a short review of process control applications monitored with electrical PT is given. Furthermore, the control system designed for the example application of this thesis is introduced and examples of industrial processes, to which the proposed control system could be modified, are given. In Chapter 5, the performance and robustness of the proposed approximate LQG controller is evaluated with numerical simulations in the case of the example application of this thesis. Furthermore, the comparison of the effect of the state estimators on control performance is done. In Chapter 6, the performance of the control system utilizing the approximate $\mathcal{H}_\infty$ controller is evaluated. Furthermore, it is investigated whether the approximate $\mathcal{H}_\infty$ controller is more suitable than the optimal linear quadratic (LQ) tracker in the case of the example application. In Chapter 7, the effect of locations of actuators on control performance in the case of the CD process is investigated. The core of the contribution of this thesis is mainly in Chapters 5, 6, and 7 and also in Section 4.2. In Chapter 8, overall discussion and conclusions are given.

2 On control problems

In this chapter, the linear quadratic Gaussian (LQG) controller and the $\mathcal{H}_\infty$ optimal controller are considered. The chapter is begun by giving short explanations to the concepts of optimal control problems, model-based control systems, and stochastic control problems. Furthermore, background information on optimal control theory is briefly reviewed.

Optimal control problems are characterized by the property that the solution, that is the optimal controller or the optimal control law, is obtained by minimizing a selected cost function (or by maximizing a performance index). The cost function reflects the objectives of the control system and combines all the available performance specifications. Unlike the so-called classical control system design methodology [15], [58], [59], in which the control system is modified on the basis of the designer's intuitive insight until acceptable performance is obtained, the optimal control design methodology yields the optimal controller directly. The only step in which modification may be required is the adjustment of the parameters in the cost function so that the cost function describes better the desired behaviour of the process. However, the number of modified parameters in the cost function is small. The need for less modification based on designer's insight is one of the main advantages of the optimal control methodology. Especially when considering high-order systems, the intuitive insight often fails.

In addition to the specification of the cost function, another important component in the formulation of the optimal control problem is the modelling of the process to be controlled. The optimal controller is based on a mathematical model of the process that leads to the use of the term a *model-based* control system. The process modelling includes also the definition of possible physical constraints on the state of the process and on the control. Due to the constraints, the range of all possible controls is reduced to the admissible ones.

In order to operate efficiently, the controller needs information on the state of the process. If the controller must operate on limited or uncertain state information or if the process is corrupted by random disturbances, the state and future controls are seen as stochastic. This leads to *a stochastic control problem* in which the cost function is a stochastic variable, and instead of minimizing the cost function as such one minimizes the expected value of the cost function given the assumptions about the statistics of the

random effects.

The first steps in the field of optimal control theory were taken in the post-war era. The development in the field was mainly influenced by two factors [60], [61]. Firstly, in many countries research efforts were focused on military and space industries, and optimal control methods were needed for launching, guidance, and tracking of missiles and space vehicles. Secondly, the improvement in the availability of high capacity digital computers enabled the computations even in the case of complex systems. In the 1950s, originating from his work on missiles, Richard Bellman formulated the *principal of optimality* and defined the optimal control problem as a multi-stage decision making problem that could be solved by using *dynamic programming*. In 1956, Lev Pontryagin proposed the *maximum principle of optimality* (also referred to as the minimum principle) that is said to form the foundation for the optimal control theory. The achievements by Bellman and Pontryagin led to extensive research in the field of optimal control theory and in the fields related to it in the next decades. During that time, one of the main contributors without a doubt was Rudolf Kalman who worked, among other things, on linear optimal control problems with quadratic performance index and on optimal filtering. In the 1960s and the 1970s, the optimal LQG control theory was mostly developed due to the achievements of many contributors. To meet the requirements of a more robust control design, the concept of $\mathcal{H}_\infty$ optimal control was introduced in the 1980s. The basic $\mathcal{H}_\infty$ theory was refined during the 1990s by John Doyle and Gunter Stein, for example.

Optimal control theory discussed in this chapter is based on the books [62], [63], [64], [65], and [66]. In this thesis, the discussion is limited to the discrete-time optimal control problems since in the control systems using PT as a sensor, the observations are typically obtained at discrete time intervals. Furthermore, only the state-space models are considered as overall process models, and the approach using, for example, the transfer function models [59], [67] or the differential (or difference) equation models [59], [67] is omitted. The state-space models are superior for high-order multiple-input and multiple-output (MIMO) systems with large state dimension which are related to distributed parameter systems (DPSs) based on partial differential equations (PDEs).

In Section 2.1, the discrete-time state-space model consisting of a linear state equation and a nonlinear observation equation is considered. In Section 2.2, the LQG optimal control problem is formulated. Firstly, the basic linear quadratic regulator (LQR) is reviewed. Then, methods for solving a tracking problem are considered, and an introduction to (non-

linear) state estimation is given. In Section 2.3, the $\mathcal{H}_\infty$ optimal control problem is formulated and the $\mathcal{H}_\infty$ controller is reviewed. Model predictive control (MPC) is briefly discussed in Section 2.4. In Section 2.5, the proportional-integral-derivative (PID) controller is briefly considered although the PID controller is not an optimal controller. In Section 2.6, the concepts of controllability and observability of control systems are discussed. The chapter is concluded with a discussion is Section 2.7.

2.1 STATE-SPACE MODEL

The state-space model considered in this thesis consists of a linear state equation and a nonlinear observation equation. The choice of such a state-space model is based on the example application of this thesis, which involves controlling of a convection-diffusion (CD) process using electrical impedance tomography (EIT) as a sensor.

The linear, nonstationary, discrete-time state equation and the nonlinear, nonstationary, discrete-time observation equation constitute the state-space model

$$x_{t+1} = A_t x_t + B_{2,t} u_t + s_{t+1} + w_{1,t} \tag{2.1}$$

$$g_t = G_t(x_t) + v_t \tag{2.2}$$

where the time index $t \in \mathbb{N}_0$ and $x_t \in \mathbb{R}^{n_x}$ denotes the state vector. In (2.1), $u_t \in \mathbb{R}^{n_u}$ is the control input vector and the vector $s_{t+1} \in \mathbb{R}^{n_x}$ describes the uncontrollable process input. The state transition matrix $A_t \in \mathbb{R}^{n_x \times n_x}$ and the control input matrix $B_{2,t} \in \mathbb{R}^{n_x \times n_u}$ are known at each time t. In (2.2), $g_t \in \mathbb{R}^{n_g}$ is the vector of observations at time t. Furthermore, the nonlinear mapping $G_t : \mathbb{R}^{n_x} \to \mathbb{R}^{n_g}$ models the dependence of the observations upon the state and is assumed to be differentiable. In (2.1), $w_{1,t} \in \mathbb{R}^{n_x}$ is the state noise and in (2.2), $v_t \in \mathbb{R}^{n_g}$ is the observation noise. The initial state x_0 is assumed to be a Gaussian random variable with known mean $\mu_{x_0} \in \mathbb{R}^{n_x}$ and known covariance $\Gamma_{x_0} \in \mathbb{R}^{n_x \times n_x}$.

The state noise $w_{1,t}$ and the observation noise v_t are assumed to be zero-mean Gaussian random variables with known covariances $\Gamma_{w_{1,t}} \in \mathbb{R}^{n_x \times n_x}$ and $\Gamma_{v_t} \in \mathbb{R}^{n_x \times n_x}$ for all t, respectively. Furthermore, it is assumed that

$$E\left[w_{1,t} w_{1,t+\tau}^T\right] = \begin{cases} 0 & , \tau \neq 0 \\ \Gamma_{w_{1,t}} & , \tau = 0 \end{cases} \tag{2.3}$$

$$E\left[v_t v_{t+\tau}^T\right] = \begin{cases} 0 & , \tau \neq 0 \\ \Gamma_{v_t} & , \tau = 0 \end{cases} \tag{2.4}$$

where $\tau \in \mathbb{Z}$. The state noise and the observation noise are also assumed to be uncorrelated so that $E\left[v_t w_{1,t+\tau}^T\right] = 0$ for all τ. It is assumed that the initial state x_0 and the state noise $w_{1,t}$ as well as the initial state x_0 and the observation noise v_t are uncorrelated, that is,

$$E\left[x_0 w_{1,t}^T\right] = E\left[x_0 v_t^T\right] = 0 \tag{2.5}$$

for all $t \in \mathbb{N}_0$. Furthermore, the assumption that the state x_t and the observation noise v_t are uncorrelated holds for all t. Thus,

$$E\left[x_t v_{t+\tau}^T\right] = 0 \tag{2.6}$$

for all τ.

2.2 LINEAR QUADRATIC GAUSSIAN CONTROL PROBLEM

One of the most widely studied stochastic optimal control problem is the LQG control problem. The objective in the LQG control is to find the optimal control law specifying how to compute the optimal control inputs that minimize the expected value of a *quadratic* cost function when only *incomplete* or *indirect* state information is available and when the process is modelled with a *linear* state equation. Furthermore, the state noise and the observation noise are modelled as *Gaussian white noise* processes.

Solving the LQG optimal control problem consists basically of two tasks. The first task is to find an optimal state estimator that yields the estimated state of the process knowing the noisy observations and the state-space model. The second task is to determine the optimal control law yielding the optimal control input knowing the state estimate. An appealing feature of the LQG optimal control problem is that it possesses a so-called certainty equivalence property [59]. For the certainty equivalent problems, the controller and the estimator design processes are separable. Thus, the state estimator can be designed without taking into account the control law. The only information needed to be transformed from the estimator to the control law is the state estimate. Furthermore, the control law can be designed as if there is perfect information about the state of the process. In other words, the certainty equivalent control law for stochastic problems is equivalent to the optimal control law for deterministic problems obtained by replacing all random variables in the state-space model with their expected values and assuming that there is perfect information about the state. The only difference is that the actual state in the control

law for deterministic problems is replaced by its estimate in the control law for stochastic problems.

Typically in the LQG control, the optimal control law is obtained as a solution to a linear quadratic regulator (LQR) problem and if the observation equation is linear, the Kalman filter, also known as the linear quadratic estimator, is employed as a optimal state estimator. In this thesis, the control law for the stochastic LQR is reviewed in Section 2.2.1. In Section 2.2.2, optimal control laws for tracking problems are considered. Furthermore, as the observation equation in this thesis is nonlinear, nonlinear state estimation is considered in Section 2.2.3.

2.2.1 Discrete-time stochastic linear quadratic regulator

In the stochastic LQR control, the expected value of a *quadratic* cost function is minimized when the state equation is *linear*, the initial conditions and the disturbance inputs are assumed to be Gaussian, and perfect state information is available. In this thesis when formulating the LQR control law, the process input vector s_{t+1} in the state equation (2.1) is assumed to be a zero vector and in Section 4.2.2, it is described how the effect of s_{t+1} is taken into account. However, it would be possible to consider $\{s_{t+1}\}$ as a random process and replace s_{t+1} with its expected value in the derivation of the control law. Thus, the state equation (2.1) gets the form

$$x_{t+1} = A_t x_t + B_{2,t} u_t + w_{1,t}. \tag{2.7}$$

The objective in the LQR control is to derive a control law that specifies the control inputs u_t, $t = 1, \ldots, N$, that minimize a selected cost function when the state x_t, $t = 1, \ldots, N$, and the state equation are known. The quadratic cost function to be minimized is typically of the form

$$J = E\left[\frac{1}{2}\left(x_N^T H x_N + \sum_{t=0}^{N-1} z_t^T z_t\right)\right] \tag{2.8}$$

where $H \in \mathbb{R}^{n_x \times n_x}$ is the weighting matrix that is specified by the designer, and the objective vector $z_t \in \mathbb{R}^{(n_x+n_u)}$ is defined as

$$z_t = C_{1,t} x_t + D_{12,t} u_t. \tag{2.9}$$

Typically in LQR control problems, the matrices $C_{1,t} \in \mathbb{R}^{(n_x+n_u)\times n_x}$ and $D_{12,t} \in \mathbb{R}^{(n_x+n_u)\times n_u}$ are defined so that

$$C_{1,t} = \begin{bmatrix} Q_t^{\frac{1}{2}} \\ 0 \end{bmatrix} \qquad \text{and} \qquad D_{12,t} = \begin{bmatrix} 0 \\ R_t^{\frac{1}{2}} \end{bmatrix} \tag{2.10}$$

where $Q_t \in \mathbb{R}^{n_x \times n_x}$ and $R_t \in \mathbb{R}^{n_u \times n_u}$ are weighting matrices that are specified by the designer. With such a choice the cost function (2.8) gets the form

$$J = E\left[\frac{1}{2}x_N^T H x_N + \frac{1}{2}\sum_{t=0}^{N-1}\left(x_t^T Q_t x_t + u_t^T R_t u_t\right)\right]. \tag{2.11}$$

It is assumed that H and Q_t are positive semidefinite matrices for all t. Furthermore, the matrix R_t is positive definite for all t. From (2.11), it can be concluded that there are two usually competing objectives, that are, to drive the state x_t to zero quickly and to choose small control inputs u_t to do that. The weighting matrices Q_t, H, and R_t set relative weights to the objectives. If, for example, it is important to drive the state to zero regardless of the size of the control inputs, the magnitude of the elements of Q_t is increased relative to the magnitude of the elements of R_t and vice versa. Also the state and measurement noise vectors weighted by matrices could be included in the objective vector z_t (2.9).

Often, it is impossible or unnecessary to control the entire state x_t. The control output specifies the part of the state that is controlled, and it is defined with the output equation

$$y_t = C_t x_t \tag{2.12}$$

where the output vector $y_t \in \mathbb{R}^{n_y}$, $n_y \leq n_x$ and $C_t \in \mathbb{R}^{n_y \times n_x}$ is the output matrix. Now the objective is to drive the output y_t to zero. Let the matrices $H = C_t^T H_y C_t$ and $Q_t = C_t^T Q_{y,t} C_t$ in (2.11). The cost function (2.11) can now be expressed in terms of the output y_t so that

$$J = E\left[\frac{1}{2}y_N^T H_y y_N + \frac{1}{2}\sum_{t=0}^{N-1}\left(y_t^T Q_{y,t} y_t + u_t^T R_t u_t\right)\right] \tag{2.13}$$

where $H_y \in \mathbb{R}^{n_y \times n_y}$ and $Q_{y,t} \in \mathbb{R}^{n_y \times n_y}$ are the positive definite for all t.

The solution to the LQR problem is the optimal control law. There are two widely used approaches, the method of dynamic programming and the variational method, to derive the optimal control law. In this thesis, the derivation utilizing dynamic programming is reviewed. The basic idea of dynamic programming is to break the optimization problem (the minimization problem in this thesis) into a sequence of simpler subproblems over time. This is enabled by the (Bellman's) principle of optimality which states that an optimal control sequence has the property that, whatever the initial state and the optimal first control may be, the remaining

controls constitute an optimal control sequence with regard to the state resulting from the first control [59].

Let u_t denote the optimal control in a process finishing at time N and starting from state x_t i.e. the optimal control at time t. Let $J_{t,N}$ denote the cost in a process finishing at time N and starting from state x_t at time t. That is,

$$J_{t,N} = E\left[\frac{1}{2}x_N^T H x_N + \frac{1}{2}\sum_{k=t}^{N-1}\left(x_k^T Q_k x_k + u_k^T R_k u_k\right)\right]. \tag{2.14}$$

Let $J_{t,N}^*$ denote the value of (2.14) using optimal control over $(N-t)$ stages finishing at time N and starting from state x_t i.e. the optimal (minimum) cost for the last $(N-t)$ stages of an N stage process. That is,

$$J_{t,N}^* = \min_{u_t,\ldots,u_{N-1}}\left\{E\left[\frac{1}{2}x_N^T H x_N + \frac{1}{2}\sum_{k=t}^{N-1}\left(x_k^T Q_k x_k + u_k^T R_k u_k\right)\right]\right\}. \tag{2.15}$$

Thus, the cost of reaching the final state x_N is

$$J_{N,N} = \frac{1}{2}x_N^T P_N x_N \tag{2.16}$$

where $P_N \in \mathbb{R}^{n_x \times n_x}$, $P_N = H$. Furthermore, the optimal cost $J_{N,N}^* = \frac{1}{2}x_N^T P_N x_N$. Correspondingly, the cost over the final interval $[N-1, N]$ is

$$\begin{aligned} & J_{N-1,N} \\ & = E\left[\frac{1}{2}\left(x_{N-1}^T Q_{N-1} x_{N-1} + u_{N-1}^T R_{N-1} u_{N-1}\right) + J_{N,N}^*\right] \\ & = \frac{1}{2}E\left[x_{N-1}^T Q_{N-1} x_{N-1} + u_{N-1}^T R_{N-1} u_{N-1} \; + x_N^T P_N x_N\right] \\ & = \frac{1}{2}\left(x_{N-1}^T Q_{N-1} x_{N-1} + u_{N-1}^T R_{N-1} u_{N-1} + E\left[x_N^T P_N x_N\right]\right) \end{aligned} \tag{2.17}$$

where x_N is related to u_{N-1} by the state equation (2.7). The cost over the interval $[N-1, N]$ is minimized with respect to u_{N-1} and the minimization problem to be solved is

$$\begin{aligned} & \min_{u_{N-1}}\{J_{N-1,N}\} \\ & \quad = \min_{u_{N-1}}\left\{\frac{1}{2}\Big\{x_{N-1}^T Q_{N-1} x_{N-1} + u_{N-1}^T R_{N-1} u_{N-1} \right. \\ & \qquad + (A_{N-1}x_{N-1} + B_{2,N-1}u_{N-1})^T P_N \\ & \qquad \left.(A_{N-1}x_{N-1} + B_{2,N-1}u_{N-1}) + \mathrm{tr}\left(P_N \Gamma_{w_{1,N}}\right)\Big\}\right\} \end{aligned} \tag{2.18}$$

where tr $(\cdot)$ denotes the trace of a matrix and $\Gamma_{w_{1,N}}$ is the covariance matrix of the state noise $w_{1,N}$. Solving the minimization problem in (2.18) yields the optimal control input

$$u_{N-1} = -K_{N-1}x_{N-1} \tag{2.19}$$

where $K_{N-1} \in \mathbb{R}^{n_u \times n_x}$, $K_{N-1} = (R_{N-1} + B_{2,N-1}^T P_N B_{2,N-1})^{-1} B_{2,N-1}^T P_N A_{N-1}$. Substituting (2.19) into (2.17) yields the optimal cost

$$J_{N-1,N}^* = \frac{1}{2} x_{N-1}^T P_{N-1} x_{N-1} + \omega_{N-1} \tag{2.20}$$

where $P_{N-1} \in \mathbb{R}^{n_x \times n_x}$,

$$\begin{aligned} P_{N-1} &= (A_{N-1} + B_{2,N-1}K_{N-1})^T P_N (A_{N-1} + B_{2,N-1}K_{N-1}) \\ &\quad + Q_{N-1} + K_{N-1}^T R_{N-1} K_{N-1}, \end{aligned} \tag{2.21}$$

and $\omega_{N-1} \in \mathbb{R}$, $\omega_{N-1} = \frac{1}{2}\text{tr}\,(P_N \Gamma_{w_{1,N}}) + \omega_N$ with $\omega_N = 0$.

It can be noted that $J_{N,N}^*$ and $J_{N-1,N}^*$ are of the same form. The process is continued further back for $N-2, N-3, \ldots$ and for the t^{th} stage of the process the expressions for the optimal control input and the minimum cost are

$$u_t = -K_t x_t, \tag{2.22}$$

$$J_{t,N}^* = \frac{1}{2} x_t^T P_t x_t + \omega_t \tag{2.23}$$

where $K_t \in \mathbb{R}^{n_u \times n_x}$, $K_t = (R_t + B_{2,t}^T P_{t+1} B_{2,t})^{-1} B_{2,t}^T P_{t+1} A_t$, is referred to as the optimal feedback gain matrix, $P_t \in \mathbb{R}^{n_x \times n_x}$,

$$\begin{aligned} P_t &= A_t^T P_{t+1} A_t + Q_t - \\ &\quad A_t^T P_{t+1} B_{2,t} \left(R_t + B_{2,t}^T P_{t+1} B_{2,t} \right)^{-1} B_{2,t}^T P_{t+1} A_t, \end{aligned} \tag{2.24}$$

and $\omega_t \in \mathbb{R}$, $\omega_t = \frac{1}{2}\text{tr}\,(P_{t+1}\Gamma_{1,t}) + \omega_{t+1}$. It can be concluded from (2.22) that the optimal controller is a linear, nonstationary, and state feedback controller.

The matrix P_t is needed when computing the control inputs (2.22). The equation (2.24) has the form of a discrete-time matrix Riccati equation [66]. The matrix P_t can be solved, for example, by recursion from $P_N = H$ using (2.24). Other numerical methods also exist [66]. If $N \to \infty$ and the matrices $A_t = A$, $B_{2,t} = B_2$, $Q_t = Q$, and $R_t = R$ are stationary, $P_t \to P$ where P is the steady-state solution of the algebraic Riccati equation

$$0 = A^T P A - P + Q - A^T P B_2 \left(R + B_2^T P B_2 \right)^{-1} B_2^T P A. \tag{2.25}$$

The use of the steady-state solution P is justified, if the control system is designed to operate for time periods that are long compared to the transient time of the solution of the Riccati equation (2.24). Such an approximation simplifies the controller structure and enables the off-line computation of the optimal feedback gain matrix K as it becomes stationary. See [66] for details on numerical methods for solving the algebraic Riccati equation.

2.2.2 Discrete-time tracking problem

The basic LQR reviewed in Section 2.2.1 is designed to drive the states (or the outputs) to zero. However in many real life applications, the problem is to design a control system that keeps the state x_t close to a given desired state $x_{d,t} \in \mathbb{R}^{n_x}$ for all $t \in \mathbb{N}_0$. The desired state $x_{d,t}$ typifies the desired process behaviour and can be nonstationary and/or non-zero. Furthermore, it is specified by the designer. The control objective can be stated also in terms of the output y_t. In such a case, the problem is to design a control system that forces the output y_t to follow a given reference input r_t as closely as possible for all t. The reference input $r_t \in \mathbb{R}^{n_y}$ is defined so that $r_t = C_t x_{d,t}$. Such control systems are referred to as *tracking systems*.

In terms of the output, the objective of a tracking system is to minimize the tracking error $\epsilon_t \in \mathbb{R}^{n_y}$, $\epsilon_t = |r_t - y_t|$, for all t. The cost function of a tracking system contains the tracking error ϵ_t and is

$$J = E\left[\frac{1}{2}\epsilon_N^T H_y \epsilon_N + \frac{1}{2}\sum_{t=0}^{N-1}\left(\epsilon_t^T Q_{y,t}\epsilon_t + u_t^T R_t u_t\right)\right] \tag{2.26}$$

where the weighting matrices H_y, $Q_{y,t}$, and R_t are defined as in Section 2.2.1.

The optimal LQ tracker is derived, for example, in [62]. The optimal control law for the tracking problem is achieved by following the derivation of the basic LQR and taking into account the required modifications resulting from the new cost function (2.26). The optimal control law is

$$u_t = -K_t x_t - K_{b,t} b_{t+1} \tag{2.27}$$

where K_t is defined in Section 2.2.1, $K_{b,t} \in \mathbb{R}^{n_u \times n_x}$,

$$K_{b,t} = (R_t + B_{2,t}^T P_{t+1} B_{2,t})^{-1} B_{2,t}^T, \tag{2.28}$$

and $b_t \in \mathbb{R}^{n_x}$,

$$b_t = (A_t^T - K_t^T B_{2,t}^T) b_{t+1} - Q_t x_{d,t}, \tag{2.29}$$

with b_N given. Thus, for computation of the control input (2.27) at each time t one has to solve b_{t+1} recursively from (2.29). Besides the optimal tracker, suboptimal trackers have been designed mostly for continuous-time systems, see [63], [68].

If the system matrices and the weighting matrices are stationary so that $A_t = A$, $B_{2,t} = B_2$, $C_t = C$, $Q_t = Q$, and $R_t = R$, a so-called non-zero-set-point regulator can be designed. In such a case, the control law is

$$u_t = \bar{u} - K(x_t - \bar{x}) \tag{2.30}$$

where $\bar{u} \in \mathbb{R}^{n_u}$ and $\bar{x} \in \mathbb{R}^{n_x}$ are the steady-state values of the control input and the state, respectively. The steady-state values are determined so that the steady-state output $\bar{y} \in \mathbb{R}^{n_y}$ equals a stationary reference input r. The non-zero set-point regulator for continuous-time systems is discussed in [69] and [66].

2.2.3 State estimation

The optimal control u_t can be found by using the control law (2.22) provided that the entire state x_t is measured perfectly. This assumption is not valid in many real life applications in which there may not be sensors capable of measuring the entire state or the cost of including such sensors is prohibitive. Therefore, the concept of state estimation is introduced, and a state estimator is incorporated into the control system. It can be shown that if the state estimates are optimal in some sense, the optimal control law produces optimal control inputs.

In this thesis, the aim is to determine the distribution of the unknown quantity (i.e. the state) on the basis of EIT observations when the unknown quantity has spatial and temporal variations. The associated nonstationary reconstruction problem of EIT can be formulated as a state estimation problem. The review of state estimation methods in this thesis is based on [5], [70] considering nonstationary inverse problems. As general references on the state estimation theory, see [71], [72], [73].

The specification of the state estimation problem is to compute the state estimate, preferably the optimal state estimate, denoted by $\hat{x}_t$ or $x_{t|k}$ on the basis of the observations $g_1, \ldots, g_k$. The estimation problem is considered from the Bayesian point of view. In Bayesian estimation, the state x_t and the observation g_t are random (vector) variables. The solution to the Bayesian estimation problem is actually the posterior density $\pi(x_t|g_i, i = 1, \ldots, k)$ of the state x_t conditioned on the observations

$g_i, i = 1, \ldots, k$, instead of a single estimate of the state x_t. The posterior density sums up the information about the state x_t after the measurements up to time k are performed.

The state estimation problem can be characterized as a prediction, a filtering, or a smoothing problem depending on the set of observations available for the computation of the state estimate at time t. If $k < t$, the state estimation problem is a prediction problem. When considering real time filtering problems, $k = t$. If real time estimation is not required, it is possible that $k > t$, and the state estimation problem is viewed as a smoothing problem. For real time feedback control systems, real time state estimation is essential, and in such a case the set of available observations at time t is $\{g_1, \ldots, g_t\}$.

A computationally feasible approach to solve the Bayesian estimation problem is to use recursive algorithms since the dimension of the problem increases linearly with time. When solving the Bayesian filtering problem, the posterior density $\pi(x_t|g_i, i = 1, \ldots, t)$ that gives the conditional probability of the state x_t conditioned on the observations g_i, $i = 1, \ldots, t$, is to be determined. In order to determine the posterior density, properties for the (state) process $\{x_t\}$, the (observation) process $\{g_t\}$, and the (noise) processes $\{w_{1,t}\}$ and $\{v_t\}$ are postulated.

The vector process $\{x_t\}$ is assumed to be a Markov process with an initial state $x_0 \sim \pi(x_0)$ and a transition kernel $\pi(x_{t+1}|x_t)$. The prior density $\pi(x_0)$ sums up the available information about the initial state x_0 prior to any measurements. The transition kernel $\pi(x_{t+1}|x_t)$ is a function specifying that the future state x_{t+1} is independent of the past states $x_0, \ldots, x_{t-1}$ conditionally to the present state x_t. Furthermore, the future state x_{t+1} depends on the past observations $g_1, \ldots, g_t$ through the present state x_t. The observation g_t is conditionally independent of the past states given the present state x_t. The likelihood function $\pi(g_t|x_t)$ describes the interrelation between the observation g_t and the state x_t. The noise processes $\{w_{1,t}\}$ and $\{v_t\}$ are sequentially uncorrelated. Furthermore, the noise vectors $w_{1,t}$ and v_s are mutually independent for all $t, s \in \mathbb{N}_0$.

Given the prior density $\pi(x_0)$, the transition kernel $\pi(x_{t+1}|x_t)$, $t = 0, 1, \ldots$, and the likelihood $\pi(g_t|x_t)$, $t = 0, 1, \ldots$, the posterior density can

be determined recursively following the steps

$$\begin{aligned}
&\pi\left(x_t|g_i, i=1,\ldots,t\right) \\
&\quad = \frac{\pi\left(g_t|x_t\right)\pi\left(x_t|g_i, i=1,\ldots,t-1\right)}{\pi\left(g_t|g_i, i=1,\ldots,t-1\right)} \qquad (2.31)\\
&\pi\left(x_t|g_i, i=1,\ldots,t-1\right) \\
&\quad = \int_{\mathbb{R}^{n_x}} \pi\left(x_{t-1}|g_i, i=1,\ldots,t-1\right)\pi\left(x_t|x_{t-1}\right)\mathrm{d}x_{t-1} \qquad (2.32)
\end{aligned}$$

where the normalizing constant

$$\begin{aligned}
&\pi\left(g_t|g_i, i=1,\ldots,t-1\right) \\
&\quad = \int_{\mathbb{R}^{n_x}} \pi\left(g_t|x_t\right)\pi\left(x_t|g_i, i=1,\ldots,t-1\right)\mathrm{d}x_t \qquad (2.33)
\end{aligned}$$

and the initial distribution is given by

$$\pi\left(x_0|g_0\right) = \frac{\pi\left(g_0|x_0\right)\pi\left(x_0\right)}{\int_{\mathbb{R}^{n_x}} \pi\left(g_0|x_0\right)\pi\left(x_0\right)\mathrm{d}x_0}. \qquad (2.34)$$

The equation (2.31) is the *measurement update* of the Bayesian recursion and (2.32) is the *time update* equation. In (2.31), $\pi\left(x_t|g_i, i=1,\ldots,t-1\right)$ is referred to as the prediction density.

The posterior density as such is difficult to visualize and analyse. However, once the posterior density is derived, different estimates can be computed to explore the density. Such estimates include point and interval (spread) estimates. The point estimates indicate the most probable value of the unknown state whereas the interval estimates yield an interval that contains the values of the unknown state with some specified probability given the observations and the prior information.

The point estimates that can be derived from the posterior density (2.31) include for example the conditional mean (CM) that is also known as the minimum mean square error estimate

$$x_{t|t}^{\mathrm{CM}} = E\left[x_t|g_i, i=1,\ldots,t\right] = \int_{\mathbb{R}^{n_x}} x_t \pi\left(x_t|g_i, i=1\ldots,t\right)\mathrm{d}x_t \qquad (2.35)$$

provided that the integral exists and the maximum a posteriori (MAP) estimate

$$x_{t|t}^{\mathrm{MAP}} = \arg\max_{x_t} \pi\left(x_t|g_i, i=1,\ldots,t\right) \qquad (2.36)$$

given the observations $g_1,\ldots,g_t$. The answer to the question which of the point estimates is the *optimal* state estimate $x_{t|t}$ depends on the definition

of the concept of optimality. A typical choice is to define that the optimal state estimate minimizes the mean square estimation error. In such a case, $x_{t|t} = x_{t|t}^{\mathrm{CM}}$. Perhaps the most widely used interval estimate is the conditional covariance defined as

$$\begin{aligned}&\operatorname{cov}(x_t|g_i, i = 1, \ldots, t)\\ &\quad = \int_{\mathbb{R}^{n_x}} (x_t - x_{t|t}^{\mathrm{CM}})(x_t - x_{t|t}^{\mathrm{CM}})^T \pi\left(x_t|g_i, i = 1, \ldots, t\right) \mathrm{d}x_t \quad (2.37)\end{aligned}$$

provided that the integral exists.

Computation of the estimates (2.35)-(2.37) is not always a trivial task. The MAP estimate (2.36) is obtained as a solution to the optimization problem that can be solved using, for example, iterative methods. In (2.35) and (2.37), the integration is typically over a high-dimensional space. Consequently, efficient alternative ways to perform the integration are needed. The sampling-based methods, such as the Markov Chain Monte Carlo (MCMC) methods, are applicable, although the computational load of such methods is large. As a general reference to the MCMC methods, see [74].

KALMAN FILTER

The well-known Kalman filter [75] is the solution to a special class of recursive Bayesian filtering problems. In these problems, both the state equation and the observation equation are linear, the state noise and the measurement noise are modelled as Gaussian white noise with known covariances, and the optimality criterion is defined as the minimum mean square criterion.

The basis of the Kalman filter is the state-space model with the linear state equation (2.1) and a linear observation equation

$$g_t = G_{1,t} x_t + v_t \quad (2.38)$$

where $G_{1,t} \in \mathbb{R}^{n_g \times n_x}$ is the observation matrix. In the state equation, the control input u_t and the process input s_t are taken to be known at respective times. The state noise $w_{1,t}$, the observation noise v_t, and the initial state x_0 are all modelled as Gaussian with known means and covariances. One may assume that they are zero mean vectors without loss of generality. It is assumed that the optimal state estimate $x_{t|t} = E\left[x_t|g_i, i = 1, \ldots, t\right]$ (the CM) and $\Gamma_{t|t} = \operatorname{cov}(x_t|g_i, i = 1, \ldots, t)$ (the conditional covariance). Furthermore, $x_{t|t-1}$ denotes the predicted state estimate and $\Gamma_{t|t-1}$ the covariance matrix of the predicted state.

In the case that the noises are modelled as additive and mutually independent of the state, the likelihood $\pi(g_t|x_t)$ and the transition kernel $\pi(x_t|x_{t-1})$ are Gaussian [5]. Furthermore, it can be shown that the prediction density $\pi\left(x_t|g_i, i=1,\ldots,t-1\right)$ corresponding to (2.32) is also a Gaussian density of $\mathcal{N}(x_{t|t-1}, \Gamma_{t|t-1})$ [5]. Given the prediction density $\pi\left(x_t|g_i, i=1,\ldots,t-1\right)$, the posterior density $\pi\left(x_t|g_i, i=1,\ldots,t\right)$ corresponding to (2.31) is determined on the basis of the observation g_t and the likelihood $\pi(g_t|x_t)$. That is, the posterior density

$$\begin{aligned}
&\pi\left(x_t|g_i, i=1,\ldots,t\right) \\
&\quad\propto \pi\left(g_t|x_t\right)\pi\left(x_t|g_i, i=1,\ldots,t-1\right) \\
&\quad\propto \exp\Big\{-\frac{1}{2}\Big(\left(g_t - G_{1,t}x_t\right)^T \Gamma_{v_t}^{-1}\left(g_t - G_{1,t}x_t\right)\Big) \\
&\qquad -\frac{1}{2}\Big(\Big(x_t - x_{t|t-1}\Big)^T \Gamma_{t|t-1}^{-1}\Big(x_t - x_{t|t-1}\Big)\Big)\Big\}
\end{aligned} \tag{2.39}$$

and it is also a Gaussian density of $\mathcal{N}(x_{t|t}, \Gamma_{t|t})$. Actually in the posterior density in (2.39), the state x_t is conditioned on all the measurements g_i, $i=1,\ldots,t$, *and* on all the control inputs u_j, $j=1,\ldots,t-1$, so that $\pi\left(x_t|g_i, i=1,\ldots,t, u_j, j=1\ldots,t-1\right)$. However in this thesis, the notation in (2.39) is used for the posterior density. As the posterior, prediction, and likelihood densities are Gaussian, the MAP estimate and the CM are identical, that is, $x_{t|t}^{\mathrm{CM}} = x_{t|t}^{\mathrm{MAP}}$.

As for all t the densities are Gaussian, one needs to update only the mean and the covariance. The optimal state estimate $x_{t|t}$, the predicted state estimate $x_{t|t-1}$, and the covariance matrices $\Gamma_{t|t}$ and $\Gamma_{t|t-1}$ can be obtained recursively using the Kalman filter equations that in this case are [71]

$$x_{t|t-1} = A_{t-1}x_{t-1|t-1} + B_{2,t-1}u_{t-1} + s_t \tag{2.40}$$

$$\Gamma_{t|t-1} = A_{t-1}\Gamma_{t-1|t-1}A_{t-1}^T + \Gamma_{w_t} \tag{2.41}$$

$$F_t = \Gamma_{t|t-1}G_{1,t}^T\left(G_{1,t}\Gamma_{t|t-1}G_{1,t}^T + \Gamma_{v_t}\right)^{-1} \tag{2.42}$$

$$x_{t|t} = x_{t|t-1} + F_t\left(g_t - G_{1,t}x_{t|t-1}\right) \tag{2.43}$$

$$\Gamma_{t|t} = \left(I - F_tG_{1,t}\right)\Gamma_{t|t-1} \tag{2.44}$$

where $F_t \in \mathbb{R}^{n_x \times n_g}$ is the Kalman gain. It should be noted that the computation of $x_{t|t}$ requires the control input u_{t-1} which is in turn computed based on the previous real time estimate $x_{t-1|t-1}$. In the control theory literature, the Kalman filter estimator is typically presented in an alternative

form in comparison with (2.40)-(2.44). The alternative formulation combines the prediction step (2.40) and the filtering step (2.43). Furthermore, the covariance matrices of the prediction and the estimate are obtained as a solution to a Riccati difference equation. The alternative formulation can be found, for example, in [63].

One of the main difficulties in many real life industrial applications is that the assumption on linearity does not hold, and nonlinear state estimation is required. In such a case, the optimal estimates can be obtained with sampling-based methods. Such methods are referred to as sequential Monte Carlo (SMC) methods, and are also known as particle filters [76], [73]. The particle filters can be formulated to prediction and smoothing problems as well as filtering problems. The computational complexity often limits the implementation of these methods in practice. Furthermore, there are recursive estimators that give a suboptimal solution to nonlinear state estimation problems. Three of such suboptimal estimators, the globally linearised Kalman filter, the extended Kalman filter, and the iterated extended Kalman filter, are reviewed in this section in the case of nonlinear observation equation. These estimators could be formulated for the case in which also the state equation is nonlinear.

GLOBALLY LINEARISED KALMAN FILTER

In the case of the state-space model (2.1)-(2.2), the basic idea of the globally linearised Kalman filter is that the nonlinear mapping G_t in (2.2) is linearised globally at a selected linearisation point $x_{\text{lp}} \in \mathbb{R}^{n_x}$ and approximated with the obtained linear mapping. Thus,

$$\begin{aligned} G_t(x_t) &\approx G_t(x_{\text{lp}}) + \mathcal{J}G_t(x_{\text{lp}})(x_t - x_{\text{lp}}) \\ &= \mathcal{J}G_t(x_{\text{lp}})x_t + \tilde{G}_t \end{aligned} \tag{2.45}$$

where the Jacobian matrix $\mathcal{J}G_t \in \mathbb{R}^{n_g \times n_x}$, $\mathcal{J}G_t = \mathcal{J}G_t(x_{\text{lp}})$, and the vector $\tilde{G}_t \in \mathbb{R}^{n_g}$, $\tilde{G}_t = G_t(x_{\text{lp}}) + \mathcal{J}G_t(x_{\text{lp}})x_{\text{lp}}$, can be computed once the vector x_{lp} is chosen. Furthermore, $\tilde{G}_t$ is independent of the state x_t but still dependent of the mapping G_t.

In the case of a nonlinear observation equation, the prediction and posterior densities are no longer Gaussian but they can be approximated with Gaussian densities. Let $\pi_G(x_t|g_i, i = 1, \ldots, t-1)$ and $\pi_G(x_t|g_i, i = 1, \ldots, t)$ denote the Gaussian approximations of the prediction density $\pi(x_t|g_i, i = 1, \ldots, t-1)$ and posterior density $\pi(x_t|g_i, i = 1, \ldots, t)$, respectively. The posterior density corresponding to

(2.31) is [5]

$$\begin{aligned}
&\pi\left(x_t|g_i, i=1,\ldots,t\right) \\
&\quad\propto \pi\left(g_t|x_t\right)\pi\left(x_t|g_i, i=1,\ldots,t-1\right) \\
&\quad\approx \pi\left(g_t|x_t\right)\pi_G\left(x_t|g_i, i=1,\ldots,t-1\right) \\
&\quad\propto \exp\Big\{-\frac{1}{2}\Big(g_t - G_t\left(x_t\right)\Big)^T\Gamma_{v_t}^{-1}\Big(g_t - G_t\left(x_t\right)\Big) \\
&\qquad -\frac{1}{2}\Big(\Big(x_t - x_{t|t-1}\Big)^T\Gamma_{t|t-1}^{-1}\Big(x_t - x_{t|t-1}\Big)\Big)\Big\}. \qquad (2.46)
\end{aligned}$$

The Gaussian approximation $\pi_G\left(x_t|g_i, i=1,\ldots,t\right)$ for the posterior density is obtained by using the linearisation (2.45) in (2.46) and it is a Gaussian density of $\mathcal{N}(x_{t|t}, \Gamma_{t|t})$.

As the state equation is linear, the computation of the predicted state $x_{t|t-1}$ and the covariance matrix $\Gamma_{t|t-1}$ is equivalent to the Kalman filter equations (2.40)-(2.41). The Kalman gain F_t, the optimal state estimate $x_{t|t}$, and the covariance matrix $\Gamma_{t|t}$ are obtained using the equations [5]

$$F_t = \Gamma_{t|t-1}\mathcal{J}G_t^T(x_{\mathrm{lp}})\Big(\mathcal{J}G_t(x_{\mathrm{lp}})\Gamma_{t|t-1}\mathcal{J}G_t^T(x_{\mathrm{lp}}) + \Gamma_{v_t}\Big)^{-1} \qquad (2.47)$$

$$x_{t|t} = x_{t|t-1} + F_t\Big(g_t - \Big(G_t(x_{\mathrm{lp}}) + \mathcal{J}G_t(x_{\mathrm{lp}})(x_{t|t-1} - x_{\mathrm{lp}})\Big)\Big) \qquad (2.48)$$

$$\Gamma_{t|t} = \Big(I - F_t\mathcal{J}G_t(x_{\mathrm{lp}})\Big)\Gamma_{t|t-1}. \qquad (2.49)$$

EXTENDED KALMAN FILTER

In the case of the state-space model (2.1)-(2.2), the basic idea of the extended Kalman filter is that instead of linearising the observation equation (2.2) globally as in the globally linearised Kalman filter, the observation equation is linearised at the predicted state $x_{t|t-1}$. Thus, the linearisation

$$G_t(x_t) \approx G_t(x_{t|t-1}) + \mathcal{J}G_t(x_{t|t-1})(x_t - x_{t|t-1}) \qquad (2.50)$$

is used when finding the Gaussian approximation of the posterior density $\pi\left(x_t|g_i, i=1,\ldots,t\right)$.

The equations for the Kalman gain F_t, the optimal state estimate $x_{t|t}$, and the covariance matrix $\Gamma_{t|t}$ are

$$\begin{aligned}
F_t &= \Gamma_{t|t-1}\mathcal{J}G_t^T(x_{t|t-1}) \\
&\quad \Big(\mathcal{J}G_t(x_{t|t-1})\Gamma_{t|t-1}\mathcal{J}G_t^T(x_{t|t-1}) + \Gamma_{v_t}\Big)^{-1} \qquad (2.51)\\
x_{t|t} &= x_{t|t-1} + F_t\big(g_t - G_t(x_{t|t-1})\big) \qquad (2.52)\\
\Gamma_{t|t} &= \Big(I - F_t\mathcal{J}G_t(x_{t|t-1})\Big)\Gamma_{t|t-1}. \qquad (2.53)
\end{aligned}$$

In conclusion, the extended Kalman filter equations consist of the time evolution update equations (2.40)-(2.41) and the observation update equations (2.51)-(2.53).

ITERATED EXTENDED KALMAN FILTER

In the case of the state-space model (2.1)-(2.2), the basic idea of the iterated extended Kalman filter is that an inner iteration loop is included into the observation update steps (2.51)-(2.53) of the extended Kalman filter.

When solving the iterated extended Kalman filter problem, the iterated extended Kalman filter estimate is obtained by minimising the quadratic functional in the exponent in the right-hand side of (2.46). An approximate numerical solution is sought. Thus,

$$\begin{aligned} x_{t|t} \quad \approx \quad & \operatorname*{sol\,min}_{x_t} \Big\{ \left(g_t - G_t\left(x_t\right)\right)^T \Gamma_{v_t}^{-1} \left(g_t - G_t\left(x_t\right)\right) \\ & + \left(x_t - x_{t|t-1}\right)^T \Gamma_{t|t-1}^{-1} \left(x_t - x_{t|t-1}\right) \Big\}. \end{aligned} \tag{2.54}$$

An approximate solution of the minimisation problem in (2.54) is obtained with the Gauss-Newton method [77]. Let $\mathcal{J}G_t^j$ denote the Jacobian $\mathcal{J}G_t(x_t^j)$. The sequence of iterates corresponding to each time $t \in \mathbb{N}_0$ yield by the Gauss-Newton method when minimising the quadratic functional (2.54) with the initial value $x_t^0 = x_{t|t-1}$ are of the form [71]

$$F_t^j = \Gamma_{t|t-1}(\mathcal{J}G_t^j)^T \left(\mathcal{J}G_t^j \Gamma_{t|t-1} (\mathcal{J}G_t^j)^T + \Gamma_{v_t}\right)^{-1} \tag{2.55}$$

$$x_t^{j+1} = x_{t|t-1} + F_t^j \left(g_t - \left(G_t(x_t^j) + \mathcal{J}G_t^j \left(x_{t|t-1} - x_t^j\right)\right)\right) \tag{2.56}$$

where $j \in \mathbb{N}_0$. The iteration is repeated until convergence. After the iteration, the estimate $x_{t|t}$ is set to x_t^j and the covariance matrix $\Gamma_{t|t}$ is computed using the state estimate $x_{t|t}$ with

$$\Gamma_{t|t} = \left(I - F_t \mathcal{J}G_t(x_{t|t})\right) \Gamma_{t|t-1}. \tag{2.57}$$

In conclusion, the iterated extended Kalman filter equations consist of the time evolution update equations (2.40)-(2.41), the iteration loop (2.55)-(2.56) and the equation for the update of the covariance matrix (2.57).

2.3 $\mathcal{H}_\infty$ CONTROL PROBLEM

The main reason behind the development of the $\mathcal{H}_\infty$ control theory was the need of a more robust optimal control method that takes into account

the uncertainty in the process modelling and in the external disturbances. The weak point of the LQG control is that the assumption of *Gaussian* state and measurement noises does not hold in many real life industrial applications. Especially, the state noise can be far from Gaussian. Furthermore, accurate modelling of the process dynamics is a challenging or even an impossible task, and there will be errors of unknown statistical nature between the model and the actual process. These errors can be compensated for by the $\mathcal{H}_\infty$ controller. However, the use of the $\mathcal{H}_\infty$ optimal controller does not automatically guarantee better results in comparison to the ones obtained using the LQG optimal controller. Especially, modelling state and measurement errors and also the discrepancies between the process model and the actual process and using these models when deriving the LQG controller will in many cases improve the performance of the LQG controller. As general references on the $\mathcal{H}_\infty$ theory, see [64], [78].

Similarly to the LQG controller, the synthesis of *the $\mathcal{H}_\infty$ measurement feedback controller* (or simply the $\mathcal{H}_\infty$ controller) can be divided into two stages. Firstly, the $\mathcal{H}_\infty$ control law is derived as if there is perfect information about the state and also about the external disturbances. Consequently, the obtained controller is referred to as the *full information controller*. Secondly, the optimal state estimator is designed. Contrary to the LQG control, the $\mathcal{H}_\infty$ state estimator depends on the full information controller and, thus, the certainty-equivalence property discussed in Section 2.2 does not hold for the H_∞ control problems. Finally, the $\mathcal{H}_\infty$ measurement feedback controller is obtained by combining the two stages. When utilizing the $\mathcal{H}_\infty$ controller, perfect information about the state and the external disturbances is not required. Instead, the state is estimated and the disturbances are taken as unknowns.

In this section, the linear state-space model that consists of the linear state equation and a linear observation equation

$$x_{t+1} = A_t x_t + B_{2,t} u_t + B_{1,t} w_t \tag{2.58}$$

$$g_t = C_{2,t} x_t + D_{21,t} w_t \tag{2.59}$$

is considered. In the state-space model (2.58)-(2.59), x_t, g_t, u_t, A_t and $B_{2,t}$ are defined in Section 2.1. Furthermore, $w_t \in \mathbb{R}^{(n_x+n_g)}$ is the exogenous disturbance input so that $w_t = [w_{1,t}^T \; v_t^T]^T$ and the noises $w_{1,t}$ and v_t are defined in Section 2.1. The matrices $B_{1,t} \in \mathbb{R}^{n_x \times (n_x+n_g)}$ and $D_{21,t} \in \mathbb{R}^{n_g \times (n_x+n_g)}$ are the state noise input matrix and the observation noise input matrix, respectively. The matrix $C_{2,t} \in \mathbb{R}^{n_g \times n_x}$ is known for all $t \in \mathbb{N}_0$. Furthermore, the objective vector corresponding to (2.9) is

$z_t \in \mathbb{R}^{n_x+n_u+(n_x+n_g)}$ so that

$$z_t = C_{1,t}x_t + D_{12,t}u_t + D_{11,t}w_t \tag{2.60}$$

where $C_{1,t} \in \mathbb{R}^{n_x+n_u+(n_x+n_g)\times n_x}$, $D_{12,t} \in \mathbb{R}^{n_x+n_u+(n_x+n_g)\times n_u}$, and $D_{11,t} \in \mathbb{R}^{n_x+n_u+(n_x+n_g)\times(n_x+n_g)}$. The state equation (2.58), the objective equation (2.60), and the observation equation (2.59) can be written in a matrix form

$$\begin{bmatrix} x_{t+1} \\ z_t \\ g_t \end{bmatrix} = \begin{bmatrix} A_t & B_{1,t} & B_{2,t} \\ C_{1,t} & D_{11,t} & D_{12,t} \\ C_{2,t} & D_{21,t} & D_{22,t} \end{bmatrix} \begin{bmatrix} x_t \\ w_t \\ u_t \end{bmatrix} \tag{2.61}$$

where $D_{22,t} \in \mathbb{R}^{n_g\times n_u}$ so that $D_{22,t}$ is a zero matrix and the initial state x_0 is a zero vector. The matrix form (2.61) is the basis when deriving the $\mathcal{H}_\infty$ controller.

The main idea in the $\mathcal{H}_\infty$ optimal control is to treat the worst-case scenario. To be more specific, the aim is to minimize some performance criterion in the presence of a worst-case external disturbance input. Consequently, performance of the system is acceptable in the presence of all possible external disturbance inputs. Below, $z = \{z_t\}$ in which $z_t \in \mathbb{R}^{n_x+n_u+(n_x+n_g)}$ and the ℓ_2-norm is defined as

$$\|z\|_{2,[0,N]} = \left(\sum_{t=0}^{N} z_t^T z_t\right)^{\frac{1}{2}}. \tag{2.62}$$

w and $\|w\|_{2,[0,N]}$ are defined accordingly. The performance criterion to be minimized is the cost function [64], [63]

$$J = \sup_{\|w\|_{2,[0,N]}\neq 0} \left\{ \frac{\|z\|_{2,[0,N]}}{\|w\|_{2,[0,N]}} \right\}. \tag{2.63}$$

Thus, the aim is to make the output z_t small relative to the size of the disturbance w_t for all $t \in [0, N]$. The direct minimization of the cost (2.63) is a difficult task. Therefore, it is typical to seek a *suboptimal* $\mathcal{H}_\infty$ controller. Assume that there exists $\gamma \in \mathbb{R}_+$ which satisfies

$$J = \sup_{\|w\|_{2,[0,N]}\neq 0} \left\{ \frac{\|z\|_{2,[0,N]}}{\|w\|_{2,[0,N]}} \right\} < \gamma. \tag{2.64}$$

In this case, γ is referred to as a performance bound. As the supremum satisfies the inequality (2.64), the inequality

$$\frac{\|z\|_{2,[0,N]}}{\|w\|_{2,[0,N]}} < \gamma \tag{2.65}$$

must hold for all $w \neq 0$. Furthermore as the strict inequality (2.65) holds, for some $\epsilon > 0$ and for all $w \neq 0$,

$$\frac{\|z\|^2_{2,[0,N]}}{\|w\|^2_{2,[0,N]}} \leq \gamma^2 - \epsilon. \tag{2.66}$$

Consequently, by rearranging the terms in (2.66) one can define a cost function J_γ, that is equivalent to (2.63), so that

$$J_\gamma = \|z\|^2_{2,[0,N]} - \gamma^2 \|w\|^2_{2,[0,N]} \leq -\epsilon \|w\|^2_{2,[0,N]} \tag{2.67}$$

for all $w \neq 0$ and for some $\epsilon > 0$.

When comparing (2.67) to the LQG cost function (2.11), one notices that the $\mathcal{H}_\infty$ cost function (2.67) has an extra term describing the effect of the (worst) external disturbance w. When minimizing the cost function J_γ, the external disturbance w_t is maximized. In summary, the solution to the suboptimal $\mathcal{H}_\infty$ control problem is a controller that achieves the bound (2.67).

The objective of the basic $\mathcal{H}_\infty$ controller is to drive the state to zero in the presence of external disturbances. The $\mathcal{H}_\infty$ controller is derived using dynamic programming respectively to the derivation of the LQG controller. However, the derivation of the $\mathcal{H}_\infty$ controller turns out to be more complicated and longer. The $\mathcal{H}_\infty$ controller is derived for example in [64]. Provided that $D^T_{12,t} D_{12,t} > 0$ and $D_{21,t} D^T_{21,t} > 0$ for all $t \in [0, N]$, the expressions for the state estimate $\hat{x}_{t+1}$ and the control input u_t are of the form

$$\hat{x}_{t+1} = \bar{A}_t \hat{x}_t + B_{2,t} u_t + L_{g,t}(g_t - \bar{G}_t \hat{x}_t) \tag{2.68}$$

$$V_{12,t} u_t = -(K_{u,t} - K_{uw,t} K_{w,t}) \hat{x}_t - L_{ug,t}(g_t - \bar{G}_t \hat{x}_t) \tag{2.69}$$

where

$$K_{u,t} = V_{12,t}(D^T_{12,t} D_{12,t} + B^T_{2,t} Z_t B_{2,t})^{-1}(D^T_{12,t} C_{1,t} + B^T_{2,t} Z_t A_t), \tag{2.70}$$

$$K_{uw,t} = V_{12,t}(D^T_{12,t} D_{12,t} + B^T_{2,t} Z_t B_{2,t})^{-1} (D^T_{12,t} D_{11,t} + B^T_{2,t} Z_t B_{1,t}), \tag{2.71}$$

$$\begin{aligned} K_{w,t} = {} & \big(D^T_{11,t} D_{11,t} + B^T_{1,t} Z_t B_{1,t} - \gamma^2 I - (D^T_{11,t} D_{12} + B^T_{1,t} Z_t B_{2,t}) \\ & (D^T_{12,t} D_{12,t} + B^T_{2,t} Z_t B_{2,t})^{-1}(D^T_{12,t} D_{11,t} + B^T_{2,t} Z_t B_{1,t})\big)^{-1} \\ & \big(D^T_{11,t} C_{1,t} + B^T_{1,t} Z_t A_t - (D^T_{11,t} D_{12,t} + B^T_{1,t} Z_t B_{2,t}) \\ & (D^T_{12,t} D_{12,t} + B^T_{2,t} Z_t B_{2,t})^{-1}(D^T_{12,t} C_{1,t} + B^T_{2,t} Z_t A_t)\big), \end{aligned} \tag{2.72}$$

and

$$
\begin{aligned}
L_{g,t} &= B_{1,t}V_{21,t}^{-1}(D_{21,t}V_{21,t}^{-1})^T \\
&\quad +\bar{A}_t X_t \bar{G}_t^T \left(D_{21,t}V_{21,t}^{-1}(D_{21,t}V_{21,t}^{-1})^T + \bar{G}_t X_t \bar{G}_t^T\right)^{-1}, \quad (2.73)\\
L_{ug,t} &= K_{uw,t}V_{21,t}^{-1}(D_{21,t}V_{21,t}^{-1})^T + (K_{u,t} - K_{uw,t}K_{w,t})X_t\bar{G}_t^T \\
&\quad \left(D_{21,t}V_{21,t}^{-1}(D_{21,t}V_{21,t}^{-1})^T + \bar{G}_t X_t \bar{G}_t^T\right)^{-1}, \quad (2.74)\\
V_{21,t}^T V_{21,t} &= -\gamma^{-2}\big(D_{11,t}^T D_{11,t} - \gamma^2 I + B_{1,t}^T Z_t B_{1,t} \\
&\quad -(D_{11,t}^T D_{12,t} + B_{1,t}^T Z_t B_{2,t})(D_{12,t}^T D_{12,t} + B_{2,t}^T Z_t B_{2,t})^{-1} \\
&\quad (D_{12,t}^T D_{11,t} + B_{2,t}^T Z_t B_{1,t})\big), \quad (2.75)\\
V_{12,t}^T V_{12,t} &= D_{12,t}^T D_{12,t} + B_{2,t}^T Z_t B_{2,t}, \quad (2.76)\\
\bar{A}_t &= A_t - B_{1,t}K_{w,t}, \quad (2.77)\\
\bar{G}_t &= C_{2,t} - D_{21,t}K_{w,t}. \quad (2.78)
\end{aligned}
$$

Given the non-negative and definite matrices Z_N and X_0, the matrices Z_t and X_t are obtained as a solution of the Riccati equations

$$
\begin{aligned}
Z_{t-1} &= A_t^T Z_t A_t + C_{1,t}^T C_{1,t} \\
&\quad - \begin{bmatrix} C_{1,t}^T D_{11,t} + A_t^T Z_t B_{1,t} & C_{1,t}^T D_{12,t} + A_t^T Z_t B_{2,t} \end{bmatrix} \\
&\quad \begin{bmatrix} D_{11,t}^T D_{11,t} + B_{1,t}^T Z_t B_{1,t} - \gamma^2 I & D_{11,t}^T D_{12,t} + B_{1,t}^T Z_t B_{2,t} \\ D_{12,t}^T D_{11,t} + B_{2,t}^T Z_t B_{1,t} & D_{12,t}^T D_{12,t} + B_{2,t}^T Z_t B_{2,t} \end{bmatrix}^{-1} \\
&\quad \begin{bmatrix} D_{11,t}^T C_{1,t} + B_{1,t}^T Z_t A_t \\ D_{12,t}^T C_{1,t} + B_{2,t}^T Z_t A_t \end{bmatrix}, \quad (2.79)\\
X_{t+1} &= \bar{A}_t X_t \bar{A}_t^T + B_{1,t}V_{21,t}^{-1}(B_{1,t}V_{21,t}^{-1})^T - \bar{D}_t \bar{S}_t \bar{D}_t^T \quad (2.80)
\end{aligned}
$$

where

$$
\begin{aligned}
\bar{D}_t &= \begin{bmatrix} B_{1,t}V_{21,t}^{-1}(K_{uw,t}V_{21,t}^{-1})^T & B_{1,t}V_{21,t}^{-1}(D_{21,t}V_{21,t}^{-1})^T \end{bmatrix} \\
&\quad +\bar{A}_t X_t \bar{C}_t^T, \quad (2.81)\\
\bar{S}_t &= \begin{bmatrix} K_{uw,t}V_{21,t}^{-1}(K_{uw,t}V_{21,t}^{-1})^T - \gamma^2 I & K_{uw,t}V_{21,t}^{-1}(D_{21,t}V_{21,t}^{-1})^T \\ D_{21,t}V_{21,t}^{-1}(K_{uw,t}V_{21,t}^{-1})^T & D_{21,t}V_{21,t}^{-1}(D_{21,t}V_{21,t}^{-1})^T \end{bmatrix} \\
&\quad +\bar{C}_t X_t \bar{C}_t^T, \quad (2.82)\\
\bar{C}_t &= \begin{bmatrix} K_{u,t} - K_{uw,t}K_{w,t} \\ \bar{G}_t \end{bmatrix}. \quad (2.83)
\end{aligned}
$$

It can be shown that the solution of the $\mathcal{H}_\infty$ measurement feedback control problem exists if and only if the Riccati equations (2.79) and (2.80) have solutions, and the condition

$$\rho(Z_t X_t) < \gamma^2 \tag{2.84}$$

is satisfied for all $t \in [0, N]$ where $\rho(\cdot)$ denotes the spectral radius. Unlike the LQG control where, provided that the standard assumptions hold, the Riccati equation always has a solution, the solutions of Riccati equations (2.79) and (2.80) do not exist if the performance bound γ is too low. The lowest value of γ for which the condition (2.84) is satisfied is searched by using numerical simulations where the controller is redesigned for decreasing values of γ.

If $N \to \infty$ and the system matrices A_t, $B_{2,t}$, $C_{1,t}$, and $C_{2,t}$ are stationary, then $Z_t \to Z$ and $X_t \to X$ where Z and X are the solutions of the algebraic Riccati equations corresponding to (2.79) and (2.80), respectively. In such a case, the coupling condition to be satisfied is $\rho(ZX) < \gamma^2$.

2.4 MODEL PREDICTIVE CONTROLLER

The idea in MPC is that the future process behaviour is predicted over a time interval and a sequence of future control inputs optimizing a given cost function related to the predicted performance are computed. The predictions are updated as new observations are obtained. By prediction of the process behaviour unwanted situations can be avoided in advance provided that there does not exist other unforeseen disturbances. The optimization problem to be solved at every time step is typically of the form of a linear programming (LP) problem or a quadratic programming (QP) problem depending on the nature of the process model and the cost function.

In the LP and the QP framework, input constraints, state constraints, and output constraints can be included directly in the problem formulation. The ability to systematically handle these constraints is one of the major advantages of MPC. There are several numerical methods for solving the LP and QP problems on-line including, for example, the active set method and the interior point methods. These methods are, unfortunately, computationally expensive for large-scale problems, and the computational load may prohibit the use on MPC in real time implementations with high-dimensional process models.

To illustrate MPC, an example of the formulation of a MPC problem is given. The formulation is based on [79]. The linear, stationary, and

discrete-time state equation and the linear, stationary, and discrete-time output equation

$$x_{t+1} = Ax_t + B_2u_t \tag{2.85}$$
$$y_t = Cx_t \tag{2.86}$$

are considered. See [79] for more information on MPC with stochastic linear models.

The finite horizon quadratic cost function can be written as

$$\begin{aligned} J &= x_{t+N}^T H x_{t+N} + (u_{t+N} - u_{t+N-1})^T S(u_{t+N} - u_{t+N-1}) \\ &\quad + \sum_{j=0}^{N-1} \left(x_{t+j}^T C^T Q C x_{t+j} + u_{t+j}^T R u_{t+j} + u_{\mathrm{d},t+j}^T S u_{\mathrm{d},t+j}\right) \end{aligned} \tag{2.87}$$

where $u_{\mathrm{d},t+j} = u_{t+j} - u_{t+j-1}$ is the change in the control input, the matrix $S \in \mathbb{R}^{n_u \times n_u}$ is a positive semidefinite matrix weighting the rate of change of the inputs, and the matrices H, Q, and R are defined in Section 2.2. Although the quadratic cost functions are popular in MPC, the performance index could also be expressed as a sum of the ∞- or 1-norm of the input and the state.

The input and output constraint can be formulated as

$$u_{\min} \leq u_{t+j} \leq u_{\max}, \qquad j = 0, 1, \ldots, N-1, \tag{2.88}$$
$$y_{\min} \leq y_{t+j} \leq y_{\max}, \qquad j = j_1, j_{1+1}, \ldots, j_2, \tag{2.89}$$
$$u_{\mathrm{d,max}} \leq u_{t+j} - u_{t+j-1} \leq u_{\mathrm{d,min}}, \qquad j = 0, 1, \ldots, N \tag{2.90}$$

where j_1 and j_2, $j_1 \geq 1$ and $j_2 \geq j_1$, are chosen constants, see [79]. The model predictive control problem at time t is to minimize the cost (2.87) with respect to a vector $u_t^N = [u_t, u_{t+1}, \ldots, u_{t+N-1}]^T$ subject to constraints (2.88)-(2.90). The vector u_t^N contains the N future control actions. Once the minimization problem is solved, the control input u_t is applied to the system and one starts again. The model predictive controller is an automatic, feedback, and model-based controller.

2.5 PROPORTIONAL-INTEGRAL-DERIVATIVE CONTROLLER

The PID controllers are widely used in industrial control systems because of their simplicity, robustness, and lack of need of complex process models. The PID controller consists of three terms operating on the output error signal. One or two of the three terms can be zero, so controllers such

as a proportional-integral (PI) controller and a proportional-derivative (PD) controller exist. The PID controllers are automatic and feedback controllers. The formulation of the PID controller in this thesis is based on [80]. It should be noted that the control input and the control output have now only temporal variations in contrast to the variables in DPSs.

The continuous-time control law for the proportional control, that is the P controller, is

$$u_{\mathrm{P}}(t) = K_{\mathrm{P}}\epsilon_{\mathrm{P}}(t) \tag{2.91}$$

where u_{P} is the control input, $K_{\mathrm{P}} \in \mathbb{R}$ is the controller gain, ϵ_{P} is the control error (or the tracking error), and $t \in \mathbb{R}$ denotes time. The control error is

$$\epsilon_{\mathrm{P}}(t) = r_{\mathrm{P}}(t) - y_{\mathrm{P}}(t) \tag{2.92}$$

where r_{P} is the reference input (or the set point) and y_{P} is the control output. Another formulation of the P controller includes a so-called set point weighting $\beta_{\mathrm{sp}} \in \mathbb{R}$ so that

$$u_{\mathrm{P,sp}}(t) = K_{\mathrm{P}}(\beta_{\mathrm{sp}} r_{\mathrm{P}}(t) - y_{\mathrm{P}}(t)). \tag{2.93}$$

In (2.93), the reference input can be weighted independently. The proportional control may lead to steady-state errors. The steady-state errors can be eliminated by adding a manually adjustable reset term $u_{\mathrm{P},0}$ to the control law. The controller is then

$$u_{\mathrm{P}_0}(t) = K_{\mathrm{P}}\epsilon_{\mathrm{P}}(t) + u_{\mathrm{P},0}(t). \tag{2.94}$$

The problem is how to find the reset term $u_{\mathrm{P},0}$ that cancels the steady-state errors in practice.

An automatic way to find $u_{\mathrm{P},0}$ is to use integral control. In the control law (2.94), the reset term is replaced with an integral term. By doing so a PI controller is obtained. The PI controller is of the form

$$u_{\mathrm{PI}}(t) = K_{\mathrm{P}}\left(\epsilon_{\mathrm{P}}(t) + \frac{1}{T_i}\int_0^t \epsilon_{\mathrm{P}}(\tilde{\tau})\mathrm{d}\tilde{\tau}\right) \tag{2.95}$$

where $T_i \in \mathbb{R}_+$ is the integral time.

In order to improve stability of the PI controller, a derivative term is included in the control law (2.95) yielding the PID controller

$$u_{\mathrm{PID}}(t) = K_{\mathrm{P}}\left(\epsilon_{\mathrm{P}}(t) + \frac{1}{T_i}\int_0^t \epsilon_{\mathrm{P}}(\tilde{\tau})\mathrm{d}\tilde{\tau} + T_d\frac{d\epsilon_{\mathrm{P}}(t)}{dt}\right) \tag{2.96}$$

where $T_d \in \mathbb{R}_+$ is the derivative time. The derivative term can be interpreted as linear extrapolation of the error T_d time units ahead.

When considering discrete-time control systems, a discrete-time approximation of the PID controller is needed. There are many ways to find the approximation and a method discussed in [80] is reviewed here. In the following, $t \in \mathbb{N}_0$ denotes the time, that is the sampling instances, and $h \in \mathbb{R}_+$ is the time between samples. For example, ϵ_t denotes the control error at time t and it is a scalar. The PID controller (2.96) can be approximated by

$$u_t = u_{\mathrm{P},t} + u_{\mathrm{I},t} + u_{\mathrm{D},t} \tag{2.97}$$

where the approximation of the proportional term, the approximation of the integral term, and the approximation of the derivative term are obtained from equations

$$u_{\mathrm{P},t} = K_{\mathrm{P}}(\beta_{\mathrm{sp}} r_t - y_t) \tag{2.98}$$

$$u_{\mathrm{I},t+1} = u_{I,t} + \frac{K_{\mathrm{P}} h}{T_i}\epsilon_t \tag{2.99}$$

$$u_{\mathrm{D},t} = \frac{T_d}{T_d + N_d h}\left(u_{\mathrm{D},t-1} - K_{\mathrm{P}} N_d (y_t - y_{t-1})\right), \tag{2.100}$$

respectively, where $N_d \in \mathbb{R}$. In the formulation, the derivative term is given by

$$\frac{T_d}{N_d}\frac{du_D}{dt} + u_D = -K_{\mathrm{P}} T_d \frac{dy}{dt}, \tag{2.101}$$

see [80] for details.

2.6 CONTROLLABILITY AND OBSERVABILITY

Before designing a controller, two important properties, controllability and observability, of the state-space system should be investigated in order to determine if it is even possible to control the system [63], [66], [81]. A rank test can be used for determining whether the system is controllable and/or observable [66], [81].

Consider a linear state-space model that consists of a linear state equation (without the state noise), a linear observation equation (without the observation noise), and an output equation so that

$$x_{t+1} = A_t x_t + B_{2,t} u_t \tag{2.102}$$

$$g_t = C_{2,t} x_t \tag{2.103}$$

$$y_t = C_t x_t. \tag{2.104}$$

The system (2.102)-(2.104) is said to be (completely) state controllable if there exists control inputs u_t, $t \in [0, N]$, that can transfer the system from any initial state x_0 to any other state x_N in a finite time N. The rank test states that the linear system (2.102)-(2.104) is state controllable if and only if the $n_x \times n_x$ matrix

$$M_{\mathrm{NS}} = \sum_{t=0}^{N} \Phi(N,t) B_{2,t} B_{2,t}^T \Phi(N,t)^T \tag{2.105}$$

is non-singular when the matrix $\Phi \in \mathbb{R}^{n_x \times n_x}$ is defined so that $\Phi(N,t) = A_{N-1}A_{N-2}\cdots A_t$ and $\Phi(0,0) = I$ where $I \in \mathbb{R}^{n_x \times n_x}$ is an identity matrix. The matrix M_{NS} is called the controllability matrix. If the matrices in the state-space model (2.102)-(2.104) are stationary so that $A_t = A$, $B_{2,t} = B_2$, $C_{2,t} = C_2$, and $C_t = C$ for all $t \in \mathbb{N}_0$, the system is state controllable if and only if the $n_x \times n_u n_x$ matrix

$$M_{\mathrm{S}} = \begin{bmatrix} B_2 & AB_2 & \cdots & A^{n_x-1}B_2 \end{bmatrix} \tag{2.106}$$

has rank n_x.

If the objective is to control the output y_t instead of the entire state x_t, the output controllability of the system (2.102)-(2.104) should be investigated. The system (2.102)-(2.104) is said to be (completely) output controllable if there exists control inputs u_t, $t \in [0, N]$, that can drive the system output y_0 to any other output y_N in a finite time N. The rank test states that the linear system (2.102)-(2.104) is output controllable if and only if the $n_y \times n_y$ matrix

$$M_{\mathrm{O,NS}} = \sum_{t=0}^{N} C_t \Phi(N,t) B_{2,t} B_{2,t}^T \Phi(N,t)^T C_t^T \tag{2.107}$$

is non-singular. If the matrices in the state-space model (2.102)-(2.104) are stationary, the system is output controllable if and only if the $n_y \times n_u n_x$ matrix

$$M_{\mathrm{O,S}} = \begin{bmatrix} CB_2 & CAB_2 & \cdots & CA^{n_x-1}B_2 \end{bmatrix} \tag{2.108}$$

has rank n_y.

The rank test states that the system is either controllable or uncontrollable. However in practice, some states/outputs can be very costly to control and thus, sometimes referred to as effectively uncontrollable. In general, the condition number of the controllability matrix can be considered as an indicator of controllability of the system. The smaller the condition number the better the controllability of the system is.

The system (2.102)-(2.104) is said to observable if and only if it is possible to determine the state x_0 from a finite time-history of the observations g_t and the control inputs u_t, $t \in [0, N]$. It can be shown that a linear system is observable if and only if the $n_x \times n_x$ matrix

$$O_{\mathrm{NS}} = \sum_{t=0}^{N} \Phi(t,0)^T C_{2,t}^T C_{2,t} \Phi(t,0) \tag{2.109}$$

is non-singular. The matrix O_{NS} is called the observability matrix. If the matrices in the state-space model (2.102)-(2.104) are stationary, the system is observable if and only if the $n_g n_x \times n_x$ matrix

$$O_{\mathrm{S}} = \begin{bmatrix} C_2 \\ C_2 A \\ \vdots \\ C_2 A^{n_x - 1} \end{bmatrix} \tag{2.110}$$

has rank n_x.

2.7 DISCUSSION

Only *discrete-time* state-space models are considered in this thesis. This choice is made because in most industrial applications the observations are obtained by sampling at discrete times. These observations are used for determining the optimal control inputs at the measurement times. Then, the control inputs are applied to the actuators and held fixed during the time between the measurements. Contrary to the observations, the state variable, that describes the evolution of an unknown quantity, is continuous in time. The situation of the continuous-time state and the discrete-time observations is handled by formally integrating the state over the time intervals between the measurements. As a consequence, a discrete-time state-space model is obtained and the discrete-time controller and the discrete-time state estimator are applied. Correspondingly, the optimal controllers and the state estimators can be derived using the continuous-time models. Optimal control methods in the case of continuous-time models are presented, for example, in [62], [66], [63]. State estimation methods, and especially the Kalman-Bucy filter, in the case of continuous-time models are presented in [82], [72].

When selecting a controller and a state estimator, the characteristics of the application of interest need to be considered. One common requirement in industrial applications is that the control systems are real time

and on-line. Consequently, only real time and on-line state estimators and controllers are feasible, and often also some additional simplifications have to be made. One example of such simplifications is to use the globally linearised Kalman filter instead of more complicated extended Kalman filters. Furthermore, for example the SMC methods are inapplicable since it is impossible to execute the required computations in real time with the current computational power. Also, off-line estimators such as the Kalman smoothers cannot be utilized since with such an estimator, for example, at time t one obtains the state estimate and, consequently, the control input for the *past* time $t - s$ where $s \in \mathbb{N}$. When considering the simplifications related to the control methods, the computations can be simplified for example by approximating the nonstationary matrices in the state-space model and the weighting matrices in the cost function with stationary matrices. In that case, the steady-state solution to the algebraic Riccati equation and the stationary optimal feedback gain matrix can be used, and the number of on-line computations is reduced significantly.

The state noise and the measurement noise were omitted from the state-space model when considering the controllability and the observability of the system in Section 2.6. One can include the noises in the model and consider then controllability and observability of the stochastic system. However, the extension of the deterministic controllability and observability concepts to stochastic systems is not straightforward and various definitions for stochastic controllability and stochastic observability exist. For more information on stochastic controllability, see [83], [84] and [85] (and the references therein). For more information on stochastic observability, see [83], [86].

When defining the concept of controllability of a system in Section 2.6, it was assumed that there are no constraints on the control input. This is not the case in many practical implementations in which, for example, the characteristics of the actuators define the set of admissible controls. If the controls are required to satisfy such constraints, the concept of constrained controllability should be investigated. An easily computable and widely used criterion for constrained controllability in the case of an arbitrary set of admissible controls has not been established. For more information on constrained controllability, see, for example, [87], [88] and the references therein.

The concept of observability was discussed in the context of linear state-space models in Section 2.6. A widely accepted definition of observability for nonlinear systems does not exist. Various methods for analysing the observability of a nonlinear discrete-time system have been

proposed, see for example [89], [90]. A simple approach to analyse the observability of a nonlinear system is to use the linearised observation model and analyse the observability of the linearised system instead.

Typically, the DPSs are not observable or controllable in the classical sense. It should be noted that the concepts of controllability and observability in this section are formulated for the finite-dimensional system. Universal corresponding definitions for controllability and observability of infinite-dimensional DPSs do not exist although the topic has been studied. See [91] for reference.

3 State-space modelling in electrical process tomography

In Chapter 2, the discrete-time state-space model for a multiple-input and multiple-output (MIMO) system was considered and used as a basis for model-based controllers and state estimators. In this chapter, the state-space model is derived for a convection-diffusion (CD) process that is monitored with electrical impedance tomography (EIT) and controlled using injectors as actuators. In Chapter 4, the state estimation and optimal control methods presented in Chapter 2 are modified to be used in the example application discussed in this thesis.

This chapter is divided into three sections. In Section 3.1, the finite-dimensional, discrete-time state equation modelling the CD process is derived. In Section 3.2, the finite-dimensional, discrete-time EIT observation equation is considered. This chapter is concluded with a discussion in Section 3.3.

3.1 STOCHASTIC CONVECTION-DIFFUSION MODEL

In the example application of this thesis, concentration of a chemical substance in a fluid flowing in a domain of interest is considered. The domain can be, for example, a pipeline, a process vessel, or a mixing tank. In this section, the objective is to write a model for a situation in which the concentration distribution is controlled at a particular subdomain of the domain by adding extra concentrate into the main fluid flow.

In a wide range of industrial processes, the fluid flow is turbulent and consists of more than one component or phase. However, a model for a laminar flow of an incompressible single-phase fluid is considered in this thesis. In such a case, the evolution of the concentration can be modelled with the CD equation with an additional source term describing the control action affecting the concentration evolution. Furthermore in process industry, nonstationary velocity fields of fluids are encountered. In this thesis, the possible nonstationary velocity field is approximated with a stationary velocity field. The uncertainties and inaccuracies in the model (for example due to the inaccurate velocity field) are approximated with stochastic terms. The finite-dimensional approximation of the CD

model is derived using the Galerkin finite element method (FEM).

In Section 3.1.1, the CD equation with an additional control source term is considered. The boundary conditions suitable for the example application of this thesis are specified in Section 3.1.2. The control action needed to achieve the control objective is modelled in Section 3.1.3. In Section 3.1.4, the Navier-Stokes equations modelling the velocity field of the fluid are reviewed briefly. In Section 3.1.5 and Appendix A, the finite element (FE) approximation of the CD model is derived.

3.1.1 Convection-diffusion equation

Let $\Omega \subset \mathbb{R}^n$, $n = 2,3$, be a bounded domain with a boundary $\Lambda = \partial\Omega$. The function $c : \Omega \times \mathbb{R}_+ \to \mathbb{R}$, $c = c(\vec{r}, t)$, describes the unknown nonstationary concentration in Ω where $\vec{r} \in \Omega$ is the spatial coordinate vector and $t \in \mathbb{R}_+$ denotes the time. The evolution of the concentration is modelled with the CD equation that is a parabolic partial differential equation (PDE) so that

$$\frac{\partial c}{\partial t} = \nabla \cdot \kappa \nabla c - \vec{v} \cdot \nabla c + q \tag{3.1}$$

where $q : \Omega \times \mathbb{R}_+ \to \mathbb{R}$, $q = q(\vec{r}, t)$, denotes the source term due to the control action. In this thesis, $\vec{v} : \Omega \to \mathbb{R}^n$, $\vec{v} = \vec{v}(\vec{r})$, is the stationary velocity field of the fluid and the diffusion coefficient $\kappa \in \mathbb{R}$ is a constant scalar. As only laminar flow of an incompressible fluid is considered in the modelling, the velocity field $\vec{v}$ is obtained as a solution of the Navier-Stokes equations described in Section 3.1.4.

3.1.2 Boundary conditions

The domain of interest in this thesis is a segment of a pipeline along which the fluid is flowing. The boundary of the domain is the union $\Lambda = \Lambda_{\text{in}} \cup \Lambda_{\text{out}} \cup \Lambda_{\text{wall}}$. The input boundary Λ_{in} refers to the cutting surface through which the flow enters the pipe and the output boundary Λ_{out} to the cutting surface through which the flow exits the pipe. Furthermore, Λ_{wall} denotes the pipe walls.

The following initial and boundary conditions are postulated for the CD equation

$$c(\vec{r}, 0) = c_0(\vec{r}), \quad \vec{r} \in \Omega \tag{3.2}$$

$$c(\vec{r}, t) = c_{\text{in}}(\vec{r}, t), \quad \vec{r} \in \Lambda_{\text{in}} \tag{3.3}$$

$$\frac{\partial c}{\partial \vec{n}}(\vec{r}, t) = 0, \quad \vec{r} \in \Lambda_{\text{wall}} \cup \Lambda_{\text{out}}, \tag{3.4}$$

where the function $c_0 : \Omega \to \mathbb{R}$ is the initial concentration, the function $c_{\text{in}} : \Lambda_{\text{in}} \times \mathbb{R}_+ \to \mathbb{R}$ is the nonstationary concentration on the input boundary Λ_{in}, and $\vec{n}$ is the outward unit normal. It should be noted that the condition (3.4) is also postulated for the output boundary Λ_{out}. For justification of such an approximate boundary condition, see [92].

Although the boundary condition for Λ_{in} is written as a Dirichlet condition, the input concentration is actually unknown and the input function c_{in} is considered as a stochastic function so that

$$c_{\text{in}}(\vec{r}, t) = \bar{c}_{\text{in}}(\vec{r}, t) + \eta(\vec{r}, t), \quad \vec{r} \in \Lambda_{\text{in}} \tag{3.5}$$

where the function $\bar{c}_{\text{in}} : \Lambda_{\text{in}} \times \mathbb{R}_+ \to \mathbb{R}$ is the deterministic part of the input, usually the spatial/temporal average of c_{in} or its estimate. If the variations of the concentration are small, c_{in} is a constant function. Furthermore, $\eta : \Lambda_{\text{in}} \times \mathbb{R}_+ \to \mathbb{R}$ is a function whose statistics should approximate the actual fluctuations of the input. It is assumed that η is a smooth function with respect to $\vec{r}$, and is, therefore, continuous and differentiable. The initial concentration c_0 is also unknown. This, however, is not a problem, since the effect of the initial concentration fades away quickly with time.

3.1.3 Control action

The objective in the example application in this thesis is to control the concentration distribution over a particular subdomain of the pipeline. To be more specific, the concentration distribution is to be regulated on the subdomain denoted by Λ_{out}. The control action taken to achieve this objective is to inject substance of high concentration into the flow through injectors. The amount of injected concentrate is controlled by adjusting the flow rates of the injectors. The injectors are located either on the pipe boundary or inside the pipe upstream of the subdomain of interest. The injected concentrate increases the concentration level near the injection point. The higher the flow rates are, the more the concentration level is increased.

The concentration on the boundary Λ_{out} is defined as $c_{\text{out}} : \Lambda_{\text{out}} \times \mathbb{R}_+ \to \mathbb{R}$,

$$c_{\text{out}}(\vec{r}, t) = c(\vec{r}, t), \quad \vec{r} \in \Lambda_{\text{out}}. \tag{3.6}$$

When modelling the injections, n_u denotes the number of injectors and it is assumed that the output of the injector j is distributed in a small

subdomain $\Omega_{\text{inj}}^{(j)} \subset \Omega$, $j = 1, \ldots, n_u$. In this thesis, the function q describes the effect of the added substance on the concentration so that for $j = 1, \ldots, n_u$

$$q(\vec{r}, t) = \begin{cases} |\Omega_{\text{inj}}^{(j)}|^{-1} u^{(j)}(t), & \vec{r} \in \Omega_{\text{inj}}^{(j)} \\ 0, & \vec{r} \notin \Omega_{\text{inj}}^{(j)} \end{cases} \tag{3.7}$$

where $|\Omega_{\text{inj}}^{(j)}|$ denotes the volume (or surface area) of $\Omega_{\text{inj}}^{(j)}$ and $u^{(j)}(t)$ is the flow rate of the j^{th}injector (mol s^{-1}).

3.1.4 Navier-Stokes equations and Reynolds number

When modelling the evolution of the concentration with the CD equation (3.1), a model for the velocity field $\vec{v}$ of the fluid is required. The motion of the fluid in this thesis is described with the Navier-Stokes equations under an incompressible flow assumption for Newtonian fluids. If the viscosity μ and the density ρ of the fluid are constant, the nonstationary Navier-Stokes equations can be written in the form [93]

$$\rho \frac{\partial \vec{v}}{\partial t} - \mu \Delta \vec{v} + \rho \vec{v} \cdot \nabla \vec{v} + \nabla p = \rho \vec{f} \tag{3.8}$$

$$\nabla \cdot \vec{v} = 0 \tag{3.9}$$

where $p : \Omega \times \mathbb{R}_+ \to \mathbb{R}$, $p = p(\vec{r}, t)$, is the pressure and $\vec{f} : \Omega \times \mathbb{R}_+ \to \mathbb{R}$, $\vec{f} = \vec{f}(\vec{r}, t)$, describes the external forces acting on the system such as gravity.

In some industrial processes, the velocity field is nearly stationary and can be approximated with a stationary velocity field. In such a case, $\vec{v}(\vec{r}, t) = \vec{v}(\vec{r})$ for all $t \in \mathbb{R}_+$. If for example, a homogeneous fluid is moving in a straight pipe under the influence of a constant pressure gradient, and that the average flow rate is relatively low, the velocity field is the solution of the stationary incompressible Navier-Stokes equations

$$-\mu \Delta \vec{v} + \rho \vec{v} \cdot \nabla \vec{v} + \nabla p = \rho \vec{f} \tag{3.10}$$

$$\nabla \cdot \vec{v} = 0 \tag{3.11}$$

where $p = p(\vec{r})$ and $\vec{f} = \vec{f}(\vec{r})$.

Suitable boundary conditions for (nonstationary) pipe flow applica-

tions are, for example,

$$\vec{v}(\vec{r},t) = 0, \quad \vec{r} \in \Lambda_{\text{wall}} \tag{3.12}$$

$$\vec{v}(\vec{r},t) = \vec{v}_{\text{in}}(\vec{r}), \quad \vec{r} \in \Lambda_{\text{in}} \tag{3.13}$$

$$\left(\mu(\nabla\vec{v}(\vec{r},t) + \nabla\vec{v}(\vec{r},t)^T) - p(\vec{r},t)I\right)\vec{n} = 0, \quad \vec{r} \in \Lambda_{\text{out}} \tag{3.14}$$

where $\vec{v}_{\text{in}} : \Lambda_{\text{in}} \to \mathbb{R}^n$, $\vec{v}_{\text{in}} = \vec{v}_{\text{in}}(\vec{r})$, is the velocity on the boundary Λ_{in} and I is an identity matrix. The non-slip boundary condition (3.12) is postulated on the liquid-solid interfaces. The inflow boundary condition (3.13) states that the velocity is known on the boundary Λ_{in}. The outflow boundary condition (3.14) is used on the boundary Λ_{out}.

From the dimensionless form of the incompressible Navier-Stokes equations, one can obtain the dimensionless Reynolds number. The motion of fluid is determined by two elementary properties that are viscosity and inertia. The dimensionless Reynolds number is a measure of the relative magnitude of inertial forces to viscous forces. The Reynolds number is defined as [93]

$$Re = \frac{v_{\text{mean}}\mathcal{L}}{\nu} \tag{3.15}$$

where v_{mean} is the mean fluid velocity, ν is the kinematic fluid viscosity, and $\mathcal{L}$ is the characteristic length of the flow region. For the pipe flow, $\mathcal{L}$ is the pipe diameter if the pipe is circular. The Reynolds number can be used to characterize flow regimes. Flows with low Reynolds numbers tend to be laminar while flows with high Reynolds numbers are turbulent. The magnitudes of "low" and "high" depend on the flow geometry. Values reported for the critical point above which the flow is turbulent vary widely, see [94] and references therein. In [94], it is stated that a close estimate for the critical point is $Re \approx 2040$.

3.1.5 Numerical approximation of the CD model

By the definition of Hadamard, a problem described by a PDE is said to be *well-posed* if

(i) a solution exists,

(ii) the solution is unique

(iii) the solution depends continuously on the data, that is, on the initial and boundary conditions.

A solution that satisfies (i)-(iii) and is sufficiently smooth (k-times continuously differentiable) is referred to as the *classical* solution of a PDE. The amount of smoothness required (the specification of k) depends on the PDE to be solved. A solution that satisfies (i)-(iii) but does not necessarily meet the smoothness requirements is called the *weak* solution of a PDE. In this section, only the weak solution of the parabolic PDE (3.1) with the initial and boundary conditions (3.2)–(3.5) is considered and a finite-dimensional approximation of the weak solution is sought using the Galerkin FEM. The existence, uniqueness, or regularity of the solution is not considered. The FE approximation of the CD equation without the additional source term was derived in [95]. A similar approach is adopted in this thesis. For more details on the FEM in general, see [96], [97]. For details on the existence and uniqueness analysis, and on the error analysis of the FEM, see [98].

Firstly, the weak solution of the PDE (3.1) with the initial and boundary conditions (3.2)–(3.5) is considered. Let $\vartheta \in H^1(\Omega)$ denote a so-called test function where $H^1(\Omega) = W^{1,2}(\Omega)$ is a Sobolev space of the first order. The weak solution of the PDE (3.1) is the solution that satisfies the weak (or variational) formulation of the original problem for all ϑ. The weak form is obtained by multiplying the PDE by the test function ϑ and integrating over the domain Ω. Thus, for all t

$$\begin{aligned}\int_\Omega \frac{\partial c(\vec{r},t)}{\partial t}\vartheta(\vec{r})\,\mathrm{d}\vec{r} &= -\int_\Omega \vec{v}(\vec{r})\cdot\nabla c(\vec{r},t)\,\vartheta(\vec{r})\,\mathrm{d}\vec{r} + \int_\Omega \kappa\Delta c(\vec{r},t)\,\vartheta(\vec{r})\,\mathrm{d}\vec{r} \\ &\quad + \int_\Omega q(\vec{r},t)\,\vartheta(\vec{r})\,\mathrm{d}\vec{r}. \end{aligned} \tag{3.16}$$

Applying the Green's formula and the Neumann boundary condition (3.4) to the second term on the right of (3.16) leads to

$$\begin{aligned}\int_\Omega \kappa\Delta c(\vec{r},t)\,\vartheta(\vec{r})\,\mathrm{d}\vec{r} &= -\int_\Omega \kappa\nabla c(\vec{r},t)\cdot\nabla\vartheta(\vec{r})\,\mathrm{d}\vec{r} + \int_{\partial\Omega}\kappa\frac{\partial c(\vec{r},t)}{\partial\vec{n}}\vartheta(\vec{r})\,\mathrm{d}S \\ &= -\int_\Omega \kappa\nabla c(\vec{r},t)\cdot\nabla\vartheta(\vec{r})\,\mathrm{d}\vec{r} \\ &\quad + \int_{\Lambda_{\text{in}}}\kappa\frac{\partial c(\vec{r},t)}{\partial\vec{n}}\vartheta(\vec{r})\,\mathrm{d}S. \end{aligned} \tag{3.17}$$

Substituting (3.17) into the weak form (3.16) yields

$$\begin{aligned}&\int_\Omega \frac{\partial c(\vec{r},t)}{\partial t}\vartheta(\vec{r})\,\mathrm{d}\vec{r} + \int_\Omega \vec{v}(\vec{r})\cdot\nabla c(\vec{r},t)\,\vartheta(\vec{r})\,\mathrm{d}\vec{r} + \int_\Omega \kappa\nabla c(\vec{r},t)\cdot\nabla\vartheta(\vec{r})\,\mathrm{d}\vec{r} \\ &\quad - \int_\Omega q(\vec{r},t)\vartheta(\vec{r})\,\mathrm{d}\vec{r} - \int_{\Lambda_{\text{in}}}\kappa\frac{\partial c(\vec{r},t)}{\partial\vec{n}}\vartheta(\vec{r})\,\mathrm{d}S = 0. \end{aligned} \tag{3.18}$$

Now, c is the weak solution of the CD model (3.1)–(3.5) if and only if (3.18) holds for all test functions ϑ. Thus, (3.18) is the starting point for the FE approximation.

The basic idea of the Galerkin FEM is to approximate the weak solution of the CD model (3.1)-(3.5) with a finite-dimensional solution. The approximate solution c^h is defined so that

$$c(\vec{r},t) \quad \approx \quad c^h(\vec{r},t) = \sum_{j=1}^{n_\varphi} c_j(t)\varphi_j(\vec{r}) \tag{3.19}$$

where φ_j, $j = 1,\ldots,n_\varphi$, are the basis functions of a finite-dimensional subspace H^h of $H^1(\Omega)$, n_φ is the number of the basis functions, and c_j are to be determined. An important question is how to choose the subspace H^h and the basis functions φ_j. Typically, H^h is chosen as a subspace of compactly supported piecewise polynomial functions of order d where $d \in \mathbb{N}$. This choice makes the FEM computationally feasible in comparison to many other techniques when seeking the approximation c^h. Furthermore, the order d is kept low, that is, 1st or 2nd order polynomial functions are used provided that adequate precision is achieved. In this thesis, H^h is a subspace of piecewise linear functions and φ_j are the (piecewise linear) basis functions of H^h.

To construct the basis functions, the domain Ω is divided into small subdomains that are referred to as elements in this thesis. The obtained FE mesh is a collection of vertices (nodes), edges between the vertices, and faces. In two dimensions, the elements can be, for example, triangles or convex quadrilaterals and in three dimensions, tetrahedra, cuboids or wedges. In this thesis, triangular elements are used in two dimensions and tetrahedral elements in three dimensions. It is defined that the basis function $\varphi_j(\vec{r}) = 1$ at the j^{th} node in the FE mesh and $\varphi_j(\vec{r}) = 0$ at other nodes. As a consequence, the total number of nodes in the FE mesh equals the number n_φ of the basis functions. Furthermore, $c_j(t)$, $j = 1,\ldots,n_\varphi$, in (3.19) is the approximated value of concentration at the j^{th} node at time t.

Also, a finite-dimensional approximation is needed for the source term q. The finite-dimensional approximation q^h for the source term q is

$$q(\vec{r},t) \quad \approx \quad q^h(\vec{r},t) = \sum_{j=1}^{n_\varphi} q_j(t)\varphi_j(\vec{r}) \tag{3.20}$$

where q_j, $j = 1,\ldots,n_\varphi$, are defined as follows. In this thesis, if a pointwise injector k, $k = 1,\ldots,n_u$, is located at the j^{th} node, the injected concentrate

is distributed to a subdomain $\Omega^{(k)}_{\text{inj,h}}$ formed by the elements connected to that node where $\Omega^{(k)}_{\text{inj,h}}$ is an approximation for the subdomain $\Omega^{(k)}_{\text{inj}}$ in (3.7). The concentration due to the injected concentrate at the j^{th} node is

$$q_j(t) = \begin{cases} |\Omega^{(k)}_{\text{inj,h}}|^{-1} u^{(k)}(t), & \text{the injector } k \text{ is in the } j^{\text{th}} \text{ node} \\ 0, & \text{the injector } k \text{ is not in the } j^{\text{th}} \text{ node} \end{cases} \tag{3.21}$$

where $u^{(k)}(t)$ denotes the flow rate of k^{th} injector at time t.

The next task in the FEM is to determine c_j, $j = 1, \ldots, n_\varphi$. In the following, $c(t) = \left[c_1(t), \ldots, c_{n_\varphi}(t)\right]^T \in \mathbb{R}^{n_\varphi}$ and $q(t) = \left[q_1(t), \ldots, q_{n_\varphi}(t)\right]^T \in \mathbb{R}^{n_\varphi}$ denote the vectors of c_j and q_j, respectively. Furthermore, the vector $c'(t) = \left[c'_1(t), \ldots, c'_{n_\varphi}(t)\right]^T \in \mathbb{R}^{n_\varphi}$ consists of the time derivatives of c_j. In the Galerkin FEM, the basis functions are used as test functions. Substituting the approximations (3.19) and (3.20) into the weak form (3.18) and reformulating the obtained equations into a matrix form yields

$$\bar{M}\left(c'(t) - q(t)\right) + \bar{K}c(t) = 0 \tag{3.22}$$

where the matrices $\bar{M} \in \mathbb{R}^{n_\varphi \times n_\varphi}$ and $\bar{K} \in \mathbb{R}^{n_\varphi \times n_\varphi}$ are defined as

$$\bar{M}(i,j) = \int_\Omega \varphi_j(\vec{r})\varphi_i(\vec{r})\,\mathrm{d}\vec{r} \tag{3.23}$$

$$\begin{aligned} \bar{K}(i,j) = {} & \int_\Omega \vec{v}(\vec{r}) \cdot \nabla\varphi_j(\vec{r})\,\varphi_i(\vec{r})\,\mathrm{d}\vec{r} + \int_\Omega \kappa \nabla\varphi_j(\vec{r}) \cdot \nabla\varphi_i(\vec{r})\,\mathrm{d}\vec{r} \\ & - \int_{\Lambda_{\text{in}}} \kappa \frac{\partial\varphi_j(\vec{r})}{\partial\vec{n}}\varphi_i(\vec{r})\,\mathrm{d}S. \end{aligned} \tag{3.24}$$

The nonhomogeneous Dirichlet boundary condition (3.3) specifies the concentration on the input boundary Λ_{in}, and it is implemented in the FE approximation. The obtained system of ordinary differential equations (ODEs) is

$$c'_{\text{o}}(t) = -M^{-1}Kc_{\text{o}}(t) + q_{\text{o}}(t) - M^{-1}\tilde{M}c'_{\text{in}}(t) - M^{-1}\tilde{K}c_{\text{in}}(t) \tag{3.25}$$

where c_{in} denotes the concentration on the input boundary nodes whereas c_{o} refers to the concentration corresponding to the nodes that are not on the input boundary Λ_{in}. Similarly, q_{o} denotes the effect of the control action on non-input nodes. The definition of the matrices in (3.25) and other details on the FE approximation are shown in Appendix A.

The system of ODEs (3.25) is solved numerically with respect to time. As (3.25) is known to be stiff, the multistep backward Euler method is

employed. The FE approximation of the CD model is of the form

$$c_{\mathrm{o},t+1} = \tilde{A}c_{\mathrm{o},t} + \tilde{Z}c_{\mathrm{in},t} + \tilde{T}c_{\mathrm{in},t+1} + \frac{1}{n_\tau}\tilde{G}\Theta u_t \tag{3.26}$$

where $t \in \mathbb{N}_0$ denotes now the discrete time index and $c_{\mathrm{o},0}$ is obtained from the initial condition (3.2). The vectors $c_{\mathrm{in},t}$ and $c_{\mathrm{in},t+1}$ are specified by the Dirichlet boundary condition (3.3). Furthermore, the control input vector u_t can be computed when $c_{\mathrm{o},t}$ is known. Thus, when computing $c_{\mathrm{o},t+1}$, the vector u_t is known. The matrices in (3.26) are defined in Appendix A.

As the input concentration in (3.5) is partly unknown, a stochastic term describing the uncertainty in $c_{\mathrm{in},t}$ and $c_{\mathrm{in},t+1}$ has to be incorporated into the model. The details are shown in Appendix A. The finite-dimensional, discrete-time evolution model for the concentration in the final form is

$$c_{t+1} = Ac_t + B_2u_t + s_{t+1} + w_{1,t} \tag{3.27}$$

where $c_t \in \mathbb{R}^{n_\varphi}$ is the discretised concentration at time t. Assuming that the velocity field $\vec{v}$ and the diffusion coefficient κ do not vary over time, the state transition matrix $A \in \mathbb{R}^{n_\varphi \times n_\varphi}$ is stationary. The vector $u_t \in \mathbb{R}^{n_u}$ denotes the flow rates of injectors (mol s^{-1}) over the time interval $[t, t+1]$, and the stationary control input matrix $B_2 \in \mathbb{R}^{n_\varphi \times n_u}$ determines how the control affects the state. The vector $s_{t+1} \in \mathbb{R}^{n_\varphi}$ is due to (formal) integration of the deterministic input $\bar{c}_{\mathrm{in}}$ in (3.5) over the time interval $[t, t+1]$. The zero-mean Gaussian state noise $w_{1,t} \in \mathbb{R}^{n_\varphi}$ consists of two parts. The first part is due to the stochastic input term η of the unknown boundary data in equation (3.5). The second part is white noise that approximates the inaccuracies in the CD model. The derivation of the covariance matrix $\Gamma_{w_{1,t}} \in \mathbb{R}^{n_\varphi \times n_\varphi}$ of the state noise $w_{1,t}$ is shown in detail in [95]. As the evolution errors are correlated, $\Gamma_{w_{1,t}}$ is not a diagonal matrix. Furthermore, since the input concentration c_{in} is the main source of uncertainty in the evolution model, the variance of the evolution errors is highest on the input boundary Λ_{in}.

The finite-dimensional approximation of the output concentration (3.6) is

$$y_t = Cc_t \tag{3.28}$$

where $y_t \in \mathbb{R}^{n_y}$ and the output matrix $C \in \mathbb{R}^{n_y \times n_\varphi}$ can be considered as a restriction matrix from $\Omega \to \Lambda_{\mathrm{out}}$. In other words, y_t is the concentration at the nodes on the boundary Λ_{out}.

3.2 EIT OBSERVATION MODEL

Electrical impedance tomography is a suitable modality for monitoring targets that possess spatial and/or temporal variations in conductivity. The basic idea in EIT is to inject electric currents into the object through electrodes that are typically attached to the object boundary and to measure the potential differences between chosen pairs of electrodes. The objective is then to reconstruct the three-dimensional electrical conductivity distribution in the object on the basis of the measured voltages.

The reconstruction problem of EIT belongs to a class of ill-posed inverse problems (see the definition of a well-posed problem in Section 3.1.5). The *forward problem* of EIT is to find a forward model for the computation of the electric potential and the voltages given the contact impedances, the injected currents and the conductivity distribution. The *inverse problem* of EIT is to reconstruct the conductivity distribution on the basis of a set of voltage measurements, the injected currents and the forward model.

In 1980, A.P. Calderon formulated mathematically the problem of determining the conductivity distribution in a domain on the basis of the boundary measurements [99]. The problem corresponds to the EIT reconstruction problem with certain assumptions. The problem has been widely studied after that. In [100], the uniqueness of the solution to the Calderon's problem was proved in $\mathbb{R}^2$ for L^∞ conductivity.

In Section 3.2.1, the complete electrode model (CEM) that is used as a forward model in EIT is reviewed and in Section 3.2.2, the FE approximation of the CEM is discussed. In Section 3.2.3, the obtained EIT observation equation is linearised for computational reasons and the nonstationary observation model is formulated in Section 3.2.4. Furthermore, data acquisition in EIT is discussed in Section 3.2.5 and a short introduction to the EIT inverse problem is given in Section 3.2.6.

3.2.1 Complete electrode model

Let $\Omega \subset \mathbb{R}^n$, $n = 2, 3$, be a bounded domain with n_e contact electrodes e_ℓ attached to its boundary $\partial\Omega$ so that $e_\ell \subset \partial\Omega$, $\ell = 1, \ldots, n_e$. The electrodes are assumed to be strictly disjoint, that is $\overline{e_\ell} \cap \overline{e_k} = \emptyset$ for $\ell \neq k$. The electric current injected into the object Ω through the electrode ℓ is denoted as $I_\ell \in \mathbb{R}$. Furthermore, $U_\ell \in \mathbb{R}$ denotes the potential on the ℓ^{th} electrode and $V_i = U_\ell - U_k$, $\ell \neq k$, the potential differences between chosen pairs of electrodes.

In this thesis, the conductivity in the domain of interest is modelled with a real-valued function $\sigma : \Omega \to \mathbb{R}_+$ which corresponds to a situation of a domain with an isotropic conductivity. The electromagnetic conditions within the domain Ω are described with the elliptic PDE

$$\nabla \cdot (\sigma(\vec{r})\nabla\phi(\vec{r})) \quad = \quad 0, \quad \vec{r} \in \Omega \tag{3.29}$$

where $\phi : \Omega \to \mathbb{R}$ is the electric potential in Ω. The PDE (3.29) can be derived from the Maxwell's equations with certain assumptions [101], [102].

For the EIT forward model various sets of boundary conditions referred to as electrode models have been proposed. The most accurate known model so far is the CEM that was first described in [103]. See [103], [101] for more details on other electrode models. The boundary conditions for the CEM are

$$\phi(\vec{r}) + \bar{z}_\ell \sigma(\vec{r}) \frac{\partial \phi(\vec{r})}{\partial \vec{n}} \quad = \quad U_\ell, \quad \vec{r} \in e_\ell, \ \ell = 1, 2, \ldots, n_e \tag{3.30}$$

$$\int_{e_\ell} \sigma(\vec{r}) \frac{\partial \phi(\vec{r})}{\partial \vec{n}} \mathrm{d}S \quad = \quad I_\ell, \quad \vec{r} \in e_\ell, \ \ell = 1, 2, \ldots, n_e \tag{3.31}$$

$$\sigma(\vec{r}) \frac{\partial \phi(\vec{r})}{\partial \vec{n}} \quad = \quad 0, \quad \vec{r} \in \partial\Omega \backslash \cup_{\ell=1}^{n_e} e_\ell \tag{3.32}$$

where $\bar{z}_\ell \in \mathbb{R}$ denotes the contact impedance between the ℓ^{th} electrode and contact material. In this thesis, the condition (3.30) takes into account the shunting effect of the electrodes and the potential drop caused by the contact impedance layer at the saline-electrode interface. The condition (3.31) specifies that the magnitude of the total charge flux through the electrode ℓ equals the injected current. Furthermore, the condition (3.32) states that through the boundary between the electrodes the current density is zero.

To ensure the existence and uniqueness of the solution of the CEM (3.29)-(3.32), additional conditions for the injected currents and electrode potentials are needed, see [101] for a proof. The vector of injected currents $\mathcal{I} = [I_1, \ldots, I_{n_e}]^T \in \mathbb{R}^{n_e}$ has to satisfy the charge conservation law

$$\textstyle\sum_{\ell=1}^{n_e} I_\ell = 0. \tag{3.33}$$

The vector $\mathcal{I}$ is referred to as a current pattern. Furthermore, the reference level of the potential has to be fixed. The vector consisting the electrode potentials is denoted as $U = [U_1, \ldots, U_{n_e}]^T \in \mathbb{R}^{n_e}$. In this thesis, it is chosen that

$$\textstyle\sum_{\ell=1}^{n_e} U_\ell = 0. \tag{3.34}$$

The condition (3.34) is one of the possible conditions for determining the reference point.

As the reconstruction problem in EIT is ill-posed, it has been often stated that it is crucial that the forward model is adequately accurate. Recent results have, however, indicated that as long as the possible inaccuracies in the observation model are modelled properly, one obtains feasible reconstructions.

3.2.2 Numerical approximation of the CEM

The solution of the CEM (3.29)-(3.34) consists of two unknowns to be determined that are the internal potential ϕ and the electrode potentials U. In this thesis, the FE approximation of the CEM is used. The FE approximation of the CEM has previously been considered in [104], [102], [105], [106], [107]. Although the formulation of the FE approximation of the CEM considered in this thesis follows the one derived in [107], a brief review of the formulation is given.

The weak solution of the CEM (3.29)-(3.34) is considered and denoted by $(\phi, U) \in H$ where the solution space $H = H^1(\Omega) \times \mathbb{R}^{n_e}$. Let $v \in H^1(\Omega)$ denote the test function for the electric potential ϕ and $\mathrm{Y} = [\mathrm{Y}_1, \ldots, \mathrm{Y}_{n_e}]^T \in \mathbb{R}^{n_e}$ the vector for the potentials on the electrodes U. The weak form of the CEM derived in [101], [107] is

$$\mathcal{B}\left((\phi, U), (v, \mathrm{Y})\right) = \sum_{\ell=1}^{n_e} I_\ell \mathrm{Y}_\ell \quad \forall (v, \mathrm{Y}) \in H \tag{3.35}$$

where $\mathcal{B} : H \times H \to \mathbb{R}$ is a bilinear form defined as

$$\begin{aligned} \mathcal{B}\left((\phi, U), (v, \mathrm{Y})\right) &= \int_\Omega \sigma(\vec{r}) \nabla \phi(\vec{r}) \cdot \nabla v(\vec{r}) \mathrm{d}\vec{r} \\ &\quad + \sum_{\ell=1}^{n_e} \frac{1}{\bar{z}_\ell} \int_{e_\ell} (\phi(\vec{r}) - U_\ell)(v(\vec{r}) - \mathrm{Y}_\ell) \mathrm{d}S. \end{aligned} \tag{3.36}$$

Now, $(\phi, U) \in H$ is the weak solution of the CEM if and only if (3.35) holds for all $(v, \mathrm{Y}) \in H$.

The weak solution (ϕ, U) is approximated with a finite-dimensional solution $(\phi^h, U) \in H^h$ where $H^h = H^{1,h} \times H^{2,h}$ so that $H^{1,h}$ is a finite-dimensional subspace of $H^1(\Omega)$ and $H^{2,h}$ is a subspace of $\mathbb{R}^{n_\ell}$ with dimension $n_\ell - 1$. The finite-dimensional approximation for ϕ is

$$\phi(\vec{r}) \approx \phi^h(\vec{r}) = \sum_{i=1}^{n_{\tilde{\varphi}}} a_i \tilde{\varphi}_i(\vec{r}) \tag{3.37}$$

where a_i, $i = 1, \ldots, n_{\tilde{\varphi}}$, are unknown coefficients and the functions $\tilde{\varphi}_i$ form the basis of $H^{1,h}$. In this thesis, the basis functions $\tilde{\varphi}_i$ are chosen as piecewise 2nd order polynomial functions. The vector of electrode potentials is written as

$$U = \sum_{i=1}^{n_e-1} \alpha_i \bar{\varphi}_i \tag{3.38}$$

where α_i, $i = 1, \ldots, n_e - 1$, are unknown coefficients and the vectors $\bar{\varphi}_i \in \mathbb{R}^{n_e}$. In this thesis, the vectors $\bar{\varphi}_i$ are chosen so that $\bar{\varphi}_1 = [1, -1, 0, \ldots, 0]^T$, $\bar{\varphi}_2 = [1, 0, -1, 0, \ldots, 0]^T$, $\ldots$, $\bar{\varphi}_{n_e-1} = [1, 0, \ldots, 0, -1]^T$. With such a choice of $\bar{\varphi}_i$, the condition (3.34) is satisfied.

The Galerkin FEM is adopted. Let $\hat{0} : \Omega \to \mathbb{R}$ be a function so that $\hat{0}(\vec{r}) = 0$. The test functions (v, Y) equal $\{(\tilde{\varphi}_1, \bar{0}), \ldots, (\tilde{\varphi}_{n_{\tilde{\varphi}}}, \bar{0}), (\hat{0}, \bar{\varphi}_1), \ldots, (\hat{0}, \bar{\varphi}_{n_e-1})\}$ where $\bar{0}$ denotes a zero vector of size n_e. Substituting (3.37) and (3.38) into the weak formulation (3.35) leads to a matrix equation

$$\mathcal{A}\theta = \tilde{I} \tag{3.39}$$

where $\theta = [a_1, \ldots a_{n_{\tilde{\varphi}}}, \alpha_1, \ldots, \alpha_{n_e-1}]^T \in \mathbb{R}^{n_{\tilde{\varphi}}+(n_e-1)}$ is the vector of unknowns. Furthermore, the vector $\tilde{I} = \left[\bar{0}^T \ \hat{I}^T\right]^T \in \mathbb{R}^{n_{\tilde{\varphi}}+(n_e-1)}$ where $\bar{0}$ is a zero vector of size $n_{\tilde{\varphi}}$ and

$$\hat{I} = \begin{bmatrix} \sum_{\ell=1}^{n_e} I_\ell (\bar{\varphi}_1)_\ell \\ \vdots \\ \sum_{\ell=1}^{n_e} I_\ell (\bar{\varphi}_{n_\ell - 1})_\ell \end{bmatrix} = \mathcal{G}^T \mathcal{I}. \tag{3.40}$$

The notation $(\bar{\varphi}_i)_\ell$ refers to the ℓ^{th} entry of the vector $\bar{\varphi}_i$. With the chosen vectors $\bar{\varphi}_i$, the sparse matrix $\mathcal{G} \in \mathbb{R}^{n_e \times (n_e-1)}$ is

$$\mathcal{G} = \begin{bmatrix} 1 & 1 & \cdots & 1 & 1 \\ -1 & 0 & \cdots & 0 & 0 \\ 0 & -1 & 0 & \cdots & 0 \\ \vdots & \ddots & \ddots & \ddots & \vdots \\ 0 & \cdots & 0 & -1 & 0 \\ 0 & 0 & \cdots & 0 & -1 \end{bmatrix}. \tag{3.41}$$

In (3.39), the sparse block matrix $\mathcal{A} \in \mathbb{R}^{(n_{\tilde{\varphi}}+n_e-1)\times(n_{\tilde{\varphi}}+n_e-1)}$ is

$$\mathcal{A}(\sigma, \bar{z}) = \begin{bmatrix} \mathcal{C}(\sigma, \bar{z}) & \mathcal{D}(\bar{z}) \\ (\mathcal{D}(\bar{z}))^T & \mathcal{E}(\bar{z}) \end{bmatrix} \tag{3.42}$$

where the vector $\bar{z} \in \mathbb{R}^{n_e}$ is $\bar{z} = [\bar{z}_1, \ldots, \bar{z}_{n_e}]^T$ and

$$\begin{aligned}
\mathcal{C}(i,j) &= \mathcal{B}((\tilde{\varphi}_i, \bar{0}), (\tilde{\varphi}_j, \bar{0})) = \int_\Omega \sigma \nabla \tilde{\varphi}_i \cdot \nabla \tilde{\varphi}_j \mathrm{d}\vec{r} + \sum_{\ell=1}^{n_e} \frac{1}{\bar{z}_\ell} \int_{e_\ell} \tilde{\varphi}_i \tilde{\varphi}_j \mathrm{d}S, \\
&\quad i,j = 1, \ldots, n_{\tilde{\varphi}}, \qquad (3.43) \\
\mathcal{D}(i,j) &= \mathcal{B}((\tilde{\varphi}_i, \bar{0}), (\hat{0}, \bar{\varphi}_j)) = -\left(\frac{1}{\bar{z}_1} \int_{e_1} \tilde{\varphi}_i \mathrm{d}S - \frac{1}{\bar{z}_{j+1}} \int_{e_{j+1}} \tilde{\varphi}_i \mathrm{d}S \right), \\
&\quad i = 1, \ldots n_{\tilde{\varphi}}, \quad j = 1, \ldots, n_e - 1, \qquad (3.44) \\
\mathcal{E}(i,j) &= \mathcal{B}((\hat{0}, \bar{\varphi}_i), (\hat{0}, \bar{\varphi}_j)) = \sum_{\ell=1}^{n_e} \frac{1}{\bar{z}_\ell} \int_{e_\ell} (\bar{\varphi}_i)_\ell (\bar{\varphi}_j)_\ell \mathrm{d}S \\
&= \begin{cases} \frac{|e_1|}{\bar{z}_1}, & i \neq j \\ \frac{|e_1|}{\bar{z}_1} + \frac{|e_{j+1}|}{\bar{z}_{j+1}}, & i = j \end{cases}, i,j = 1, \ldots, n_e - 1 \qquad (3.45)
\end{aligned}$$

where $|e_j|$ is the measure of the j^{th} electrode and $\mathcal{C}(i,j)$, $\mathcal{D}(i,j)$, and $\mathcal{E}(i,j)$ denote the entries of the corresponding matrices. For details on the computation of the integrals in (3.43)-(3.45), see [108], [107].

For the computation of the integrals in (3.43)-(3.45), a finite-dimensional approximation for the conductivity is needed. Typically, when deriving the FE approximation for the CEM, piecewise constant functions are used in the finite-dimensional approximation of the conductivity, see for example [108], [107]. In this thesis, however, piecewise linear functions are used as in [109], [92]. This choice is adopted since it allows for a straightforward mapping between the state evolution model and the observation model if the FE bases for conductivity and concentration are equal. The finite-dimensional approximation for the conductivity is

$$\sigma(\vec{r}) \approx \sigma^h(\vec{r}) = \sum_{i=1}^{n_\varphi} \sigma_i \varphi_i(\vec{r}) \qquad (3.46)$$

where the functions φ_i form the basis for H^h that is a finite-dimensional subspace of $H^1(\Omega)$, n_φ is the number of basis functions φ_i, and σ_i is the approximate value of conductivity in the i^{th} node. From this on, $\sigma = [\sigma_1, \ldots, \sigma_{n_\varphi}]^T \in \mathbb{R}^{n_\varphi}$ denotes the finite-dimensional representation of the conductivity.

The approximate solution of the forward problem is obtained by solving (3.39) as

$$\theta = \mathcal{A}^{-1} \tilde{I}. \qquad (3.47)$$

The first $n_{\tilde{\varphi}}$ entries of the vector θ yield the coefficients a_i and as a result, the values of the internal potential ϕ^h in the FE nodes can be computed. The last $n_e - 1$ entries of the vector θ are the values of the coefficients α_i. The vector of potentials on the electrodes U is obtained according to (3.38).

In EIT, the potential differences between chosen electrodes are measured. In this thesis, the vector $V = [V_1, \ldots, V_{n_V}]^T \in \mathbb{R}^{n_V}$ denotes the actual EIT observations where n_V is the number of measurements conducted corresponding to one current injection and the matrix $\mathcal{M} \in \mathbb{R}^{n_V \times n_e}$ is a measurement matrix specifying the electrodes between which the voltages are measured. The matrix $\mathcal{M}$ is also referred to as the measurement pattern. Thus, the voltage vector

$$V = \mathcal{M}U. \tag{3.48}$$

When the matrix $\mathcal{F} \in \mathbb{R}^{(n_e-1)\times(n_{\tilde{\varphi}}+n_e-1)}$ is defined so that $\mathcal{F} = [O \; I]$ where $O \in \mathbb{R}^{(n_e-1)\times n_{\tilde{\varphi}}}$ is a zero matrix and $I \in \mathbb{R}^{(n_e-1)\times(n_e-1)}$ is an identity matrix, it can be shown that the voltage vector is of the form

$$V = \mathcal{M}\mathcal{G}\mathcal{F}\mathcal{A}^{-1}\mathcal{F}^T\mathcal{G}^T\mathcal{I} = \mathcal{R}(\sigma, \bar{z})\mathcal{I}. \tag{3.49}$$

In (3.49), the matrix $\mathcal{R} \in \mathbb{R}^{n_V \times n_e}$ is referred to as the resistance matrix and is defined as $\mathcal{R} = \mathcal{M}\mathcal{G}\mathcal{F}\mathcal{A}^{-1}\mathcal{F}^T\mathcal{G}^T$. Furthermore in (3.49), the vector $\mathcal{I}$ is the current pattern, and, therefore, it can be concluded that the dependence between the voltages V and the injected currents $\mathcal{I}$ is linear. By contrast, the dependence between the voltages V and the conductivity σ is nonlinear. In this thesis, an approximation for the contact impedances is used. Thus, the vector $\bar{z}$ in (3.49) is known. Consequently, the resistance matrix depends only on the conductivity, that is, $\mathcal{R}(\sigma, \bar{z}) = \mathcal{R}(\sigma)$. The contact impedances can also be estimated simultaneously with the conductivity as shown in [110], [111], [112], [113].

When the nonlinear function $\bar{R} : \mathbb{R}^{n_\varphi} \to \mathbb{R}^{n_V}$ is defined so that $\bar{R}(\sigma) = \mathcal{R}(\sigma)\mathcal{I}$, the finite-dimensional observation model of EIT is

$$V = \mathcal{R}(\sigma)\mathcal{I} + v = \bar{R}(\sigma) + v, \tag{3.50}$$

where the vector $v \in \mathbb{R}^{n_V}$ denotes the observation noise. In this thesis, the observation noise is modelled as Gaussian noise so that $v \sim N(0, \Gamma_v)$ where $\Gamma_v \in \mathbb{R}^{n_V \times n_V}$ is the covariance matrix of the observation noise. The covariance matrix Γ_v can be determined, for example, by analysing the measurement system properties with a set of repeated measurements [114], [110].

The unknown quantity in this thesis is the concentration of a chemical substance in a pipe segment. As the EIT forward model is stated in terms of the conductivity, a mapping from the concentration to the conductivity is required. In this thesis, a linear model is used although the dependence between the conductivity and the concentration is often nonlinear. If the FE bases for approximating the conductivity and the concentration are equal, the model describing the dependence between the conductivity and the concentration in that case is $\tilde{\sigma} : \mathbb{R}^{n_\varphi} \to \mathbb{R}^{n_\varphi}$, $\sigma = \tilde{\sigma}(c) = kc$ where $k \in \mathbb{R}_+$.

The EIT observation model in terms of the concentration corresponding to (3.50) is

$$V = \bar{R}(\tilde{\sigma}(c)) + v = \tilde{R}(c) + v \tag{3.51}$$

where $\tilde{R} : \mathbb{R}^{n_\varphi} \to \mathbb{R}^{n_V}$ is the nonlinear composite function $\tilde{R}(c) = (\bar{R} \circ \tilde{\sigma})(c)$.

3.2.3 Linearisation of the EIT observation model

As the EIT observation model (3.51) is nonlinear, nonlinear state estimation methods are needed. A simple approach to handle the nonlinearity is to approximate the nonlinear observation model with a linearised model. The mapping $\tilde{R}$ is linearised around a linearisation point $c_{\text{lp}} \in \mathbb{R}^{n_\varphi}$. In this thesis, c_{lp} is chosen to be a vector $c_{\text{lp}} = [c_{\text{a}}, c_{\text{a}}, \ldots, c_{\text{a}}]^T$ representing a homogeneous concentration distribution in the pipe where $c_{\text{a}} \in \mathbb{R}_+$ is the approximate spatial and temporal average concentration. The average concentration is approximated on the basis of prior knowledge. Thus, the linearised observation model is

$$V \approx \tilde{R}(c_{\text{lp}}) + \mathcal{J}\tilde{R}(c_{\text{lp}}) \left(c - c_{\text{lp}}\right) + v \tag{3.52}$$

where $\mathcal{J}\tilde{R} \in \mathbb{R}^{n_V \times n_\varphi}$ is the Jacobian matrix of the mapping $\tilde{R}$. The differentiability of the mapping $\tilde{R}$ is not considered in this thesis. The Jacobian matrix $\mathcal{J}\tilde{R}$ in (3.52) is obtained applying the chain rule of differentiation so that

$$\mathcal{J}\tilde{R}(c) = \mathcal{J}\bar{R}(\tilde{\sigma}(c))\mathcal{J}\tilde{\sigma}(c) \tag{3.53}$$

where $\mathcal{J}\bar{R} \in \mathbb{R}^{n_V \times n_\varphi}$ and $\mathcal{J}\tilde{\sigma} \in \mathbb{R}^{n_\varphi \times n_\varphi}$ denote the Jacobians of the functions $\bar{R}$ and $\tilde{\sigma}$, respectively.

The Jacobian matrix of the mapping $\bar{R}$ with respect to the conductivity

$$\mathcal{J}\bar{R}(\sigma) = \left[\frac{\partial \bar{R}(\sigma)}{\partial \sigma_1}, \ldots, \frac{\partial \bar{R}(\sigma)}{\partial \sigma_{n_\varphi}} \right] \tag{3.54}$$

is computed as in [115]. See also [102]. From (3.49) and (3.50), it can be concluded that

$$\bar{R}(\sigma) = \mathcal{M}\mathcal{G}\mathcal{F}\mathcal{A}^{-1}\mathcal{F}^T\mathcal{G}^T\mathcal{I} \tag{3.55}$$

where $\mathcal{A} = \mathcal{A}(\sigma)$. The partial derivatives of $\bar{R}$ with respect to the conductivity σ_k, $k = 1, \ldots, n_\varphi$, are

$$\begin{aligned}
\frac{\partial \bar{R}(\sigma)}{\partial \sigma_k} &= \frac{\partial}{\partial \sigma_k}(\mathcal{M}\mathcal{G}\mathcal{F}\mathcal{A}^{-1}\mathcal{F}^T\mathcal{G}^T\mathcal{I}) \\
&= \mathcal{M}\mathcal{G}\mathcal{F}\frac{\partial \mathcal{A}^{-1}(\sigma)}{\partial \sigma_k}\mathcal{F}^T\mathcal{G}^T\mathcal{I} \\
&= -\mathcal{M}\mathcal{G}\mathcal{F}\mathcal{A}^{-1}(\sigma)\frac{\partial \mathcal{A}(\sigma)}{\partial \sigma_k}\mathcal{A}^{-1}(\sigma)\mathcal{F}^T\mathcal{G}^T\mathcal{I}
\end{aligned} \tag{3.56}$$

since only the matrix $\mathcal{A}$ in (3.55) depends on the conductivity, and it can be shown that $\frac{\partial \mathcal{A}^{-1}(\sigma)}{\partial \sigma_k} = -\mathcal{A}^{-1}(\sigma)\frac{\partial \mathcal{A}(\sigma)}{\partial \sigma_k}\mathcal{A}^{-1}(\sigma)$. In the block matrix $\mathcal{A}$, only the block $\mathcal{C}$ depends on the conductivity. Consequently,

$$\frac{\partial \mathcal{A}(\sigma)}{\partial \sigma_k} = \begin{bmatrix} \frac{\partial \mathcal{C}(\sigma)}{\partial \sigma_k} & 0 \\ 0 & 0 \end{bmatrix} \tag{3.57}$$

where

$$\begin{aligned}
\frac{\partial \mathcal{C}(\sigma)}{\partial \sigma_k} &= \frac{\partial}{\partial \sigma_k}\left(\int_\Omega \sigma(\vec{r})\nabla\varphi_i(\vec{r}) \cdot \nabla\varphi_j(\vec{r})\mathrm{d}\vec{r}\right) \\
&= \frac{\partial}{\partial \sigma_k}\left(\int_\Omega \sum_{i=1}^{n_\varphi} \sigma_j\varphi_j(\vec{r})\nabla\varphi_i(\vec{r}) \cdot \nabla\varphi_j(\vec{r})\mathrm{d}\vec{r}\right) \\
&= \int_\Omega \varphi_k(\vec{r})\nabla\varphi_i(\vec{r}) \cdot \nabla\varphi_j(\vec{r})\mathrm{d}\vec{r}.
\end{aligned} \tag{3.58}$$

It should be noted that (3.58) is valid only when the piecewise linear basis functions are used in the approximation of the conductivity σ. The Jacobian matrix $\mathcal{J}\bar{R}$ could be computed using also the adjoint differentiation considered in [116].

The Jacobian matrix $\mathcal{J}\tilde{\sigma}$ is a diagonal matrix

$$\mathcal{J}\tilde{\sigma}(c) = \mathrm{diag}\left(\frac{\partial \tilde{\sigma}_1(c)}{\partial c_1}, \ldots, \frac{\partial \tilde{\sigma}_{n_\varphi}(c)}{\partial c_{n_\varphi}}\right). \tag{3.59}$$

Often, the FE bases for the conductivity and the concentration are different due to computational reasons. As an example, when approximating the CEM with the FEM, the FE mesh has to be quite dense near

the electrodes in order to avoid large approximation errors. Such a mesh structure is unnecessary when approximating the CD model, and making the FE mesh denser would only increase the computational load. In such a case, interpolation between the two different FE meshes is required. A simple method to tackle the problem is the linear interpolation. Let $\sigma_{\mathrm{CEM}} \in \mathbb{R}^{n_{CEM}}$ and $\sigma_{\mathrm{CD}} \in \mathbb{R}^{n_{CD}}$ denote the conductivity approximated in the FE mesh for the CEM and the CD model, respectively. Now $\sigma_{\mathrm{CEM}} = \bar{J}\sigma_{\mathrm{CD}} = k\bar{J}c_{\mathrm{CD}}$ where $\bar{J} \in \mathbb{R}^{n_{CEM} \times n_{CD}}$ is a linear interpolation matrix and $c_{\mathrm{CD}} \in \mathbb{R}^{n_{CD}}$ is the finite-dimensional approximation of the concentration in the FE mesh for the CD model. Furthermore, the Jacobian matrix in this case is

$$\mathcal{J}\tilde{\sigma}(c) = \bar{J}\mathrm{diag}\left(\frac{\partial\tilde{\sigma}_1(c)}{\partial c_1}, \ldots, \frac{\partial\tilde{\sigma}_{n_{CD}}(c)}{\partial c_{n_{CD}}}\right). \tag{3.60}$$

3.2.4 Nonstationary EIT observation model

The concentration of a chemical substance has both spatial and temporal variations. Thus, a nonstationary observation model corresponding to (3.51) is needed. Let $c_t \in \mathbb{R}^{n_\varphi}$ denote the finite-dimensional approximation of the concentration at the measurement time t. Furthermore, the vector $\mathcal{I}_t \in \mathbb{R}^{n_e}$ denotes the current pattern applied at time t and $V_t \in \mathbb{R}^{n_V}$ the voltage observations corresponding to that current pattern. The nonstationary EIT observation model corresponding to (3.51) is

$$V_t = \tilde{R}_t(c_t) + v_t \tag{3.61}$$

where the mapping $\tilde{R}_t : \mathbb{R}^{n_\varphi} \to \mathbb{R}^{n_V}$ corresponds to the current pattern $\mathcal{I}_t$ and $v_t \in \mathbb{R}^{n_V}$ denotes the observation noise at time t.

The globally linearised nonstationary EIT observation model corresponding to (3.52) is

$$V_t \approx \tilde{R}_t(c_{\mathrm{lp}}) + \mathcal{J}\tilde{R}_t(c_{\mathrm{lp}})\left(c_t - c_{\mathrm{lp}}\right) + v_t \tag{3.62}$$

where $\mathcal{J}\tilde{R}_t \in \mathbb{R}^{n_V \times n_\varphi}$ is the Jacobian matrix of the mapping $\tilde{R}_t$. The linearised nonstationary observation model (3.62) can be rearranged to

$$V_{1,t} = \mathcal{J}\tilde{R}_t(c_{\mathrm{lp}})c_t + v_t \tag{3.63}$$

where $V_{1,t} = V_t - \tilde{R}_t(c_{\mathrm{lp}}) - \mathcal{J}\tilde{R}_t(c_{\mathrm{lp}})c_{\mathrm{lp}}$.

3.2.5 Data acquisition in EIT

When designing the EIT measurement system, it is essential that the voltage measurements provide maximal information on the unknown quantity. To achieve that goal in EIT, the issues to be considered are the current injection and the voltage measurement strategies. These strategies are mainly developed for the two-dimensional EIT. In this thesis, the current injection and voltage measurement strategies are discussed only briefly. Furthermore, the EIT hardware is not considered. For information on EIT hardware, see [117], [118], [119], [120], [121], [1], [122], [123], [124], [125], [126].

The current injection strategies can be divided into two categories that are the *pair-drive methods* and the *multiple-drive methods*. In the pair-drive methods, the current is applied between two electrodes at a time. Thus, only one current generator is needed. The two widely used pair-drive methods in EIT are the *adjacent drive method* and the *opposite (polar) drive method*. In the adjacent drive method, the current is injected sequentially through adjacent electrode pairs [127], [128]. It has been shown that the current density produced by the adjacent method is non-uniform leading to good sensitivity in the regions near the drive electrodes and poor sensitivity in the central region of the domain [129]. In opposite drive method, the current is injected sequentially through diametrically opposite electrode pairs [128], [130]. The method produces a more uniform current density than the adjacent method. Especially, in the central regions of the domain the sensitivity is better [129].

The multiple-drive methods can produce the most uniform current density into the domain [131], [132]. In the multiple-drive methods, currents are applied to all electrodes simultaneously by using multiple current generators. The challenge in such methods is the selection of the patterns of applied current to obtain the best overall sensitivity. The optimal current pattern is known to depend on the structure of the unknown quantity distribution. There are also different definitions for optimality in the case of optimal current patterns and the choice of the definition of optimality has an effect on the optimal current pattern.

The theory of optimal current patterns in EIT has been widely investigated. In [131], [133], the concept of distinguishability was discussed. To be more specific, the current pattern that best distinguishes one conductivity distribution from another was considered. The so-called *trigonometric current patterns* were introduced in the publications. The trigonometric current patterns are the optimal current patterns when the target distri-

bution is rotationally invariant.

Practical EIT systems have constraints that limit the total amount of current that can be applied and the maximum current on individual electrodes. In [133], [130], [134], [135], it was shown that the constraints have an impact on the optimal current patterns. In [136], [137], [138], an adaptive process for producing the optimal current pattern on the basis of EIT measurements was described. It should be noted that this experimental process does not require prior knowledge of the target distribution inside the object. In [139], iterative and direct methods to determine optimal current patterns on the basis of physical measurements were considered. The problem of determining the optimal current patterns in statistical inversion framework when imaging stationary targets was considered in [140]. In [141], the method was extended to nonstationary targets. It was shown that the use of only a small number of current injection patterns repetitively instead of several different patterns yielded accurate estimates since the target itself was moving.

Only a few studies on current patterns in three-dimensional EIT have been published. In [142], three current injection strategies (and voltage measurement strategies) were studied with simulations when imaging stationary targets. In [143], a modified opposite current injection procedure was developed for reducing the measurement time when monitoring a multiphase flow in real time. The procedure was evaluated with laboratory experiments.

In EIT, the voltages can be measured in different ways. One possibility is to fix a reference electrode and to measure the voltages with respect to that electrode. Another possibility is to measure the voltages between, for example, adjacent or opposite electrodes without any fixed reference electrode.

3.2.6 Inverse problem in EIT

The reconstruction problem in EIT is a nonlinear and ill-posed inverse problem. The methods for solving the EIT reconstruction problem can be divided into two categories depending on whether the unknown quantity is stationary or nonstationary.

In stationary EIT, it is assumed that the unknown quantity does not change during a set of current injections. Consequently, several measurement sets are available for reconstructing the distribution of the unknown quantity. The stationary inversion can be considered from the deterministic viewpoint or the statistical viewpoint. The main difference between

statistical inversion and deterministic inversion is in how the quantities are defined. In statistical inversion, the quantities in the model are considered as random variables. In deterministic inversion, the quantity of interest is considered unknown but deterministic. For more information on stationary inverse problems, see [5].

If the unknown quantity has (rapid) temporal variations, the nonstationary inversion methods produce better reconstructions than the stationary inversion methods. Nonstationary quantities are typical in process control applications in which, for example, monitoring of fast moving fluids is needed. The nonstationary inverse problem can be stated as a problem to obtain information on the spatially and temporally varying unknown quantity on the basis of observations given the density of the initial state. This leads to the concept of a state estimation problem specified in Section 2.2.3. When solving nonstationary inverse problems, the Bayesian filtering methods are used. It should be noted that even if the temporal variations of the unknown quantity are slow, incorporating an evolution model into the inversion algorithm may enhance the results. For more information on nonstationary inverse problems, see [5].

STATIONARY INVERSE PROBLEMS

The firstly reported reconstruction methods in EIT were the backprojection method and the sensitivity coefficient method that are often referred to as qualitative inversion methods. These methods have been and still are widely-used although they produce biased reconstructions. On the other hand, these methods are fast and do not require accurate process modelling.

The backprojection algorithm was introduced in [144] in the context of EIT. The method was also discussed in [145]. An iterative extension based on the conjugate residual method to the algorithm was proposed in [146]. The filtered backprojection algorithm was used in [129]. The sensitivity coefficient method was discussed in [147]. In [148], the sensitivity weighted back-projection algorithm was introduced. In [142], the sensitivity method was used in three-dimensional EIT.

In addition to the qualitative inversion methods, also other approaches to solve the stationary inverse problem in EIT have been proposed. Below, the deterministic inversion in EIT is considered. The EIT inverse problem is to determine the concentration c (or the conductivity σ) on the basis of the measurements V and the forward model $\tilde{R}$. If one formulates the problem as a least squares problem, the aim is to find c that minimizes

the functional

$$\|V - \tilde{R}(c)\|_2^2. \tag{3.64}$$

As the EIT inverse problem is ill-posed, minimizing the functional (3.64) as such leads to a nonunique and highly unstable solution that is, consequently, intolerant to even small measurement noise and modelling errors.

One approach to handle the ill-posedness of the problem is to use regularization. The basic idea of a regularization method is not to solve the original minimization problem but to seek an approximate problem that has a stable solution and to solve that problem. For example in the Levenberg-Marquardt method and in the Tikhonov regularization that have been applied in EIT, such a problem is obtained by adding a penalty term into the functional to be minimized. This penalty term is typically chosen *ad hoc* in deterministic inversion. In addition to the standard Levenberg-Marquardt and Tikhonov regularization methods, various modifications of them have been proposed in the case of EIT, see [149] as an example. Furthermore, other regularization methods are, for example, regularization by singular value truncation and regularization by truncated iterative methods (e.g. the Landweber-Fridman iteration, the Kaczmarz iteration, and the Krylov subspace method) [5].

The Levenberg-Marquardt method was first applied to EIT in [150]. In [151], the method proposed in [150] was shown to be inapplicable in a real measurement situation. In [152], the Levenberg-Marquardt was applied to stabilize the image reconstruction process in the presence of modelling errors and measurement noise. An experimental evaluation of the methods proposed in [152] was presented in [153]. A convergence analysis of the Levenberg-Marquardt method was shown in [154]. In [155], a combination of the steepest descent and the Levenberg-Marquardt methods with additional anatomical information was introduced.

One of the most common regularization methods in EIT is the generalized Tikhonov regularization [156]. The Tikhonov regularization was used in EIT, for example, in [151], [157], [105], [106], [158]. In the generalized Tikhonov regularization, the problem of minimizing the functional (3.64) is replaced with a problem of minimizing a functional with an additional penalty term

$$\|V - \tilde{R}(c)\|_2^2 + \beta_{\text{tr}}^2 \|L_{\text{tr}}(c - c_{\text{pr}})\|_2^2 \tag{3.65}$$

where $\beta_{\text{tr}} > 0$ is the regularization parameter (constant), $L_{\text{tr}} \in \mathbb{R}^{n_L \times n_\varphi}$ is the regularization matrix, n_L is the number of rows in L_{tr}, and $c_{\text{pr}} \in \mathbb{R}^{n_\varphi}$ is

the initial guess for the concentration. With a proper choice of the penalty term, the minimization problem has a stable solution. The existence and uniqueness of the solution is not discussed in this thesis. Minimizing the functional (3.65) in EIT is a nonlinear minimization problem that can be solved with iterative methods such as the Newton-Raphson method and the Gauss-Newton method. In [107], several iterative methods for solving the EIT inverse problem were discussed.

In deterministic inversion, the regularization matrix L_{tr}, the initial guess for the unknown c_{pr}, and the regularization parameter β_{tr} are typically chosen *ad hoc* by the designer. A simple choice is to set $L_{\text{tr}} = I$ where I is an identity matrix [157]. If the concentration is assumed to be smooth, a difference-type matrix can be used [158]. In [105], a regularization matrix that takes into account the prior assumptions of the target was constructed. The choice of the regularization parameter β_{tr} depends on the measurement noise level. Several methods for choosing the regularization parameter have been proposed such as the Morozov discrepancy principle, the L-curve method and the generalized cross validation.

Below, the statistical inversion in EIT is considered. In the statistical inversion theory, the inverse problem is considered from the Bayesian point of view. The basic idea in statistical inversion is to view all quantities included in the models as random variables. The solution of the inverse problem is a (posterior) probability density of the unknown quantity instead of a single estimate produced by the classical deterministic inversion methods. As the solution is a probability density, point and interval estimates can be computed, and at the same time the reliability of the obtained estimates can be evaluated. In this thesis, the principles of statistical inversion theory are reviewed only briefly. The review is mainly based on [5]. For more information about the statistical inversion theory in general, see [5], [4]. The statistical inversion methods in EIT were considered in [109], [116], [159], [160], [114], [161].

For solving an inverse problem using the statistical inversion approach, one needs to formulate the prior and likelihood densities and to derive the posterior density. The prior density is formulated for the unknown quantity that in this thesis is the concentration, and it is denoted as $\pi_{\text{pr}}(c)$. Constructing the prior density can be a complicated task when solving an inverse problem. The qualitative information about the unknown has to be transformed into a quantitative prior density. The most widely used priors in EIT, and in the field of inverse problems in general, are the Gaussian priors. The Gaussian priors lead to estimators that are of simple form. Furthermore, the Gaussian densities are often adequate approximations of

the non-Gaussian densities.

The Gaussian priors applied in statistical inversion in EIT include the white noise prior [116], the smoothness priors [162], [116], [5], and the anisotropic smoothness prior [109], [114]. The white noise prior models the unknown parameters as mutually uncorrelated. If the unknown quantity does not change abruptly, and, hence, has only smooth spatial changes, the smoothness priors can be employed. The anisotropic smoothness priors are considered when the unknown quantity is expected to have large changes or discontinuity in some direction and to be smooth in other directions. Furthermore, Gaussian Markov random field priors can be used when the unknown has rapid changes or discontinuities (at known locations) [5].

The non-Gaussian priors used in EIT are, for example, the total variation prior [163], [164], [116] and the L^1 prior [165], [116]. The total variation prior is a suitable choice when the distribution of the unknown quantity is piecewise constant. When using the L^1 prior, the unknown quantity is assumed to contain small and well localized objects in a relatively homogeneous background. In [166], [167], Markov Chain Monte Carlo (MCMC) methods were applied in EIT, and sophisticated non-Gaussian prior models were introduced. In the publications, different types of materials existed in the domain of interest, and the conductivities of the materials varied.

The likelihood density contains the forward model and information about the noise and the measurement uncertainties. When constructing the likelihood function in EIT, an additive noise model is typically employed, and it is assumed that the noise is independent of the unknown concentration c. The joint probability density of V and c in the case of additive noise can be written as [116]

$$\pi(V, c) = \pi_{\text{pr}}(c)\pi(V|c) = \pi_{\text{pr}}(c)\pi_{\text{noise}}(V - \tilde{R}(c)) \tag{3.66}$$

where $\pi_{\text{noise}}(\cdot)$ is the probability density of the measurement noise v. The probability density $\pi(V|c)$ is the likelihood density and can be expressed as $\pi(V|c) = \pi_{\text{noise}}(V - \tilde{R}(c))$ in the case of additive noise model. The likelihood density expresses the likelihood of different measurement outcomes with c given. A more complex model for the relation between the concentration, the observations, and the noise can be derived if needed. In EIT, the measurement noise is often modelled as zero-mean Gaussian.

When the prior and likelihood densities are formulated, the posterior probability density, that is, the solution of the inverse problem, is com-

puted. The posterior density is

$$\pi_{\text{post}}(c) = \pi(c|V) = \frac{\pi_{\text{pr}}(c)\pi(V|c)}{\pi(V)} \quad \propto \quad \pi_{\text{pr}}(c)\pi(V|c) \qquad (3.67)$$

where the marginal density $\pi(V)$ can be considered as a norming constant.

A widely used point estimate when considering statistical inverse problems is the maximum a posteriori (MAP) estimate. The most popular interval estimate is the conditional covariance. If the likelihood function is Gaussian with an additive noise model and a Gaussian prior is used, the problem of finding the MAP estimate in statistical inversion corresponds to the Tikhonov regularization problem (3.65) when choosing $c_{\text{pr}} = E[c]$ and $\beta_{\text{tr}}^2 L_{\text{tr}}^T L_{\text{tr}} = \Gamma_c^{-1}$ where Γ_c is the covariance matrix of the Gaussian prior density of the concentration. It should be noted, however, that in deterministic inversion c_{pr}, β_{tr}, and L_{tr} are chosen *ad hoc* whereas in statistical inversion the key issue is to find a proper prior model for the concentration.

In the above discussion, absolute inversion was considered as the aim was to determine the absolute values of the unknown quantity. By contrast in difference imaging, the basic idea is to monitor the changes in the unknown quantity instead of the absolute values of the quantity. In difference imaging, the reconstructions are based on the difference between the voltage measurements corresponding to the unknown distribution of the concentration and the reference voltage measurements corresponding to a reference concentration distribution that often is a homogeneous distribution. The difference methods are known to produce the reconstructions fast as the reconstruction algorithm is quite simple. Furthermore, the methods are relatively tolerant to modelling errors. For example, the systematic errors may be partly compensated when comparing the actual measurements to the reference measurements if both are corrupted with a similar error. In [143], difference imaging in EIT was considered and laboratory experiments were presented. In [168], difference imaging of mixing of two miscible liquids was considered in the case of EIT.

NONSTATIONARY INVERSE PROBLEMS

In nonstationary inversion, the number of observations is typically significantly smaller than the number of the unknowns. Therefore, the inverse problem in nonstationary EIT is severely ill-posed. In such a case, the nonstationary EIT inverse problem can be viewed as a state estimation

problem. In the state estimation approach, the evolution model describes the temporal variations of the unknown quantity and is often PDE-based. In the case of rapidly moving fluids typical in process control applications, fluid dynamical models can be utilized as evolution models. Sometimes the state-space model is inadequate although the temporal variations of the unknown are taken into account and one does not obtain stable estimates even if the observations are noiseless. In such a case, additional spatial information of the unknown has to be incorporated into the state estimation scheme [169], [170], [171].

In [172], the state estimation approach in EIT was evaluated with numerical simulations. A model corresponding to the (linearised) CEM (3.52) was used as an observation model and a random walk model as a state evolution model. The Kalman filter estimates of the resistivity distribution in a two-dimensional domain representing a section of a human thorax were presented. Also in [171], the random walk evolution model and the CEM were employed. The Kalman filter estimates and the fixed-interval Kalman smoother estimates of the nonstationary simulated impedance distribution in a two-dimensional domain were computed. In [173], the state estimation approach using the random walk evolution model and the CEM was evaluated with laboratory experiments. In the experiments, a cylindrical tank was filled with saline and a plastic cylindrical object was moved in the tank to simulate a nonstationary target. The Kalman filter estimates and the fixed-interval Kalman smoother estimates of the two-dimensional resistivity distribution inside the tank were presented. In [174], the results using also the fixed-lag Kalman smoother were shown.

Also the extended Kalman filter has been used in solving the state estimation problem in EIT. In [175], [176], cylindrical objects were moved in a tank filled with saline to simulate nonstationary targets. The resistivity distribution in the tank was estimated. The state-space model consisted of the random walk evolution model and the nonlinear CEM (3.61). The known internal structures were taken into account in the modelling. The approach was evaluated with numerical simulations and laboratory experiments. In [177], the extended Kalman filter was used in estimating the conductivities in a two-dimensional domain representing a section of a human thorax. The random walk model was used as a state model. Both numerical simulations and laboratory experiments were presented.

The state estimation approach has been employed successfully to monitoring a CD process using EIT as a sensor in simulation studies and in laboratory experiments. In a case of a CD process, the simple random

walk model is often inadequate. In [92], a stochastic CD model was used as an evolution model and the CEM (3.52) as an observation model when estimating the simulated two-dimensional concentration distribution of a substance in a fluid moving along a pipeline using the Kalman filter. In [92], also the fixed-lag Kalman smoother estimates of the concentration were presented. In [95], the Kalman filter estimates and the fixed-interval Kalman smoother estimates and in [113], the iterated extended Kalman filter estimates were computed when estimating the simulated three-dimensional concentration distribution. An experimental evaluation of the state estimation approach in the case of a CD process monitored with EIT was performed in [178], [113], [179]. In the publications, monitoring the concentration distribution in the object of interest (a pipe or a tank) was considered. There were extra objects in the moving fluid. For example in [178], a saline-filled table tennis ball was placed in a fluid in a cylindrical tank and the contents of the tank were stirred with an impeller. In [178], the estimates of the two-dimensional concentration distribution and in [113], [179], the estimates of the three-dimensional concentration distribution were shown.

3.3 DISCUSSION

In this chapter, the state-space model consisting of the CD evolution model and the EIT observation model was considered. The key issue in the modelling was to take uncertainties and inaccuracies related to the evolution model and the observation model into account by finding proper models for the state noise process and the observation noise process. In this thesis, the state noise covariance matrix was far from the standard *ad hoc* choice that is a diagonal matrix with equal diagonal entries. Actually, such an *ad hoc* choice would render the state estimation approach infeasible. In this thesis, the observation noise was modelled as a Gaussian noise and the covariance matrix of the observation noise was of simple structure. However, if there are uncertainties and inaccuracies related to the observation model that are not Gaussian, one can analyse their statistical properties and formulate a proper model for the observation noise process. This matter is discussed further in Section 5.2.3.

In this thesis, only a stationary laminar flow was considered. However in a wide range of industrial processes, nonstationary turbulent flows are encountered. The advantage of turbulent flows is their ability to transport and mix components of the flow fast and effectively. Furthermore if

chemical reactions are involved in a process, the use of turbulence may increase reactant contact and decrease reaction times. However even in the case of a single-phase non-reactive flow, modelling the fundamentals of turbulence can be a complex task. Various computational fluid dynamic (CFD) models for turbulent, reactive and non-reactive flows have been developed. Such models include, for example, the $k - \epsilon$ model and Reynolds stress models [180], [93]. Unfortunately, the solution of the turbulent models require extensive computations. For real-time process control applications, the computational time is a crucial issue and, therefore, the CFD models as such are often inapplicable. If such a feasible and more realistic flow model is available, it could replace the laminar flow model used in this thesis.

The presented single-phase model is not likely the most appropriate model in the context of industrial processes. For example, the separation and mixing processes discussed in Section 4.3 typically involve two or more components of similar or dissimilar phases. Therefore, attention should be directed to multiphase flows consisting of more than one component or phase. The modelling of multiphase flows, whether it is experimental, theoretical or computational, is a challenging task due to the complexity of such flows. The complexity is multiplied if turbulence is encountered in a multiphase flow. Despite that fact, CFD models for different kind of multiphase flows have been proposed although the computer power and speed needed for solving the related equations can be a prohibitive issue in real-time process control implementations [181], [182], [183], [184]. If computational resources allow the use of a more complex multiphase process model, such a model can replace the CD model. In addition to computational reasons, approximating the multi-phase flow with a single-phase flow model is reasonable if the flow phenomena are dominated by one phase and the amounts or effects of other phases are insignificant.

The injections of extra concentrate into the flow in the CD equation were modelled as point-wise injections that are distributed to a small volume near the injection point. To model the injections more accurately, the injections could be written as boundary conditions for the velocity and the concentration at the point of injection. Such a model would take into account the change in the velocity field inside the pipe due to the injections in addition to the change in the concentration. Most likely if the flow rates of injectors are high, the flow in the pipe becomes turbulent due to the injections, and a turbulent flow model would be needed. Whether the flow is laminar or turbulent, the changes in the velocity field would necessitate

recomputation of the velocity field after each injection that could be too time-consuming for an real-time process control implementation with fast sampling. By assuming that the concentration of the injected substance is very high, the flow rates of the injectors can be considered to be low. Hence, the change in the velocity due to the injections is relatively small. An elegant approach to overcome the problem of time-consuming recomputation of the velocity field is to write the CD model with the stationary velocity field and construct a state noise process that accommodates for the modelling errors due to this approximation [185]. Such an approach could benefit also the example application of this thesis.

A stochastic term describing the inaccuracies in the CD model could be included in the continuous CD equation (3.1). Such a term would take into account the modelling uncertainties, for example, in the velocity field and in the diffusion coefficient. In this thesis, this term is added to the state noise w_t after discretisation. For more information on the stochastic formulation of the CD equation, see [186].

Overall, the simplifications of the evolution model (including those described above) are often feasible since the control system that is designed in Chapter 4 is based not only on the evolution model of the process but also on the EIT measurements. If the approximative evolution model is slightly inaccurate, the controller obtains compensatory information on the process via the EIT measurement, and the control performance is not deteriorated substantially. In [187], [188], [143], multiphase flows were monitored successfully with EIT even when an evolution model was not used. The key issue was that the conductivities of the components in a multiphase flow were different. Furthermore, a simplified multiphase model or even a single-phase model approximating a multiphase flow may be adequate in some processes. In [178], [113], [179], a CD model was formulated for a fluid flow in a pipeline. There were non-diffusing tracer objects with low conductivity drifting with the flow and the objects were successfully monitored with EIT despite the single-phase evolution model. If the considered process is very complex and the development of even an adequately accurate process model is impossible, system identification methods could be used. For example in many web forming processes, system identification is essential in modelling the spatial response of the actuators [189], [190].

In this thesis, the FEM was utilized in the numerical evaluation of the CD model. In addition to the FEM, mesh-based numerical methods for PDEs include, for example, the finite difference method (FDM) and the finite volume method (FVM) which could be also considered. However,

the advantage of the FEM is its ability to handle complex geometries and non-trivial boundary conditions. On the other hand, the FDM and the FVM are easier to implement and less time-consuming. In [191], [192], the FDM was used successfully to approximate the CD equation describing the concentration of a substance in a pipe flow. Contrary to the approach chosen in this thesis, the source term due to the control action was incorporated into a boundary condition instead of the CD equation itself. Furthermore, also numerous meshless methods exist for solving the CD problems [193], [194] as well as combinations of meshless and FE methods [195].

It is well-known that the FEM yields quite accurate results for diffusion-dominated problems. By contrast, if the diffusion coefficient is small, the problem becomes convection-dominated, and the standard FE discretisation may lead to oscillatory and even unstable approximate solutions. The oscillations are due to the so-called boundary layers that are small subregions of the domain in which the derivatives of the solution are large. To eliminate the oscillations, the mesh size has to be set sufficiently small or some FE stabilization method has to be applied. Such methods include, for example, the streamline upwind Petrov-Galerkin (SUPG) method [196], the Galerkin least squares (GLS) method [197], and the local discontinuous Galerkin (LDG) method [198]. Often, the stabilization methods improve the approximation properties and reduce the oscillatory behaviour of the solution in comparison to the standard Galerkin FEM. There are numerous studies on the stabilization methods applied to different kind of CD problems. For example in [199], a comparison of several stabilized FE methods for solving the convection-diffusion-reaction (CDR) equation that is the CD equation with an additional reaction term, was presented. In [200], [201], the GLS stabilization method was investigated in the case of the one-dimensional CD equation with a control action term as in (3.1).

In this thesis, the CEM was approximated with the FEM. In [202], [203], [112], the use of the boundary element method (BEM) for solving the CEM numerically was investigated. In [202], the location of a non-conducting inclusion in a domain of known homogeneous conductivity was estimated. In [203], [112], estimation of a piecewise homogeneous conductivity distribution in a domain containing subdomains of different conductivity was considered. In the publications, the unknown conductivity distribution was stationary. In general, the BEM is suitable only for piecewise homogeneous domains whereas the FEM can be used also for non-homogeneous domains. In the case of piecewise homogeneous

domains with simple geometries, the BEM is less time-consuming and demands less computational resources in comparison to the FEM as only the boundaries of the inhomogeneities are discretised instead of the whole domain. However, when estimating, for example, the non-homogeneous, non-stationary conductivity distribution of a chemical substance in a fluid flow as in this thesis, the BEM is infeasible.

It is well-known that the spatial resolution in EIT is quite poor in comparison to many other imaging modalities. However, adequate reconstructions have been obtained in both medical and industrial applications. The low spatial resolution could become a problem when the components in a multiphase flow are too small to be distinguished. In such a case instead of imaging individual components, an estimate of the ratio of the components may provide adequate information. By contrast, the temporal resolution in EIT is good. This is a huge benefit when controlling fast moving fluids since without accurate real time information, the control system is unable to react to the undesirable situations on time.

4 Process control using electrical process tomography

In Chapter 3, the discrete-time state-space model for the convection-diffusion (CD) process and the electrical impedance tomography (EIT) observations was discussed. The state equation described the spatial and temporal variations of the concentration of a substance in a fluid flowing in a pipe segment. The process was controlled by injecting extra concentrate into the main flow through injectors. The observation equation defined the link between the concentration and the EIT boundary measurements. In this chapter, the focus is on designing a control system for the CD process. In Chapter 5, the feasibility of the control system is evaluated with simulations.

This chapter is divided into four sections. In Section 4.1, publications considering controlling of industrial processes monitored with electrical process tomography (PT) are discussed. A control system suitable for the CD process monitored with EIT is designed in Section 4.2. In Section 4.3, examples of industrial processes to which this kind of control system could be applied are given. The chapter ends with a discussion in Section 4.4.

4.1 ELECTRICAL PROCESS TOMOGRAPHY IN PROCESS CONTROL

As the potential of electrical PT in process control has been recognized, various controllers for industrial processes have been developed when electrical PT is used for process monitoring. In this section, the discussed publications are grouped according to the type of the controller. In Section 4.1.1, the controller in the publications is the proportional-integral-derivative (PID) controller. In Section 4.1.2, publications consider applications with other automatic, real time controllers. In Section 4.1.3, model-based controllers are considered in the publications. The focus is on two electrical PT techniques that are EIT and electrical capacitance tomography (ECT).

4.1.1 PID controllers and electrical PT

Most of the published control systems employing data from electrical PT include a PID controller. The idea of a real time, automatic, and feedback control system using EIT as a sensor was first proposed in [204]. The controller in the control system was a PID controller. In the publication, control of an air-water bubble column was considered. The aim was to adjust the air flow rate in order to maintain a desired flow condition ensuring high reaction efficiency. The performance of the PID controller was evaluated with laboratory experiments in [205]. In [206], the aim was to control a pneumatic conveying system transporting polyethylene pieces using a proportional-integral (PI) controller and ECT as a sensor. The PI controller was designed to adjust the velocity of the conveying air in order to maintain a dilute phase flow at a predescribed level in a conveying pipe. The control system was evaluated with laboratory experiments. In [207], control of material moisture content of wet materials in a batch fluidised bed dryer was studied. The moisture content was determined on-line using ECT. A PI controller was designed to achieve a desired drying rate for wet materials by adjusting the inlet gas velocity. The proposed process model considered the bulk moisture content. The performance of the control system was evaluated with simulations. In [208], EIT measurements were used for determining the separation status of a pilot-scale solid-liquid separator by measuring the air core size and position. A PID controller was designed to automatically maintain the desired air core formation by manipulating the inlet flow rate. The proposed control system was tested with laboratory experiments.

The PI and PID controllers are widely used in process control but, however, they have several weaknesses especially in comparison to model-based optimal controllers considered in this thesis. Although the PID and PI controllers are automatic, real time, and feedback controllers, they require proper tuning of the control parameters in order to achieve good control performance. Furthermore, feedforward control is implemented more accurately using a model-based controller than a PID controller since the process behaviour can be predicted more accurately when the controller is based on an actual process model. Also the PID controller is not able to adapt to changing conditions automatically or recognize dead times. Furthermore, the PI and PID controllers aim to control a scalar process variable (they are used typically for single-input and single-output systems). For example in [207], the proposed process model described the bulk moisture content instead of a spatial distribution of the moisture

content. As the aim in this thesis is to control a distributed parameter system (DPS) modelled with partial differential equations (PDEs), the PI and PID controllers are unsuitable.

In the above mentioned publications, only stationary electrical PT techniques were considered. If the state of the process changes during a set of measurements, that is often the case in many industrial applications involving, for example, fast moving fluids, the stationary PT techniques yield unsatisfactory results. The state estimation approach adopted in this thesis accommodates for the temporal variations of the process.

4.1.2 Other automatic, real time controllers and electrical PT

In addition to the PID controllers, other automatic and feedback controllers using data obtained with electrical PT have been proposed. In [209], electrical resistance tomography (ERT) data was used for real time monitoring of a water-oil separation process in a hydrocyclone. The aim was to keep the separation effectiveness high and the core offset low by changing the input pressure of the liquid inflow. The control strategy was quite simplistic, and the input pressure was adjusted only if preset limits set on the separation effectiveness and on the core offset were violated. The simplicity of the controller was partly due to the requirement of the controller to operate in real time. The proposed control system was evaluated with numerical simulations. In the publication, the separation process was not described with a mathematical model and only the stationary tomographic techniques were considered.

In [210], ECT was used to provide data on dune formation of polypropylene pellets in a pneumatic flow rig to a neural network (NN) controller. The automatic and real time multilayer perceptron (MLP) based NN controller adjusted the air flow rate of the pneumatic flow rig to control the dune formation. The NN controllers are known to be especially useful when considering nonlinear processes. Furthermore, the advantage of the NN controller over the PID controller is that the NN controller takes into account the dynamics of the process in a neural network model. However, the model parameters in the neural network model do not have any physical significance whereas the model parameters in the PDE-based models considered in this thesis do. In [210], the aim was to control a scalar output process variable by adjusting a scalar input variable. In other words, the process was not considered as a DPS. Furthermore, only the stationary tomographic techniques were considered.

4.1.3 Model-based optimal controllers and electrical PT

Model-based (optimal) controllers have many benefits in comparison to non-model-based controllers such as PID controllers. The model-based controllers adapt automatically to changing process conditions without needing tuning of the controller parameters. The model-based controllers recognize dead times and can avoid undesirable situations by predicting the process behaviour in advance. Furthermore, feedforward control can be used in addition to feedback control as a process model exists. Although the benefits of using a model-based controller are clear, the majority of the controllers implemented in industrial applications are non-model-based (PID) controllers. The lack of implemented model-based controllers originates partly from the fact that process models of good quality, if existing, are often complex. Thus, they need sophisticated simplifications without reducing the quality of the model and considerable computational resources to be applied in control systems. Despite the challenges, a few model-based optimal controllers employing PT as a sensor have been designed.

In [28], distributed parameter control of a batch fluidised bed dryer was considered. ECT was used as a sensor to monitor the distributed permittivity in the bed. The objective of the designed control system was to maintain a desired shape of the permittivity distribution. The control input was the inlet air velocity of the dryer. The values for the control input with respect to a set of selected moisture content values were obtained as a solution of a simple optimization problem. Experimental results were used to evaluate the performance of the control system. In [28], the aim was to control only the shape of the permittivity distribution rather than to match the distribution to a certain desired distribution that would be advantageous in many cases. Furthermore, only stationary tomographic techniques were considered.

In [191], [192], the starting point of the study was similar to the one presented in this thesis. The idea in [191], [192] was to utilize EIT as a sensor for a model-based controller when controlling fast moving fluids. The controller was aimed for regulating the concentration distribution of a chemical substance in a fluid flow. The state-space model of the process and the observations was formed so that the concentration evolution was described with the CD equation and the observation equation was derived using the CEM. Although the idea of estimating the state of the process on the basis of tomographic observations was discussed, in the presented simulations, the state was assumed to be known and the state estimation

was not used. Several control strategies were discussed in [191] and simulations using a PI controller to regulate the average concentration at a particular point of the pipe were shown. The PI controller was designed also in [192].

The first automatic, feedback, and model-based optimal controllers obtaining data from EIT measurements were developed in [53], [54], [44], [57] by the author of this thesis. In the publications, the basis of the control system was the state-space model of the CD process and the EIT observations similar to the one derived in Chapter 3. One of the advantages of the state-space approach in process control is that the state estimate of the process can be used directly in a control system. Consequently, the need for post-processing reconstructions is avoided. In the publications, an approximate linear quadratic Gaussian (LQG) controller was designed (see Section 4.2.2), and the performance and the robustness of the controller was investigated with numerical simulations. Similar results as in the publications are presented in Section 5.1. Furthermore, the $\mathcal{H}_\infty$ optimal control in the case of EIT measurements was considered in [57]. The formulation of the approximate $\mathcal{H}_\infty$ controller proposed in this thesis differs from the one presented in [57]. The proposed approach of this thesis is evaluated with simulations presented in Section 6.

4.2 CONTROLLER FOR THE CD PROCESS MONITORED WITH EIT

In this section, a control system for the CD process is designed. In Section 4.2.1, the objective of the control system is illustrated. The LQG controller and the $\mathcal{H}_\infty$ controller discussed in Chapter 2 are modified to suit the features of the CD process in Sections 4.2.2 and 4.2.3, respectively. Furthermore, the controllability and the observability of the state-space model described in Chapter 3 are addressed briefly in Section 4.2.4. The computational aspects of the state estimation and the control algorithms are considered in Section 4.2.5.

4.2.1 Objective of the control system

The objective of the control system designed in this thesis is to control the concentration of a chemical substance in a fluid moving along a pipeline. The computational domain in this thesis is a finite segment of a pipe, see Figure 4.1. The fluid enters the pipe through the input boundary Λ_{in} and exits through the output boundary Λ_{out}. The direction of flow in

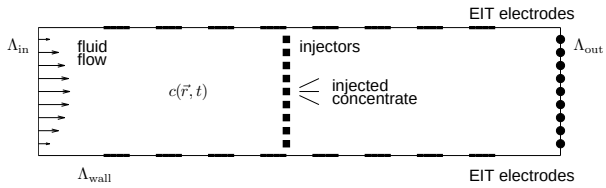

Figure 4.1: Illustration of the control system for controlling the concentration of a substance in a fluid.

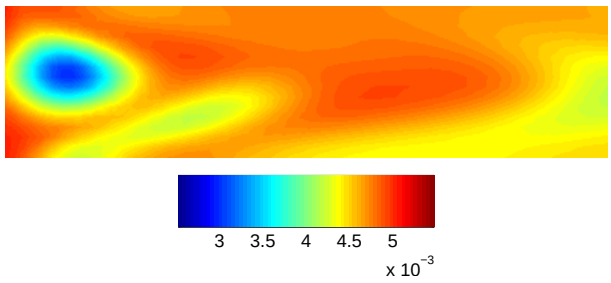

Figure 4.2: The concentration distribution in the pipe at a selected time.

the pipe is from left to right. In Figure 4.2, the concentration distribution in the pipe is illustrated at a selected time when process control has not been applied. The objective of the controller is to match the concentration distribution over the boundary Λ_{out} (at the end of the pipe) to a predetermined desired distribution as well as possible. The desired distribution is a uniform distribution that remains constant during the operation time. In Figure 4.2, it can be seen that the concentration over the boundary Λ_{out} is not homogeneous. Thus, the controller has to bring the concentration distribution close to the desired distribution as quickly as possible after the start-up and then to compensate for the concentration variations in the fluid.

In this thesis, EIT is utilized as a sensor in the control system. The EIT electrodes are attached to the (inner) wall of the pipe, see Figure 4.1. In the three-dimensional studies, the electrodes form several circular layers on the pipe boundary, see Figure 5.17 in Section 5.2. In addition to a monitoring system, an actuation mechanism is needed for adjusting the concentration of the substance along the pipe. In this thesis, a series of injectors placed in the pipe or on the pipe boundary serve as actuators. Through the injectors, strong concentrate is injected into the flow. Due to

the fluid flow, the injected concentrate drifts to the region downstream of the injectors and mixes with the main fluid. The flow rates of injectors are considered as control inputs. Thus, by adjusting the flow rates, the concentration distribution over Λ_{out} is aimed to match the desired distribution. It should be noted that the injectors can only add extra substance into the flow, and cannot remove it. Therefore, the concentration level downstream of the injectors can be increased but not decreased when injecting strong concentrate. If one wants to decrease the concentration level, for example, water or some other suitable liquid can be injected into the flow in addition to the strong concentrate.

4.2.2 Approximate LQG controller for the CD process

The basis for the formulation of the approximate LQG controller in this thesis is the CD state equation (3.27), the nonlinear EIT observation equation (3.61), and the output equation (3.28), that is,

$$\begin{aligned} c_{t+1} &= Ac_t + B_2 u_t + s_{t+1} + w_{1,t} && (4.1)\\ V_t &= \tilde{R}_t(c_t) + v_t && (4.2)\\ y_t &= Cc_t. && (4.3) \end{aligned}$$

The objective of the controller is to specify the flow rates of the injectors u_t so that the concentration distribution over Λ_{out}, that is, the output concentration y_t matches the desired distribution as well as possible. The solution to the presented control problem consists of two tasks. The first task is to estimate the concentration distribution in the pipe on the basis of the EIT observations and the state-space model (4.1)-(4.2). The second task is to determine the control inputs u_t that minimise the difference between the output concentration y_t and the reference input r_t. The reference input describes the predetermined desired concentration distribution over the boundary Λ_{out}. In this thesis, the desired profile is stationary and uniform so that for all $t \in \mathbb{N}_0$, $r_t = \beta_y \mathbf{1}$ where $\beta_y \in \mathbb{R}_+$ is the desired concentration level and $\mathbf{1} = [1\ , \ldots, 1]^T \in \mathbb{R}^{n_y}$. In the following, y_{ref} denotes the reference input.

There are several issues that need to be emphasized when designing the controller in this thesis. The reference input y_{ref} is non-zero and, thus, a basic LQG controller that drives the output to zero is inadequate. To overcome this problem, a tracking system discussed in Section 2.2.2 can be considered or, as in this thesis, a feedforward element can be incorporated into the controller. Furthermore, there is an additional source term s_{t+1} in

the state equation (4.1) describing the process input and that term has to be included into the controller design. Therefore, neither the basic LQG controller nor the linear quadratic (LQ) tracker can be applied as such. In this thesis, the effect of the process source term is taken into account using the feedforward element. Also as the injectors can only add more substance into the fluid and cannot remove it, the constraint $u_t^{(j)} \geq 0$ has to be valid for all t and $j = 1, \ldots, n_u$.

In this thesis, the approximate LQG controller is designed by defining variables describing perturbations from a predetermined steady-state of the system and by using the perturbation variables when deriving the control law (2.30). The perturbation variables $\tilde{c}_t \in \mathbb{R}^{n_\varphi}$, $\tilde{u}_t \in \mathbb{R}^{n_u}$, and $\tilde{y}_t \in \mathbb{R}^{n_y}$ are defined so that

$$\tilde{c}_t = c_t - \bar{c} \tag{4.4}$$

$$\tilde{u}_t = u_t - \bar{u} \tag{4.5}$$

$$\tilde{y}_t = y_t - \bar{y} \tag{4.6}$$

where $\bar{c} \in \mathbb{R}^{n_\varphi}$, $\bar{u} \in \mathbb{R}^{n_u}$, and $\bar{y} \in \mathbb{R}^{n_y}$ are the steady-state values of the state, the control input, and the control output, respectively. To be more specific, $\bar{u}$ is the steady-state control input, that is, the steady rates of injectors required to achieve the steady-state response $\bar{c}$ so that steady-state output $\bar{y} = C\bar{c} = y_{\text{ref}}$.

The computation of the steady-state values can be decoupled from the computation of the feedback control gains provided that the matrices in the state equation (4.1) and in the output equation (4.3) are stationary. In such a case, the steady-state values can be determined before the process start-up. The steady-state values are defined with equations

$$\bar{c} = A\bar{c} + B_2\bar{u} + \bar{s} \tag{4.7}$$

$$\bar{y} = C\bar{c} \tag{4.8}$$

where $\bar{s} \in \mathbb{R}^{n_\varphi}$ is a stationary approximation for s_{t+1}. If $\{s_{t+1}\}$ is considered as a random process whose distribution is known, then $\bar{s}$ can be set to $E[s_{t+1}]$ and one can assume that the variations from $\bar{s}$ are included in the state noise term $w_{1,t}$. It will be shown that such an approximation is adequate in the example application.

Eliminating $\bar{c}$ from the equations (4.7) - (4.8) leads to

$$\bar{y} = C\left(I - A\right)^{-1}\left(B_2\bar{u} + \bar{s}\right). \tag{4.9}$$

As the problem is to define the steady-state control $\bar{u}$ such that the output $\bar{y}$ equals the reference input y_{ref}, the error $(\bar{y} - y_{\text{ref}})$ is to be minimized

with respect to $\bar{u}$. The minimisation problem to be solved is

$$\min_{\bar{u}} \|\bar{y} - y_{\text{ref}}\|_2 = \min_{\bar{u}} \|C\left(I - A\right)^{-1}\left(B_2\bar{u} + \bar{s}\right) - y_{\text{ref}}\|_2. \tag{4.10}$$

As the control inputs are assumed to be non-negative, the minimisation problem (4.10) is solved with the non-negative least squares estimation [211]. Given the steady-state control input $\bar{u}$, the steady-state concentration $\bar{c}$ is computed as

$$\bar{c} = \left(I - A\right)^{-1}\left(B_2\bar{u} + \bar{s}\right). \tag{4.11}$$

This kind of formulation of the steady-state values can be considered as a feedforward element in the controller. It should be noted that if the desired distribution is nonstationary, the steady-state values have to be recomputed every time the desired distribution changes. Furthermore, as the formulation is based on the CD evolution model, the model needs to be adequately accurate. An inaccurate model could lead to a controller that drives the output systematically to an undesired state. In the numerical simulations, the controller is tested with an inaccurate process model to determine whether it can compensate for this kind of systematic errors.

The state equation and the output equation in terms of the perturbation variables are

$$\tilde{c}_{t+1} = A\tilde{c}_t + B_2\tilde{u}_t + w_{1,t} \tag{4.12}$$

$$\tilde{y}_t = C\tilde{c}_t. \tag{4.13}$$

Now, the control problem is to determine $\tilde{u}_t$ that bring $\tilde{y}_t = y_t - y_{\text{ref}}$, that is, the output error from its initial state to zero as quickly as possible and hold $\tilde{y}_t$ close to zero in the presence of the process input and the disturbances. The quadratic cost function to be minimized including the output $\tilde{y}_t$ and the control input $\tilde{u}_t$ is of the form

$$J = E\left[\tilde{y}_N^T H_y \tilde{y}_N + \sum_{t=0}^{N-1} \tilde{y}_t^T Q_y \tilde{y}_t + \tilde{u}_t^T R \tilde{u}_t\right] \tag{4.14}$$

where $H_y \in \mathbb{R}^{n_y \times n_y}$, $Q_y \in \mathbb{R}^{n_y \times n_y}$, and $R \in \mathbb{R}^{n_u \times n_u}$. In (4.14), the matrix $Q_y = \beta_Q I$ defines the importance for the output concentration $\bar{y}_t$ to match the reference input y_{ref} over Λ_{out}. As the objective is to regulate the concentration distribution over the whole boundary Λ_{out}, all the entries in $\tilde{y}_t$ are equally weighted. The weighting matrix $R = \beta_R I$ in (4.14) is used to impose a penalty on the use of excessive control inputs $\tilde{u}_t$ which

may exceed the operating range of the injectors, for example. As the injectors work similarly, the penalty imposed is the same for all entries of $\tilde{u}_t$. The key issue in choosing the weighting matrices is the magnitude of the entries of Q_y relative to the entries of R. When increasing the scalar β_Q relative to the scalar β_R, the controller attempts to minimise the error between the actual output concentration and the reference input regardless of the possible excessive control inputs. By contrast, decreasing β_Q relative to β_R limits the control inputs but at the same time allows larger output errors. Thus, the choice of the weighting matrices is always a trade-off between matching the output concentration distribution to the desired distribution and avoiding excessive control inputs.

The control law for the model (4.12)-(4.13) when minimizing (4.14) can be found by following the derivation discussed in Section 2.2.1. The optimal control law is

$$\tilde{u}_t \quad = \quad -K_t \tilde{c}_t \tag{4.15}$$

where $K_t \in \mathbb{R}^{n_u \times n_\varphi}$ is the discrete-time feedback gain. Substituting the perturbation variables (4.5) and (4.4) into the control law (4.15) yields the actual control inputs

$$u_t \quad = \quad \bar{u} - K_t \left(c_t - \bar{c} \right). \tag{4.16}$$

In this thesis, the input constraint $u_t^{(j)} \geq 0$ is handled in a quite simple manner. If the entries of the control input vector u_t are negative in spite of the computation of the steady-state values with the non-negative least squares, those entries are set to zero.

The computation of the control input u_t requires the state c_t. The state c_t is unknown and it is replaced with the state estimate $c_{t|t} \in \mathbb{R}^{n_\varphi}$ in (4.16). The globally linearised Kalman filter or the iterated extended Kalman filter described in Section 2.2.3 are used for obtaining the state estimate $c_{t|t}$.

4.2.3 Approximate $\mathcal{H}_\infty$ controller for the CD process

In this thesis, the approximate $\mathcal{H}_\infty$ controller is designed to control the CD process in a situation in which there are errors of unknown statistical nature between the model and the actual process. To be more specific, the input concentration (3.5) that was partly unknown when designing the approximate LQG controller is now unknown. Consequently, the process source term s_{t+1} due to the approximated average input concentration is

not in the CD state equation (3.27) and the input concentration acts as an unknown external disturbance to the process.

The objective of the approximate $\mathcal{H}_\infty$ controller is to match the control output y_t to the reference input y_{ref} in the presence of external disturbances. The external disturbances are the state and measurement noises and also the unknown input concentration. A new state variable $c^\infty \in \mathbb{R}^{(n_\varphi+n_y)}$,

$$c_t^\infty = \begin{bmatrix} c_t \\ y_{\text{ref}} \end{bmatrix}, \tag{4.17}$$

is considered and it consists of the concentration c_t and the reference input y_{ref}. The new state variable is introduced in order to provide the approximate $\mathcal{H}_\infty$ controller with information on the reference input. It should be noted that the reference input could be nonstationary in the formulation. The objective vector $z_t \in \mathbb{R}^{(n_y+n_u)}$ is defined as

$$z_t = \begin{bmatrix} Q_y^{\frac{1}{2}}(y_t - y_{\text{ref}}) \\ R^{\frac{1}{2}}u_t \end{bmatrix} = \begin{bmatrix} Q_y^{\frac{1}{2}} \\ 0 \end{bmatrix}(y_t - y_{\text{ref}}) + \begin{bmatrix} 0 \\ R^{\frac{1}{2}} \end{bmatrix} u_t. \tag{4.18}$$

The state equation of the state variable (4.17), the objective vector (4.18), and the observation equation (3.63) can be written in matrix form

$$\begin{bmatrix} c_{t+1}^\infty \\ z_t \\ V_{1,t} \end{bmatrix} = \begin{bmatrix} A_1 & B_{11} & B_{12} \\ C_1 & D_{11} & D_{12} \\ C_{2,t} & D_{21} & D_{22} \end{bmatrix} \begin{bmatrix} c_t^\infty \\ w_t \\ u_t \end{bmatrix} \tag{4.19}$$

where the external input $w_t \in \mathbb{R}^{(n_\varphi+n_V)}$, $w_t = \begin{bmatrix} w_{1,t}^T & v_t^T \end{bmatrix}^T$. The state noise $w_{1,t}$ encompasses the external disturbance input due to the unknown input boundary data. The system matrices are defined as

$$\begin{aligned} A_1 &= \begin{bmatrix} A & 0 \\ 0 & I \end{bmatrix} & B_{11} &= \begin{bmatrix} I & 0 \\ 0 & 0 \end{bmatrix} & B_{12} &= \begin{bmatrix} B_2 \\ 0 \end{bmatrix} \\ C_1 &= \begin{bmatrix} Q_y^{\frac{1}{2}}C & -Q_y^{\frac{1}{2}} \\ 0 & 0 \end{bmatrix} & D_{11} &= \begin{bmatrix} 0 & 0 \\ 0 & 0 \end{bmatrix} & D_{12} &= \begin{bmatrix} 0 \\ R^{\frac{1}{2}} \end{bmatrix} \\ C_{2,t} &= \begin{bmatrix} \mathcal{J}\tilde{R}_t(c_{\text{bh}}) & 0 \end{bmatrix} & D_{21} &= \begin{bmatrix} 0 & I \end{bmatrix} & D_{22} &= 0 \end{aligned}. \tag{4.20}$$

The approximate $\mathcal{H}_\infty$ controller is formulated on the basis of the theory reviewed in Section 2.3. In the formulation, the matrices D_{11} and $D_{12}^T C_1$ are zero matrices and the equations can be simplified accordingly.

4.2.4 Controllability and observability of the control system

When intuitively considering the controllability of the example application, it is evident that the concentration upstream of the injectors cannot be altered by injecting extra concentrate into the flow. This is due to the fact that the process is assumed to be dominated by the convection, and the rate of diffusion is slow. Thus, by intuition the system is not state controllable but may be output controllable. However when considering a diffusion process, it is impossible to obtain a output concentration distribution with sharp concentration variations such as an exactly piece-wise constant output concentration. The state controllability and the output controllability of the system are formally tested with the rank test specified in Section 2.6. As the state transition and the control input matrices in the state equation (4.1) are stationary, the state controllability matrix (2.106) and the output controllability matrix (2.108) are computed in Chapter 5. However, it is worth emphasizing that even if all the states were controllable, the desired state is reached within a finite time N. Thus, during the time $[0, N-1]$ the state may be far from the desired state. This inference is valid also for the output.

Correspondingly, when considering intuitively the observability of the system, it can be noted that the measurement system can observe only the states downstream of the first and upstream of the last EIT electrodes in the pipe. However, the concentration in regions upstream of the first electrode pair and downstream of the last electrode pair can be estimated as the evolution model provides information about the process in those regions. Furthermore, as the reconstruction problem in nonstationary EIT is highly underdetermined (i.e. the number of states is far greater than the number of measurements), the system is typically not observable in the classical sense. As the observation model (4.2) is nonlinear, a simple approach to formally test the observability of the system is to use the globally linearised observation model (3.63) and compute the observability matrix (2.109), see Chapter 5.

It should be noted that although the system might not be controllable and/or observable in the classical sense, one may be able to control it up to a point. In fact, one of the aims of this thesis is to determine if it is even possible to control a CD process using EIT observations when the associated state-space system is clearly neither state controllable nor observable.

4.2.5 Computational issues

When controlling processes involving rapid variations, the controller must obtain information frequently about the process in order to be able to respond to undesirable situations. Consequently, the time between EIT measurements should be short. As the aim is to design a real time controller, in the time between the consecutive EIT measurements one must be able to process the measurements as well as to compute the state estimate and the control input. As the state dimension is typically very high in the case of PDE-based DPSs, the state estimation and control algorithms must be very efficient. An essential fact when considering the algorithms is that all possible computations are performed off-line prior to the actual operation of the control system.

In the EIT observation model (3.61), the mapping $\tilde{R}_t$ depends on the current pattern $\mathcal{I}_t$. In this thesis, 16 different current patterns are used repeatedly. For example, $\mathcal{I}_1 = \mathcal{I}_{17}$. Consequently, the mappings $\tilde{R}_t$ corresponding to times $t = 1$ and $t = 17$ are identical. In the globally linearised Kalman filter, the mapping $\tilde{R}_t$ is linearised around a linearisation point c_{lp}. The Jacobians $\mathcal{J}\tilde{R}_t$ of the mappings $\tilde{R}_t$ can be computed prior to data acquisition and stored. Corresponding to the equal current patterns $\mathcal{I}_1$ and $\mathcal{I}_{17}$, for example, the Jacobians for times $t = 1$ and $t = 17$ are equal. Thus, one has to store only 16 Jacobians. Given the initial covariance matrix $\Gamma_{1|0}$ and the Jacobians $\mathcal{J}\tilde{R}_t$, also the covariance matrices $\Gamma_{t|t}$ and $\Gamma_{t|t-1}$ as well as the Kalman gains F_t can be computed prior to data acquisition. It should be noticed that the measurements g_t affect only the measurement update equation (2.43). Storing also the covariance matrices and Kalman gains may be inconvenient, if the process is run for a long time (that is, t is large). However, one actually needs to store only the asymptotic covariance matrices and Kalman gains corresponding to different current patterns. By asymptotic covariances and Kalman gains one means the matrices to which the covariances $\Gamma_{t|t}$ and $\Gamma_{t|t-1}$ and the Kalman gains F_t converge for each current pattern after sufficiently many Kalman filter recursions.

In this thesis, the employed current patterns are not optimised in any way. In [141], a single optimized current pattern was found to be sufficient in a particular nonstationary EIT application. In the case of a single current pattern, the precomputations and the number of matrices to be stored is decreased further from the case described in this thesis.

The iterated extended Kalman filter does not allow any precomputations. Due to the inner iteration required for the minimisation of the

functional (2.54), the Jacobians $\mathcal{J}\tilde{R}_t$ and the Kalman gains F_t have to be recomputed several times for each time $t \in \mathbb{N}_0$. Furthermore, the covariance matrices $\Gamma_{t|t}$ and $\Gamma_{t|t-1}$ have to be recomputed at each $t \in \mathbb{N}_0$.

The most time-consuming part of the approximate LQG control law computation is the computation of the solution of the Riccati equation (2.24). If the final time $N \to \infty$, and the state transition matrix and the control input matrix are stationary, that is, $A_t = A$ and $B_{2,t} = B_2$, then P_t in (2.24) converges to a steady-state solution P. As a result, also the LQG feedback gain matrix K_t defined in (2.22) is stationary, that is, $K_t = K$ for all $t \in \mathbb{N}_0$. The steady-state matrices P and K are used in the simulations in Chapter 5.

In the approximate $\mathcal{H}_\infty$ control law computation, the use of the steady-state solution of the Riccati equation (2.79), that is, $Z_t = Z$ leads to stationary matrices $K_{u,t} = K_u$, $K_{uw,t} = K_{uw}$, $K_{w,t} = K_w$, $\bar{A}_t = \bar{A}$, $V_{12,t} = V_{12}$, and $V_{21,t} = V_{21}$. The stationary matrices can be precomputed off-line and they are used in the simulations in Chapter 5. Especially, the precomputation of Z reduces the on-line computational load substantially. By contrast, as the $\mathcal{H}_\infty$ observation matrix $C_{2,t}$ is nonstationary, the Riccati equation (2.80) must be computed recursively on-line. It should, however, be noticed that $C_{2,t}$ depends on time only through the current pattern $\mathcal{I}_t$. Therefore, the steady-state solutions could be computed for each different current pattern which would reduce the computational burden.

4.3 POTENTIAL INDUSTRIAL APPLICATIONS

In this section, several industrial processes to which the control system described in Section 4.2 could be applied are discussed. Although the process model derived in Chapter 3 does not fully describe any existing real industrial process and the control system designed does not fully correspond to any existing control system, the basic idea of the designed control system can be adopted with required modifications to controlling many different kind of industrial processes. In this section, the focus is on three industrial processes. The separation and mixing processes encountered especially in the chemical and mineral industries and the web forming processes (also referred to as film and sheet forming processes) are considered.

The separation and mixing processes are selected as examples since those processes have been successfully monitored with electrical PT (references are given below). Furthermore, suitable actuation mechanisms for

those processes can be designed even though the actuation mechanism is not necessarily the same as the one described in Section 4.2.1. The web forming processes are selected as examples since the two-dimensional dynamics of the example application discussed in this thesis is somewhat similar to the dynamics of these processes.

The discussion is broadened from processes featuring a single-phase flow that is considered in this thesis to processes featuring multiphase flows to show the variety of potential applications. Furthermore, the actuation mechanism and the control variable described in Sections 4.2.1 and 3.1.3, respectively, are suitable only for special kind of processes and, thus, examples of other possibilities are given. The separation and mixing processes discussed in this section are monitored with electrical PT techniques unless mentioned otherwise and process control is not considered in any of the given publications. By contrast, the web forming processes discussed in this section are not monitored with EIT and various control systems for those processes have been proposed.

The separation of components of different phases in multiphase flows is encountered not only in chemical and mineral industries but also in other fields. The two widely used separators for solid-solid and solid-liquid separation in a liquid continuum are the hydrocyclones and the dense medium cyclones [212], [12]. The hydrocyclones are also applicable in liquid-liquid separation provided that the liquids have different densities such as oil and water in a deoiling process [187]. Typically, the hydrocyclones and the dense medium cyclones consist of one or more feed inlets and two outlets (overflow and underflow). While operating a vortex, sometimes an air core is formed inside the separator. The average diameter and the dynamic oscillation of the air core is stated to reflect the efficiency of the separator. As a consequence, the performance of the separator can be controlled by adjusting the operational parameters that are known to affect the formation of the air core. For solid-liquid separators, such parameters include, for example, the feed flow rate and the concentration of the solid particles in the feed. In the deoiling hydrocyclones, the control variable, that is adjusted to neutralise the air core, could be selected as the feed flow rate of the oily water, the concentration of oil in the mixture, or the back pressure of the hydrocyclone underflow.

In mixing processes, the objective is to produce a homogeneous mixture of two or more components of a similar or dissimilar phase. There are various types of industrial mixing processes including mixing of miscible liquids, solid-liquid mixing, and gas-liquid mixing. The mixing in such processes is typically executed in a tank, in a stirred vessel, or in a

pipeline. The contents can be mixed with impellers, jets, or tees. When mixing with impellers, rotating impellers are placed in a stirred vessel or in a tank. The basic principal in jet mixing encountered in mixing processes involving liquids is that a fast moving jet stream of liquid is injected into a slowly moving or stationary bulk liquid. The injected liquid can either be an additional chemical or a part of the original liquid drawn through a pump and returned as a high-velocity jet back to the mixture. The tee mixers include side tees and opposed tees. A side tee mixer is formed by two pipe sections joined at a suitable angle and, thus, resembles the jet mixer. In an opposed tee mixer, two streams enter from opposite directions, mix as they converge, and leave through a pipe that is perpendicular to the pipes from which the streams enter.

The mixing of miscible liquids in a pipeline is required for example when additional chemicals are injected via jets into the main stream. In [213], [143], [214], [215], mixing of miscible liquids was successfully monitored with EIT. A more specific application is a system for mixing of paper making chemicals into the main process stream [216], [215]. The chemical is fed into the main stream via a jet injection mixer system by exploiting a high speed injection stream. In [215], an EIT system was applied to imaging the efficiency of mixing of such a system. The injection points as well as the EIT electrodes were located on the pipe boundary. In such a case, the flow rate of injectors and/or the concentration of the injected solution could be controlled to achieve a homogeneous mixture. Furthermore, controlling the angle of the jet stream could improve the quality of mixing.

In addition to mixing of miscible fluids in a pipeline, the mixing of components of a similar or dissimilar phase in a stirred vessel has been studied in the case of EIT. In [217], [6], [218], [219], [220], the mixing of miscible liquids in a stirred vessel was considered when EIT was used for process monitoring. The solid-liquid [182], [10] and gas-liquid mixing [121], [221], [222], [204] in a stirred vessel have also been successfully monitored with EIT. In the above-mentioned processes involving mixing in a stirred vessel, controlling the impeller speed could improve the quality of mixing. Furthermore, if addition of extra liquid or gas is required, the amount (and in some cases the concentration) of the injected component could be selected as the control variable.

Also additional baffles could be placed inside a pipeline, a stirred vessel, or a tank and the position of the baffles could be controlled in order to direct the fluid and, thereby, to homogenize a mixture. When considering, for example, the CD process discussed in this thesis, the baffles

would change the velocity field inside the object and, actually, one would control the concentration by controlling the velocity field. However, the dependence of the concentration and the velocity field in the CD model is nonlinear and, thus, the control problem would also be nonlinear.

Many mixing processes involve simultaneous local chemical reactions. If one considers, for example, a CD process involving a chemical reaction, the process could be described with a convection-diffusion-reaction (CDR) model taking into account both the changes of concentration of some chemical substances and the chemical reaction. The (coupled) CDR systems have been used for simulating, for example, the dynamic behaviour of fluidized bed and packed bed reactors [26], [223], [224], chemical reactions in chaotic flows [225], and precipitation processes [226]. In the above-mentioned publications, EIT was not used. The process described in this thesis could be expanded to cover also chemical reactions. To give an example, if the fluid consists of several substances that are involved in chemical reactions, the behaviour of each substance could be modelled with the CDR equation that are dependent with respect to the chemical reactions. The injections could consist of one or more components of the fluid aiming for a homogeneous mixture. This would naturally lead to a more complicated process model and extended processing times.

In addition to EIT, there are also other methods to determine concentration variations in chemical processes. For example in [227], [228], [229], chemical species tomography was considered. In [227], [228], imaging of hydrocarbon concentration distribution and mixing within a combustion chamber was investigated using near infra-red absorption tomography. In [229], magnetic resonance measurements were used in determining the distribution of species in a multi-component flow. Controllers for such processes could be also designed.

Some specific processes such as the web forming processes [33], [190], [230] are essentially two-dimensional distributed parameter processes that have some similarities to the example process of this thesis. The web forming processes include for example paper making [231], [232], [230], polymer film extrusion [33], and a wide range of coating processes. In the web forming process, a delivery mechanism supplies material through a narrow slit to form a continuous web [33]. The material is moving downstream of the delivery mechanism. The properties of the material being controlled vary in two-dimensions over the surface of the material web. The control system, referred to as a cross-directional control system, aims to regulate the nonstationary property of the material and, thus, to increase the uniformity of the final product. In the web forming processes,

the sensing system is usually an array of static sensors or a single sensor moving back and forth along the material web. An array of actuators is located across the web at the start of the process upstream of the sensor(s). Typical features of the web forming processes are that they are high dimensional DPSs, there are constraints on the actuator inputs, and the development of high-quality models for such processes is a challenging task.

In paper making, the important process properties are basis weight, moisture, calliper, and coat weight. For each of these properties specific control systems can be designed, see [230] for a detailed review. For example, the basis weight control system aims to distribute the fibres evenly over the width of the headbox using either slice lip actuators or dilution actuators. The dilution actuators change the consistency of the pulp stock with a flow of low consistency water and, thus, locally reduce the basis weight. The flow rate of actuators is adjusted on the basis of the measurements. In the polymer film extrusion, the thickness of the film can be controlled with a heater set which continuously vary the thermal properties of the material web [33].

4.4 DISCUSSION

In this chapter, a control system for the CD process was designed. Two controllers, the approximate LQG controller and the approximate $\mathcal{H}_\infty$ controller, were formulated. The formulation of the approximate controllers followed the formulation of the basic controllers shown in Chapter 2 with the exceptions of the feedforward element introduced in the context of the approximate LQG controller and the new state variable in the context of the approximate $\mathcal{H}_\infty$ controller. Without these elements, the performance of the controllers would naturally be inadequate.

In industrial processes, the actuators may have physical constraints. In the example application considered in this thesis, several physical constraints on the injectors need to be considered. Firstly, the injectors can only add substance to the flow. Secondly, the flow rate of an injector has a maximum value depending on the injection mechanism. Thirdly, it may not be possible to adjust the injection rate fast enough for extremely fast processes. The first two physical constraints result in a nonlinear and constrained actuation mechanism. In general, the constraints on control inputs, states, and outputs are difficult to implement in the LQG framework. In this thesis, only the first constraint was taken into consideration

in the LQG control and it was handled in a straightforward manner as explained in Section 4.2.2. Another sub-optimal and one of the simplest manners to handle the first two constraints would be to choose the parameters when defining the weighting matrices in the cost function so that the values of the control inputs lie within a required range. Furthermore, the constraints could be included more formally using model predictive control (MPC).

The third constraint on injectors is related to the response of the injectors. Specifically, the dynamic response of the injectors has to be faster than the dynamic response of the process in order to compensate for the unwanted events in time. The dynamic response of processes involving fast moving fluids is mainly determined by the convection rate of the flow. The effect of diffusion is often less significant. The dynamic response of the injectors depends on the speed of the actual flow valve adjusting the injection rate. In practice, this constraint sets high demands on the development of the flow valve.

A problem when monitoring industrial processes with EIT is that typically the domain of interest, whether it is a pipeline, a vessel, or a tank, is made of electrically conducting metallic material. In such a case, the domain acts like a large electrode, and the injected current leaks away through the wall. In order to overcome the problem of conducting boundaries, the electrodes in industrial processes must be located on the inner boundary of the domain [1]. Thus, the electrodes are invasive as they penetrate the domain boundary but non-intrusive. However, the invasive electrodes alone do not solve the problem, and, therefore, additional methods are needed. In [123], several approaches to handle the problem were reviewed. For example, the domain boundaries can be composed of an electrically non-conducting material or the electrodes can be electrically insulated. The latter approach may, however, lead to reconstructions of poor quality. Furthermore, a grouped-node technique developed in [123] can be applied to model the conducting wall of the domain.

The questions of how many EIT electrodes are needed and where to place them depend on the process. When the object of interest is a tank, a stirred vessel, or a pipeline, the electrodes are typically arranged in several layers on the object boundary. It is stated that in such a case the state estimation accuracy is the highest in the middle region of the area covered by the sensors. Recently, a novel approach of using only a single electrode layer was proposed [113]. Furthermore, additional internal electrodes could be placed inside the object to improve the quality of the EIT data provided that it suits the characteristics of the pro-

cess [233], [234], [235], [236], [237]. For web forming processes, for example, a different arrangement of electrodes is needed. An arrangement with electrodes at the edges of the web would likely be inappropriate.

The placement of the injectors depends on the considered process. For web forming processes, the injectors are located in a line across the web. For mixing processes, the injectors are located on the domain boundary. A challenge when boundary injectors are used is how to get the concentrate into the middle regions of the pipe effectively. In Section 5.3, the simulation results indicate that it is possible to achieve adequate control performance with boundary injectors if the flow rates of the injectors are high enough. The high flow rates, however, affect the velocity field inside the pipe and the velocity field becomes nonstationary and dependent of the flow rates. This fact needs to be addressed in the process modelling. Also the location of the injectors with respect to the EIT electrodes and the output boundary has an influence on the control performance. The concept of injector placement in a specific application is considered in Section 7.

If the controller and the observer are based on a spatial discretisation of the PDE models, properties like controllability and observability may depend on the discretisation method and on the number and the locations of the discretisation points. However, if the discretisation is done properly and the finite-dimensional model is a good approximation of the infinite-dimensional model, then the analysis of the finite-dimensional model generally yields adequate information about the properties of the infinite-dimensional system. In Section 4.2.4, the controllability and the observability analysis of the system was discussed on the basis of the finite-dimensional approximations of the infinite-dimensional models. One could also consider the controllability and observability of the infinite-dimensional models in the case of an infinite-dimensional controller. A theoretical controllability and observability analysis of the state-space model consisting of the CD state equation and the EIT observation equation as in this thesis could be based on the formulation of the model in [186].

5 Simulations using approximate linear quadratic Gaussian controller

In Chapter 4, a control system for monitoring and controlling a convection-diffusion (CD) process on the basis of electrical impedance tomography (EIT) observations was designed. The aim of the control system was to control the concentration distribution of a chemical substance in a fluid flow over a cross-section at a particular point of a pipeline. In this chapter, the performance of the designed control system is evaluated with numerical simulations when the controller is the approximate linear quadratic Gaussian (LQG) controller. The simulations are executed in the Matlab® platform.

In Section 5.1, two-dimensional simulation results when the approximate LQG controller is utilized are presented and the robustness of the controller is tested [53], [54], [44], [57]. In Section 5.2, the performance of the approximate LQG controller is evaluated with three-dimensional simulations. In Section 5.3, boundary actuators are used and the velocity field inside the pipe changes due to the boundary injections [56]. In Section 5.4, the effects of two different state estimators, the globally linearised Kalman filter and the iterated extended Kalman filter, on control performance are compared [55].

5.1 TWO-DIMENSIONAL APPROXIMATE LQG CONTROLLER SIMULATIONS

Firstly in this section, the simulation of the concentration evolution corresponding to the actual process in practical implementations is considered. Secondly, the simulation of the EIT observations corresponding to the observations obtained from the EIT measurements in practical implementations is considered. Thirdly, the computation of the concentration estimates and the control inputs using the globally linearised Kalman filter and the approximate LQG controller, respectively, is considered.

The simulation of the concentration evolution, the simulation of the EIT observations, and the computation of the control inputs are not separable (see Figure 5.1) although they are considered separately. For the simulation of the concentration evolution, one needs the control inputs.

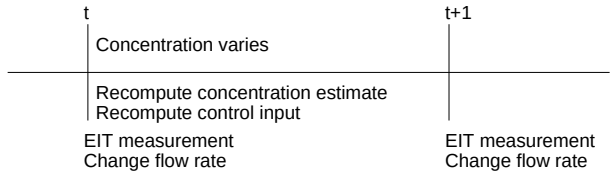

Figure 5.1: The timeline of the control process.

The flow rates of the injectors change only at the measurement times. It should be noted, however, that the concentration varies during the time between the EIT measurements. When computing the control input corresponding to a measurement time, one needs the estimate of the concentration distribution corresponding to that time. For the computation of the concentration estimate, one needs the simulated EIT observation. And finally for the simulation of the EIT observation, one needs the concentration distribution corresponding to the measurement time.

5.1.1 Simulation of the concentration evolution

In the two-dimensional simulations, a finite segment of a pipe illustrated in Figure 4.1 is considered. The pipe width is 10 cm and the pipe length 40 cm. The spatial and temporal variations of the concentration in the pipe are modelled with the CD model (3.1)-(3.5) where $\vec{r} \in \mathbb{R}^2$. The concentration variations in the fluid are mainly due to low concentration inclusions entering the pipe through the boundary Λ_{in}. The concentration on the boundary Λ_{in} is modelled with the input concentration (3.5). In this section, the motion of fluid is modelled with the stationary incompressible Navier-Stokes equations (3.10)-(3.11).

The concentration evolution in the pipe is simulated using the finite-dimensional approximation of the CD model. The finite element method (FEM) is employed to obtain the finite-dimensional approximation. In the finite-dimensional approximation of the concentration, the basis functions are piecewise linear functions (piecewise 1^{st} order polynomial functions). The finite element (FE) mesh used in the approximation is shown in Figure 5.2(a). For the backward Euler method, one needs to select a suitable time step in order to obtain an accurate numerical solution of the CD model. A suitable time step Δt can be chosen on the basis of prior knowledge or from a set of simulations. In this thesis, $\Delta t = 2.5$ ms is chosen from a set

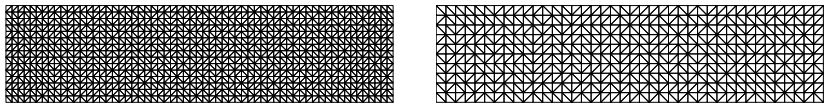

(a) (b)

Figure 5.2: The finite element meshes for approximating the CD model. (a) The mesh employed when constructing the evolution model for the simulation of the concentration evolution. (b) The mesh employed when constructing the evolution model for the state estimator and the controller.

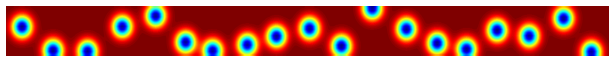

Figure 5.3: The input concentration.

of simulations by trial and error.

The finite-dimensional approximation of the input concentration is shown in Figure 5.3 in which dark blue indicates low and dark red high concentration. The concentration of the homogeneous background is 5.0×10^{-3} mol^{-1}cm^2 and the minimum value of the concentration in the low concentration inclusions is 2.5×10^{-3} mol^{-1}cm^2. Time evolves from right to left. A vertical cross-section in Figure 5.3 corresponds to the concentration on the boundary Λ_{in} at one time instant.

The solution of the Navier-Stokes equations (3.10)-(3.11) is the parabolic velocity field

$$\vec{v}_{\vec{r}_1}(\vec{r}) = \frac{3}{2} v_{\vec{r}_1,\text{mean}} \left[1 - \left(\frac{|\vec{r}_2 - \vec{r}_{2,0}|}{\tilde{r}} \right)^2 \right], \qquad \vec{v}_{\vec{r}_2}(\vec{r}) = 0 \tag{5.1}$$

where $v_{\vec{r}_1,\text{mean}}$ is the spatial average of the velocity in the horizontal direction of the pipe, $\vec{r}_{2,0}$ is the $\vec{r}_2$-coordinate of the pipe center, and $\tilde{r}$ is the pipe width. In the simulations, the average velocity is selected to be $v_{\vec{r}_1,\text{mean}} = 50$ cms^{-1} and the diffusion coefficient $\kappa = 5$ cm^{2}s^{-1}. The velocity field (5.1) is depicted in Figure 5.4. Assuming that the fluid is saline and taking into account the pipe diameter, it is noted that with the selected spatial average of the velocity the flow is actually turbulent (the Reynolds number is of order 10^4) and the true velocity profile is neither stationary nor parabolic. The effects of turbulent mixing (and other temporal changes in the velocity) are modelled by increasing the diffusion

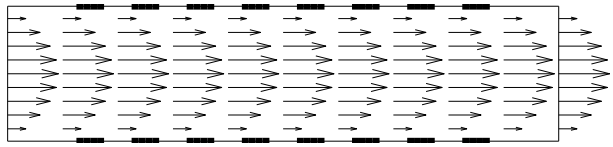

Figure 5.4: The parabolic velocity field.

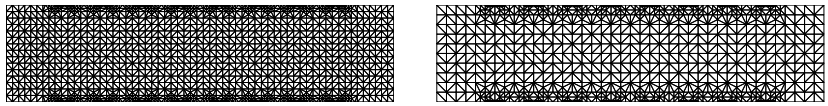

(a) *(b)*

Figure 5.5: The finite element meshes when approximating the CEM. (a) The mesh employed when constructing the observation model for simulating the measurements. (b) The mesh employed when constructing the observation model for the state estimator and the controller.

coefficient κ [98].

5.1.2 Simulation of the EIT observations

The EIT observations are modelled with the complete electrode model (CEM) (3.29)–(3.34) where $\vec{r} \in \mathbb{R}^2$. The finite-dimensional approximation of the CEM is used when simulating the observations and it is obtained with the FEM. The mesh used in the FEM is illustrated in Figure 5.5(a). The EIT mesh is refined in the subregions near the electrodes where the electric potential is known to have rapid changes. The refinement of the mesh in those regions reduces substantially the errors that result from the spatial discretisation. In the finite-dimensional approximation of the electric potential, the basis functions are chosen as piecewise 2^{nd} order polynomial functions. By contrast, the conductivity is approximated using piecewise linear functions.

In the simulations, the currents are injected between opposite electrodes. As illustrated in Figure 5.6 in this thesis, the concept of opposite has a slightly different meaning in comparison to other implementations. The dashed lines connect the opposite electrodes. Firstly, the current is injected between the first and the ninth electrode, secondly between the second and the tenth electrode and so forth. The voltages corresponding

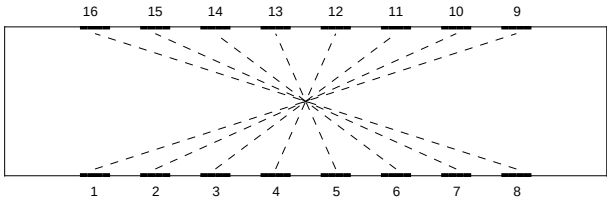

Figure 5.6: The opposite electrode pairs.

to one current injection are measured between all opposite electrode pairs. Consequently, 16 voltage measurements are made corresponding to one current injection.

In this thesis, the time between the current injections Δt_{EIT} is selected as 50 ms. Hence, the concentration moves 2.5 cm on average during the time between the consecutive current injections due to the flow. All the voltage measurements corresponding to each current injection are executed simultaneously and instantly, so that the concentration is taken to be non-varying during that time.

The voltages corresponding to 64 current injections are simulated. The voltages are corrupted with observation noise. The observation noise is assumed to be zero-mean and Gaussian. The noise consists of two components. Firstly, noise with standard deviation of 1% of the value of an individual observation is added to that observation. Secondly, noise with standard deviation of 0.1% of the voltage range, that is, the difference between the maximum and the minimum voltage is added to all observations. This is a more or less standard error model of practical EIT measurement systems.

5.1.3 Construction of the state estimator and the approximate LQG controller

The objective of the controller is to obtain a uniform concentration distribution over the boundary Λ_{out} when there are nine injectors located across the pipe (see Figure 4.1). The desired output concentration (5.1×10^{-3} $\mathrm{mol}^{-1}\mathrm{cm}^2$) is selected to be higher than the concentration of the homogeneous background (5.0×10^{-3} $\mathrm{mol}^{-1}\mathrm{cm}^2$). As a consequence, the controller has to take into account the concentration variations due to the low concentration inclusions and even if there are no inclusions to increase

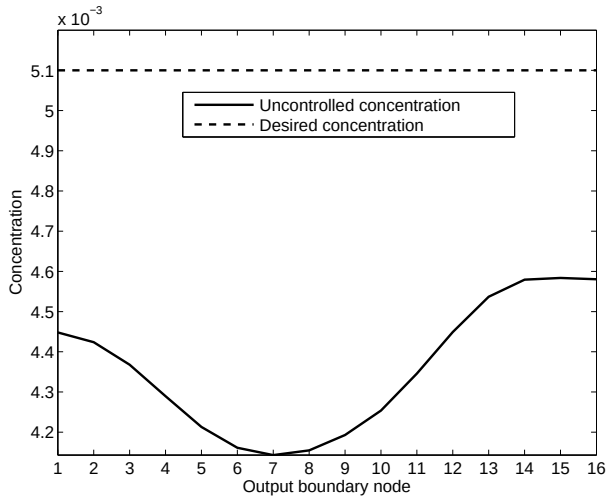

Figure 5.7: The uncontrolled concentration distribution and the desired concentration distribution over the boundary Λ_{out} as an inclusion passes the boundary.

the output concentration so that it matches the desired output concentration. In Figure 5.7, the concentration distribution over the boundary Λ_{out} is depicted at time $t = 1.70$ s. The concentration distribution corresponds to a situation when a low concentration inclusion passes the boundary Λ_{out} and control is not employed. Also, the desired uniform distribution is plotted. The concentration distribution at the entire pipe at that time is visualised in Figure 5.8(a).

For the construction of the globally linearised Kalman filter and the approximate LQG controller, a finite-dimensional approximation of the CD model (3.1)-(3.5) and of the CEM (3.29)–(3.34) is needed. When approximating both the CD model and the CEM with the FEM, coarse FE meshes illustrated in Figures 5.2(b) and 5.5(b) are employed in the spatial discretisation. The use of the same meshes as in the simulations of the concentration evolution and the EIT observations would lead to unrealistically good estimates. The use of different meshes (models) is a standard procedure to avoid the unrealistically good results in the control theory and in the inverse problems theory. In order to operate with different meshes, interpolation between meshes is required. In this thesis, the linear interpolation method is used. The sizes of the FE meshes are given in Table 5.1 in which the number of nodes and elements for each FE mesh

Table 5.1: Number of nodes and elements in the FE meshes used for approximating the CD model and the CEM in two-dimensional simulations. The abbreviation CDM refers to the CD model. The term "actual" refers to the FE meshes used for approximating the models for the simulation of the concentration evolution and the EIT observations. The term "inverse" refers to the FE meshes used for approximating the models for the construction of the state estimator and the controller.

	Nodes	Elements
CDM actual	992	1830
CEM actual, 1$^{\text{st}}$order basis functions	1346	2440
CEM actual, 2$^{\text{nd}}$order basis functions	5131	2440
CDM inverse	451	800
CEM inverse, 1$^{\text{st}}$order basis functions	707	1248
CEM inverse, 2$^{\text{nd}}$order basis functions	2661	1248

is listed. The mesh sizes and, consequently, the computational load in the two-dimensional simulations are moderate.

When approximating the solution of the CD model with the FEM, the input concentration (3.5) is (partly) unknown. The input concentration is approximated with a uniform concentration distribution the level of which equals the concentration of the homogeneous background.

Once the discrete-time state-space model (4.1)–(4.2) is obtained, the controllability and the observability of the numerical system are tested by computing the state controllability matrix (2.106), the output controllability matrix (2.108), and the observability matrix (2.109). The globally linearised observation model (3.63) is used when testing the observability. The rank tests indicate that the system is neither state controllable nor observable. This fact is also intuitively clear. By contrast, the numerical system is output controllable. However, the required sequence of control inputs that transfers the output to a desired output may not be applicable in practice (negative and unrealistically large entries).

For the globally linearised Kalman filter, the covariance matrices $\Gamma_{w_{1,t}}$ and Γ_{v_t} as well as the initial state c_0 and the initial covariance matrix $\Gamma_{0|0}$ are selected as follows. Let $c_{\text{bh}} \in \mathbb{R}^{n_\varphi}$ denote a constant vector whose entries equal the concentration of the homogeneous background $\beta_{\text{bg}} = 5.0 \times 10^{-3}$ mol^{-1}cm^2. The structure of the state noise covariance matrix $\Gamma_{w_{1,t}}$ is described in Appendix A. The computation of $\Gamma_{w_{1,t}}$ requires the specification of the matrices Γ_{η_t} and Γ_{ξ_t}. It is assumed that the input noise

covariance matrix is $\Gamma_{\eta_t} = \beta_\eta^2 I$ where the standard deviation β_η is selected to be the presumed standard deviation of the input concentration $c_{\text{in},t}$ so that $\beta_\eta = \frac{1}{8} \times \beta_{\text{bg}}$. The nodal noise covariance matrix $\Gamma_{\xi_t} = \beta_\xi^2 I$ where the standard deviation $\beta_\xi = \frac{1}{40} \times \beta_{\text{bg}}$.

The observation noise consists of two components as explained above. However in this thesis, the observation noise covariance matrix is $\Gamma_{v_t} = \beta_v^2 I$ where the standard deviation β_v is taken to be 0.1% of the voltage range. Such an approximation is shown to be adequate. Furthermore, the initial covariance matrix is $\Gamma_{0|0} = (\frac{1}{10})^2 I$ and the initial concentration is $c_{0|0} = c_{\text{bh}}$. Often, the initial concentration is not known. To take into account the uncertainty of the initial state, the initial covariance is set relatively large. Thus, the uncertainty is reflected in the variances of the first estimates, but the transition effect fades out soon.

When using the approximate LQG controller described in Section 4.2.2, the weighting matrices should be selected. Feasible scalars β_Q and β_R are determined from simulations that are different from the simulation study the results of which are shown in this section.

5.1.4 Two-dimensional simulation results using the approximate LQG controller

The effect of control on the process is illustrated in Figure 5.8. In Figure 5.8(a), the uncontrolled concentration evolution is shown. When simulating the uncontrolled concentration evolution, the control term is omitted from the CD model. In Figure 5.8(b), the change in the concentration due to the injected concentrate is shown. In the simulation of the concentration change, the input concentration $c_{\text{in}} = 0$. Thus, the finite-dimensional model for the concentration change is

$$c_{\text{c},t+1} \quad = \quad A c_{\text{c},t} + B_2 u_t \tag{5.2}$$

where $c_{\text{c},t} \in \mathbb{R}^{n_\varphi}$ and $c_{\text{c},0} \in \mathbb{R}^{n_\varphi}$ is a zero vector. In Figure 5.8(c) and 5.8(d), the controlled concentration evolution and the globally linearised Kalman filter estimates of the controlled concentration are shown, respectively.

Especially from the last four subfigures corresponding to times $t = 1.65, ..., 1.80$ s in Figure 5.8(d), it can be seen that the low concentration inclusions cannot be observed at the beginning of the pipe. At those times, the current is injected between electrodes that are located in the middle of the pipe (at time 1.75 s between the third and the eleventh electrode and at time 1.80 s between the fourth and the twelfth electrode). Overall, the

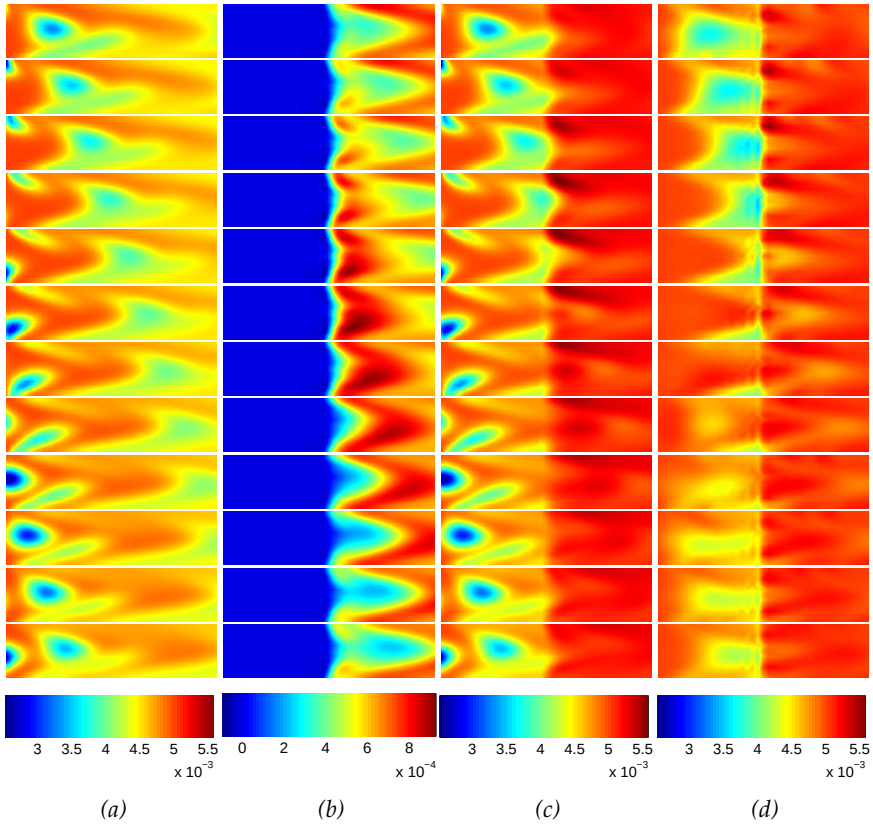

Figure 5.8: (a) The uncontrolled concentration evolution, (b) the change of concentration, (c) the controlled concentration evolution, and (d) the globally linearised Kalman filter estimates of the controlled concentration at times $t = 1.25, 1.30, \ldots, 1.75, 1.80$ *s.*

estimates, however, provide the controller with adequate information on the process. Consequently, when a low concentration inclusion passes the array of injectors, the flow rates of injectors are increased. This can be seen particularly at times $t = 1.35, ..., 1.60$ s in Figure 5.8. As a consequence of the injections, the concentration over the boundary Λ_{out} is regulated and it matches the desired concentration quite well.

The uncontrolled concentration and the controlled concentration over the boundary Λ_{out} are shown in Figure 5.9 in which the concentration values on the FE nodes on Λ_{out} are plotted at each time t. In Figure 5.10, the predicted output concentration is plotted. By predicted output

concentration one means the globally linearised Kalman filter predictions (see Equation (2.40)). It should be noticed that when computing the FE approximation for the controlled concentration and the predicted concentration, the FE meshes are of different size (see Table 5.1). Thus, the number of the FE nodes on Λ_{out} is also different. When comparing Figures 5.9 and 5.10, it can be seen that the predicted output concentration is lower than the actual output concentration. This leads to control inputs that are larger than would actually be required and the controlled output concentration is at some time instances above the desired output concentration. However, it can be stated that the controlled output concentration matches quite adequately the desired output concentration.

Furthermore, the control performance of the system is evaluated with a function

$$\delta(t) = \left(\int_{\Lambda_{\text{out}}} |y_{\text{ref}}(\vec{r}, t) - c_{\text{out}}(\vec{r}, t)|^2 \mathrm{d}S \right)^{\frac{1}{2}} \tag{5.3}$$

where the constant function $y_{\text{ref}} : \Lambda_{\text{out}} \times \mathbb{R}_+ \to \mathbb{R}$, $y_{\text{ref}} = y_{\text{ref}}(\vec{r}, t)$, is the desired output concentration. The function (5.3) is a measure of output (or tracking) errors, that is, the differences between the desired output concentration and the controlled output concentration. The integral (5.3) is computed using the FE approximation of the output concentration. The output errors for the uncontrolled and controlled output concentration are depicted in Figure 5.11. Also the output errors for the predicted output concentration are shown. The output errors for the controlled output concentration are notably smaller than the output errors for the uncontrolled output concentration. Furthermore, the output errors for the controlled output concentration are smaller than the ones for the predicted output concentration.

It can be seen from Figures 5.9 and 5.11 that there is an initial transient before the controller is able to bring the controlled output concentration close to the desired concentration. The length of the initial transient depends on the distance between the injectors and the output boundary. The closer the injectors are to the boundary Λ_{out} the shorter the length of the initial transient as the injected concentrate reaches the boundary Λ_{out} faster. In this case, the transient error decays to zero sufficiently fast.

5.1.5 Effects of mismodelling velocity fields

In this thesis, the robustness of the control system is examined with simulations in which the model for the fluid dynamics of the process is inac-

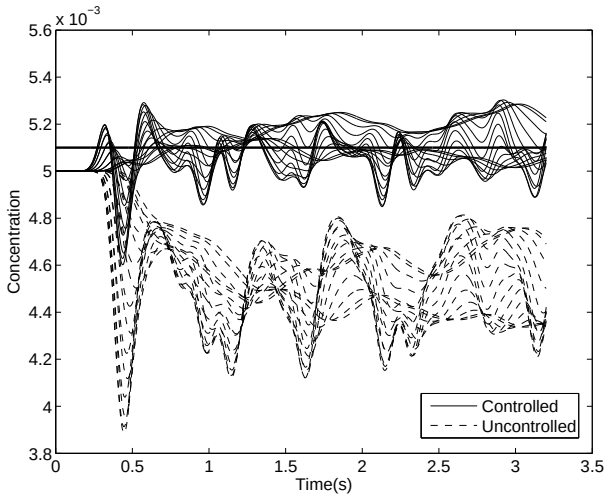

Figure 5.9: The uncontrolled concentration and the controlled concentration on the FE nodes on Λ_{out}. The thick black line indicates the desired output concentration.

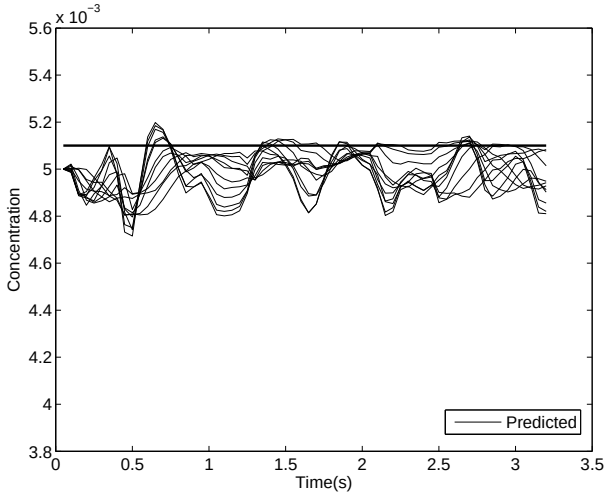

Figure 5.10: The predicted concentration on the FE nodes on Λ_{out}. The thick black line indicates the desired output concentration.

curate. When considering the control system designed in this thesis, it is

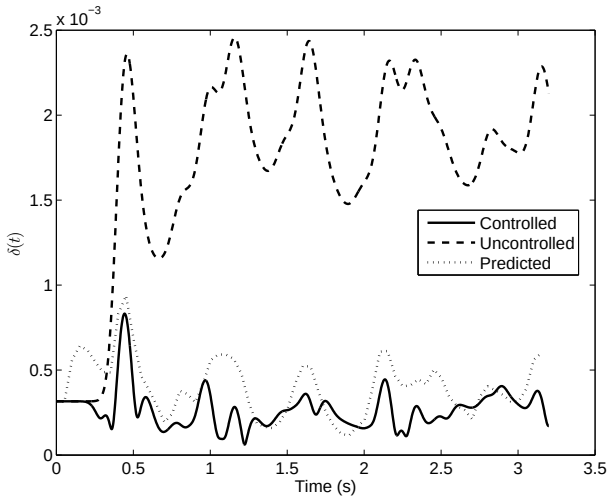

Figure 5.11: The output errors for the uncontrolled concentration, the controlled concentration, and the predicted concentration.

assumed that the main source of uncertainty is in the modelling of the velocity field. By contrast, the diffusion coefficient is assumed to be known relatively accurately. In the simulations, an inaccurate spatial average of the velocity in the horizontal direction is used in the CD model when constructing the globally linearised Kalman filter and the approximate LQG controller. Only the spatial average of the velocity is altered and the velocity profile is still parabolic. In [238], the effect of using an incorrect velocity field on the accuracy of the state estimates was investigated in a simulation study similar to the one presented in this section. However in [238], process control was not considered.

In the first robustness test, the inaccurate spatial average of the velocity is selected to be $v_{\vec{r}_1,\text{mean}} = 45$ cms^{-1} whereas the actual spatial average of the velocity is $v_{\vec{r}_1,\text{mean}} = 50$ cms^{-1}. Thus when simulating the concentration evolution, $v_{\vec{r}_1,\text{mean}} = 50$ cms^{-1} and when constructing the globally linearised Kalman filter and the approximate LQG controller, $v_{\vec{r}_1,\text{mean}} = 45$ cms^{-1}. In Figure 5.12, the uncontrolled output concentration and the controlled output concentration when the inaccurate spatial average of the velocity is used are plotted. Furthermore in Figure 5.12, the controlled output concentration when the accurate spatial average of the velocity is used is plotted for comparison. In Figure 5.13, the output

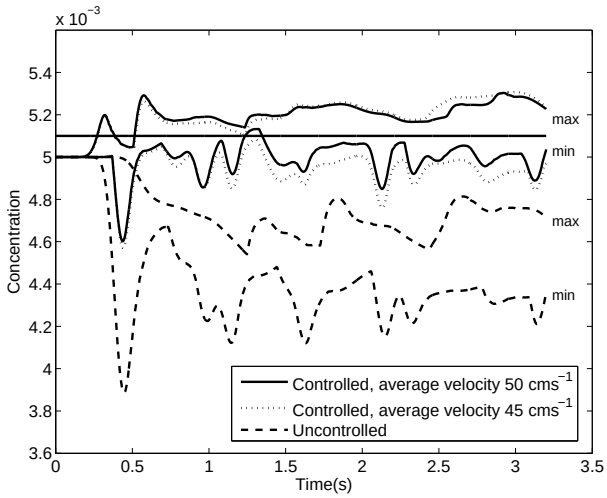

Figure 5.12: The minimum and the maximum value of the uncontrolled concentration and the controlled concentration on the FE nodes on Λ_{out} at each time when $v_{\vec{r}_1,\text{mean}} = 45$ cms^{-1} (incorrect) and $v_{\vec{r}_1,\text{mean}} = 50$ cms^{-1} (correct). Average velocity refers to the spatial average of the velocity $v_{\vec{r}_1,\text{mean}}$. The thick black line indicates the desired output concentration.

errors are presented. It can be seen from Figures 5.12 and 5.13 that the result with a slightly mismodelled velocity field is satisfactory.

In the second robustness test, a large error is applied to the spatial average of the velocity so that $v_{\vec{r}_1,\text{mean}} = 20\ \text{cms}^{-1}$. In Figure 5.14, the uncontrolled output concentration and the controlled output concentration are plotted when the inaccurate spatial average of the velocity $v_{\vec{r}_1,\text{mean}} = 20$ cms^{-1} is used when constructing the state estimation and the controller. Furthermore in Figure 5.14, the controlled output concentration when the accurate spatial average of the velocity $v_{\vec{r}_1,\text{mean}} = 50\ \text{cms}^{-1}$ is used is computed for comparison. In Figure 5.15, the output errors are presented. It can be concluded from Figures 5.14 and 5.15 that the control performance degrades considerably. However, the controller is still able to control the inhomogeneities up to a point. The explanation for the loss of control performance can be seen in Figure 5.16. In Figure 5.16(a), the evolution of the controlled concentration is represented. The globally linearised Kalman filter estimates of the controlled concentration are shown in Figure 5.16(b) and the evolution of the change in the concentration in Figure 5.16(c). It can be seen from the subfigures at times $t = 1.25, \ldots, 1.50$ (the top six

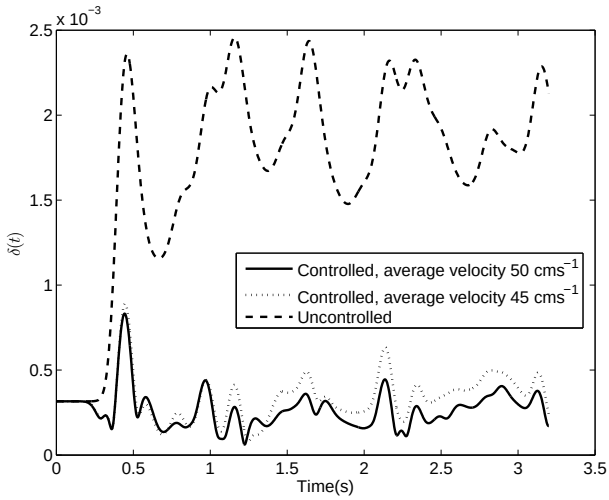

Figure 5.13: The output errors for the uncontrolled concentration and the controlled concentration when $v_{\vec{r}_1,\text{mean}} = 45\ cms^{-1}$ (incorrect) and $v_{\vec{r}_1,\text{mean}} = 50\ cms^{-1}$ (correct). Average velocity refers to the spatial average of the velocity $v_{\vec{r}_1,\text{mean}}$.

subfigures) that when the inaccurate (lower) spatial average of the velocity is used in the CD model, the inclusions are estimated to move slower than they actually do. Thus, the controller is operating on the basis of misinformation, and delays occur in injecting the strong concentrate. The selected times are equivalent to those shown in Figure 5.8 in which the results with the correct velocity field are shown.

5.1.6 Discussion of two-dimensional approximate LQG controller simulations

In Section 5.1, the performance of the approximate LQG controller designed for controlling a CD process was evaluated with two-dimensional simulations. The simulation results indicated that in this case it is possible to base an automatic and model-based controller on tomographic observations. It is noted that the output concentration exhibited some minor deviations from the desired output concentration but with only a finite number of pointwise injectors an uniform concentration distribution is difficult or even impossible to achieve.

In practical process control applications, there are inevitable distur-

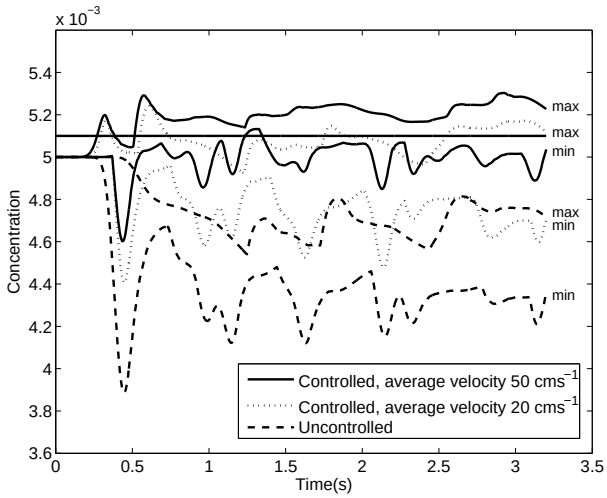

Figure 5.14: The minimum and the maximum value of the uncontrolled concentration and the controlled concentration on the FE nodes on Λ_{out} at each time when $v_{\vec{r}_1,\text{mean}} = 20$ cms^{-1} (incorrect) and $v_{\vec{r}_1,\text{mean}} = 50$ cms^{-1} (correct). The thick black line indicates the desired output concentration. Average velocity refers to the spatial average of the velocity $v_{\vec{r}_1,\text{mean}}$.

bance inputs. Such disturbance inputs include for example different kind of measurement and modelling errors. In this thesis, the partly unknown input concentration can be considered as a non-Gaussian disturbance input. The basic LQG controller can overcome the effects of zero-mean Gaussian disturbance inputs. Thus in order to control the CD process adequately with the approximate LQG controller, the input concentration was modelled as a stochastic function. By doing this, the uncertainty in the input concentration was taken into account. This kind of procedure actually made process control feasible in this example.

As the model-based control system is designed on the basis of a mathematical model of the process and if simplifying assumptions are made in process modelling, one can not automatically guarantee acceptable performance or even stability when implementing the controller in practice. For example, most flows in process control applications are turbulent and/or multiphase flows that can be challenging to model and, thus, approximations are sometimes used. Furthermore in high dimensional real time control problems, the computational load has to be minimized and model

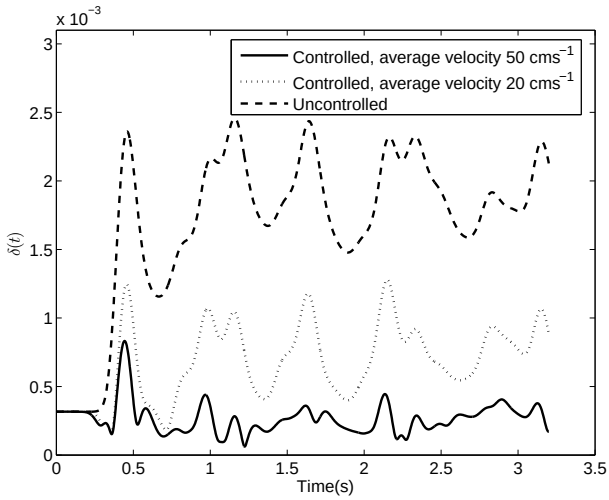

Figure 5.15: The output errors for the uncontrolled concentration and the controlled concentration when $v_{\vec{r}_1,\text{mean}} = 20\ cms^{-1}$ (incorrect) and $v_{\vec{r}_1,\text{mean}} = 50\ cms^{-1}$ (correct). Average velocity refers to the spatial average of the velocity $v_{\vec{r}_1,\text{mean}}$.

reduction is often considered. In such cases, by investigating the robustness of the control system, one is able to find out whether the control system is sensitive to inaccuracies in the process modelling. In Section 5.1.5, the robustness of the developed control system was tested with two sets of simulations. The results indicated that as long as the observations and the overall stochastic structure of the process dynamics are adequately accurately modelled, the state estimation and control schemes are relatively tolerant to misspecification of such quantities as the velocity field. These results are also supported by the results in [238] and [44]. One could also estimate such unknown quantities as the velocity field simultaneously with the concentration distribution as proposed in [239], [240]. However, such an approach is computationally demanding and could be challenging to implement in practical real time process control applications.

In this thesis, a homogeneous and stationary reference input was used since typically in practical industrial process control applications the (homogeneous or nonhomogeneous) reference input is stationary or is changed only infrequently. In the simulations, the reference input could be chosen to be nonhomogeneous and/or nonstationary. The designed

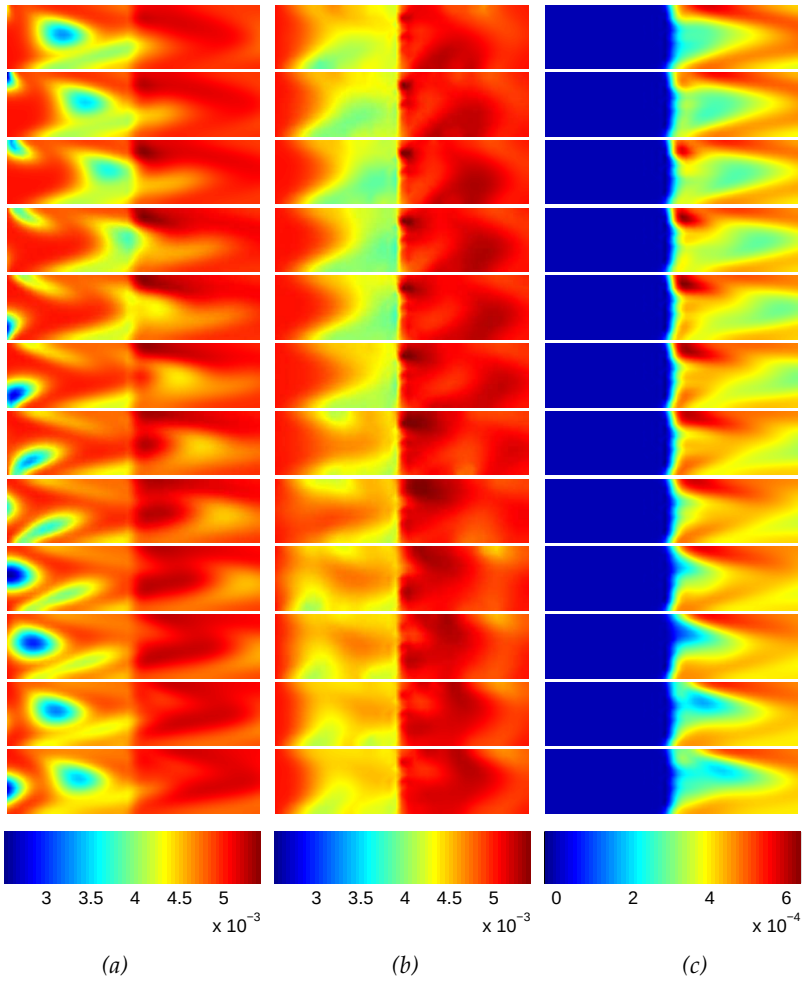

Figure 5.16: (a) The controlled concentration evolution, (b) the Kalman filter estimates, and (c) the change in the concentration at times $t = 1.25, 1.30, \ldots, 1.75, 1.80$ *s when* $v_{\vec{r}_1,\text{mean}} = 20\ cms^{-1}$.

control system can be modified easily to accommodate such requirements, and simulations indicate that the control system works well also in those kind of situations. A change in the reference input would, however, require recomputation of the steady-state values of the concentration and the control input that are used when constructing the approximate controller. Furthermore, a change in the reference input would create a tran-

sient error that would, however, in most cases decay to zero quickly.

5.2 THREE-DIMENSIONAL APPROXIMATE LQG CONTROLLER SIMULATIONS

There are industrial processes that are essentially two-dimensional in nature such as the web forming processes. When designing control systems for such processes, the control system can be described as a two-dimensional distributed parameter control system whose performance can be evaluated with two-dimensional simulations similar to the ones shown in Section 5.1. Furthermore, there are industrial processes that are essentially three-dimensional in nature such as the mixing and separation processes in tanks, pipelines or process vessels. The control systems for those processes are three-dimensional in nature and are modelled as three-dimensional distributed parameter control systems. In this section, a three-dimensional control system is designed for a specific CD process monitored with EIT and simulation results to evaluate the performance of the control system are shown.

Controlling a process that is three-dimensional in nature with boundary actuators is often a difficult task. For example, if one wants to control the concentration distribution of a substance in a fluid flowing in a pipeline with injectors located on the pipe boundary, the challenge is how to get the injected concentrate efficiently and accurately into the middle regions of the pipe. By contrast, monitoring a process that is three-dimensional in nature with EIT is less difficult than monitoring an essentially two-dimensional process when considering for example the location of the sensors.

5.2.1 Simulation of the concentration evolution, simulated EIT observations, and construction of the control system

The domain of interest in the three-dimensional simulations is a pipe illustrated in Figure 5.17. The pipe radius is 5 cm and the pipe length 20 cm. The electrodes are placed in four layers so that there are 16 electrodes per layer. Consequently, there are 64 electrodes altogether. The control performance with two different injector settings is evaluated. In the first case referred to as Case 1, 4 boundary injectors are located 8 cm downstream of the boundary Λ_{in}, see Figure 5.17. In the second case referred to as Case 2, there are 13 points from which the extra substance is added to

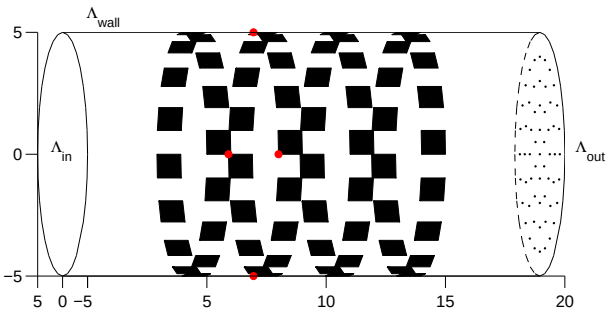

Figure 5.17: Case 1. Illustration of the pipe in the three-dimensional simulations. Boundary patches describe the EIT electrodes. Injectors are denoted by red circles and the black dots refer to the FE nodes on the boundary Λ_{out}.

the fluid flow over a vertical cross-section of the pipe 8 cm downstream of the boundary Λ_{in}. Case 2 simulates, for example, a situation in which the extra substance is injected so that it reaches also the middle regions of the pipe. In Figure 5.18, the formation of the injectors in Case 2 is depicted in detail. In both cases, the objective of the control system is to regulate the concentration profile over the boundary Λ_{out}, see Figure 5.17.

Firstly, the simulation of the concentration evolution in the pipe is considered. The concentration is modelled with the CD model (3.1)-(3.5) where $\vec{r} \in \mathbb{R}^3$. In the three-dimensional simulations, the low concentration inclusions are of the form of a sphere. In the interior of the sphere, the concentration decreases as the center of the sphere is approached. The minimum and the maximum concentration values are selected as in the two-dimensional simulations. The low concentration inclusions enter the pipe through the input boundary Λ_{in}. The concentration on Λ_{in} is modelled with the input concentration (3.5). The velocity field in (3.1) is modelled with the three-dimensional stationary Navier-Stokes equations (3.10)-(3.11).

The finite-dimensional approximation of the CD model (3.1)-(3.5) is used for the simulation of the concentration evolution. The CD model is approximated with the FEM. In the finite-dimensional approximation of the concentration, the basis functions are piecewise linear functions. The

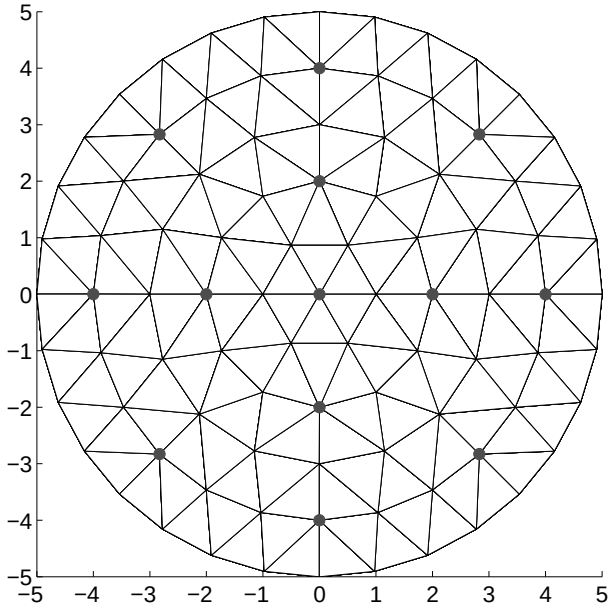

Figure 5.18: Case 2. Formation of the injectors and the FE mesh on the injector layer.

velocity field is parabolic so that

$$\begin{aligned} \vec{v}_{\vec{r}_3}(\vec{r}_1,\vec{r}_2,\vec{r}_3) &= 2v_{\vec{r}_3,\text{mean}}\left(1-\frac{\vec{r}_1^{\,2}+\vec{r}_2^{\,2}}{\tilde{r}^2}\right), \\ \vec{v}_{\vec{r}_1}(\vec{r}_1,\vec{r}_2,\vec{r}_3) &= \vec{v}_{\vec{r}_2}(\vec{r}_1,\vec{r}_2,\vec{r}_3)=0 \end{aligned} \tag{5.4}$$

where the spatial average of the velocity in the horizontal direction of the pipe is chosen as $v_{\vec{r}_3,\text{mean}} = 50$ cms^{-1}. Furthermore, the diffusion coefficient in the simulations is $\kappa = 5$ cm^{2}s^{-1}.

Secondly, the simulation of the EIT observations is considered. The finite-dimensional approximation of the CEM (3.29)–(3.34) where $\vec{r} \in \mathbb{R}^3$ is used in the simulation. The CEM (3.29)–(3.34) is approximated with the FEM. In the finite-dimensional approximation of the internal potential, the basis functions are chosen as piecewise 2$^{\text{nd}}$ order polynomial functions. By contrast in the finite-dimensional approximation of the conductivity, the basis functions are piecewise linear functions.

The time between the consecutive EIT measurements is taken to be 50 ms. The concentration distribution changes considerably during the time

Table 5.2: Number of nodes and elements in the FE meshes used for approximation of the CD model and the CEM in three-dimensional simulations. The abbreviation CDM refers to the CD model. The term "actual" refers to the FE meshes used for approximating the models for the simulation of the concentration evolution and the EIT observations. The term "inverse" refers to the FE meshes used for approximating the models for the construction of the state estimator and the controller.

	Nodes	Elements
CDM actual	7667	40800
CEM actual, 1$^{\text{st}}$order basis functions	2646	13080
CEM actual, 2$^{\text{nd}}$order basis functions	19229	13080
CDM inverse	1911	8880
CEM inverse, 1$^{\text{st}}$order basis functions	1911	8880
CEM inverse, 2$^{\text{nd}}$order basis functions	13489	8880

interval between the measurements. The currents are injected between electrodes that are located on opposite sides of the pipe and in different electrode layers. The voltages are measured between opposite electrodes of the same electrode layer. Consequently, 64 voltage measurements are executed corresponding to each current injection. In total, 64 current injections are applied. See [143] for more details on the measurement protocol. The voltage observations are corrupted with zero-mean Gaussian observation noise that consists of two components as in the two-dimensional simulations presented in Section 5.1.

Thirdly, the construction of the globally linearised Kalman filter and the approximate LQG controller is considered. The specification of parameters for the globally linearised Kalman filter and the approximate LQG controller follows the explanation given in Section 5.1. There are only a few minor changes. The computation of the covariance matrix $\Gamma_{w_{1,t}}$ is performed as described in Section 5.1 and Appendix A. However in the three-dimensional simulations, $\beta_\eta = \frac{1}{4} \times c_{\text{bg}}$ and $\beta_{\tilde{\varsigma}} = \frac{1}{100} \times c_{\text{bg}}$.

One of the challenges in the three-dimensional simulations is the size of the FE meshes. Table 5.2 summarizes the number of nodes and tetrahedral elements in the FE meshes. In comparison to the FE mesh sizes in the two-dimensional simulations presented in Table 5.1, the number of nodes and elements has now increased notably.

5.2.2 Three-dimensional simulation results using the approximate LQG controller

The objective of the controller is to regulate the concentration distribution over the boundary Λ_{out} so that the concentration on the FEM nodes matches the desired concentration (5.1×10^{-3} mol^{-1}cm^2). Firstly, the performance of the approximate LQG controller is investigated when the boundary injectors depicted in Figure 5.17 are used (Case 1). The uncontrolled concentration evolution, the change in the concentration, and the controlled concentration evolution are illustrated in Figure 5.19(a), 5.19(b), and 5.19(c), respectively. Concentration on five vertical layers located 2 cm, 6.5 cm, 11 cm, 15.5 cm, and 20 cm downstream of the boundary Λ_{in} are shown. The last layer is actually the boundary Λ_{out} and is, therefore, the most interesting one. It can be seen that the injectors are not able to distribute the injected concentrate to the inner regions of the pipe. Thus, the concentration over the boundary Λ_{out} matches a desired concentration only near the pipe walls.

The uncontrolled concentration and the controlled concentration over the output boundary Λ_{out} are depicted in Figure 5.20 for Case 1. In Figure 5.20, the lines corresponding to the minimal values of the uncontrolled concentration and the minimal values of the controlled concentration lie on top of each other at most times t indicating that the minimum values of the uncontrolled and controlled concentrations are equal at those times. Consequently, the injected concentrate is distributed only to some regions of the pipe and other regions are unaffected by the control action. From Figure 5.19, it can be concluded that the concentration in the middle regions of the pipe cannot be adjusted efficiently.

Furthermore, the control performance of the system is evaluated by investigating the output errors $\|y_{\text{ref}} - Cc_t\|_2$ that are computed using the FE approximation of the concentration. The output errors for the uncontrolled concentration and the controlled concentration are plotted in Figure 5.21. Despite the difficulties evident in Figure 5.20, the output errors are smaller for the controlled concentration in comparison to the uncontrolled concentration once the effect of the initial conditions has faded.

Secondly, the performance of the approximate LQG controller is investigated when using the injector setting illustrated in Figure 5.18 (Case 2). The uncontrolled concentration evolution, the change in the concentration, and the controlled concentration evolution are shown in Figure 5.22(a), 5.22(b), and 5.22(c), respectively. Contrary to the case shown in Figure 5.19, the controller is now able to regulate the output concentration,

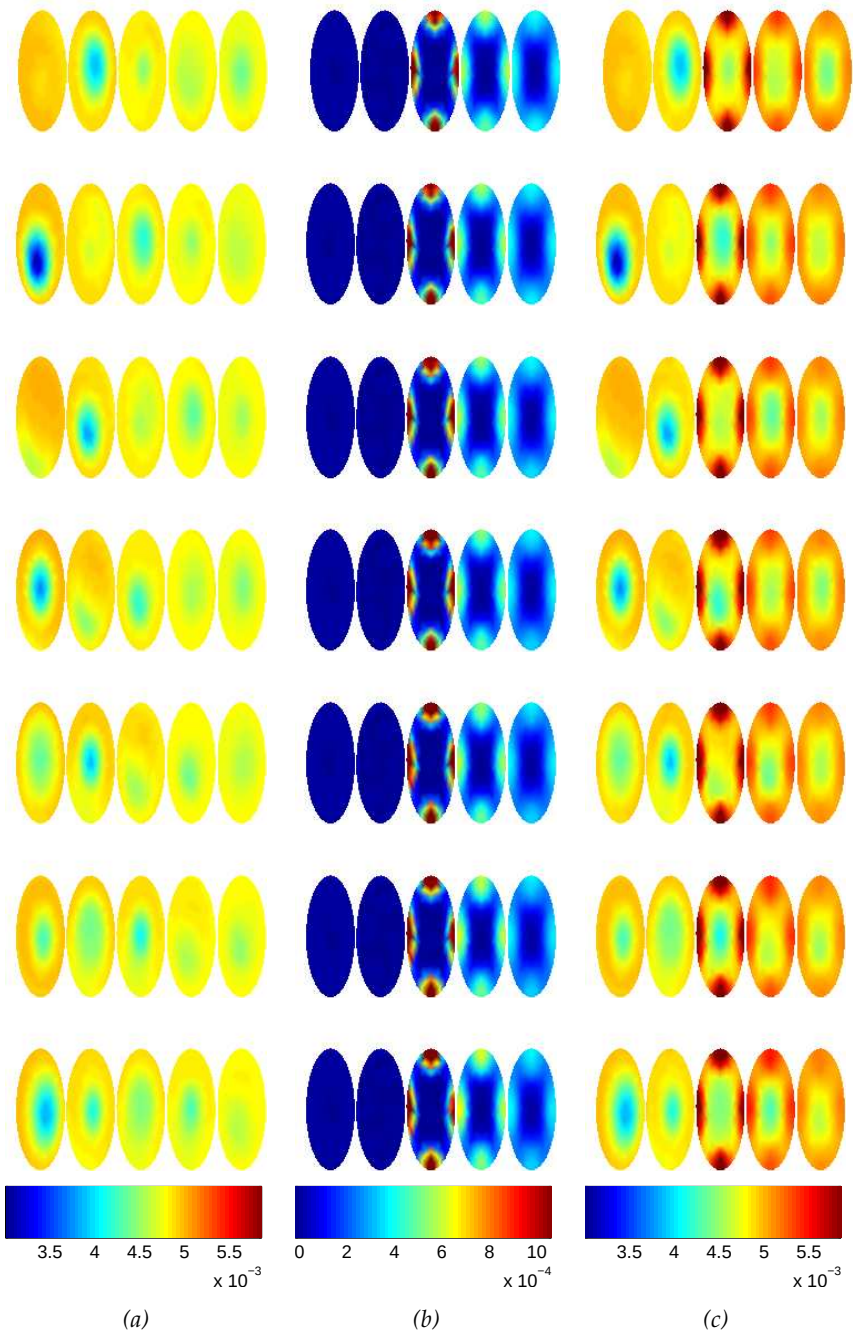

Figure 5.19: Case 1. (a) The uncontrolled concentration evolution, (b) the change in the concentration, and (c) the controlled concentration evolution at times $t = 2.90, 2.95, \ldots, 3.15, 3.20$ *s.*

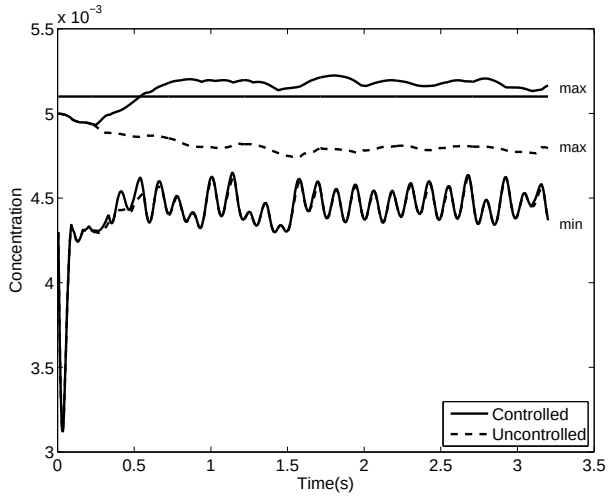

Figure 5.20: Case 1. The minimum and the maximum value of the uncontrolled concentration and the controlled concentration on the FE nodes on Λ_{out}. The thick black line indicates the desired output concentration.

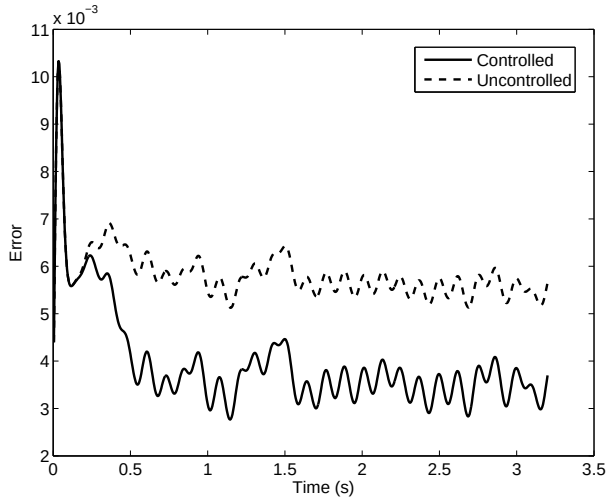

Figure 5.21: Case 1. The output errors for the uncontrolled concentration and the controlled concentration.

and the output concentration matches the desired output concentration.

The uncontrolled concentration and the controlled concentration over the boundary Λ_{out} are depicted in Figure 5.23. It can be concluded that due to the injected concentrate, the output concentration reaches the desired output concentration throughout the pipe. The output errors for the uncontrolled concentration and the controlled concentration are plotted in Figure 5.24. The output errors are notably smaller for the controlled concentration than for the uncontrolled concentration.

5.2.3 Discussion of three-dimensional approximate LQG controller simulations

The three-dimensional modelling of the process and observations is essential when designing a control system for processes that are three-dimensional in nature. Such processes include for example processes involving fluid flowing in a pipe, in a tank or in a process vessel. The simulation results shown in this section indicated that it is possible to control a three-dimensional CD process when EIT is used as a sensor for the controller. The tracking performance and the disturbance rejection of the proposed controller were adequate at least in Case 2. Robustness of the designed control system could be investigated with similar simulations as described in Section 5.1.5.

One simplification was made in the simulations involving the modelling of the velocity field. In practical implementations, the injectors are typically located on the pipe boundary and the flow rates of injectors are often so high that the velocity field changes due to the injections. In the simulations, the velocity field was assumed to be stationary due to computational reasons. To compensate for this simplifying approximation, the effects of small scale turbulent mixing were modelled by increasing the diffusion coefficient. Furthermore, the injector setting in Case 2 was constructed to simulate the case in which the flow rates of injectors are high, and the injected concentrate diffuses to the middle regions of the pipe.

The computational complexity of the system is a crucial issue especially in three-dimensional simulations. The dimension of the state variable is inevitably very large since the number of unknowns equals the number of nodes in the FE mesh. The FE meshes in turn have to be fine for the solution to have an adequate level of accuracy. There are effective methods to overcome the problem of dense discretisation. One of them, the approximation error approach, is considered below. Such an approach

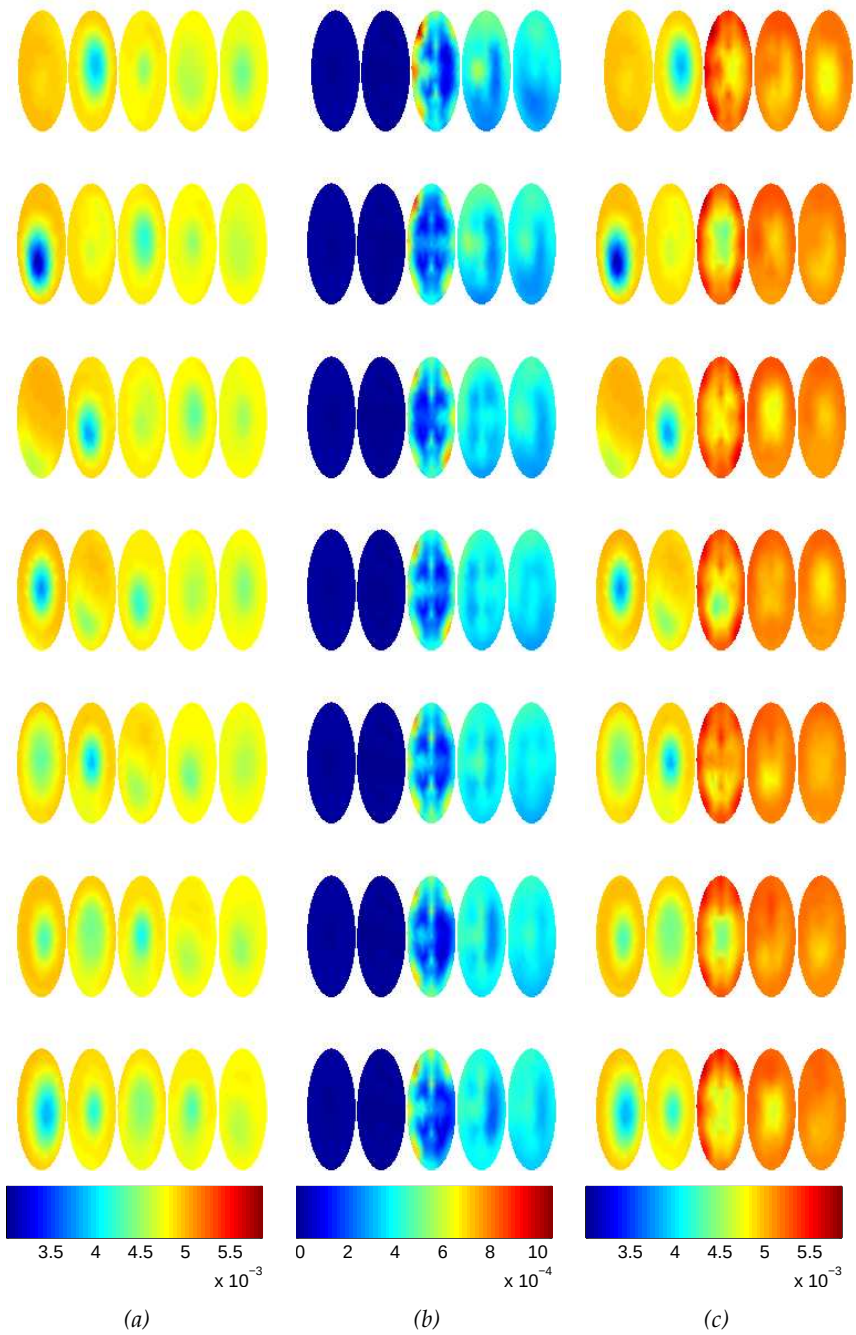

Figure 5.22: Case 2. (a) The uncontrolled concentration evolution, (b) the change in the concentration, and (c) the controlled concentration evolution at times $t = 2.90, 2.95, \ldots, 3.15, 3.20$ *s.*

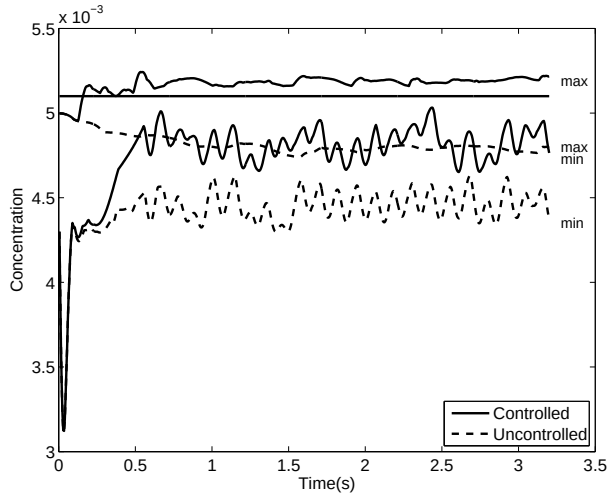

Figure 5.23: Case 2. The minimum and the maximum value of the uncontrolled concentration and the controlled concentration on the FE nodes on Λ_{out}. The thick black line indicates the desired output concentration.

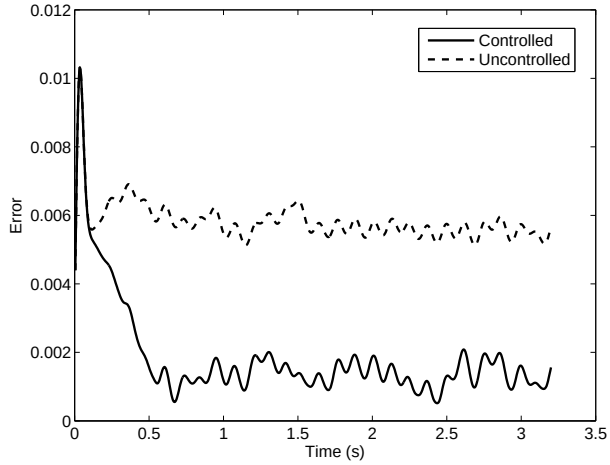

Figure 5.24: Case 2. The output errors for the uncontrolled concentration and the controlled concentration.

could be adopted if the process control methods presented in this thesis are used in practical implementations.

The basic idea in the approximation error method is to analyse the statistical properties of the error processes related to the state and observation models prior to actual measurements, and to incorporate that information into the models. An example related to the application discussed in this thesis is the reduction of the computational complexity of the EIT forward model. Due to the ill-posed nature of the EIT estimation problem, the spatial discretisation of the forward model should be fine leading to a high-dimensional forward model. However, the use of a high-dimensional forward model may lead to excessive computational times and, thus, the dimensionality of the forward model should be reduced especially in the real time industrial applications. If the modelling errors due to the reduced discretisation are neglected, the solution of the EIT estimation problem can be inadequate. If the discretisation errors are appropriately modelled, a reduced observation model can be employed in process monitoring as the uncertainty in the model is taken into account.

The approximation error approach was first proposed in [5] (see also [51]) where the discretisation errors were accommodated for in stationary inverse problems. In addition to model reduction, the method has also been applied to problems in which the errors are caused by (partially) unknown geometry [241], by truncation of the computational domain [242], [243], by (partially) unknown boundary conditions [179], and by linearisation of the observation model [244]. The approximation error method for the (linear and nonlinear) nonstationary inverse problems was presented in [49], [50]. In [185], the nonstationary approximation error approach was applied in monitoring of a CD process in which the nonstationary velocity fields were unknown. The stationary approximation error method was evaluated with EIT laboratory experiments in [241], [243] and the nonstationary approximation error method in [179].

5.3 APPROXIMATE LQG CONTROLLER SIMULATIONS WITH NONSTATIONARY VELOCITY FIELDS

In real life process control applications in which pipelines or tanks are involved, actuators are typically located on the boundary of the object. This may lead to certain challenges when designing the whole control system. If one uses, for example, boundary actuators injecting extra substance into the flow, the injection rate has to high enough so that the injected

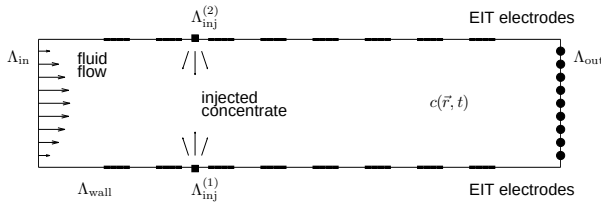

Figure 5.25: Illustration of the pipe with boundary injection points denoted by black squares.

substance reaches also the middle regions of the object. As a consequence of the high injection rate, the injections alter the velocity field inside the object. Furthermore, nonstationary velocity fields are typical in practical industrial implementations even without the impact of a controller. The question is whether in such a case modelling the velocity field inside the pipe as stationary and unaffected by the injections as in Section 5.1 leads to adequate control performance.

The starting point for the simulation study in this section corresponds to the one presented in Section 5.1 with the exception of the nonstationary velocity fields and the boundary injections. In this section, the domain of interest is a pipe with two injection boundaries located on the opposite walls of the pipe as illustrated in Figure 5.25. The situation can be compared to a system involving side-tee mixers when the flow rate of the injected concentrate is controlled using a flow valve. The objective of the approximate LQG controller is to regulate the concentration over the boundary Λ_{out} on the basis of EIT observations. The performance of the control system is evaluated with two-dimensional simulations.

5.3.1 Simulation of the concentration evolution and the EIT observations

The concentration is modelled with the CD model (3.1)-(3.5) where $\vec{r} \in \mathbb{R}^2$ and the velocity field $\vec{v}$ is nonstationary. The variations in the concentration are due to low concentration inclusions that enter the pipe through the boundary Λ_{in}. The concentration on boundary Λ_{in} is modelled with the input concentration (3.5). Although the injection points are on the boundary of the domain, the effect of the injected concentrate is modelled as described in Section 3.1.3 and not as a boundary condition for the CD equation. Such a boundary condition depending on the flow rate on the

injection boundary could also be formulated.

The nonstationary velocity field is modelled with the nonstationary Navier-Stokes equations (3.8)-(3.9) with the initial and boundary conditions (3.12)-(3.14). Furthermore, an additional boundary condition is postulated for the modelling of the velocity field on the injection boundaries. Let $\Lambda_{\text{inj}}^{(j)} \subset \Lambda_{\text{wall}}$, $j = 1, 2$, denote the part of the boundary through which the concentrate is injected into the main stream. The velocity field on the injection boundary is defined as

$$\vec{v}(\vec{r}, t) \quad = \quad \vec{v}_{\text{inj}}^{(j)}(\vec{r}, t), \quad \vec{r} \in \Lambda_{\text{inj}}^{(j)} \tag{5.5}$$

where $\vec{v}_{\text{inj}}^{(j)}$ refers to the velocity field on the j^{th} injection boundary $\Lambda_{\text{inj}}^{(j)}$, $j = 1, 2$. The flow on the j^{th} injection boundary $\Lambda_{\text{inj}}^{(j)}$ is a plug flow so that when $\vec{r} \in \Lambda_{\text{inj}}^{(j)}$,

$$\vec{v}_{\text{inj},\vec{r}_1}^{(j)}(\vec{r}, t) \quad = \quad 0 \tag{5.6}$$

$$\vec{v}_{\text{inj},\vec{r}_2}^{(j)}(\vec{r}, t) \quad = \quad v_{\text{inj},0}^{(j)}(t). \tag{5.7}$$

where the velocity $v_{\text{inj},0}^{(j)}(t)$ in the vertical direction at time t depends on the flow rate $u^{(j)}(t)$ on the j^{th} injection boundary. It can be shown that if the density ρ and the molar mass M_f of the fluid, and the velocity on $\Lambda_{\text{inj}}^{(j)}$ are constant, the velocity

$$v_{\text{inj},0}^{(j)}(t) = (-1)^{j+1} \frac{u^{(j)}(t) M_f}{\rho |\Lambda_{\text{inj}}^{(j)}|} \tag{5.8}$$

where $|\Lambda_{\text{inj}}^{(j)}|$ is the size of the injection boundary.

The finite-dimensional approximation of the CD model (3.1)-(3.5) is derived utilizing the FEM as in Section 5.1 with the exception that the velocity field is nonstationary. To obtain an approximation for the velocity field $\vec{v}$, the boundary value problem (3.8)-(3.9) with initial and boundary conditions (3.12)-(3.14) and (5.5) is solved numerically using the FE solver in COMSOL Multiphysics®. The external forces acting on the system are nonexisting in this study and, thus, $\vec{f} = 0$. Furthermore, the velocity field $\vec{v}_{\text{in}}$ on the boundary Λ_{in} is parabolic (see equation (5.1)) where the spatial average of the velocity in the horizontal direction is $v_{\text{in},\vec{r}_1,\text{mean}} = 50\ \text{cms}^{-1}$.

When approximating the Navier-Stokes equations with the FEM, the computational domain is taken to be twice as long as the original pipe.

The interesting region is in the middle of the new computational domain. Such a choice compensates for the effects of the unknown boundary data on boundaries Λ_{in} and Λ_{out} on the velocity field. Furthermore, the FE mesh when approximating the Navier-Stokes equations is denser than the FE meshes for approximating the CD model and the CEM (Table 5.1) in order to guarantee adequate numerical accuracy. The number of nodes is 17245 and the number of elements is 33760 when approximating the Navier-Stokes equations. The linear interpolation method is applied for the interpolation between the different meshes.

The finite-dimensional and discrete-time approximation of the CD model corresponds to (3.27) with the exception that the state transition matrix, the control input matrix, and the process source term are in this case nonstationary and dependent of the velocity field at time t. Thus, the evolution model is

$$c_{t+1} = A_t(\vec{v}_t)c_t + B_{2,t}(\vec{v}_t)u_t + s_{t+1}(\vec{v}_t) + w_t. \tag{5.9}$$

When simulating the concentration evolution (corresponding to the actual process), the velocity field $\vec{v}_t$, the matrices A_t and B_t, and the vector s_{t+1} have to be recomputed as each time t.

The EIT observations are modelled with the CEM (3.29)–(3.34) where $\vec{r} \in \mathbb{R}^2$. The current injection and the voltage measurement patterns are similar to the ones described in Section 5.1. Furthermore, the finite-dimensional approximation of the CEM is derived as in Section 5.1.

5.3.2 Construction of the control system

The control inputs are obtained with the approximate LQG controller designed in Section 4.2.2. The globally linearised Kalman filter is used as a state estimator. In the FE approximation of the CD model (3.1)-(3.5) for constructing the globally linearised Kalman filter and the approximate LQG controller, the nonstationary velocity field is replaced with an approximate stationary velocity field. The approximate velocity field is parabolic and modelled with (5.1). As a consequence of the stationary velocity field, the matrices and the process input vector in the state equation (5.9) are stationary so that $A_t = A$, $B_t = B$, and $s_t = \bar{s}$ for all t. Thus, the computational load of the state estimator and the controller is decreased and tolerable for real time application. The parameters for the globally linearised Kalman filter are specified in Section 5.1.3. The parameters for the weighting matrices needed when constructing the approximate LQG controller are determined from a set of simulations.

5.3.3 Simulation results with nonstationary velocity fields

The uncontrolled concentration evolution is shown in Figure 5.26(a). When computing the uncontrolled concentration evolution, there are no injections affecting the velocity field. Thus, the velocity field is approximately parabolic. The controlled concentration evolution is shown in Figure 5.26(c) and the change in the concentration in Figure 5.26(b). In these computations, the velocity field is nonstationary and changing according to the flow rates of the injectors. It can be seen that even though the flow rates of injectors are high, the injected concentrate does not reach the middle regions of the pipe. Consequently, the concentration in the middle regions of the pipe is lower than the concentration near the pipe walls. Correspondingly on the boundary Λ_{out}, the concentration near the pipe walls is higher and the concentration in the middle of the boundary Λ_{out} is lower than the desired output concentration.

In Figure 5.26(d), the globally linearised Kalman filter estimates of the controlled concentration are shown. It can be seen from the last four subfigures that the estimated output concentration is lower than the actual output concentration. Especially in the regions near the pipe boundaries, the estimates are less accurate. Furthermore from the subfigures from the fourth subfigure to the eight subfigure, it can be concluded that the low concentration inclusions are estimated to move slower than they actually do. These inaccuracies in the state estimates deteriorate the control performance.

Although the concentration on the boundary Λ_{out} does not fully match the desired output concentration, the benefit of control on the process is clear. In Figure 5.27, the uncontrolled concentration and the controlled concentration over the boundary Λ_{out} are depicted. The controlled output concentration is increased and it matches better the desired output concentration. Furthermore in Figure 5.28, the output errors are shown. The output errors are smaller for the controlled concentration.

5.3.4 Discussion of simulations with nonstationary velocity fields

In this section, boundary actuators were considered and the effect of boundary injections on the velocity field was accounted for. The simulations showed that the boundary actuators can be used to control the CD process considered in this thesis up to a point if the flow rate of the injected substance is high enough. The problem of using such a injection system is evidently how to distribute the injected substance to the mid-

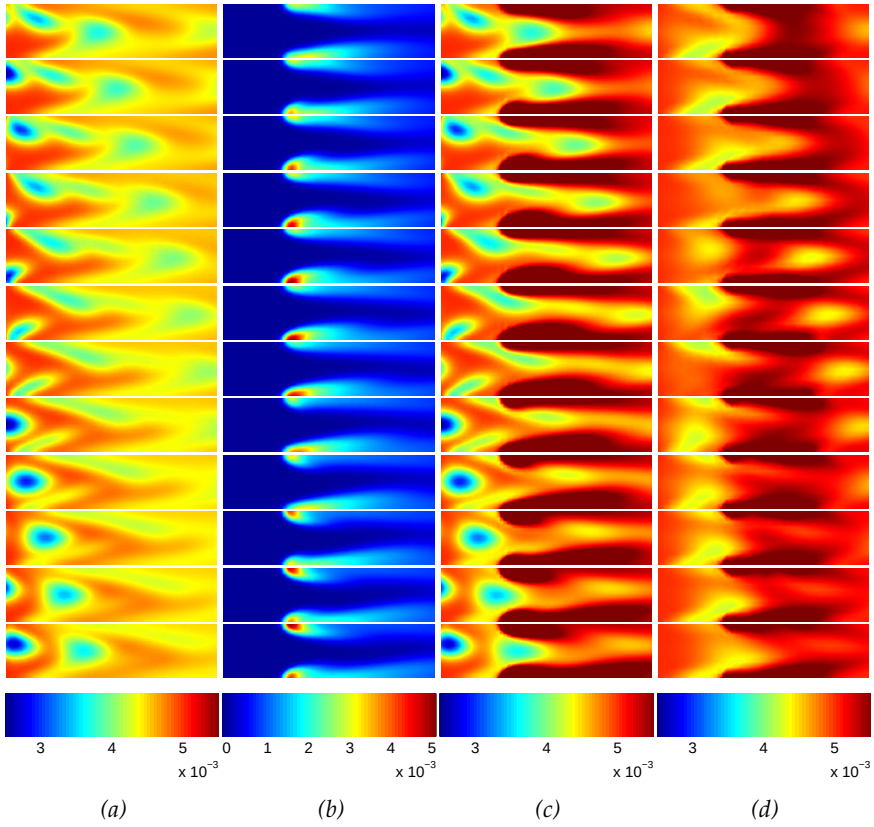

Figure 5.26: (a) The uncontrolled concentration evolution, (b) the change in the concentration, (c) the controlled concentration evolution, and (d) the globally linearised Kalman filter estimates of the controlled concentration at times $t = 1.70, \ldots, 2.25$ *s.*

dle regions of the pipe so that the concentration near the pipe walls does not increase to an undesirable level. Especially if the injection points are close to the region in which the concentration is aimed to match to the desired concentration, controlling the concentration distribution with only boundary actuators is challenging.

If boundary actuators are used in practical implementations, one needs an actuation system that is able to inject the extra substance in a fast flow rate in comparison to the rate of the main process flow. With such a system, also the middle regions of the object of interest are affected with the added substance. Furthermore, several injections points on boundary of

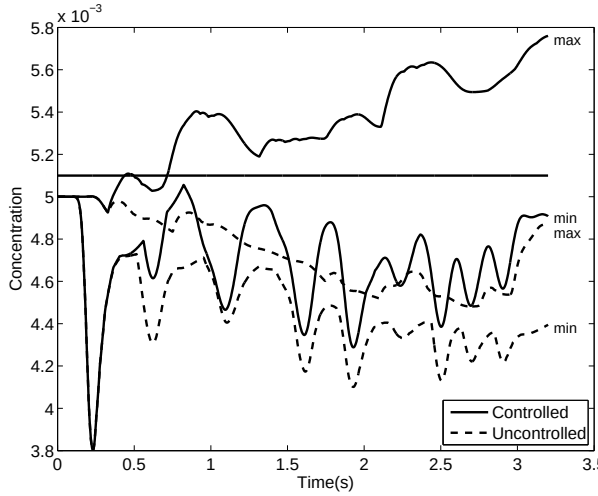

Figure 5.27: The minimum and the maximum value of the uncontrolled concentration and the controlled concentration on the FE nodes on Λ_{out} at each time. The thick black line indicates the desired output concentration.

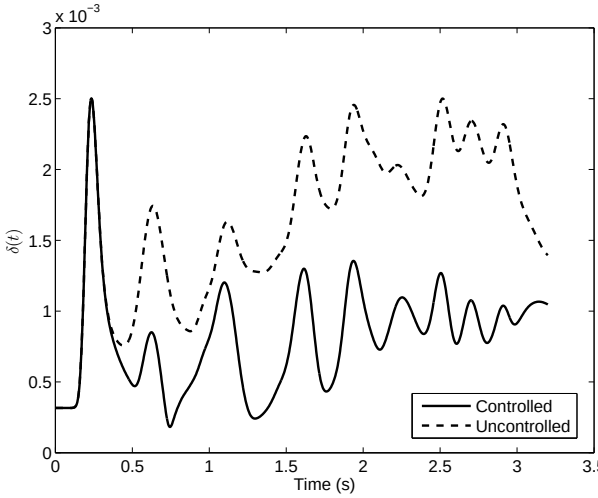

Figure 5.28: The output errors for the uncontrolled concentration and the controlled concentration.

the object may be required to obtain a satisfactory outcome, a homogeneous mixture for example. It is also intuitively clear that making very small and/or pinpoint concentration changes inside the object using only boundary actuators is a very difficult task. However, one may be able to control the spatial and temporal average of the concentration with such a system.

Due to computational reasons the nonstationary velocity field was replaced with an stationary approximation when constructing the state estimator and the controller. The simulations indicated that approximating the nonstationary velocity fields was acceptable in this case although the state estimates have inaccuracies. However, this approach is essential when considering real time processes involving rapid changes in which the time for computations is limited. The recomputation of the velocity field at each time would lead to recomputation of the matrices in the state equation which in turn would lead to a nonstationary feedback gain matrix. These computations would most likely make the implementation of a real time controller impossible in the case of high dimensional systems. In [185], estimation of the concentration when the effect of the nonstationary velocity fields was taken into account using the approximation error approach was investigated. A similar approach could be adopted in this case.

There are also other stationary approximations than the parabolic velocity field for the nonstationary velocity field. One approach would be to compute several velocity fields corresponding to selected flow rates of the injections prior to the actual operation of the system. Then the approximation that closely corresponds to the actual flow rates could be chosen from the set of the computed velocity fields using bilinear interpolation.

The velocity field inside the pipe was taken to be laminar and was modelled with the Navier-Stokes equations. If the flow rates on the injection boundaries are very high in practical implementations, the flow is likely to turbulent and turbulent flow models could be used. It is emphasized, that the laminar flow model could be replaced in the computations with a turbulent flow model if such is needed. However, the use of turbulent flow models may increase the computational load. Furthermore, the performance of the control system may be adequate even if approximate flow models are used when the overall structure of the process is properly modelled. These issues are also addressed in Section 3.3.

5.4 COMPARISON OF EFFECTS OF TWO STATE ESTIMATORS ON CONTROL PERFORMANCE

State estimators such as the globally linearised Kalman filter, the extended Kalman filter, and the iterated extended Kalman filter have successfully been applied in EIT, see Section 3.2.6. However, all of the publications have focused only on state estimation. Process control or effects of the selection of the state estimator on control performance have not been considered in the publications. It is often stated that the effect of linearising the EIT observation model is not large on the outcome. Especially if the variations of the quantity to be estimated are not very large, the globally linearised Kalman filter estimates are said to be feasible provided that the linearisation point is properly selected. This is the case for example in a mixing process in which the monitoring and control systems are situated after a main mixer and the aim is to detect inhomogeneities in the fluid and to make fine adjustments. However, it is relevant to ask whether the globally linearised Kalman filter yield adequately accurate state estimates for process control when the variations of the estimated quantity cannot be considered as small.

Furthermore, the measurements in the field are never noiseless. The noise level depends on the industrial application and on the imaging modality in question, and can be determined, for example, with a set of repeated measurements. Also the noise level affects the selection of the state estimator and this topic is investigated in the case of the CD process monitored with EIT. In this thesis, two state estimators, the globally linearised Kalman filter and the iterated extended Kalman filter, are employed and in both cases, the performance of the approximate LQG controller designed in Section 4.2.2 is evaluated with two-dimensional simulations.

5.4.1 Simulation of the concentration evolution and the EIT observations

The starting point for this study is similar to the one described in Section 5.1 with a few exceptions. In Section 5.1, the input concentration consisted of low concentration inclusions in a homogeneous background and the level of the background concentration was constant in the simulations. Furthermore, the difference between the background concentration and the minimum concentration in the inclusions was small. It was established that the globally linearised Kalman filter estimates were feasible for control purposes in such a case. When simulating the input concentra-

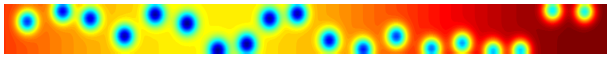

Figure 5.29: The input concentration when the background concentration is temporally varying.

tion in this section, the concentration of the background changes smoothly with respect to time so that the value of the background concentration decreases from 5×10^{-3} mol^{-1}cm^2 to 3×10^{-3} mol^{-1}cm^2 and then starts to increase again. The low concentration inclusions are simulated as in Section 5.1 with the exception that the minimum value of concentration in the inclusions is now 0.1×10^{-3} mol^{-1}cm^2. Thus, the difference between the background concentration and the minimum concentration value in the inclusions is slightly larger than in Section 5.1. The simulated input concentration is shown in Figure 5.29.

The EIT observations are simulated as in Section 5.1 with the exception of the added observation noise. In this section, to each observation, firstly, noise with standard deviation of 1%, 10%, or 30% of the value of that observation and, then, noise with standard deviation of 0.1%, 1%, or 3% of the voltage range is added, respectively. The three different noise levels are denoted by the 1/0.1% noise level, the 10/1% noise level, and the 30/3% noise level.

5.4.2 Construction of the state estimators and the approximate LQG controller

The parameters for the state estimator and the approximate LQG controller are selected as in Section 5.1 with a few exceptions. As the concentration on the boundary Λ_{in} has now larger variations than in Section 5.1, the standard deviation of the input noise β_η is changed accordingly. The covariance matrix $\Gamma_{\eta_t} = \beta_\eta^2 I$ is still diagonal, but in this case $\beta_\eta = \frac{1}{5} \times c_{\text{bg}}$ where c_{bg} is an stationary approximation of the concentration. As the background concentration is not homogeneous, the selection of c_{bg} is not as straightforward as in Section 5.1. If the variations of the concentration are not known in advance, c_{bg} has to be chosen on a basis of prior knowledge. In this section, $c_{\text{bg}} = 4.7 \times 10^{-3}$ mol^{-1}cm^2. The covariance matrix of the observation noise is approximated with a uniform diagonal matrix $\Gamma_{v_t} = \beta_v^2 I$ where β_v is 0.1%, 1%, or 3% of the assumed voltage range corresponding to the employed noise level. The parameters β_Q and β_R for

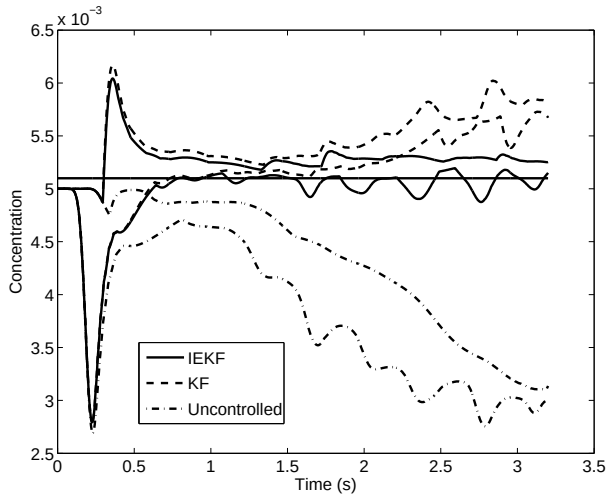

Figure 5.30: The minimum and the maximum value of the uncontrolled concentration and the controlled concentration on the FE nodes on Λ_{out} when using the globally linearised Kalman filter (KF) and the iterated extended Kalman filter (IEKF). The straight line indicates the desired output concentration. The noise level is $1/0.1\%$.

the weighting matrices $Q_y = \beta_Q I$ and $R = \beta_R I$ are selected from a set of simulations.

5.4.3 Simulation results using two different state estimators

The simulation results when the noise level is the $1/0.1\%$ noise level are firstly considered. In Figure 5.30, the uncontrolled concentration and the controlled concentration over the boundary Λ_{out} are shown when using the globally linearised Kalman filter and the iterated extended Kalman filter. The output concentration when using the globally linearised Kalman filter is higher than the desired output concentration especially from the time $t = 1.5$ s onwards.

The output errors (5.3) for the uncontrolled concentration and the controlled concentration are shown in Figure 5.31 when the noise level is $1/0.1\%$. The output errors when the iterated extended Kalman filter is used as a state estimator are notably smaller than the errors when the globally linearised Kalman filter is used.

In this numerical study, the control performance using the iterated extended Kalman filter is substantially better that the control performance

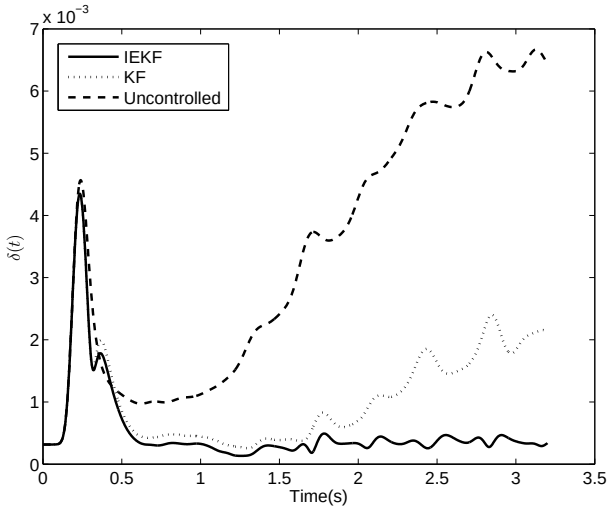

Figure 5.31: The output errors for the uncontrolled concentration and the controlled concentration using the globally linearised Kalman filter (KF) and the iterated extended Kalman filter (IEKF). The noise level is 1/0.1%.

using the globally linearised Kalman filter, see Figures 5.30 and 5.31. The reason for the difference in the control performance can be traced to the state estimates yielded by the estimators. The state estimates for the concentration using the two state estimators are shown in Figure 5.32. In Figure 5.32(a) and 5.32(c), the images of the controlled concentrations are shown at times $t = 2.40, \ldots, 2.95$ s. In Figure 5.32(a), the globally linearised Kalman filter and in Figure 5.32(c), the iterated extended Kalman filter is used as a state estimator. During the selected times, the background concentration is at its lowest. In Figure 5.32(b), the globally linearised Kalman filter estimates and in Figure 5.32(d), the iterated extended Kalman filter estimates of the controlled concentration are shown. Especially, the top three subfigures in Figures 5.32(b) and 5.32(d) illustrate the difference in the state estimates. When using the iterated extended Kalman filter, the low concentration inclusions are estimated more accurately than when using the globally linearised Kalman filter. Furthermore, the globally linearised Kalman filter is unable to estimate the average level of the controlled concentration in the regions after the injectors. The concentration estimates in those regions including also the boundary Λ_{out} are too low, and, therefore, control inputs are too high. It can be concluded

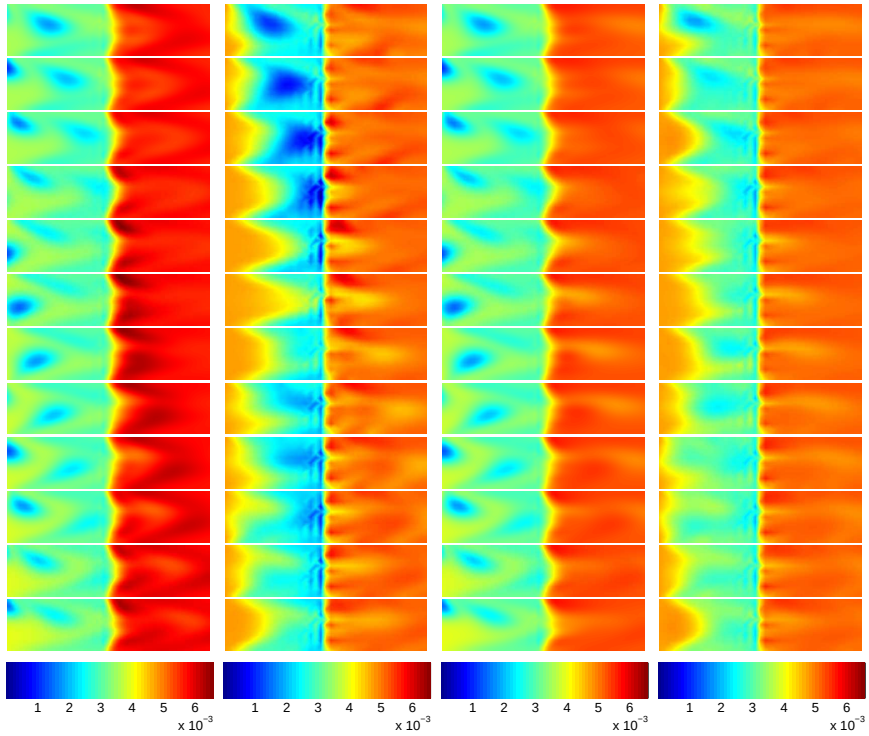

Figure 5.32: (a) The controlled concentration evolution using the globally linearised Kalman filter, (b) the globally linearised Kalman filter estimates, (c) the controlled concentration evolution using the iterated extended Kalman filter, and (d) the iterated extended Kalman filter estimates at times $t = 2.40, \ldots, 2.95$ *s. The noise level is* $1/0.1\%$.

from Figures 5.32 and 5.30 that in this numerical study as the level of the average concentration decreases, the globally linearised Kalman filter is unable to adapt to the new situation. By contrast, the iterated extended Kalman filter yields adequate state estimates to the controller also in this case. The inner iteration loop ensures that the linearisation point in the iterated extended Kalman filter corresponds more accurately to the actual average concentration level.

In Figure 5.33, the uncontrolled concentration and the controlled concentration over Λ_{out} are shown in the case of the $10/1\%$ noise level. The corresponding output errors (5.3) are plotted in Figure 5.34. When considering the $10/1\%$ noise level, the difference between the control per-

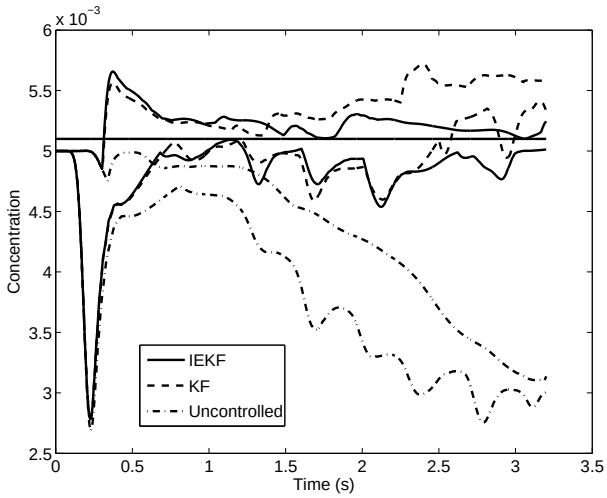

Figure 5.33: The minimum and the maximum value of the uncontrolled concentration and the controlled concentration on the FE nodes on Λ_{out} using the globally linearised Kalman filter (KF) and the iterated extended Kalman filter (IEKF). The noise level is 10/1%.

formances using the iterated extended Kalman filter and the globally linearised extended Kalman filter decreases. However, the control performance using the iterated extended Kalman filter is better especially when the average concentration varies from the initial background concentration (approximately from the time $t = 2.40$ s onwards).

In Figure 5.35, the uncontrolled concentration and the controlled concentration over Λ_{out} are shown in the case of the 30/3% noise level. The corresponding output errors (5.3) are plotted in Figure 5.36. Neither the globally linearised Kalman filter nor the iterated extended Kalman filter yield adequate estimates for the controller to perform well. The results presented in Figure 5.35 show that the controller is not able to regulate the low concentration inclusions or even to match the average output concentration to the desired output concentration. The concentration over Λ_{out} is increased but not enough. Furthermore, the control performance using the globally linearised Kalman filter corresponds to the control performance using the iterated extended Kalman filter.

Time-averaged output errors for the globally linearised Kalman filter and the iterated extended Kalman filter are shown in Table 1. The noise levels are 1/0.1%, 10/1%, and 30/3%. The time-averaged output error for

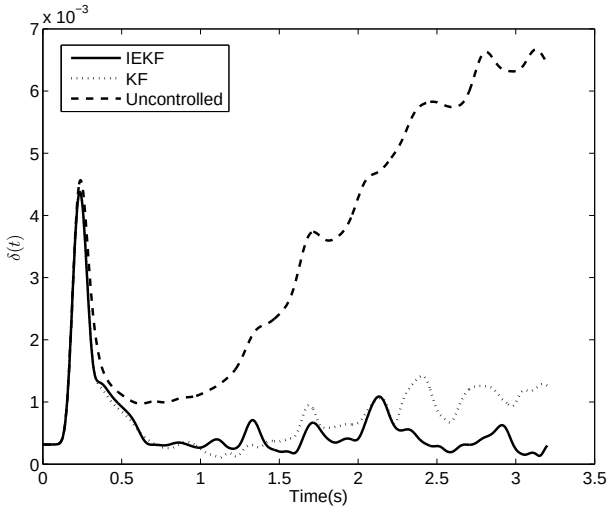

Figure 5.34: The output errors for the uncontrolled concentration and the controlled concentration using the iterated extended Kalman filter (IEKF) and the globally linearised extended Kalman filter (KF). The noise level is 10/1%.

the iterated extended Kalman filter is significantly smaller than the one for the globally linearised Kalman filter when the noise level is 1/0.1% or 10/1%. When the noise level is 30/3%, the difference between the time-averaged output errors for the state estimators is small. In this case, the time-averaged output error for the globally linearised Kalman filter is slightly smaller. Furthermore, it can be noticed that the smallest time-averaged output error for the globally linearised Kalman filter is achieved when the noise level is the 10/1% noise level and not the 1/0.1% noise level. This is due to the fact that if the measurement noise level is low, the effect of the evolution model is small in comparison to the effect of the observation model when computing the estimates. Consequently as the observation model is biased (the linearisation point does not correspond to the actual level of the concentration), also the estimates are biased.

It can be concluded from Table 1 and Figures 5.30, 5.31, 5.33, and 5.34 that in this numerical study the iterated extended Kalman filter performs better than the globally linearised extended Kalman filter when the noise level of the measurement system is low (in this case 1/0.1% or 10/1%). The iterated extended Kalman filter yields more accurate state estimates, and better quality of the estimates usually leads to better control perfor-

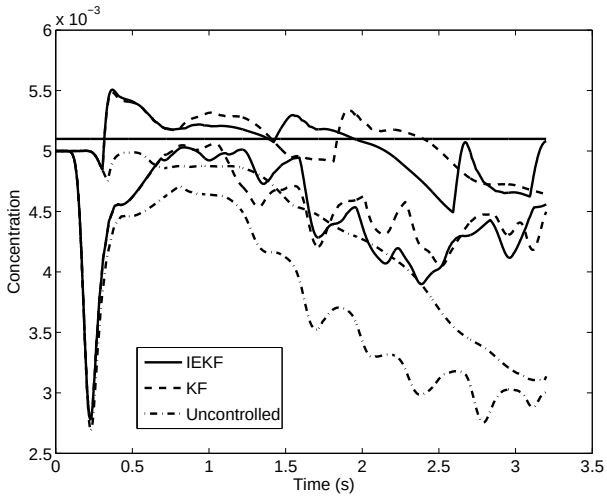

Figure 5.35: The minimum and the maximum value of the uncontrolled concentration and the controlled concentration on the FE nodes on Λ_{out} using the globally linearised Kalman filter (KF) and the iterated extended Kalman filter (IEKF). The noise level is 30/3%.

mance. When the noise level increases, the advantage of using a more complex state estimation algorithm diminishes. This can be seen from Figures 5.35 and 5.36 in which the noise level is 30/3%.

5.4.4 Discussion of simulations using two different state estimators

In general, choosing an appropriate state estimator when controlling a specific industrial process monitored with electrical process tomography (PT) always depends on the characteristics of the process and on the control objective to be attained. As the control inputs are based on the state estimates, the estimates should be relatively accurate in order to achieve adequate control performance. Furthermore, in real time implementations with fast sampling, the state estimation algorithm is also required to be fast. Simulations, like the ones presented in this section, provide information on the computational times and on the estimation accuracy, and this information can be taken into account when designing control systems.

In this section, the objective was to investigate the effect of two different state estimators, the globally linearised Kalman filter and the iter-

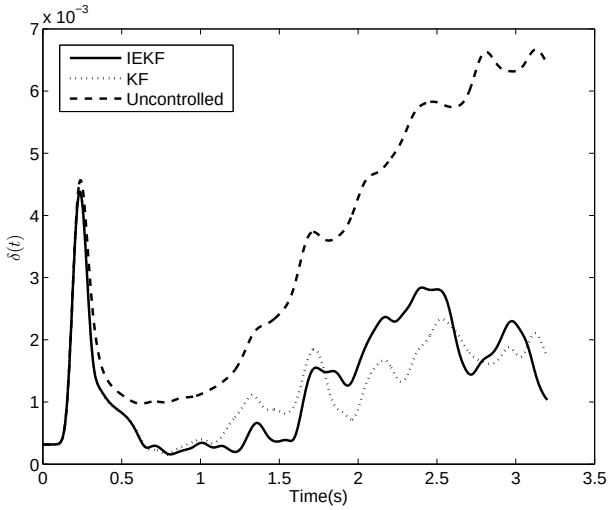

Figure 5.36: The output errors for the uncontrolled concentration and the controlled concentration using the globally linearised Kalman filter (KF) and the iterated extended Kalman filter (IEKF). The noise level is 30/3%.

ated extended Kalman filter, on control performance when controlling the concentration distribution in a CD process monitored with EIT. As the EIT observation model was nonlinear, the basic Kalman filter was inapplicable. As expected, the simulation results indicated that the iterated extended Kalman filter yields state estimates that are adequate for control purposes even when the concentration variations are quite large. However, the simulations verified that one cannot automatically conclude that the iterated extended Kalman filter is more suitable for process control implementations than the globally linearised Kalman filter. Even though the iterated extended Kalman filter performed better in general, the control performance with the globally linearised Kalman filter was essentially as good as the performance with the iterated extended Kalman filter when the noise level of the measurement system was 30/3%. Therefore, in such a case, the computational complexity of the system can be decreased by applying the globally linearised Kalman filter without a significant loss in control performance. However, in such a case the performance of the controller was altogether quite poor. By contrast, if the measurement system was very accurate, the advantage of using the iterated extended Kalman filter was clear.

Table 5.3: Time-averaged output errors and the ratio of errors for the globally linearised Kalman filter (KF) and the iterated extended Kalman filter (IEKF) corresponding to the employed noise levels.

Noise level (%)	KF	IEKF	IEKF/KF
1/0.1	0.0032	0.0014	0.44
10/1	0.0024	0.0016	0.67
30/3	0.0036	0.0038	1.1

If the computational time is a crucial issue, the computationally simple algorithm is preferable to the more accurate and expensive algorithm. In such a case, the globally linearised Kalman filter is usually more suitable than the iterated extended Kalman filter provided that the estimate quality is adequate. In high-dimensional problems, the use of the iterated extended Kalman filter may lead to excessive computation times and is, therefore, not feasible for real time operations unless the dimensionality of problem is reduced in a proper manner. The approximation error method [49], [50] discussed in Section 5.2.3 could be used for model reduction which would enable the use of a more computationally demanding state estimation algorithm.

The link between the noise level and the performance of the state estimators shown in the simulations suggests that developing and improving just one procedure of the whole controller chain is useless. For example, choosing a state estimator that generally yields more accurate estimates does not automatically guarantee better control performance if the measurement system is inaccurate and vice versa.

6 Simulations using approximate $\mathcal{H}_\infty$ controller

In this chapter, the performance of the approximate $\mathcal{H}_\infty$ controller discussed in Section 4.2.3 is evaluated with two-dimensional simulations. One of the benefits of the $\mathcal{H}_\infty$ controller is its ability to handle non-Gaussian disturbances which are often encountered in practical process control applications. The disturbance inputs include the modelling and the measurement errors and other unknown (but not necessarily random) external disturbances.

In the two-dimensional simulations in Section 5.1, the input concentration (3.5) was partly unknown. The inclusion of the average input concentration $\bar{c}_{\text{in}}$ led to feasible state estimates and good control performance. Furthermore, it was reasonable to assume that the state noise in Section 5.1 was zero-mean Gaussian noise. In this chapter, the input concentration (3.5) is treated as an external disturbance to the process. The simulations aim to test the approximate $\mathcal{H}_\infty$ controller in the case of the unknown boundary data and the results are compared to the ones obtained with the optimal linear quadratic (LQ) tracker reviewed in Section 2.2.2.

6.1 CONSTRUCTION OF THE APPROXIMATE $\mathcal{H}_\infty$ CONTROLLER

The starting point of this study is similar to the one described in Section 5.1. The concentration evolution is simulated as in Section 5.1 with the exception that the diffusion coefficient $\kappa = 10$ cm^{2}s^{-1}. By increasing the diffusion coefficient, it is easier for the controller to match the output concentration to the desired uniform output concentration. It should be noticed that when simulating the concentration evolution, the input concentration (3.5) is known. Furthermore, the electrical impedance tomography (EIT) observations are simulated as in Section 5.1.

When approximating the solution of the convection-diffusion (CD) model with the finite element method (FEM) for constructing the approximate $\mathcal{H}_\infty$ controller, the input concentration (3.5) is unknown. An approximate boundary condition (3.4) is postulated also for the input boundary Λ_{in} instead of the Dirichlet condition (3.3). Thus, (3.3) and (3.4) are re-

placed with

$$\frac{\partial c}{\partial \vec{n}}(\vec{r},t) \quad = \quad 0, \;\; \vec{r} \in \Lambda. \tag{6.1}$$

The finite element (FE) approximation of the CD equation (3.1) with the initial condition (3.2) and the boundary condition (6.1) is obtained following the approach shown in Section 3.1.5 and Appendix A. The discrete-time state equation is

$$c_{t+1} = Ac_t + B_2 u_t + w_{1,t} \tag{6.2}$$

where the state noise $w_{1,t}$ encompasses also the errors due to the unknown input boundary data. The state-space system consisting of the state equation (6.2) and the observation equation (3.63) is output controllable, but is neither state controllable nor observable.

The objective of the controller is to regulate the concentration distribution over the boundary Λ_{out}. The desired output concentration is 5.1×10^{-3} mol^{-1}cm^2 as in Section 5.1. The approximate $\mathcal{H}_\infty$ controller is derived on the basis of the theory in Section 2.3 with the modifications shown in Section 4.2.3. The only parameters to be specified in the approximate $\mathcal{H}_\infty$ controller are the performance bound γ and the weighting matrices Q_y and R. The lowest feasible performance bound and the weighting matrices are chosen from a set of simulations.

6.2 APPROXIMATE $\mathcal{H}_\infty$ CONTROLLER SIMULATION RESULTS

The uncontrolled concentration evolution, the change in the concentration, and the controlled concentration evolution are shown in Figures 6.1(a), 6.1(b), and 6.1(c), respectively. In Figure 6.1(d), the state estimates of the controlled concentration are shown. As expected, the concentration on the boundary Λ_{in} is not estimated accurately. Also the estimates on the other regions of the pipe are not as accurate as in the approximate linear quadratic Gaussian (LQG) control simulations in Section 5.1. However, with respect to the fact that the input concentration is now completely unknown and an approximate boundary condition is postulated for the boundary Λ_{in}, the estimates are adequate. The effect of postulating a Dirichlet boundary condition for the boundary Λ_{in} in the approximate LQG control simulations can be seen in Figures 5.8(d) and 5.16(b). In those figures, the estimated concentration on the boundary Λ_{in} always equals to the concentration of the homogeneous background due to the

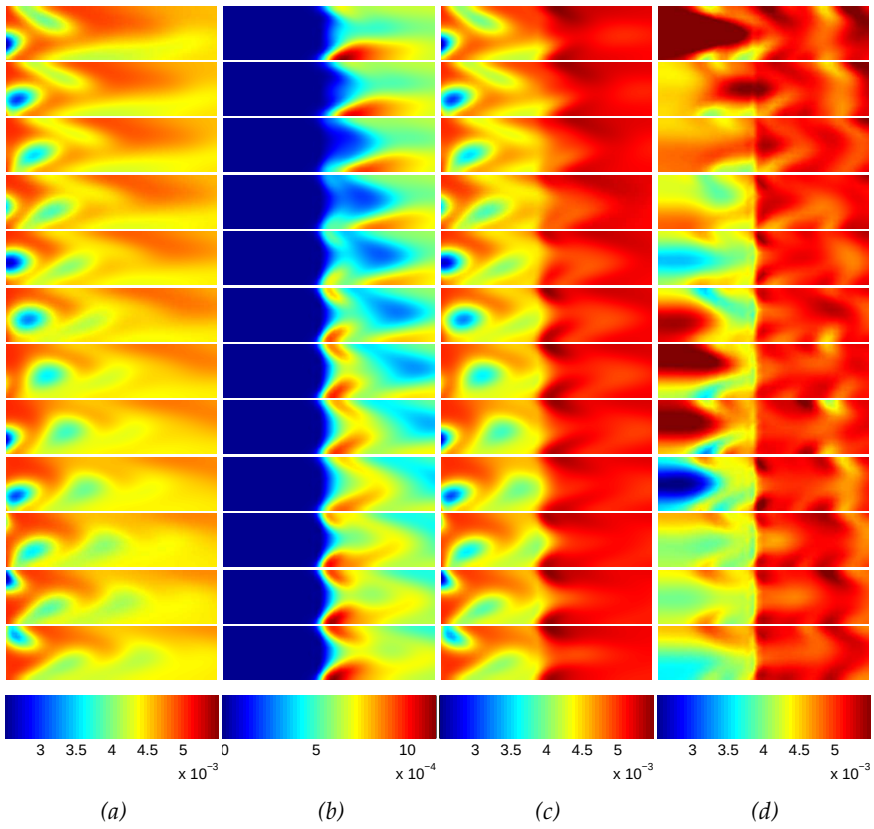

Figure 6.1: (a) The uncontrolled concentration evolution, (b) the change in the concentration, (c) the controlled concentration evolution, and (d) the estimated controlled concentration at times $t = 1.55, \ldots, 2.10$ *s.*

approximation for $\bar{c}_{\text{in}}$. In Figure 6.1(d), the estimated concentration on the boundary Λ_{in} can be far from the homogeneous background concentration. Although the state estimates are only moderately accurate, the approximate $\mathcal{H}_\infty$ controller is able to regulate the output concentration.

The uncontrolled concentration and the controlled concentration over the boundary Λ_{out} are depicted in Figure 6.2. It can be seen that the controlled output concentration matches well the desired output concentration after the initial transient. The output errors are plotted in Figure 6.3. As expected, the output errors are smaller when control is employed.

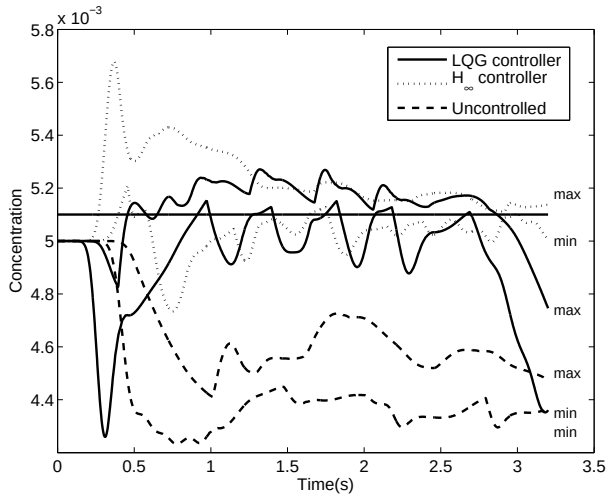

Figure 6.2: The minimum and the maximum value of the uncontrolled concentration and the controlled concentration on the FE nodes on Λ_{out} when using the approximate $\mathcal{H}_\infty$ controller and the LQG controller. The thick black line indicates the desired output concentration.

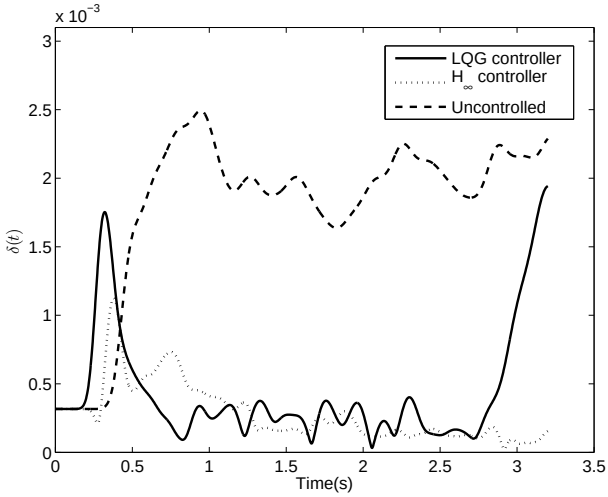

Figure 6.3: The output errors for the uncontrolled concentration and the controlled concentration when using the approximate $\mathcal{H}_\infty$ controller and the LQG controller.

6.3 COMPARISON OF THE OPTIMAL LQ TRACKER AND THE APPROXIMATE $\mathcal{H}_\infty$ CONTROLLER

The performance of the approximate $\mathcal{H}_\infty$ controller is compared to the performance of the LQ tracker. The derivation of the optimal LQ tracker is reviewed in Section 2.2.2. The state estimation method used in the simulations is the globally linearised Kalman filter introduced in Section 2.2.3. In (2.29), the final state $b_N \in \mathbb{R}^{n_\varphi}$ is taken to be a zero vector. The weighting matrices Q_y and R are chosen on the basis of simulations.

The uncontrolled concentration evolution, the change in the concentration, and the controlled concentration evolution when using the optimal LQ tracker are shown in Figures 6.4(a), 6.4(b), and 6.4(c), respectively. The selected times correspond to the times in Figure 6.1. When comparing the controlled concentration evolution in Figure 6.4(c) to the controlled concentration evolution obtained with the approximate $\mathcal{H}_\infty$ controller in Figure 6.1(c), it can be concluded that both controllers are able to increase the output concentration to the desired level in general. However, the approximate $\mathcal{H}_\infty$ controller can regulate the low concentration inclusion better than the LQ tracker. This fact is also seen in Figures 6.1(b) and 6.4(b) in which the injected concentrate when using the approximate $\mathcal{H}_\infty$ controller matches better to the shape and the size of the low concentration inclusion than when using the LQ tracker.

The difference in the performance of the controllers is partly due to the state estimates. In Figure 6.4(d), the state estimates of the controlled concentration when using the LQ tracker are shown. It is evident that the Kalman filter is unable detect the low concentration inclusions when the boundary condition (6.1) is used. Although the state estimates when using the approximate $\mathcal{H}_\infty$ controller in Figure 6.1(d) are not as good as the state estimates with the partly known input boundary data in Section 5.1, the state estimates in Figure 6.1(d) are much better than the state estimates using the LQ tracker in Figure 6.4(d). Actually, the state estimates shown in Figure 6.4(d) are nearly useless.

The uncontrolled concentration and the controlled concentration over the boundary Λ_{out} when using the approximate $\mathcal{H}_\infty$ controller and the optimal LQ tracker are depicted in Figure 6.2. It can be seen that the output concentration using the approximate $\mathcal{H}_\infty$ controller matches better the desired output concentration than when using the LQ tracker. However, the performance of the LQ tracker is also fairly satisfactory. The tracking error of the LQ tracker from time $t = 2.75$ onwards is due to the final condition b_N. Furthermore, the LQ tracker does not overshoot after the initial

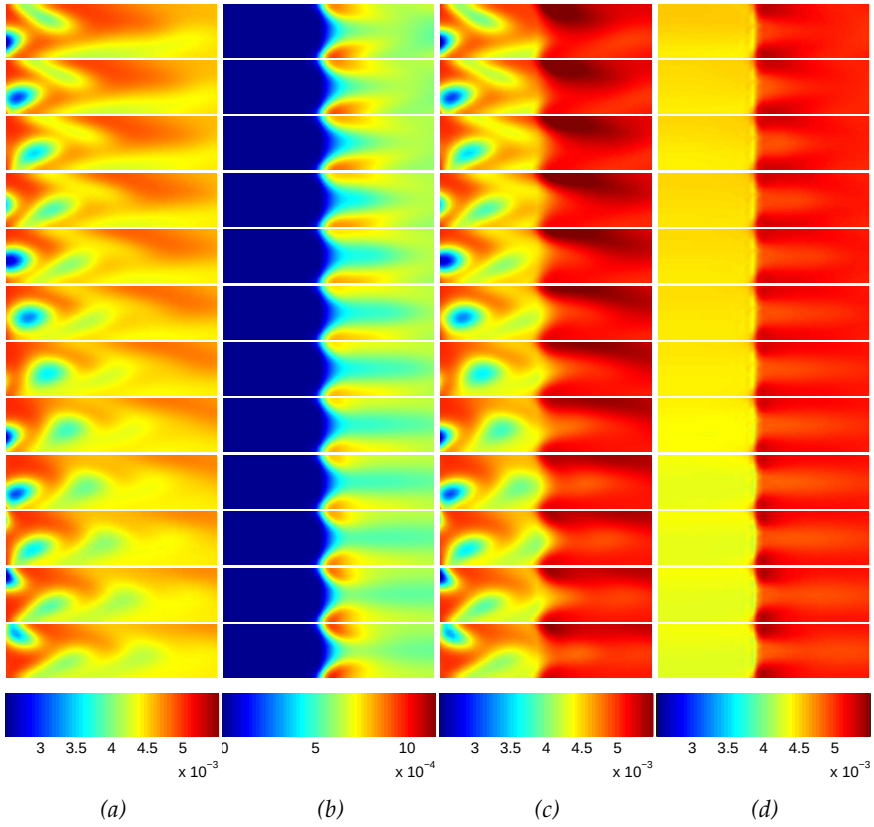

Figure 6.4: (a) The uncontrolled concentration evolution, (b) the change in the concentration, (c) the controlled concentration evolution, and (d) the estimated controlled concentration at times $t = 1.55, \ldots, 2.10$ *s.*

transient as does the approximate $\mathcal{H}_\infty$ controller. The output errors for the approximate $\mathcal{H}_\infty$ controller and the LQ tracker are plotted in Figure 6.3. The output errors are generally smaller when the approximate $\mathcal{H}_\infty$ controller is used.

The reason that the control performance of the LQ tracker is adequate is the effect of diffusion. The LQ tracker is able to increase the mean level of concentration on the basis of the poor state estimates that leads to the adequate control performance. If the diffusion coefficient was smaller, the performance of the LQ tracker would deteriorate (as would also the performance of the approximate $\mathcal{H}_\infty$ controller).

6.4 DISCUSSION OF APPROXIMATE $\mathcal{H}_\infty$ CONTROLLER SIMULATIONS

In this section, the performance of the approximate $\mathcal{H}_\infty$ controller was evaluated. The $\mathcal{H}_\infty$ controller is known to be more robust to external disturbances than the LQG controller. The simulation results indicated that it is possible to design an approximate $\mathcal{H}_\infty$ controller for the CD process when there are external disturbances to the process. The simulations also indicated that the tracking performance and the disturbance rejection of the proposed controller are adequate.

When the input boundary data was unknown and the approximate boundary condition was postulated for Λ_{in}, the approximate $\mathcal{H}_\infty$ controller performed (slightly) better than the optimal LQ tracker. Especially, the low concentration inclusions were detected more precisely and regulated better when using the approximate $\mathcal{H}_\infty$ controller. If the diffusion coefficient was smaller as in Section 5.1 and the concentration variations were larger as in Section 5.4, the performance of the LQ tracker would be even poorer. In such a case, the homogenising effect of diffusion would be lesser and since the LQ tracker is not able to regulate the low concentration inclusions, the output concentration would differ more from the desired concentration.

In many publications, the standard view is that the $\mathcal{H}_\infty$ controller performs generally better than the LQG controller in the case of non-Gaussian disturbances. However, if one is able to formulate proper models for the disturbances and take those models into account when designing the LQG controller, the performance of the LQG controller may easily be better than the performance of the $\mathcal{H}_\infty$ controller designed so that the disturbances are not modelled. For example, the approximation error method discussed in Section 5.2.3 could be applied when analysing the statistical properties of the modelling errors.

7 Optimal injector setting

In some process control applications, the control performance can be enhanced by proper layout of control actuators and/or measurement sensors. In practice, the possible actuator and sensor positions are to a great extent defined by the physical characteristics of the process and the designers often choose them based on physical intuition and experience. For simple system, such decisions are adequate. However as the system becomes more complex geometrically or structurally, decision-making based on intuition may deteriorate the performance of the control system. The optimal positions of actuators and sensors can be determined on the basis of simulations, for example, by inspecting some appropriate performance criterion.

Not only the actuator positions but also the number of actuators has an effect on the control performance. The effect in practical implementations is typically so significant that it is relevant to determine the suitable number of actuators. It is obvious that as the actuator number increases the control performance improves up to a point. The key question in practice is how many actuators are needed for adequate control performance. As an example, one can consider the TrumpJet® injection system for mixing paper making chemicals into the main process stream [216]. The system is designed to operate with only a few injection points located on the pipe boundary.

When considering processes modelled with partial differential equations (PDEs), determining the optimal positions of actuators should be formulated for that infinite-dimensional system instead of the finite-dimensional approximation of the system. Such a formulation would, however, be inapplicable in practice. Thus, a general approach is to use the finite-dimensional approximation and to show that the solution to the optimal actuator problem which is obtained on the basis of the finite-dimensional system is near-optimal in the sense that it approaches the optimal solution to the actuator position problem for the infinite-dimensional system [43], [245], [246], [247], [248]. Furthermore, the topic on optimal sensor positions for distributed parameter systems (DPSs) has been studied in [43], [246], [247], [248], [249]. The publications consider, however, only one-dimensional cases.

In the example application of this thesis, it is assumed that the positions of the electrical impedance tomography (EIT) electrodes are fixed

but the positions and the number of injectors can be modified. Intuitively, if the injectors are close to the boundary Λ_{out} and the diffusion coefficient is small, it is impossible to obtain a uniform or even a smooth concentration distribution on the boundary Λ_{out} with only a few pointwise injectors. Once the injectors are located further back from the boundary Λ_{out}, the injected concentrate has more time to diffuse. Thus, by finding the optimal injector setting the homogenising effect of diffusion can be fully exploited. Furthermore, with only a few injectors regardless of their position one may be able to regulate the mean level of concentration but is more than likely unable to make fine adjustments to remove effects of the low concentration inclusions.

Also intuitively, by locating the injectors in the region in which the state estimation accuracy is as high as possible, the control performance can be improved. Bias in the state estimates creates bias to the optimal control inputs, that in turn results in inadequate concentration distribution on the boundary Λ_{out}. The state estimation accuracy can be deduced, for example, by inspecting the mean state noise variance, that is, time-averaged diagonals of the state estimate covariance. When considering the observability of the motivating application in Section 4.2.4, it was concluded that the estimation accuracy is high downstream of the first electrode pair. The uncertainty of the state estimates very near the input boundary Λ_{in} is typically high, because the input concentration is the primary unknown of the system.

Although one can consider the suitable injector positions and the suitable number of injectors in this example intuitively, the optimal positions and the optimal number of injectors are not clear for example due the (joint) effect of factors such as the state estimation accuracy and the diffusion. Thus in this chapter, the problem of finding the optimal injector positions and the optimal number of injectors for the example application of this thesis is studied with two-dimensional simulations. The aim is to study only one example situation in which parameters such as the diffusion coefficient and the desired concentration level are fixed.

7.1 SIMULATION OF THE CONCENTRATION EVOLUTION AND THE EIT OBSERVATIONS

In this study, six different positions for a series of injectors illustrated in Figure 7.1 are considered. In those positions, the injectors are located in a straight vertical line. Consecutive injectors could be considered for

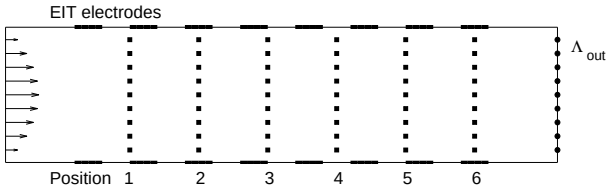

Figure 7.1: The considered injector positions in the pipe segment when $n_k = 9$.

example in a situation in which the flow rates of injectors are not high enough to inject a required amount of strong concentrate.

The set of selected injector numbers to be tested is $N_k = \{1, 3, 5, 7, 9\}$. The single injector is located in the middle of the pipe. There are, actually, commercial systems that are trying to achieve similar goals as in this thesis with just one actuator. When more than one injector is used, the injectors are added symmetrically in a vertical line around the single injector. The maximum number of injectors in this example is chosen to be nine. Nine injectors cover sufficiently the region between the pipe walls. In this section, one of the aims is to determine if adequate control performance can be achieved with fewer than nine injectors. The control performance is evaluated for every position illustrated in Figure 7.1 and for every number of injectors $n_u \in N_k$.

The concentration evolution and the EIT observations are simulated as described in Section 5.1. The only difference is that the structure of the control input matrix B_2 in the convection-diffusion (CD) state equation changes to correspond to the different injector positions and the number of injectors. The globally linearised Kalman filter is used as the state estimator, and the control inputs are computed using the approximate linear quadratic Gaussian (LQG) controller formulated in Section 4.2.2.

7.2 SIMULATION RESULTS USING DIFFERENT INJECTOR SETTINGS

A natural choice to evaluate the performance of the control system is to compute the minimum cost corresponding to (4.14), see [63] for details. Furthermore, the main aim of the control system is to obtain a desired output concentration distribution. The output errors (5.3) reflect this aim and are also considered. It is noted that the distance between the injectors

and the boundary Λ_{out} affects the time required for the controller to bring the concentration on Λ_{out} from its initial state close to the desired level. Thus, the closer the injectors are to the boundary Λ_{out} the shorter is the initial transient and the smaller the output errors. Therefore, the first time instances are excluded from the evaluations of the time-averaged output errors in order to eliminate the error due to the different transient performance. This is reasonable since if a control system is designed to operate for a long time period, the first time instances are irrelevant.

The benefit of control on the process in general is seen in Figure 7.2. In Figure 7.2(a), the uncontrolled concentration evolution is shown. In Figure 7.2(b), nine injectors are in position 1, in Figure 7.2(c), nine injectors are in position 3, and in Figure 7.2(d), nine injectors are in position 6. When the injectors are in position 1, the controller is not able to regulate the low concentration inclusions and the output concentration is lower than the desired output concentration (see especially the bottom six subfigures in Figure 7.2(b)). When the injectors are in position 3, the control system seems to work adequately. When the injectors are in position 6, the controller is able to regulate the low concentration inclusions but the concentration distribution on the boundary Λ_{out} is not as smooth as in the case in which the injectors are in position 3.

The costs for different injector positions and numbers of injectors are computed and plotted in Figure 7.3. As expected, the smallest costs are obtained with nine injectors, and the costs increase as the number of injectors decreases. Furthermore when the injectors are near the boundary Λ_{in}, the uncertainty in the input concentration increases the costs. If one investigated only the costs, one would place nine injectors in position 6.

The output errors for different injector positions when nine injectors are used are plotted in Figure 7.4. The injector positions 3 and 4 have the smallest output errors almost at all times after the initial transient. In Table 7.1, the time-averaged output errors are shown. The time-averaged output errors are smallest for position 3. The time-averaged output errors for different injector positions and numbers of injectors are shown in Figure 7.5. The time-averaged output errors with one injector indicate that if the injector is near the boundary Λ_{in} of the pipe, one is able to regulate the mean concentration level with the help of diffusion. However, with a single injector one cannot remove the effect of the low concentration inclusions. Once the single injector is moved towards the boundary Λ_{out}, the extra concentrate has less time to diffuse and the time-averaged output errors are larger. Especially using five injectors or more, the controller seem to be able to regulate the mean concentration level and also to remove the

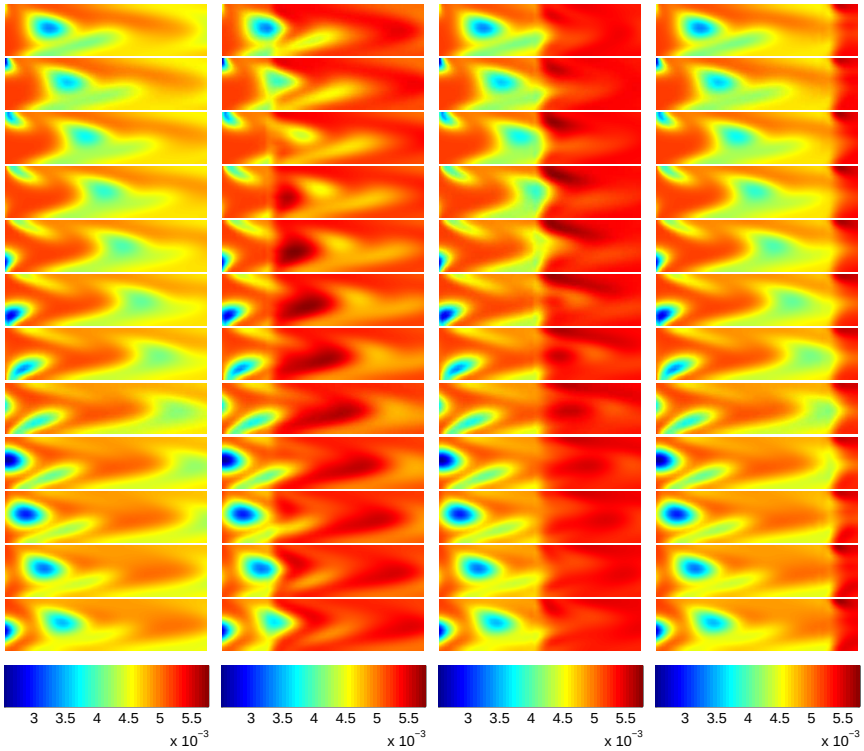

Figure 7.2: (a) The uncontrolled concentration evolution. (b) The controlled concentration evolution when the injectors are in position 1. (c) The controlled concentration evolution when the injectors are in position 3. (d) The controlled concentration evolution when the injectors are in position 6. Nine injectors are used.

effect of the low concentration inclusions.

The output errors for different injector numbers are depicted in Figure 7.6 when the injectors are in position 3. Similarly to the consideration of the costs, the smallest output errors are achieved with nine injectors. The result in this example is obvious since it is difficult to obtain a smooth output concentration profile with only a few injectors despite the diffusion property of the process. However, the output errors for seven injectors are almost as small as for nine injectors. In this case, therefore, the improvements that are obtained by adding more injectors may be of little significance in comparison to the expenses needed to do so.

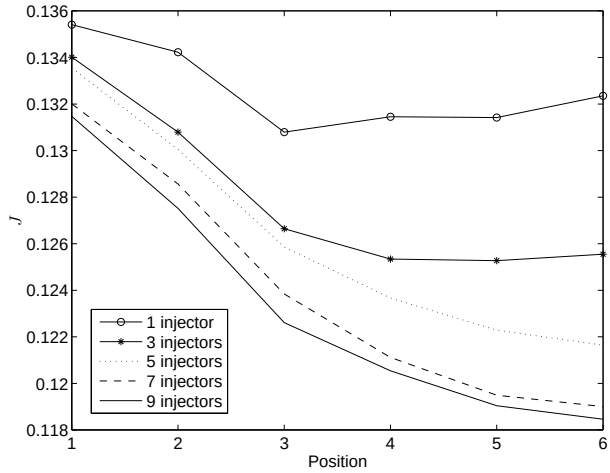

Figure 7.3: The costs J for different injector positions and number of injectors.

Table 7.1: Time-averaged output errors ($\cdot 10^{-3}$) for different injector position and number of injectors.

Position	1 injector	3 injectors	5 injectors	7 injectors	9 injectors
1	1.399	1.023	0.888	0.729	0.619
2	1.320	0.731	0.574	0.469	0.371
3	1.217	0.513	0.381	0.288	0.248
4	1.387	0.651	0.477	0.334	0.304
5	1.515	0.685	0.481	0.327	0.338
6	1.668	0.917	0.535	0.368	0.361

7.3 DISCUSSION OF OPTIMAL INJECTOR SETTING

In this section, the problem of finding the suitable injector positions for the example application of this thesis was investigated. Furthermore, the number of injectors needed to achieve adequate control performance was considered. It was shown that finding the optimal injector setting can improve the performance of the control system in this example. The simulations also indicated that considering the injector positions and the number of injectors intuitively may be difficult if the control performance is

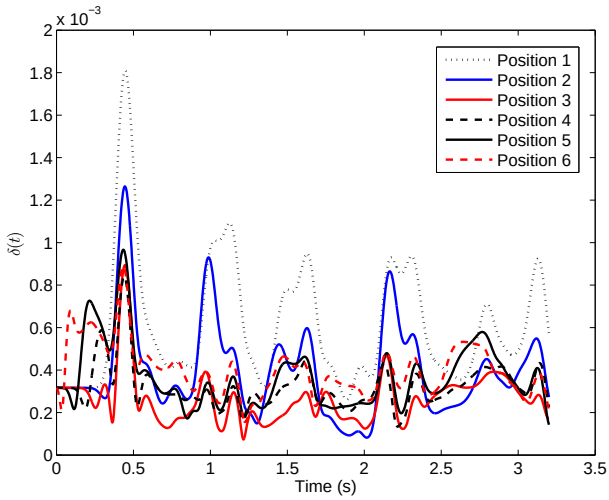

Figure 7.4: The output errors for different injector positions when nine injectors are used.

affected by several factors.

In this example, the homogenising effect of diffusion is closely related to the question of the optimal injector position and the optimal number of injectors. If the effect of diffusion was larger, adequate control performance would be achieved with fewer injectors and the injectors could be located in the regions nearer to the output boundary Λ_{out}. However, with only one injector or with injectors close to the output boundary, the low concentration inclusions could not be regulated even if the effect of diffusion was larger.

The optimal actuator positions could also be studied by considering the conditional number of the output controllability matrix of the state-space system (without the state noise and the measurement noise) provided that the output controllability matrix is of full rank. The condition number of the controllability matrix is an indicator of controllability of the system and small condition numbers indicate ”better” controllability. Thus, by minimizing the conditional number of the controllability matrix with respect to the actuator positions, optimal positions could be found.

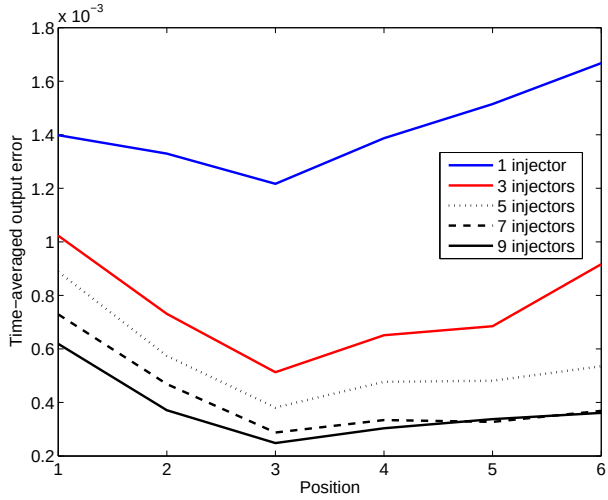

Figure 7.5: Time-averaged output errors for different injector position and number of injectors.

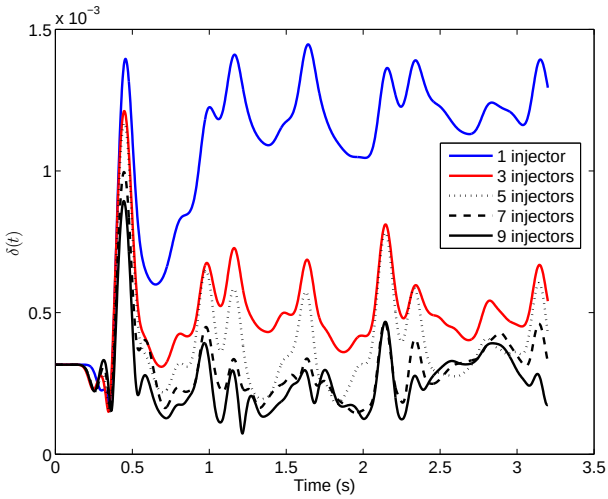

Figure 7.6: The output errors for different injector number when the injectors are in position 3.

8 Conclusions

Since the 1990s, the potential of electrical process tomography (PT) to be used for industrial process monitoring in process control has been recognized. However, only a few practical implementations have been designed. The main reason limiting the use of electrical PT in process control is that the reconstructed images have traditionally been qualitative in nature. For automatic control, quantitative reconstructions are usually needed. The challenge in providing the controller quantitative information about the process using electrical PT is that the reconstruction problem of electrical PT is an ill-posed inverse problem and, thus, sensitive to modelling and measurement errors. Often when controlling an industrial process, modelling and measurement errors cannot be avoided. Thus, one of the key questions is whether the information provided by electrical PT is sufficient for process control when such errors are present.

Furthermore in the practical process control implementations using electrical PT as a sensor, the proportional-integral-derivative (PID) controller has typically been used instead of a physical model-based controller. One of the challenges related to the model-based controllers is how to combine the process models with the data provided by electrical PT. Furthermore, adequate process models can often be complex and, therefore, unsuitable for real time control systems.

In certain types of processes, the information provided by electrical PT may be sufficient for process control. In this thesis, it was shown that it is possible to control a convection-diffusion (CD) process using model-based approximate optimal controllers when the process was monitored with electrical impedance tomography (EIT). As the controlled quantity had both spatial and temporal variations, the CD process was described as a distributed parameter system (DPS) modelled with partial differential equations (PDEs). Also the forward model in EIT was PDE-based. The reconstruction problem of EIT was formulated as a state estimation problem. Previously, the state estimation approach has been shown to produce feasible reconstructions for nonstationary targets. In this thesis, there were uncertainties related to (partly) unknown boundary conditions in the process model. Such uncertainties are typical for PDE models describing industrial processes. The key issue in obtaining sufficient state estimates for the controller was to model the uncertainties related to the unknown boundary conditions and to take these models into account when design-

ing the state estimator and the controller.

When aiming for a real time control system, some simplifications and approximations are often needed in the modelling. Such approximations could be related, for example, to nonstationary flows typically encountered in industrial processes. In this thesis, it was shown that approximating the nonstationary flow with a stationary flow led to adequate control performance as long as the overall process dynamics were adequately accurately modelled. Thus in some cases, the use of such stationary approximations may be reasonable. However, ignoring the time-dependence of the flow fields and modelling them as stationary may in other cases lead to intolerable estimation errors and poor control performance. In such a case, the question is how to take the time-dependence of the flow fields into account when constructing the controller. One approach would be to use the recently developed approximation error method [70], [49] and to model the errors caused by the use of the stationary approximations for nonstationary flow fields [185]. Furthermore in [240], a novel approach to estimate the reduced-order representation of the nonstationary flow field simultaneously with other primary unknown process quantities was introduced when using EIT as a sensor. The reduce-order representation was based on the concept of proper orthogonal decomposition. The above mentioned methods could be applied with minor modifications also to the example application of this thesis if needed.

The models related to the PDE-based DPSs are typically high-dimensional as noticed also in this thesis. If one aims for a real time controller, employing high-dimensional models may prevent real time computations. The traditional and commonly used model reduction techniques in the field of control theory do not take into account the ill-posedness of inverse problems and may lead to approximation errors that can cause poor control performance. The above mentioned approximation error method provides also a way to reduce the dimensionality of the models in the case of inverse problems without destroying the state estimates and, thus, may enable the use of PT as a sensor for real time and model-based optimal controllers. In [250], a reduced-order observation model in stationary EIT was constructed based on the concept of proper orthogonal decomposition and the approximation error approach. In [251], the approach proposed in [250] was extended to deriving reduced-order approximations of both the evolution and observation models in nonstationary EIT. The above mentioned methods could be applied with minor modifications also to the control system discussed in this thesis.

In this thesis, the approximate linear quadratic Gaussian (LQG) controller and the approximate $\mathcal{H}_\infty$ controller were employed. It was shown that the performance of controllers was adequate even when there were non-Gaussian uncertainties related to the process model. In general in the LQG control, the state and measurement noises are assumed to be Gaussian. Furthermore, it is often stated that the $\mathcal{H}_\infty$ controller performs better than the LQG controller if there are non-Gaussian disturbances to the process as shown also in this thesis. This claim, however, is not necessarily valid. If one is able to model the disturbances and utilise those models in the controller design, the performance of the LQG controller may be adequate or even better than the performance of the $\mathcal{H}_\infty$ controller.

When considering industrial processes, there may be physical constraints on the actuators resulting from their operation range and/or on the controlled process quantities resulting from the characteristics of the process. Actuator constraints are typical for web forming processes, for example. When designing a controller, often these constraints cannot be ignored in order to obtain adequate control performance. In this thesis, the constraints on the injectors were taken into account by including a feedforward term in the controller. Typically in the LQG control and the $\mathcal{H}_\infty$ control, the constraints are handled in an *ad hoc* and often quite simple manner. A problem arises when there are several constraints and one tries to find the optimal control input that satisfies them all. When constraints are present, one might want to consider a model predictive controller instead of the LQG controller or the $\mathcal{H}_\infty$ controller. In model predictive control (MPC), the constraints are included in the controller design. The disadvantage of MPC is the computational burden related to the computations especially if the prediction horizon is long. However, proper model reduction might enable real time computations.

In this thesis, model-based controllers were considered. If it is known that there are errors of unknown statistical nature between the actual process and the model, one may obtain better control performance with a PID controller than with a model-based controller. It should be noticed that a single PID controller is typically inapplicable in distributed parameter control systems as it can control only a scalar quantity. However, a comparison between multiple PID controllers and the optimal controllers considered in this thesis could provide interesting additional information in this case. A similar comparison between an auto-tuned PID controller and an adaptive predictive controller can be found for example in [252]. Also an interesting idea that has been previously stated is to use the PID controller together with a feedforward controller. In this case, the process

dynamics would be accounted for in the feedforward part of the controller and the PID controller would regulate the possible remaining deviations of the process output from the desired output.

In general, the control scheme discussed in this thesis can be applied also to other industrial processes besides the CD process and to other imaging modalities besides EIT, provided that proper process and observation models can be derived. Many processes, especially in the chemical industry, are distributed and nonlinear in nature. Electrical PT techniques and the state estimation algorithms can easily be modified for such processes. By contrast, the controllers discussed in this thesis are not applicable as such if the process models are nonlinear. However, it should be noticed that when linearising a process model, an additional model could be derived for linearisation errors. Such an approximative linearised process model taking into account the linearisation errors may be adequate when designing a controller for nonlinear processes.

In the future, the objective is to evaluate the performance of the control system with laboratory experiments. Three-dimensional state estimation of the concentration in a fluid flowing in a pipe has already been successfully tested in a laboratory scale when using a CD process model and EIT observations [179], [113]. As in many industrial processes the unknown quantity has rapid variations and the models are high-dimensional, the approximation error method may be needed to enable real time operations. Furthermore, as the multi-phase flows are typical in practical industrial applications, multi-phase flow models may in some cases improve the control performance. However, the computational burden related to multi-phase flow models is greater than the burden when using a single-phase flow model. As the controller is not based only on the process model but also on the information provided by the electrical PT, a single-phase model may be an adequate approximation for the control of a multi-phase flow.

Bibliography

[1] T. York, "Status of electrical tomography in industrial applications," in *Proceedings of SPIE - Process Imaging for Automatic Control*, Vol. 4188 (2000), pp. 175–190, Boston, Massachusetts, USA, November 5–6.

[2] D. M. Scott and H. McCann, eds., *Process Imaging for Automatic Control* (CRC Press, 2005).

[3] R. A. Williams and M. S. Beck, eds., *Process Tomography: Principles, Techniques and Applications* (Butterworth-Heinemann Ltd, 1995).

[4] A. Tarantola, *Inverse Problem Theory and Methods for Model Parameter Estimation* (SIAM, 2005).

[5] J. P. Kaipio and E. Somersalo, *Statistical and Computational Inverse Problems* (Springer, 2004).

[6] O. M. Ilyas, R. A. Williams, R. Mann, P. Ying, A. M. El-Hamouz, F. J. Dickin, R. B. Edwards, and A. Rushton, "Advances in and prospects for the use of electrical impedance tomography for modelling and scale-up of liquid/liquid and solid/liquid processes," in *Tomographic Techniques for Process Design and Operation* (1993), pp. 251–264.

[7] R. A. Williams, "A journey inside mineral separation processes," *Mineral Engineering* **8,** 721–737 (1995).

[8] R. A. Williams, "Tomographic imaging for modelling and control of mineral processes," *Chemical Engineering Journal* **59,** 71–85 (1995).

[9] S. J. R. Simons, "Control of mixing processes using tomographic data," in *Fluid Mixing 5* (1996), pp. 143–153.

[10] H. Tabe, S. J. R. Simons, J. Savery, R. M. West, and R. A. Williams, "Modelling of multiphase processes using tomographic data for optimisation and control," in *Proceedings of 1st World Congress on Industrial Process Tomography* (1999), pp. 84–89, Buxton, UK, April 14–17.

[11] R. A. Williams, X. Jia, R. M. West, M. Wang, J. C. Cullivan, J. Bond, I. Faulks, T. Dyakowski, S. J. Wang, N. Climpson, J. A. Kostuch, and

D. Payton, "Industrial monitoring of hydrocyclone operation using electrical resistance tomography," *Minerals Engineering* **12,** 1245–1252 (1999).

[12] J. A. Gutiérrez, T. Dyakowski, M. S. Beck, and R. A. Williams, "Using electrical impedance tomography for controlling hydrocyclone underflow discharge," *Powder Technology* **108,** 180–184 (2000).

[13] H. McCann and D. M. Scott, eds., *Proceedings of SPIE, Process Imaging for Automatic Control*, Vol. 4188, (SPIE, 2000).

[14] Y. Dai, A. D. Pachowko, and M. Wang, "The control of polymer addition to raw waste sludge using electrical resistance tomography - a preliminary study," *Particle & Particle Systems Characterization* **21,** 228–233 (2004).

[15] R. Isermann, *Digital Control Systems* (Springer-Verlag, 1989).

[16] M. Morari and J. H. Lee, "Model predictive control: past, present and future," *Computers & Chemical Engineering* **23,** 667–682 (1999).

[17] J. B. Rawlings, "Tutorial overview of model predictive control," *IEEE Control Systems Magazine* **20,** 38–52 (2000).

[18] S. J. Qin and T. A. Badgwell, "A survey of industrial model predictive control technology," *Control Engineering Practice* **11,** 733–764 (2003).

[19] A. Jutan, J. D. Wright, and J. F. MacGregor, "Part III. On-line linear quadratic stochastic control studies," *AIChE Journal* **23,** 751–758 (1977).

[20] J. P. Sorensen, "Experimental investigation of the optimal control of a fixed-bed reactor," *Chemical Engineering Science* **32,** 763–774 (1977).

[21] K. Clement, S. B. Jorgensen, and J. P. Sorensen, "Fixed bed reactor Kalman filtering and optimal control– II Experimental investigation of discrete time case with stochastic disturbances," *Chemical Engineering Science* **55,** 1231–1236 (1980).

[22] W. H. Ray, "Some recent applications of distributed parameter systems theory– A survey," *Automatica* **14,** 281–287 (1978).

[23] D. Dochain, J. P. Babary, and N. Tali-Maamar, "Modelling and adaptive control of nonlinear distributed parameter bioreactors via orthogonal collocation," *Automatica* **28,** 873–883 (1992).

[24] A. A. Patwardhan, G. T. Wright, and T. F. Edgar, "Nonlinear model-predictive control of distributed-parameter system," *Chemical Engineering Science* **47,** 721–735 (1992).

[25] J. Tervo, M. Vauhkonen, P. J. Ronkanen, and J. P. Kaipio, "A three-dimensional finite element model for the control of certain non-linear bioreactors," *Mathematical Methods in the Applied Sciences* **23,** 357–377 (2000).

[26] P. D. Christofides and P. Daoutidis, "Nonlinear control of diffusion-convection-reaction processes," *Computers & Chemical Engineering* **20,** S1071–S1076 (1996).

[27] S. Godasi, A. Karakas, and A. Palazoglu, "Control of nonlinear distributed parameter processes using symmetry groups and invariance conditions," *Computers & Chemical Engineering* **26,** 1023–1036 (2002).

[28] J. A. Villegas, S. R. Duncan, H. G. Wang, W. Q. Yang, and R. S. Raghavan, "Distributed parameter control of a batch fluidised bed dryer," *Control Engineering Practice* **17,** 1096–1106 (2009).

[29] P. D. Christofides and P. Daoutidis, "Feedback control of hyperbolic PDE systems," *AIChE Journal* **42,** 3063–3086 (1996).

[30] M. N. Contou-Carrere and P. Daoutidis, "Model reduction and control of multi-scale reaction-convection processes," *Chemical Engineering Science* **63,** 4012–4025 (2008).

[31] G. E. Stewart, D. M. Gorinevsky, and G. A. Dumont, "Feedback controller design for a spatially distributed system: The paper machine problem," *IEEE Transactions on Control Systems Technology* **11,** 612–628 (2003).

[32] A. Rigopoulos and Y. Arkun, "Reduced order cross-directional controller design for sheet forming processes," *IEEE Transactions on Control Systems Technology* **11,** 746–756 (2003).

[33] P. E. Wellstead, M. B. Zarrop, and S. R. Duncan, "Signal processing and control paradigms for industrial web and sheet manufacturing," *International Journal of Adaptive Control and Signal Processing* **14,** 51–76 (2000).

[34] J. M. Chourot, L. Boillereaux, M. Havet, and A. L. Bail, "Numerical modeling of high pressure thawing: Application to water thawing," *Journal of Food Engineering* **34,** 63–75 (1997).

[35] H. Fibrianto, L. Boillereaux, and J. M. Flaus, "Hybrid automata for linearizing the model of high-pressure thawing," *Control Engineering Practice* **11,** 1253–1262 (2003).

[36] C. C. Doumanidis, "Multiplexed and distributed control of automated welding," *IEEE Control Systems Magazine* **14,** 13–24 (1994).

[37] C. C. Doumanidis and N. Fourligkas, "Temperature distribution control in scanned thermal processing of thin circular parts," *IEEE Transactions on Control Systems Technology* **9,** 708–717 (2001).

[38] P. D. A. Jones, S. R. Duncan, T. Rayment, and P. S. Grant, "Control of temperature profile for a spray deposition process," *IEEE Transactions on Control Systems Technology* **11,** 656–667 (2003).

[39] V. A. Tsachouridis, P. Jones, and S. Duncan, "Control of a sprayform tooling process in rapid manufacture," *Transactions of the Institute of Measurement and Control* **28,** 309–322 (2006).

[40] A. Emami-Naeini, J. L. Ebert, D. de Roover, R. L. Kosut, M. Dettori, L. M. L. Porter, and S. Ghosal, "Modeling and control of distributed parameter systems," *IEEE Transactions on Control Systems Technology* **11,** 668–683 (2003).

[41] H. Shang, J. F. Forbes, and M. Guay, "Model predictive control for quasilinear hyperbolic distributed parameter systems," *Industrial and Engineering Chemistry Research* **43,** 2140–2149 (2004).

[42] M. Nihtilä, J. Tervo, and J. P. Kaipio, "Simulation of a nonlinear distributed parameter bioreactor by FEM approach," *Simulation Practice and Theory* **5,** 199–216 (1997).

[43] M. Yoshida and S. Matsumoto, "Controller design for parabolic distributed parameter systems using finite integral transform techniques," *Journal of Process Control* **6,** 359–366 (1996).

[44] A. R. Ruuskanen, A. Seppänen, S. Duncan, E. Somersalo, and J. P. Kaipio, "Using process tomography as a sensor for optimal control," *Applied Numerical Mathematics* **56,** 37–54 (2006).

[45] P. D. Christofides and P. Daoutidis, "Finite-dimensional control of parabolic PDE systems using approximate inertial manifolds," *Journal of Mathematical Analysis and Applications* **216,** 398–420 (1997).

[46] S. Y. Shvartsman and I. G. Kevrekidis, "Nonlinear model reduction for control of distributed systems: a computer-assisted study," *AIChE Journal* **44,** 1579–1595 (1998).

[47] N. Mahaveden and K. A. Hoo, "Wavelet-based model reduction of distributed parameter systems," *Chemical Engineering Science* **55,** 4271–4290 (2000).

[48] J. Baker and P. D. Christofides, "Finite-dimensional approximation and control of non-linear parabolic PDE systems," *International Journal of Control* **73,** 439–456 (2000).

[49] J. M. J. Huttunen and J. P. Kaipio, "Approximation errors in nonstationary inverse problems," *Inverse Problems and Imaging* **1,** 77–93 (2007).

[50] J. M. J. Huttunen and J. P. Kaipio, "Approximation error analysis in nonlinear state estimation with an application to state-space identification," *Inverse Problems* **23,** 2141–2157 (2007).

[51] J. P. Kaipio and E. Somersalo, "Statistical inverse problems: Discretization, model reduction and inverse crimes," *Journal of Computational and Applied Mathematics* **198,** 493–504 (2007).

[52] A. R. Ruuskanen, A. Seppänen, and J. P. Kaipio, "Optimal actuator placement for controlling concentration profiles via process tomography," *Inverse Problems in Science and Engineering* **14,** 819–836 (2006).

[53] A. R. Ruuskanen, A. Seppänen, S. Duncan, E. Somersalo, and J. P. Kaipio, "Optimal control in process tomography," in *Proceedings of 3rd World Congress on Industrial Process Tomography* (2003), pp. 245–251, Banff, Canada, September 2–5.

[54] A. R. Ruuskanen, A. Seppänen, S. Duncan, E. Somersalo, and J. P. Kaipio, "Using tomographic measurements in process control," in *Proceedings of 43rd IEEE Conference on Decision and Control* (2004), FrB04.1, Paradise Island, The Bahamas, December 14-17.

[55] A. R. Ruuskanen, A. Seppänen, E. Somersalo, and J. P. Kaipio, "The effect of linearizing the EIT observation model in concentration control problems," in *Proceedings of 4th World Congress on Industrial Process Tomography* (2005), pp. 873–878, Aizu, Japan, September 2–5.

[56] A. R. Ruuskanen and J. P. Kaipio, "Model-based control of concentration profile with impedance tomographic measurements," in *Proceedings of Control Systems 2006* (2006), pp. 141–146, Tampere, Finland, June 6–8.

[57] S. Duncan, J. Kaipio, A. R. Ruuskanen, M. Malinen, and A. Seppänen, "Control systems," in *Process Imaging for Automatic Control* (2005), pp. 237–262.

[58] R. H. Middleton and G. C. Goodwin, *Digital Control and Estimation: A Unified Approach* (Prentice-Hall, Inc., 1990).

[59] O. L. R. Jacobs, *Introduction to Control Theory* (Oxford University Press, 1993).

[60] S. Bennett, "A brief history of automatic control," *Control Systems Magazine* **16,** 17–25 (1996).

[61] J. G. Balchen, "How have we arrived at the present state of knowledge in process control? Is there a lesson to be learned?," *Journal of Process Control* **9,** 101–108 (1999).

[62] B. D. O. Anderson and J. B. Moore, *Optimal Control, Linear Quadratic Methods* (Prentice-Hall, Inc., 1989).

[63] J. B. Burl, *Linear Optimal Control, $\mathcal{H}_2$ and $\mathcal{H}_\infty$ Methods* (Addison Wesley Longman, Inc., 1999).

[64] M. Green and D. J. N. Limebeer, *Linear Robust Control* (Prentice-Hall, Inc., 1995).

[65] D. E. Kirk, *Optimal Control Theory, An Introduction* (Dover Publications, Inc., 1998).

[66] R. F. Stengel, *Optimal Control and Estimation* (Dover Publications, Inc., 1994).

[67] S. M. Shinners, *Modern Control System Theory and Design* (John Wiley & Sons, Inc., 1998).

[68] F. L. Lewis, "Optimal Control," in *The Control Handbook* (1996), pp. 759–778.

[69] G. F. Franklin, J. D. Powell, and A. Emami-Naeini, *Feedback Control of Dynamic Systems* (Addison-Wesley, 1993).

[70] J. P. Kaipio, S. Duncan, A. Seppänen, E. Somersalo, and A. Voutilainen, "State estimation," in *Process Imaging for Automatic Control* (2005), pp. 207–235.

[71] A. Gelb, ed., *Applied Optimal Estimation* (The M.I.T. Press, 1974).

[72] B. D. O. Anderson and J. B. Moore, *Optimal Filtering* (Prentice-Hall, Inc., 1979).

[73] A. Doucet, N. de Freitas, and N. Gordon, eds., *Sequential Monte Carlo Methods in Practice* (Spinger, 2001).

[74] W. Gilks, S. Richardson, and D. Spiegelhalter, *Markov Chain Monte Carlo in Practice* (Chapman and Hall, 1996).

[75] R. E. Kalman, "A new approach to linear filtering and prediction problems," *Transactions of the ASME– Journal of Basic Engineering* **82,** 35–45 (1960).

[76] A. Doucet, S. Godsill, and C. Andrieu, "On sequential Monte Carlo sampling methods for Bayesian filtering," *Statistics and Computing* **10,** 197–208 (2000).

[77] Å. Björck, *Numerical Methods for Least Squares Problems* (SIAM, 1996).

[78] K. Zhou, J. C. Doyle, and K. Glover, *Robust and Optimal Control* (Prentice Hall, Inc., 1996).

[79] K. R. Muske and J. B. Rawlings, "Model predictive control with linear models," *AIChE Journal* **39,** 262–287 (1993).

[80] K. J. Åström, "PID Control," in *The Control Handbook* (1996), pp. 198–209.

[81] L. C. Westphal, *Handbook of Control Systems Engineering* (Kluwer Academic Publisher, 2001).

[82] R. E. Kalman and R. S. Bucy, "New results in linear filtering and prediction theory," *Transactions of the ASME– Journal of Basic Engineering* **83,** 95–108 (1961).

[83] H. F. Chen, "On stochastic observability and controllability," *Automatica* **16,** 179–190 (1980).

[84] Y. Sunahara, T. Kabeuchi, Y. Asada, S. Aihara, and K. Kishino, "On stochastic controllability for nonlinear systems," *IEEE Transactions on Automatic Control* **19,** 49–54 (1974).

[85] J. Klamka, "Stochastic controllability of systems with variable delay in control," *Bulletin of the Polish Academy of Sciences* **56,** 279–284 (2008).

[86] Z. Y. Li, Y. Wang, B. Zhou, and G. R. Duan, "Detectability and observability of discrete-time stochastic systems and their applications," *Automatica* **45,** 1340–1346 (2009).

[87] Z. Benzaid, "On the constrained controllability of linear time-varying discrete systems," *IEEE Transactions on Automatic Control* **44,** 608–612 (1999).

[88] J. Klamka, "Controllability of dynamical systems," *Matematyka Stosowana* **9,** 57–75 (2008).

[89] F. Albertini and D. D'Alessandro, "Observability and forward-backward observability of discrete-time nonlinear systems," *Mathematics of Control, Signals, and Systems* **15,** 275–290 (2002).

[90] K. Rieger, K. Schlacher, and J. Holl, "On the observability of discrete-time dynamic systems – A geometric approach," *Automatica* **44,** 2057–2062 (2008).

[91] D. L. Russell, "Optimal Control," in *The Control Handbook* (1996), pp. 1169–1175.

[92] A. Seppänen, M. Vauhkonen, P. J. Vauhkonen, E. Somersalo, and J. P. Kaipio, "State estimation with fluid dynamical evolution models in process tomography– An application to impedance tomography," *Inverse Problems* **17,** 467–483 (2001).

[93] M. Griebel, T. Dornseifer, and T. Neunhoeffer, *Numerical Simulations in Fluid Dynamics* (SIAM, 1998).

[94] K. Avila, D. Moxey, A. de Lozar, M. Avila, D. Barkley, and B. Hof, "The onset of turbulence in pipe flow," *Science* **333,** 192–196 (2011).

[95] A. Seppänen, M. Vauhkonen, P. J. Vauhkonen, A. Voutilainen, and J. P. Kaipio, "State estimation in process tomography– Three-dimensional impedance imaging of moving fluids," *International Journal for Numerical Methods in Engineering* **73,** 1651–1670 (2008).

[96] G. Strang and G. J. Fix, *An Analysis of the Finite Element Method* (Prentice Hall, Inc., 1973).

[97] S. C. Brenner and L. R. Scott, *The Mathematical Theory of Finite Element Methods* (Springer-Verlag, 1994).

[98] K. W. Morton, *Numerical Solution of Convection-Diffusion Problems* (Chapman & Hall, 1996).

[99] A. P. Calderón, "On an inverse boundary value problem," in *Seminar on Numerical Analysis and its Applications to Continuum Physics* (1980), pp. 65–73, Rio de Janeiro, Brazil.

[100] K. Astala and L. Päivärinta, "Calderon's inverse conductivity problem in plane," *Annals of Mathematics* **163,** 265–299 (2006).

[101] E. Somersalo, M. Cheney, and D. Isaacson, "Existence and uniqueness for electrode models for electric current computed tomography," *SIAM Journal on Applied Mathematics* **52,** 1023–1040 (1992).

[102] M. Vauhkonen, *Electrical Impedance Tomography and Prior Information*, PhD thesis (University of Kuopio, 1997).

[103] K. S. Cheng, D. Isaacson, J. C. Newell, and D. G. Gisser, "Electrode models for electric current computed tomography," *IEEE Transactions on Biomedical Engineering* **36,** 918–924 (1989).

[104] K. Paulson, W. Breckon, and M. Pidcock, "Electrode modelling in electrical impedance tomography," *SIAM Journal on Applied Mathematics* **52,** 1012–1022 (1992).

[105] M. Vauhkonen, D. Vadasz, P. A. Karjalainen, E. Somersalo, and J. P. Kaipio, "Tikhonov regularization and prior information in electrical impedance tomography," *IEEE Transactions on Medical Imaging* **17,** 285–293 (1998).

[106] P. J. Vauhkonen, M. Vauhkonen, T. Savolainen, and J. P. Kaipio, "Three-dimensional electrical impedance tomography based on the complete electrode model," *IEEE Transactions on Biomedical Engineering* **46,** 1150–1160 (1999).

[107] P. J. Vauhkonen, *Image Reconstruction in Three-Dimensional Electrical Impedance Tomography*, PhD thesis (University of Kuopio, 2004).

[108] P. J. Vauhkonen, *Second Order and Infinite Elements in Three Dimensional Electrical Impedance Tomography*, Phil.Lic. thesis (University of Kuopio, 1999).

[109] J. P. Kaipio, V. Kolehmainen, M. Vauhkonen, and E. Somersalo, "Inverse problems with structural prior information," *Inverse Problems* **15,** 713–729 (1999).

[110] L. M. Heikkinen, T. Vilhunen, R. M. West, and M. Vauhkonen, "Simultaneous reconstruction of electrode contact impedances and internal electrical properties: II. Laboratory experiments," *Measurement Science and Technology* **13,** 1855–1861 (2002).

[111] T. Vilhunen, J. P. Kaipio, P. J. Vauhkonen, T. Savolainen, and M. Vauhkonen, "Simultaneous reconstruction of electrode contact

impedances and internal electrical properties: I. Theory," *Measurement Science and Technology* **13,** 1848–1854 (2002).

[112] R. G. Aykroyd and B. A. Cattle, "A boundary-element approach for the complete-electrode model of EIT illustrated using simulated and real data," *Inverse Problems in Science and Engineering* **15,** 441–461 (2007).

[113] A. Voutilainen, A. Lehikoinen, M. Vauhkonen, and J. P. Kaipio, "Three-dimensional nonstationary electrical impedance tomography with a single electrode layer," *Measurement Science and Technology* **21,** 035107 (2010).

[114] L. M. Heikkinen, *Statistical Estimation Methods for Electrical Process Tomography*, PhD thesis (University of Kuopio, 2005).

[115] A. Seppänen, *State Estimation in Process Tomography*, PhD thesis (University of Kuopio, 2005).

[116] J. P. Kaipio, V. Kolehmainen, E. Somersalo, and M. Vauhkonen, "Statistical inversion and Monte Carlo sampling methods in electrical impedance tomography," *Inverse Problems* **16,** 1487–1522 (2000).

[117] J. C. Newell, D. G. Gisser, and D. Isaacson, "An electric current tomograph," *IEEE Transactions on Biomedical Engineering* **35,** 828–833 (1988).

[118] R. D. Cook, G. J. Saulnier, D. G. Gisser, J. C. Goble, J. C. Newell, and D. Isaacson, "ACT3: A high-speed, high-precision electrical impedance tomograph," *IEEE Transactions on Biomedical Engineering* **41,** 713–722 (1994).

[119] R. W. M. Smith, I. L. Freeston, and B. H. Brown, "A real-time electrical impedance tomography system for clinical use – Design and preliminary results," *IEEE Transactions on Biomedical Engineering* **42,** 133–139 (1995).

[120] T. Savolainen, J. P. Kaipio, and P. A. Karjalainen, "An electrical impedance tomography measurement system for experimental use," *Review of Scientific Instruments* **67,** 3605–3609 (1996).

[121] R. Mann, F. J. Dickin, M. Wang, T. Dyakowski, R. A. Williams, R. B. Edwards, A. E. Forrest, and P. J. Holden, "Application of electrical resistance tomography to interrogate mixing processes at plant scale," *Chemical Engineering Science* **52,** 2087–2097 (1997).

[122] T. Savolainen, L. M. Heikkinen, M. Vauhkonen, and J. P. Kaipio, "A modular, adaptive electrical impedance tomography system," in *Proceedings of 3rd World Congress on Industrial Process Tomography* (2003), pp. 50–55, Banff, Canada, September 2–5.

[123] M. Wang, Y. Ma, N. Holliday, Y. Dai, R. A. Williams, and G. Lucas, "A high-performance EIT system," *IEEE Sensors Journal* **5,** 289–299 (2005).

[124] J. Kourunen, T. Savolainen, A. Lehikoinen, M. Vauhkonen, and L. M. Heikkinen, "A PXI-based electrical impedance tomography system for industrial use," *Measurement Science and Technology* **20,** 015503 (2009).

[125] B. D. Grieve, S. Murphy, A. Burnett-Thompson, and T. A. York, "An accessible electrical impedance tomograph for 3D imaging," *Transactions of the Institute of Measurement and Control* **32,** 31–50 (2010).

[126] Industrial Tomography Systems, ITS, http://www.itoms.com (valid 22.2.2013).

[127] D. C. Barber and B. H. Brown, "Applied potential tomography," *Journal of Physics E: Scientific Instruments* **17,** 723–733 (1984).

[128] N. J. Avis and D. C. Barber, "Adjacent or polar drive?: Image reconstruction implications in electrical impedance Tomography systems employing filtered back projection," in *Proceedings of 14th Annual International Conference of the IEEE Engineering in Medicine and Biology Society* (1992), pp. 1689–1690, Paris, France, October 29–November 1.

[129] N. J. Avis and D. C. Barber, "Image reconstruction using non-adjacent drive configurations," *Physiological Measurement* **15,** A153–A160 (1994).

[130] B. M. Eyüboglu and T. C. Pilkington, "Comments on distinguishability in electrical impedance imaging," *IEEE Transactions on Biomedical Engineering* **40,** 1328–1330 (1993).

[131] D. Isaacson, "Distinguishability of conductivities by electrical current computed tomography," *IEEE Transactions on Medical Imaging* **5,** 91–95 (1986).

[132] K. S. Cheng, S. J. Simske, D. Isaacson, J. C. Newell, and D. G. Gisser, "Errors due to measuring voltage on current-carrying electrodes in electric current computed tomography," *IEEE Transactions on Biomedical Engineering* **37,** 60–65 (1990).

[133] M. Cheney and D. Isaacson, "Distinguishability in impedance imaging," *IEEE Transactions on Biomedical Engineering* **39,** 852–860 (1992).

[134] A. Köksal and B. M. Eyüboglu, "Determination of optimum injected current patterns in electrical impedance tomography," *Physiological Measurement* **16,** A99–A109 (1995).

[135] W. R. B. Lionheart, J. Kaipio, and C. N. McLeod, "Generalized optimal current patterns and electrical safety in EIT," *Physiological Measurement* **22,** 85–90 (2001).

[136] D. G. Gisser, D. Isaacson, and J. C. Newell, "Current topics in impedance imaging," *Clinical Physics and Physiological Measurement* **8,** A39–A46 (1987).

[137] D. G. Gisser, D. Isaacson, and J. C. Newell, "Theory and performance of an adaptive current tomography system," *Clinical Physics and Physiological Measurement* **9,** A35–A41 (1988).

[138] D. G. Gisser, D. Isaacson, and J. C. Newell, "Electric current computed tomography and eigenvalues," *SIAM Journal on Applied Mathematics* **50,** 1623–1634 (1990).

[139] P. Hua, E. J. Woo, J. G. Webster, and W. J. Tompkins, "Improved methods to determine optimal currents in electrical impedance tomography," *IEEE Transactions on Medical Imaging* **11,** 488–495 (1992).

[140] J. P. Kaipio, A. Seppänen, E. Somersalo, and H. Haario, "Posterior covariance related optimal current patterns in electrical impedance tomography," *Inverse Problems* **20,** 919–936 (2004).

[141] J. P. Kaipio, A. Seppänen, A. Voutilainen, and H. Haario, "Optimal current patterns in dynamical electrical impedance tomography imaging," *Inverse Problems* **23,** 1201–1214 (2007).

[142] P. Metherall, D. C. Barber, R. H. Smallwood, and B. H. Brown, "Three-dimensional electrical impedance tomography," *Nature* **380,** 509–512 (1996).

[143] L. M. Heikkinen, J. Kourunen, T. Savolainen, P. J. Vauhkonen, J. P. Kaipio, and M. Vauhkonen, "Real time three-dimensional electrical impedance tomography applied in multiphase flow imaging," *Measurement Science and Technology* **17,** 2083–2087 (2006).

[144] D. C. Barber, B. H. Brown, and I. L. Freeston, "Imaging spatial distributions of resistivity using applied potential tomography," *Electronic Letters* **19,** 933–935 (1983).

[145] D. C. Barber and B. H. Brown, "Recent developments in applied potential tomography– APT," in *Information Processing in Medical Imaging* (1986), pp. 106–121.

[146] F. Santosa and M. Vogelius, "A backprojection algorithm for electrical impedance imaging," *SIAM Journal on Applied Mathematics* **50,** 216–243 (1990).

[147] C. J. Kotre, "A sensitivity coefficient method for the reconstruction of electrical impedance tomography," *Clinical Physics and Physiological Measurement* **10,** 275–281 (1989).

[148] C. J. Kotre, "EIT image reconstruction using sensitivity weighted filtered backprojection," *Physiological Measurement* **15,** A125–A136 (1994).

[149] M. A. Player, J. van Weereld, J. M. S. Hutchison, A. R. Allen, and L. Shang, "An electrical impedance tomography algorithm with well-defined spectral properties," *Measurement Science and Technology* **10,** L9–L14 (1999).

[150] T. J. Yorkey, J. G. Webster, and W. J. Tompkins, "Comparing reconstruction algorithms for electrical impedance tomography," *IEEE Transactions on Biomedical Engineering* **34,** 843–852 (1987).

[151] P. Hua, E. J. Woo, J. G. Webster, and W. J. Tompkins, "Iterative reconstruction methods using regularization and optimal current patterns in electrical impedance tomography," *IEEE Transactions on Medical Imaging* **10,** 621–628 (1991).

[152] E. J. Woo, P. Hua, J. G. Webster, and W. J. Tompkins, "A robust image reconstruction algorithm and its parallel implementation in electrical impedance tomography," *IEEE Transactions on Medical Imaging* **12,** 137–146 (1993).

[153] W. Ruan, R. Guardo, and A. Adler, "Experimental evaluation of two iterative reconstruction methods for induced current electrical impedance tomography," *IEEE Transactions on Medical Imaging* **15,** 180–187 (1996).

[154] D. C. Dobson, "Convergence of a reconstruction method for the inverse conductivity problem," *SIAM Journal on Applied Mathematics* **52,** 442–458 (1992).

[155] M. Glidewell and K. T. Ng, "Anatomically constrained electrical impedance tomography for anisotropic bodies via two-step approach," *IEEE Transactions on Medical Imaging* **13,** 498–503 (1995).

[156] A. N. Tihonov, "Solution of incorrectly formulated problems and the regularization method," *Doklady Mathematics* **4,** 1035–1038 (1963).

[157] K. Paulson, W. Lionheart, and M. Pidcock, "POMPUS: an optimized EIT reconstruction algorithm," *Inverse Problems* **11,** 425–437 (1995).

[158] L. M. Heikkinen, M. Vauhkonen, T. Savolainen, K. Leinonen, and J. P. Kaipio, "Electrical process tomography with known internal structures and resistivities," *Inverse Problems in Engineering* **9,** 431–454 (2001).

[159] V. Kolehmainen, *Novel Approach to Image Reconstruction in Diffusion Tomography*, PhD thesis (University of Kuopio, 2001).

[160] R. M. West, R. G. Aykroyd, S. Meng, and R. A. Williams, "Markov chain Monte Carlo techniques and spatial-temporal modelling for medical EIT," *Physiological Measurement* **25,** 181–194 (2004).

[161] R. M. West, S. Meng, R. G. Aykroyd, and R. A. Williams, "Spatial-temporal modeling for electrical impedance imaging of a mixing process," *Review of Scientific Instruments* **76,** 073703 (2005).

[162] A. Adler and R. Guardo, "Electrical impedance tomography: regularized imaging and contrast detection," *IEEE Transactions on Medical Imaging* **15,** 170–179 (1996).

[163] E. Somersalo, J. Kaipio, M. Vauhkonen, D. Baroudi, and S. Järvenpää, "Impedance imaging and Markov chain Monte Carlo methods," in *Proceedings of SPIE 42nd Annual Meeting, Computational Experimental and Numerical Methods for Solving Ill-posed Inverse Problems: Medical and Nonmedical Applications* (1997), pp. 175–185, San Diego, California, USA, July 27– August 1.

[164] V. Kolehmainen, E. Somersalo, P. J. Vauhkonen, M. Vauhkonen, and J. P. Kaipio, "A Bayesian approach and total variation priors in 3D electrical impedance tomography," in *Proceedings of the 20th Annual International Conference of the IEEE Engineering in Medicine and Biology Society*, Vol. 20 (1998), pp. 1028–1031, Hong Kong, October 29–November 1.

[165] T. Martin and J. Idier, "A FEM-based nonlinear MAP estimator in electrical impedance tomography," in *Proceedings of IEEE International Conference on Image Processing*, Vol. 2 (1997), pp. 684–687, Santa Barbara, California, USA, October 26–29.

[166] C. Fox and G. Nicholls, "Sampling conductivity images via MCMC," in *Proceedings of Leeds Annual Statistical Research Workshop, The Art and Science of Bayesian Image Analysis* (1997), pp. 91–100, Leeds, UK, June 30–July 2.

[167] G. K. Nicholls and C. Fox, "Prior modelling and posterior sampling in impedance imaging," in *Proceedings of SPIE, Bayesian Inference for Inverse Problems*, Vol. 3459 (1998), pp. 116–127, San Diego, California, USA, July 23–24.

[168] J. Kourunen, L. M. Heikkinen, M. Vauhkonen, R. Käyhkö, J. Matula, and J. Käyhkö, "Imaging of mixing of two miscible liquids using electrical impedance tomography," in *Proceedings of 5th World Congress on Industrial Process Tomography* (2007), pp. 803–809, Bergen, Norway, September 3–6.

[169] D. Baroudi, J. Kaipio, and E. Somersalo, "Dynamical electric wire tomography: a time series approach," *Inverse Problems* **14,** 799–813 (1998).

[170] J. P. Kaipio and E. Somersalo, "Nonstationary inverse problems and state estimation," *Journal of Inverse and Ill Posed Problems* **7,** 273–282 (1999).

[171] J. P. Kaipio, P. A. Karjalainen, E. Somersalo, and M. Vauhkonen, "State estimation in time-varying electrical impedance tomography," *Annals of the New York Academy of Sciences* **873,** 430–439 (1999).

[172] M. Vauhkonen, P. A. Karjalainen, and J. P. Kaipio, "A Kalman filter approach to track fast impedance changes in electrical impedance tomography," *IEEE Transactions on Biomedical Engineering* **45,** 486–493 (1998).

[173] P. J. Vauhkonen, M. Vauhkonen, T. Mäkinen, P. A. Karjalainen, and J. P. Kaipio, "Dynamic electrical impedance tomography– Phantom studies," *Inverse Problems in Engineering* **8,** 495–510 (2000).

[174] P. J. Vauhkonen, M. Vauhkonen, and J. P. Kaipio, "Fixed-lag smoothing and state estimation in dynamic electrical impedance tomography," *International Journal for Numerical Methods in Engineering* **50,** 2159–2209 (2001).

[175] K. Y. Kim, B. S. Kim, M. C. Kim, Y. J. Lee, and M. Vauhkonen, "Image reconstruction in time-varying electrical impedance tomography based on the extended Kalman filter," *Measurement Science and Technology* **12,** 1032–1039 (2001).

[176] K. Y. Kim, S. I. Kang, M. C. Kim, S. Kim, Y. J. Lee, and M. Vauhkonen, "Dynamic image reconstruction in electrical impedance tomography with known internal structures," *IEEE Transactions on Magnetics* **38,** 1301–1304 (2002).

[177] F. C. Trigo, R. Gonzalez-Lima, and M. B. P. Amato, "Electrical impedance tomography using the extended Kalman filter," *IEEE Transactions on Biomedical Engineering* **51,** 72–81 (2004).

[178] A. Seppänen, L. Heikkinen, T. Savolainen, A. Voutilainen, E. Somersalo, and J. P. Kaipio, "An experimental evaluation of state estimation with fluid dynamical models in process tomography," *Chemical Engineering Journal* **127,** 23–30 (2007).

[179] A. Lipponen, A. Seppänen, and J. P. Kaipio, "Nonstationary approximation error approach to imaging of three-dimensional pipe flow: experimental evaluation," *Measurement Science and Technology* **22,** 1–13 (2011).

[180] T. J. Chung, *Computational Fluid Dynamics* (Cambridge University Press, 2002).

[181] M. Manninen, V. Taivassalo, and S. Kallio, "On mixture model for multiphase flow," *VTT Publications* **288** (1996).

[182] R. A. Williams, X. Jia, and S. L. McKee, "Development of slurry mixing models using electrical resistance tomography," *Powder Technology* **87,** 21–27 (1996).

[183] B. G. M. van Wachem and A. E. Almstedt, "Methods for multiphase computational fluid dynamics," *Chemical Engineering Journal* **96,** 81–89 (2003).

[184] C. E. Brennen, *Fundamentals of Multiphase Flow* (Cambridge University Press, 2005).

[185] A. Lipponen, A. Seppänen, J. Hämäläinen, and J. P. Kaipio, "Nonstationary inversion of convection-diffusion problems - recovery from unknown nonstationary velocity fields," *Inverse Problems and Imaging* **4,** 463–483 (2010).

[186] H. K. Pikkarainen, *A Mathematical Model for Electrical Impedance Process Tomography*, PhD thesis (Helsinki University of Technology, 2005).

[187] M. A. Bennett and R. A. Williams, "Monitoring the operation of an oil/water separator using impedance tomography," *Minerals Engineering* **17,** 605–614 (2004).

[188] M. Wang, "Impedance mapping of particulate multiphase flows," *Flow Measurement and Instrumentation* **16,** 183–189 (2005).

[189] P. E. Wellstead, W. P. Heath, and A. P. Kjaer, "Identification and control of web processes: polymer film extrusion," *Control Engineering Practice* **6,** 321–331 (1998).

[190] S. Duncan, "Cross directional control," in *IEE Proceedings on Control Theory and Applications*, Vol. 149 (2002), pp. 412–413.

[191] S. Duncan, "Using process tomography as a sensor in a system for controlling concentration in fluid flow," in *Proceedings of 2nd World Congress on Industrial Process Tomography* (2001), pp. 378–386, Hannover, Germany, August 29–31.

[192] S. Duncan, "Regulating concentration profile in fluid flow using process tomography," in *Proceedings of 15th IFAC World Congress on Automatic Control* (2002), pp. 1283–1288, Barcelona, Spain, July 21–26.

[193] E. Oñate, S. Idelsohn, O. C. Zienkiewicz, and R. L. Taylor, "A finite point method in computational mechanics. Application to convective transport and fluid flow," *International Journal for Numerical Methods in Engineering* **39,** 3839–3866 (1996).

[194] H. Lin and S. N. Atluri, "Meshless local Petrov-Galerkin (MLPG) method for convection-diffusion problems," *Computer Modeling in Engineering & Sciences* **1,** 45–60 (2000).

[195] O. Shipilova, H. Haario, and A. Smolianski, "Particle transport method for convection problems with reaction and diffusion," *International Journal for Numerical Methods in Fluids* **54,** 1215–1238 (2007).

[196] A. N. Brooks and T. J. R. Hughes, "Streamline upwind/Petrov-Galerkin formulations for convection dominated flows with particular emphasis on the incompressible Navier-Stokes equations," *Computer Methods in Applied Mathematics and Engineering* **32,** 199–259 (1982).

[197] T. J. R. Hughes, L. P. Franca, and G. M. Hulbert, "A new finite element formulation for computational fluid dynamics: VIII. The Galerkin/least-squares method for advective-diffusive equations," *Computer Methods in Applied Mechanics and Engineering* **73,** 173–189 (1989).

[198] B. Cockburn and C. W. Shu, "The local discontinuous Galerkin method for time-dependent convection-diffusion systems," *SIAM Journal on Numerical Analysis* **35,** 2440–2463 (1998).

[199] R. Codina, "Comparison of some finite element methods for solving the diffusion-convection-reaction equation," *Computer Methods for Applied Mechanics and Engineering* **156,** 185–210 (1998).

[200] B. B. King and D. A. Krueger, "The 1D convection diffusion equation: Galerkin least squares approximation and feedback control," in *Proceedings of 43rd IEEE Conference on Decision and Control* (2004), WeA04.1, Paradise Island, The Bahamas, December 14-17.

[201] D. A. Krueger, *Stabilized Finite Element Methods for Feedback Control of Convection Diffusion Equations*, PhD thesis (Virginia Polytechnic Institute and State University, 2004).

[202] R. Duraiswami, G. L. Chahine, and K. Sarkar, "Boundary element techniques for efficient 2-D and 3-D electrical impedance tomography," *Chemical Engineering Science* **52,** 2185–2196 (1997).

[203] R. G. Aykroyd and B. A. Cattle, "A flexible statistical and efficient computation approach to object location applied to electric tomography," *Statistics and Computing* **16,** 363–375 (2006).

[204] M. Wang, X. Jia, M. Bennet, and R. A. Williams, "Electrical tomographic imaging for bubble column measurement and control," in *Proceedings of SPIE - Process Imaging for Automatic Control*, Vol. 4188 (2000), pp. 114–121, Boston, Massachusetts, USA, November 5–6.

[205] M. Wang, X. Jia, M. Bennet, and R. A. Williams, "Flow regime identification and optimum interfacial area control of bubble columns using electrical impedance imaging," in *Proceedings of 2nd World Congress on Industrial Process Tomography* (2001), pp. 726–734, Hannover, Germany, August 29–31.

[206] R. Deloughry and E. Pickup, "Investigation of the closed loop control of a pneumatic conveying system using tomographic imaging," in *Proceedings of SPIE - Process Imaging for Automatic Control*, Vol.

4188 (2000), pp. 103–113, Boston, Massachusetts, USA, November 5–6.

[207] J. A. Villegas, M. Li, S. R. Duncan, H. G. Wang, and W. Q. Yang, "Feedback control of moisture in a batch fluidised bed dryer using tomographic sensor," in *Proceedings of 5th World Congress on Industrial Process Tomography* (2007), pp. 405–413, Bergen, Norway, September 3–6.

[208] J. A. Gutiérrez-Gnecchi and E. Marroquín-Pineda, "Control of a pilot-scale, solid-liquid separation plant using electrical impedance tomography measurements," *Particle & Particle System Characterization* **25,** 306–313 (2008).

[209] R. G. Aykroyd, B. A. Cattle, and R. M. West, "A boundary element approach for real-time monitoring and control from electrical resistance tomographic data," in *Proceedings of 4th World Congress on Industrial Process Tomography* (2005), pp. 637–642, Aizu, Japan, September 5–8.

[210] R. Deloughry, I. Ibrahim, P. V. S. Ponnapalli, P. Lingard, and D. Benchebra, "PXI-based electrical capacitance tomographic imaging system applied to flow control and mass flow measurement," in *Proceedings of 5th World Congress on Industrial Process Tomography* (2007), pp. 495–502, Bergen, Norway, September 3–6.

[211] G. Golub and C. von Loan, *Matrix Computations* (The Johns Hopkins University Press, 1996).

[212] R. A. Williams, O. M. Ilyas, T. Dyakowski, F. J. Dickin, J. A. Gutierrez, M. Wang, M. S. Beck, C. Shah, and A. Rushton, "Air core imaging in cyclonic separators: implications for separator design and modelling," *Chemical Engineering Journal* **56,** 135–141 (1995).

[213] R. B. White, K. Simic, and P. R. Strode, "The combined use of flow visualisation, electrical resistance tomography and computational fluid dynamics modelling to study mixing in a pipe," in *Proceedings of 2nd World Congress on Industrial Process Tomography* (2001), pp. 610–617, Hannover, Germany, August 29–31.

[214] D. R. Stephenson, M. Cooke, A. Kowalski, and T. A. York, "Determining jet mixing characteristics using electrical resistance tomography," *Flow Measurement and Instrumentation* **18,** 204–210 (2007).

[215] J. Kourunen, R. Käyhkö, J. Matula, J. Käyhkö, M. Vauhkonen, and L. M. Heikkinen, "Imaging of mixing of two miscible liquids using electrical impedance tomography and linear impedance sensor," *Flow Measurement and Instrumentation* **19,** 391–396 (2008).

[216] TrumpJet®– a new system for effective mixing of papermaking chemicals and additives, Wetend Technologies Ltd., http://www.wetend.com (valid 22.2.2013).

[217] O. M. Ilyas, R. A. Williams, R. Mann, P. Ying, A. Rushton, and R. B. Edwards, "Investigation of batch mixing using multiple-plane impedance tomography," in *Proceedings of 2nd Meeting of the European Concerted Action on Process Tomography (ECAPT), Process Tomography - A strategy for industrial exploitation* (1993), pp. 268–271, Karlsruhe, Germany, March 25–27.

[218] P. J. Holden, M. Wang, R. Mann, F. J. Dickin, and R. B. Edwards, "Imaging stirred-vessel macromixing using electrical resistance tomography," *AIChE Journal* **44,** 780–790 (1998).

[219] S. Kim, A. N. Nkaya, and T. Dyakowski, "Measurement of mixing of two miscible liquids in a stirred vessel with electrical resistance tomography," *International Communications in Heat and Mass Transfer* **33,** 1088–1095 (2006).

[220] T. L. Rodgers, D. R. Stephenson, M. Cooke, T. A. York, and R. Mann, "Tomographic imaging during semi-batch reactive precipitation of barium sulphate in a stirred vessel," *Chemical Engineering Research and Design* **87,** 615–626 (2009).

[221] P. J. Holden, M. Wang, R. Mann, F. J. Dickin, and R. B. Edwards, "On detecting mixing pathologies inside a stirred vessel using electrical resistance tomography," *Transactions IChemE, Part A* **77,** 709–712 (1999).

[222] M. Wang, A. Dorward, D. Vlaev, and R. Mann, "Measurements of gas-liquid mixing in a stirred vessel using electrical resistance tomography (ERT)," *Chemical Engineering Journal* **77,** 93–98 (2000).

[223] P. D. Christofides, "Robust control of parabolic PDE systems," *Chemical Engineering Science* **53,** 2949–2965 (1998).

[224] C. Nagaiah, G. Warnecke, S. Heinrich, and M. Peglow, "Numerical simulation of temperature and concentration distributions in fluidized beds with liquid injection," *Chemical Engineering Science* **62,** 1567–1590 (2007).

[225] F. J. Muzzio and M. Liu, "Chemical reactions in chaotic flows," *Chemical Engineering Journal* **64,** 117–127 (1996).

[226] V. John, T. Mitkova, M. Roland, K. Sundmacher, L. Tobiska, and A. Voigt, "Simulations of population balance systems with one internal coordinate using finite element methods," *Chemical Engineering Science* **64,** 733–741 (2009).

[227] S. J. Carey, H. McCann, F. P. Hindle, K. B. Ozanyan, D. E. Winterbone, and E. Clough, "Chemical species tomography by near infrared absorption," *Chemical Engineering Journal* **77,** 111–118 (2000).

[228] P. Wright, N. Terzija, J. L. Davidson, S. Garcia-Castillo, C. Garcia-Stewart, S. Pegrum, S. Colbourne, P. Turner, S. D. Crossley, T. Litt, S. Murray, K. B. Ozanyan, and H. McCann, "High-speed chemical species tomography in a multi-cylinder automotive engine," *Chemical Engineering Journal* **158,** 2–10 (2010).

[229] L. F. Gladden, B. S. Akpa, L. D. Anadon, J. J. Heras, D. J. Holland, M. D. Mantle, S. Matthews, C. Mueller, M. C. Sains, and A. J. Sederman, "Dynamic MR imaging of single- and two-phase flows," *Chemical Engineering Research and Design* **84,** 272–281 (2006).

[230] T. Mäenpää, *Robust Model Predictive Control for Cross-Directional Processes*, PhD thesis (Helsinki University of Technology, 2006).

[231] G. A. Dumont, I. M. Jonsson, M. S. Davies, F. T. Ordubadi, K. Natarajan, C. Lindeborg, and E. M. Heaven, "Estimation of moisture variations on paper machines," *IEEE Transactions on Control Systems Technology* **1,** 101–113 (1993).

[232] K. Kristinsson and G. A. Dumont, "Cross-directional control on paper machines using Gram polynomials," *Automatica* **32,** 533–548 (1996).

[233] B. M. Eyüboglu and T. C. Pilkington, "Intracavity electrical impedance tomography," in *Proceedings of 12th Annual International Conference of the IEEE Engineering in Medicine and Biology Society*, Vol. 12 (1990), pp. 130, Philadelphia, Pennsylvania, USA, November 1–4.

[234] M. Tarvainen, M. Vauhkonen, T. Savolainen, and J. P. Kaipio, "Boundary element method and internal electrodes in electrical impedance tomography," *International Journal for Numerical Methods in Engineering* **50,** 809–824 (2001).

[235] L. M. Heikkinen, M. Vauhkonen, T. Savolainen, and J. P. Kaipio, "Modelling of internal structures and electrodes in electrical process tomography," *Measurement Science and Technology* **12,** 1012–1019 (2001).

[236] S. C. Murphy and T. A. York, "Electrical impedance tomography with non-stationary electrodes," *Measurement Science and Technology* **17,** 3042–3052 (2006).

[237] S. C. Murphy, R. K. Y. Chin, and T. A. York, "Design of an impeller-mounted electrode array for EIT imaging," *Measurement Science and Technology* **19,** 094009 (2008).

[238] A. Seppänen, M. Vauhkonen, P. J. Vauhkonen, E. Somersalo, and J. P. Kaipio, "Fluid dynamical models and state estimation in process tomography: Effect due to inaccuracies in flow fields," *Journal of Electronic Imaging* **10,** 630–640 (2001).

[239] A. Seppänen, A. Voutilainen, and J. P. Kaipio, "State estimation in process tomography– Reconstruction of velocity fields using EIT," *Inverse Problems* **25,** 085009 (2009).

[240] A. Lipponen, A. Seppänen, and J. P. Kaipio, "Reduced-order estimation of nonstationary flows with electrical impedance tomography," *Inverse Problems* **26,** 074010 (2010).

[241] A. Nissinen, L. M. Heikkinen, and J. P. Kaipio, "The Bayesian approximation error approach for electrical impedance tomography– experimental results," *Measurement Science and Technology* **19,** 015501 (2008).

[242] A. Lehikoinen, S. Finsterle, A. Voutilainen, L. M. Heikkinen, M. Vauhkonen, and J. P. Kaipio, "Approximation errors and truncation of computational domains with application to geophysical tomography," *Inverse Problems and Imaging* **1,** 371–389 (2007).

[243] A. Nissinen, L. M. Heikkinen, V. Kolehmainen, and J. P. Kaipio, "Compensation of errors due to discretization, domain truncation and unknown contact impedances in electrical impedance tomography," *Measurement Science and Technology* **20,** 105504 (2009).

[244] S. Pursiainen, "Two-stage reconstruction of a circular anomaly in electrical impedance tomography," *Inverse Problems* **22,** 1689–1703 (2006).

[245] C. Antoniades and P. D. Christofides, "Computation of optimal actuator locations for nonlinear controllers in transport-reaction processes," *Computers & Chemical Engineering* **24,** 577–583 (2000).

[246] C. Antoniades and P. D. Christofides, "Integrating nonlinear output feedback control and optimal actuator/sensor placement for transport-reaction processes," *Chemical Engineering Science* **56,** 4517–4535 (2001).

[247] C. Antoniades and P. D. Christofides, "Integrated optimal actuator/sensor placement and robust control of uncertain transport-reaction processes," *Computers & Chemical Engineering* **26,** 187–203 (2002).

[248] Y. Lou and P. D. Christofides, "Optimal actuator/sensor placement for nonlinear control of the Kuramoto-Sivashinsky equation," *IEEE Transactions on Control System Technology* **11,** 737–745 (2003).

[249] A. A. Alonso, C. E. Frouzakis, and I. G. Kevrekidis, "Optimal sensor placement for state reconstruction of distributed process systems," *AIChE Journal* **50,** 1438–1452 (2004).

[250] A. Lipponen, A. Seppänen, and J. P. Kaipio, "Reduced-order model for electrical impedance tomography based on proper orthogonal decomposition," *Submitted to Inverse Problems* (2012).

[251] A. Voutilainen, A. Lipponen, T. Savolainen, A. Lehikoinen, M. Vauhkonen, and J. P. Kaipio, "Fast adaptive 3-D nonstationary electrical impedance tomography based on reduced-order modeling," *IEEE Transactions on Instrumentation and Measurement* **61,** 2665–2681 (2012).

[252] G. A. Dumont, J. M. Martin-Sanchez, and C. C. Zervos, "Comparison of an auto-tuned PID regulator and an adaptive predictive control system on an industrial bleach plant," *Automatica* **25,** 33–40 (1989).

A FE approximation of stochastic CD model and construction of state noise covariance matrix

In this thesis, the finite element (FE) approximation of the convection-diffusion (CD) model (3.1)-(3.5) is a modification of the FE approximation of a CD model without the additional control source term that was presented in [95]. The Dirichlet boundary condition (3.3) can be incorporated into the matrix form (3.22). Let n_{in} denote the number of nodes on boundary Λ_{in} and n_{o} the number of all other nodes. As the coefficients c_j and c'_j on the boundary Λ_{in} are specified by (3.3), the terms corresponding to the input boundary nodes are moved to the right hand side of equation (3.22). Furthermore, the basis functions corresponding to the boundary Λ_{in} are removed and, thus, the number of test functions decreases to $n_{\text{o}} = n_{\varphi} - n_{\text{in}}$.

Let $N_{\text{in}} = \{N_{\text{in},1}, \ldots, N_{\text{in},n_{\text{in}}}\}$ denote a subset including the indices of the nodes on the boundary Λ_{in} and $N_{\text{o}} = \{N_{\text{o},1}, \ldots, N_{\text{o},n_{\text{o}}}\}$ be a subset of indices of all the other nodes. Now, $c_{\text{o}}(t) \in \mathbb{R}^{n_{\text{o}}}$ and $c_{\text{in}}(t) \in \mathbb{R}^{n_{\text{in}}}$ are the coefficient vectors corresponding to the index sets N_{o} and N_{in}, respectively. The obtained matrix equation with respect to (3.22) is

$$\begin{aligned} M\left(c'_{\text{o}}(t) - q_{\text{o}}(t)\right) + Kc_{\text{o}}(t) &= -\tilde{M}\left(c'_{\text{in}}(t) - q_{\text{in}}(t)\right) - \tilde{K}c_{\text{in}}(t) \\ &= -\tilde{M}c'_{\text{in}}(t) - \tilde{K}c_{\text{in}}(t) \end{aligned} \tag{A.1}$$

where the matrices $M \in \mathbb{R}^{n_{\text{o}} \times n_{\text{o}}}$, $K \in \mathbb{R}^{n_{\text{o}} \times n_{\text{o}}}$, $\tilde{M} \in \mathbb{R}^{n_{\text{o}} \times n_{\text{in}}}$ and $\tilde{K} \in \mathbb{R}^{n_{\text{o}} \times n_{\text{in}}}$ are of the form

$$M(i,j) = \int_{\Omega} \varphi_{N_{\text{o,j}}}(\vec{r})\varphi_{N_{\text{o,i}}}(\vec{r})\mathrm{d}\vec{r}, \tag{A.2}$$

$$\begin{aligned} K(i,j) &= \int_{\Omega} \vec{v}(\vec{r}) \cdot \nabla\varphi_{N_{\text{o,j}}}(\vec{r})\varphi_{N_{\text{o,i}}}(\vec{r})\mathrm{d}\vec{r} \\ &\quad + \int_{\Omega} \kappa\nabla\varphi_{N_{\text{o,j}}}(\vec{r}) \cdot \nabla\varphi_{N_{\text{o,i}}}(\vec{r})\mathrm{d}\vec{r}, \end{aligned} \tag{A.3}$$

$$\tilde{M}(i,j) = \int_{\Omega} \varphi_{N_{\text{in},j}}(\vec{r})\varphi_{N_{\text{in},i}}(\vec{r})\mathrm{d}\vec{r}, \tag{A.4}$$

$$\begin{aligned} \tilde{K}(i,j) &= \int_{\Omega} \vec{v}(\vec{r}) \cdot \nabla\varphi_{N_{\text{in},j}}(\vec{r})\varphi_{N_{\text{o,i}}}(\vec{r})\mathrm{d}\vec{r} \\ &\quad + \int_{\Omega} \kappa\nabla\varphi_{N_{\text{in},j}}(\vec{r}) \cdot \nabla\varphi_{N_{\text{o,i}}}(\vec{r})\mathrm{d}\vec{r}. \end{aligned} \tag{A.5}$$

It should be noted that $q_{\text{in}}(t) \in \mathbb{R}^{n_{\text{in}}}$ is a zero vector and $q_{\text{o}}(t) \in \mathbb{R}^{n_{\text{o}}}$.

The system of differential equations

$$c'_{\text{o}}(t) = -M^{-1}Kc_{\text{o}}(t) + q_{\text{o}}(t) - M^{-1}\tilde{M}c'_{\text{in}}(t) - M^{-1}\tilde{K}c_{\text{in}}(t) \tag{A.6}$$

is obtained and its solution is approximated with the backward Euler method. Thus,

$$\begin{aligned} c_{\text{o},t+1} &\approx c_{\text{o},t} + \Delta t c'_{\text{o},t+1} \\ &= c_{\text{o},t} - \Delta t M^{-1}Kc_{\text{o},t+1} - \Delta t M^{-1}\tilde{M}c'_{\text{in},t+1} \\ &\quad -\Delta t M^{-1}\tilde{K}c_{\text{in},t+1} + \Delta t q_{\text{o},t+1} \end{aligned} \tag{A.7}$$

where $t \in \mathbb{N}_0$ denotes the discrete time index and Δt is the time step between t and $t+1$. Furthermore, $c_{\text{o},t+1}$, $c'_{\text{in},t+1}$, $c_{\text{in},t+1}$, and $q_{\text{o},t+1}$ are the discrete-time counterparts of $c_{\text{o}}(t+1)$, $c'_{\text{in}}(t+1)$, $c_{\text{in}}(t+1)$, and $q_{\text{o}}(t+1)$, respectively. The backward Euler approximation is also written for the input concentration

$$c_{\text{in},t+1} \approx c_{\text{in},t} + \Delta t\, c'_{\text{in},t+1} \tag{A.8}$$

leading to

$$c'_{\text{in},t+1} \approx \frac{1}{\Delta t}(c_{\text{in},t+1} - c_{\text{in},t}). \tag{A.9}$$

Let $\Delta c_{\text{in},t+1} = c_{\text{in},t+1} - c_{\text{in},t}$. Substituting the approximations (A.8) into (A.7) yields

$$\begin{aligned} c_{\text{o},t+1} &= c_{\text{o},t} - \Delta t M^{-1}Kc_{\text{o},t+1} - M^{-1}(\tilde{M} + \Delta t\tilde{K})\Delta c_{\text{in},t+1} \\ &\quad -\Delta t M^{-1}\tilde{K}c_{\text{in},t} + \Delta t q_{\text{o},t+1}. \end{aligned} \tag{A.10}$$

Thus,

$$\begin{aligned} (I + \Delta t\, M^{-1}K)c_{\text{o},t+1} &= c_{\text{o},t} - M^{-1}(\tilde{M} + \Delta t\,\tilde{K})\Delta c_{\text{in},t+1} \\ &\quad -\Delta t\, M^{-1}\tilde{K}c_{\text{in},t} + \Delta t q_{\text{o},t+1} \end{aligned} \tag{A.11}$$

where $I \in \mathbb{R}^{n_{\text{o}} \times n_{\text{o}}}$ is an identity matrix. Let the matrix $W \in \mathbb{R}^{n_{\text{o}} \times n_{\text{o}}}$ be defined so that $W = (I + \Delta t\, M^{-1}K)^{-1}$. Furthermore, the control term $q_{\text{o},t+1}$ is defined as

$$q_{\text{o},t+1} = Tu_t \tag{A.12}$$

where $T \in \mathbb{R}^{n_o \times n_u}$ is a matrix specifying the size of the area (the elements) the injections affect and $u_t \in \mathbb{R}^{n_u}$ is a vector of the flow rates of injectors

at time t. Thus given the initial state c_0, the FE approximation of the CD model is of the form

$$c_{\mathrm{o},t+1} = Wc_{\mathrm{o},t} + \Xi c_{\mathrm{in},t} + \Psi \Delta c_{\mathrm{in},t+1} + \Theta u_t \tag{A.13}$$

where the matrices $\Xi \in \mathbb{R}^{n_\mathrm{o} \times n_\mathrm{in}}$, $\Psi \in \mathbb{R}^{n_\mathrm{o} \times n_\mathrm{in}}$, and $\Theta \in \mathbb{R}^{n_\mathrm{o} \times n_u}$ are

$$\Xi = -\Delta t\, WM^{-1}\tilde{K}, \tag{A.14}$$

$$\Psi = -WM^{-1}\tilde{M} + \Xi, \tag{A.15}$$

$$\Theta = \Delta t WT. \tag{A.16}$$

THE MULTISTEP BACKWARD EULER METHOD

For the backward Euler method one needs to determine a suitable time step Δt so that an accurate numerical solution of the CD model is obtained. In Section 5.1, the time between the electrical impedance tomography (EIT) measurements $\Delta t_{\mathrm{EIT}} = 50$ ms. However, Δt_{EIT} turned out to be too long to be selected as Δt. Therefore, the multistep backward Euler method is employed. In the multistep method, Δt_{EIT} is divided into n_τ substeps so that the step length $\Delta t = \Delta t_{EIT}/n_\tau$ is small enough in order to guarantee satisfactory numerical accuracy of the CD model. In this case, $n_\tau = 20$.

Let $c_{\mathrm{o},t}^{(0)}, c_{\mathrm{o},t}^{(1)}, \ldots, c_{\mathrm{o},t}^{(n_\tau)} \in \mathbb{R}^{n_\mathrm{o}}$ denote the vectors of coefficients corresponding to the index set N_o on n_τ substeps. In that case, $c_{\mathrm{o},t} = c_{\mathrm{o},t}^{(0)}$ and $c_{\mathrm{o},t+1} = c_{\mathrm{o},t}^{(n_\tau)}$. Similar notations are used for the coefficient vectors corresponding to the index set N_in, $c_{\mathrm{in},t}^{(0)}, \ldots, c_{\mathrm{in},t}^{(n_\tau)} \in \mathbb{R}^{n_\mathrm{in}}$. The change of the input is constant during the time Δt_{EIT}, that is,

$$\Delta c_{\mathrm{in},t}^{(1)} = \Delta c_{\mathrm{in},t}^{(2)} = \ldots = \Delta c_{\mathrm{in},t}^{(n_\tau)} = \frac{1}{n_\tau} \Delta c_{\mathrm{in},t+1}. \tag{A.17}$$

Furthermore, the control input is constant between measurements. Thus,

$$u_t^{(0)} = u_t^{(1)} = \cdots = u_t^{(n_\tau - 1)} = \frac{1}{n_\tau} u_t. \tag{A.18}$$

The coefficient vector on the first substep is obtained from (A.13) and

$$c_{\mathrm{o},t}^{(1)} = Wc_{\mathrm{o},t}^{(0)} + \Xi c_{\mathrm{in},t}^{(0)} + \Psi \Delta c_{\mathrm{in},t}^{(1)} + \Theta u_t^{(0)} \tag{A.19}$$

where the matrices W, Ξ, Ψ and Θ correspond to time step $\Delta t = \Delta t_{\mathrm{EIT}}/n_\tau$.

Similarly, the second substep yields

$$\begin{aligned} c_{\mathrm{o},t}^{(2)} &= Wc_{\mathrm{o},t}^{(1)} + \Xi c_{\mathrm{in},t}^{(1)} + \Psi\Delta c_{\mathrm{in},t}^{(2)} + \Theta u_t^{(1)} \\ &= W(Wc_{\mathrm{o},t}^{(0)} + \Xi c_{\mathrm{in},t}^{(0)} + \Psi\Delta c_{\mathrm{in},t}^{(1)} + \Theta u_t^{(0)}) + \Xi c_{\mathrm{in},t}^{(1)} + \Psi\Delta c_{\mathrm{in},t}^{(2)} \\ &\quad +\Theta u_t^{(1)} \\ &= W^2 c_{\mathrm{o},t}^{(0)} + W\Xi c_{\mathrm{in},t}^{(0)} + W\Psi\Delta c_{\mathrm{in},t}^{(1)} + W\Theta u_t^{(0)} + \Xi c_{\mathrm{in},t}^{(1)} + \Psi\Delta c_{\mathrm{in},t}^{(2)} \\ &\quad +\Theta u_t^{(1)} \\ &= W^2 c_{\mathrm{o},t} + (W\Xi + \Xi)c_{\mathrm{in},t} + \frac{1}{n_\tau}(W\Psi + \Psi + \Xi)\Delta c_{\mathrm{in},t+1} \\ &\quad +\frac{1}{n_\tau}(W + I)\Theta u_t \end{aligned} \tag{A.20}$$

since

$$c_{\mathrm{o},t}^{(0)} = c_{\mathrm{o},t}, \tag{A.21}$$

$$c_{\mathrm{in},t}^{(0)} = c_{\mathrm{in},t}, \tag{A.22}$$

$$c_{\mathrm{in},t}^{(1)} = c_{\mathrm{in},t}^{(0)} + \Delta c_{\mathrm{in},t}^{(1)}, \tag{A.23}$$

$$\Delta c_{\mathrm{in},t}^{(1)} = \Delta c_{\mathrm{in},t}^{(2)} = \frac{1}{n_\tau}\Delta c_{\mathrm{in},t+1}, \tag{A.24}$$

$$u_t^{(0)} = u_t^{(1)} = \frac{1}{n_\tau}u_t. \tag{A.25}$$

The recursion is repeated and after n_τ substeps

$$\begin{aligned} c_{\mathrm{o},t}^{(n_\tau)} &= W^{n_\tau}c_{\mathrm{o},t} + (W^{n_\tau-1} + W^{n_\tau-2} + \ldots + W + I)\Xi c_{\mathrm{in},t} \\ &\quad +\frac{1}{n_\tau}\Big[(W^{n_\tau-1} + W^{n_\tau-2} + \ldots + W + I)\Psi \\ &\quad +(W^{n_\tau-2} + 2W^{n_\tau-3} + \ldots + (n_\tau-2)W + (n_\tau-1)I)\Xi\Big]\Delta c_{\mathrm{in},t+1} \\ &\quad +\frac{1}{n_\tau}\left(W^{n_\tau-1} + W^{n_\tau-2} + \ldots + W + I\right)\Theta u_t. \end{aligned} \tag{A.26}$$

Equation (A.26) can be written in the form

$$\begin{aligned} c_{\mathrm{o},t+1} &= \tilde{A}c_{\mathrm{o},t} + \tilde{Q}c_{\mathrm{in},t} + \tilde{T}\Delta c_{\mathrm{in},t+1} + \frac{1}{n_\tau}\tilde{G}\Theta u_t \\ &= \tilde{A}c_{\mathrm{o},t} + \tilde{Z}c_{\mathrm{in},t} + \tilde{T}c_{\mathrm{in},t+1} + \frac{1}{n_\tau}\tilde{G}\Theta u_t \end{aligned} \tag{A.27}$$

since $\Delta c_{\text{in},t+1} = c_{\text{in},t+1} - c_{\text{in},t}$ and

$$\tilde{A} = W^{n_\tau}, \tag{A.28}$$
$$\tilde{Q} = \tilde{G}\,\Xi, \tag{A.29}$$
$$\tilde{G} = \sum_{j=0}^{n_\tau-1} W^j, \tag{A.30}$$
$$\tilde{T} = \frac{1}{n_\tau}(\tilde{P} + \tilde{S}), \tag{A.31}$$
$$\tilde{P} = \tilde{G}\,\Psi, \tag{A.32}$$
$$\tilde{S} = \sum_{j=0}^{n_\tau-2} (n_\tau - 1 - j)\, W^j\, \Xi, \tag{A.33}$$
$$\tilde{Z} = \tilde{Q} - \tilde{T}. \tag{A.34}$$

STATE NOISE COVARIANCE MATRIX

The stochastic terms are included into the CD model after the discretisation. It is assumed that the modelling errors are Gaussian so that $\xi_t \sim \mathcal{N}(0, \Gamma_{\xi_t})$ with $\Gamma_\xi = \beta_\xi^2 I \in \mathbb{R}^{n_\text{o} \times n_\text{o}}$. The stochastic process η_t is also approximated as Gaussian, that is, $\eta_t \sim \mathcal{N}(0, \Gamma_{\eta_t})$. The stochastic process η_t models the uncertainty of the input concentration so that

$$c_{\text{in},t+1} = \bar{c}_{\text{in},t+1} + \eta_{t+1}. \tag{A.35}$$

Combining equations (A.27) and (A.35) yields

$$c_{t+1} = Ac_t + B_2 u_t + s_{t+1} + w_{1,t}. \tag{A.36}$$

In (A.36), the matrices $A \in \mathbb{R}^{n_\varphi \times n_\varphi}$ and $B_2 \in \mathbb{R}^{n_\varphi \times n_u}$ are

$$A(N_{\text{in},i}, j) = 0, \tag{A.37}$$
$$A(N_{\text{o},i}, N_{\text{in},j}) = \tilde{Z}(i,j), \tag{A.38}$$
$$A(N_{\text{o},i}, N_{\text{o},j}) = \tilde{A}(i,j) \tag{A.39}$$

and

$$B_2(N_{\text{in},i}, j) = 0, \tag{A.40}$$
$$B_2(N_{\text{o},i}, N_{\text{in},j}) = \frac{1}{n_\tau}\tilde{G}\Theta(i,j). \tag{A.41}$$

Furthermore, the source terms s_{t+1} and $w_{1,t}$ are of the form

$$s_{t+1} = \tilde{Y}\bar{c}_{\text{in},t+1}, \tag{A.42}$$
$$w_{1,t} = \tilde{Y}\eta_t + \tilde{H}\xi_t \tag{A.43}$$

where the matrices $\tilde{Y} \in \mathbb{R}^{n_\varphi \times n_{\text{in}}}$ and $\tilde{H} \in \mathbb{R}^{n_\varphi \times n_{\text{o}}}$ are defined as

$$\tilde{Y}(N_{\text{in},i}, j) = \delta_{ij}, \tag{A.44}$$
$$\tilde{Y}(N_{\text{o},i}, j) = \tilde{T}(i, j) \tag{A.45}$$

and

$$\tilde{H}(N_{\text{in},i}, j) = 0, \tag{A.46}$$
$$\tilde{H}(N_{\text{o},i}, j) = \delta_{ij} \tag{A.47}$$

where δ_{ij} is the Kronecker delta. It should be noted that $w_{1,t} \sim \mathcal{N}(0, \Gamma_{w_{1,t}})$ with the covariance matrix

$$\Gamma_{w_{1,t}} = \tilde{Y}\Gamma_{\eta_t}\tilde{Y}^T + \tilde{H}\Gamma_{\xi_t}\tilde{H}^T \tag{A.48}$$

since the processes $\{\eta_t\}$ and $\{\xi_t\}$ are uncorrelated.

Anna Kaasinen

Optimal Control in Process Tomography

One of the key issues in process control is that quantitative and reliable information about the process is obtained in real time. In this thesis, the feasibility of electrical impedance tomography (EIT) for process monitoring in a model-based optimal control system is studied. The simulation results indicate that in this case the quality of the data provided by EIT is adequate for process control even when there are inevitable modelling and measurement errors.

UNIVERSITY OF
EASTERN FINLAND

Publications of the University of Eastern Finland
Dissertations in Forestry and Natural Sciences

ISBN 978-952-61-1278-7